CLRC

COUNCIL FOR THE CENTRAL LABORATORY
OF THE RESEARCH COUNCILS

ISIS 2000

The Rutherford Appleton Laboratory
ISIS Facility Annual Report
1999-2000

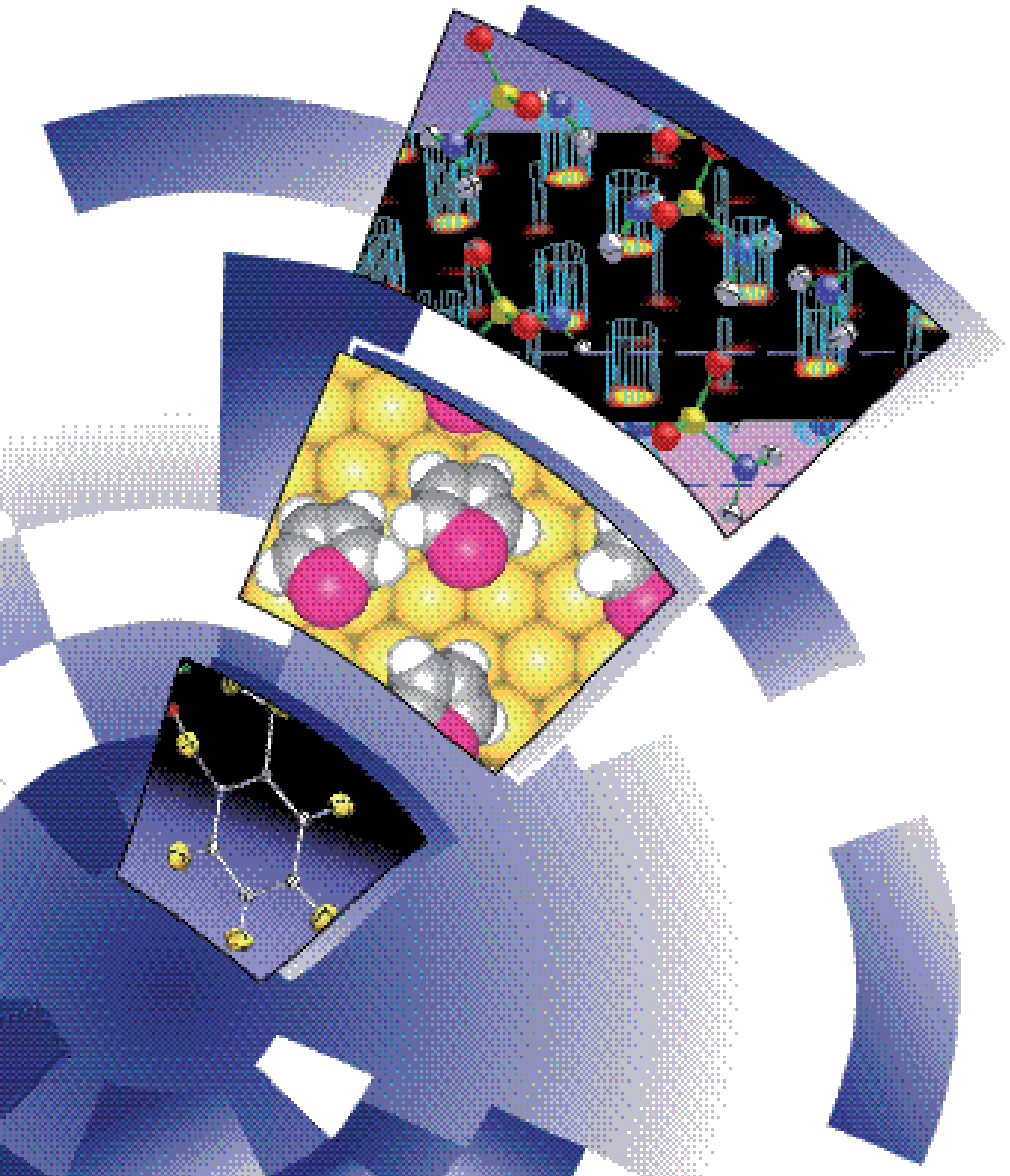

ISIS

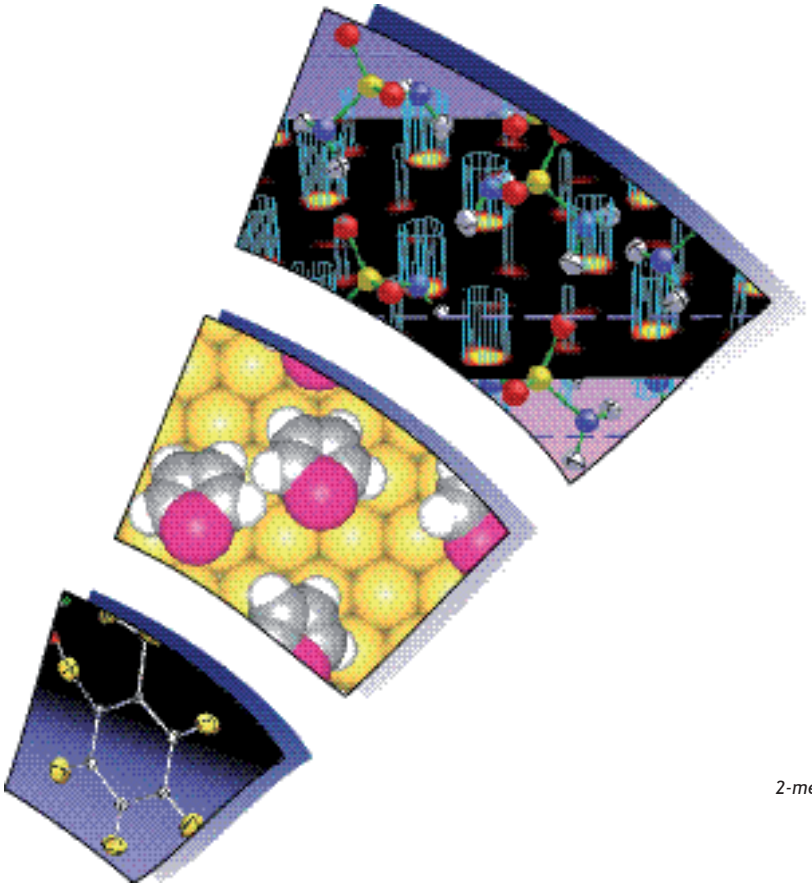

structure solution of pharmaceutical compounds from neutron powder diffraction data (page 26).

Studies of catalysts such as Co-Mo Al_2O_3 used for thiophene hydrodesulphurisation (page 18).

The O-H...N hydrogen bond in the crystalline aduct of 2-methylpyridine and pentachlorophenol is the shortest such bond studied to date using neutron diffraction (page 9).

ISIS 2000

ISIS 2000 was prepared for the ISIS Facility, CLRC Rutherford Appleton Laboratory, Chilton, Oxfordshire, OX11 0QX, UK

ISIS Director, Dr Andrew Taylor	(01235) 446681
User Office	(01235) 445592
Fax:	(01235) 445103
e-mail:	isisuo@rl.ac.uk
Web:	www.isis.rl.ac.uk

ISIS 2000 Production Team:
Philip King, Dean Adams, Rob Bewley, Mark Daymond, Roger Eccleston, Sam Foster, Chris Frost, Spencer Howells, Freddie Akeroyd, Nigel Diaper.

Printed by CLRC Photographic and Reprographic Services and ESP, Swindon
Diagrams drawn by Ampersand Design Ltd, Abingdon.

September 2000

Contents

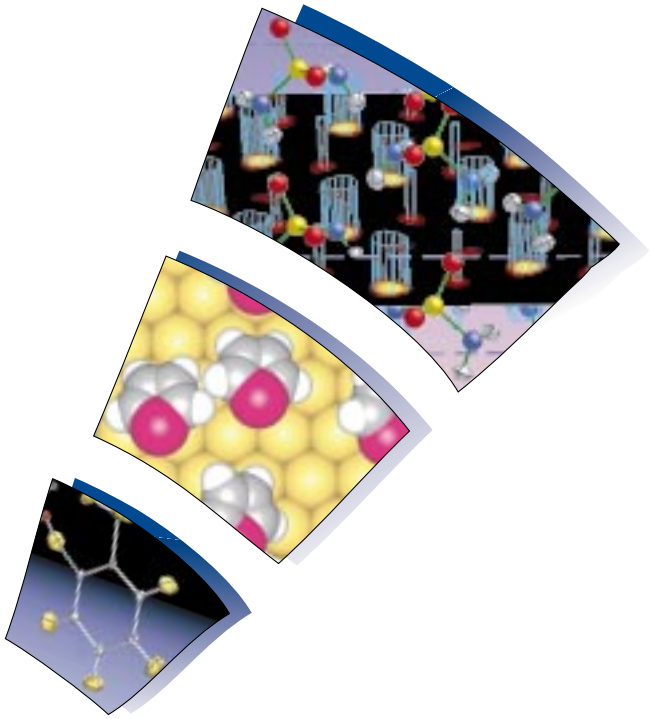

Foreword

Progress continues on all fronts !

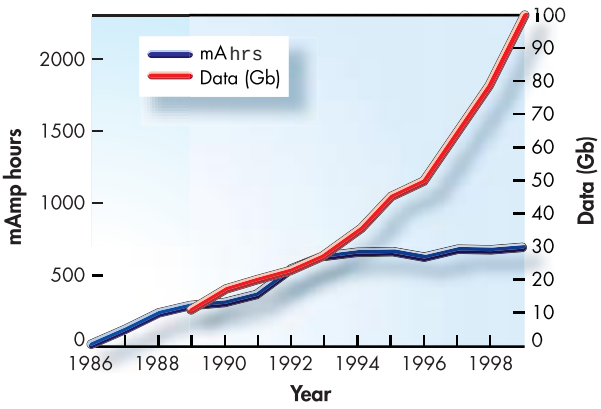

ISIS data production compared with the integrated beam current.

In March this year the Rutherford Laboratory was confirmed as the site of the New Synchrotron Light Source. This is tremendously exciting news both for ISIS and for the Laboratory as a whole. Together these two sources will firmly establish RAL as a world centre for investigating matter on the Ångstrom to micron scale. The co-location of the New Synchrotron with ISIS will provide great opportunities for the users of the facilities. From a scientific point of view it is important to ensure that the complementarity of neutrons and X-rays is fully exploited and that cross fertilisation of ideas between the two probes is maximised. For technical and instrument developments, the sharing of expertise will clearly be of great mutual benefit.

It was a great pleasure to welcome so many people to the User Consultation Meeting in May and to receive such a strong endorsement for the ISIS Second Target Station. The Second Target Station will greatly enhance our experimental capability in soft matter, advanced materials and bio-molecular science, and will strengthen the potential synergy with the New Synchrotron.

The ISIS Second Target Station is the Laboratory's highest priority in the new government Spending Review. It represents a major development of the facility, doubling the capacity for instruments and providing a qualitatively different source of neutrons to enhance and extend the scientific programme. It is the key development needed to maintain our position in the world of pulsed neutron scattering in the next decade. And for the future, we are investigating options to increase the power of ISIS to 1 MW and beyond.

The accelerator development programme is bearing fruit. Commissioning of the RFQ on its test stand and development of the prototype dual harmonic RF cavity are both well underway. Our aim is to install them in the long shutdown of 2002 and to begin to wind the ISIS current up towards the 300 μA mark.

Protons are not the only thing accelerating at ISIS. The volume of data gathered by the community last year – a broad brush measure of the productivity of the facility - exceeded 100 Gbytes, more than an order of magnitude greater than a decade ago. This data revolution is set to continue as MAPS and GEM leave their commissioning phases and move into full production mode. These state-of-the-art instruments are truly stunning. My heartiest congratulations to all of you in the community and in the facility who have worked so hard to make them such a success.

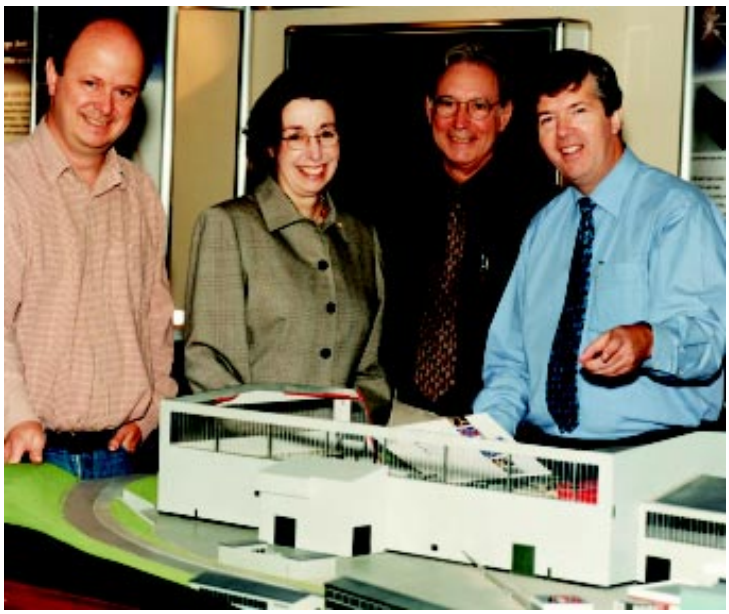

Top left: The House of Lords Select Committee on Science and Technology visiting the new GEM instrument during their tour of ISIS in May (00RC2867). Top right: Dr Pat Dehmer and Dr Iran Thomas from the US Department of Energy learning about ISIS from Andrew Taylor and Bill David (ISIS) (00RC3531). Right: Professor Helen Garnet, ANSTO Executive Director, discussing ISIS reflectometry with Jeff Penfold (ISIS) (00RC3223). Bottom left: The International Committee on Future Accelerators visited the facility in February (00RC1391). Bottom right: Richard Nelmes (ISIS) talks about high pressure studies at ISIS to members of the CLRC Council (00RC3092).

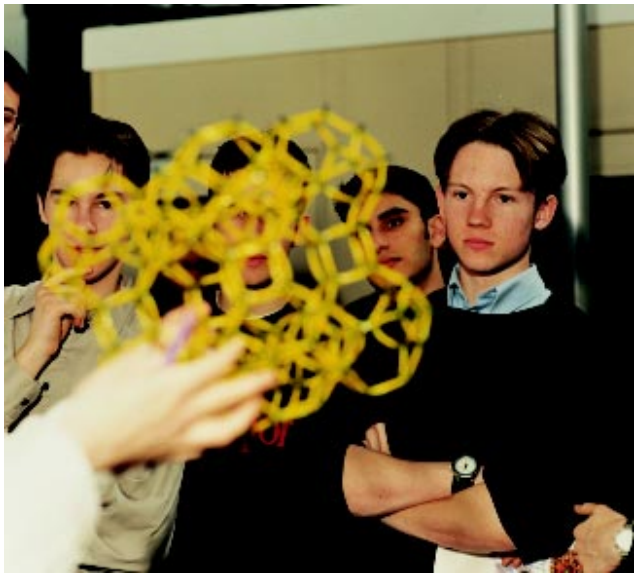

Upper left: Professor Jaques Joffrin (Orsay University) and Professor Geoffrey Bodenhausen (Ecole Normale Superieure) visited ISIS in May as part of the Five Nations Expert Group (00RC2951). Upper right: Dr Claude Detraz (Directeur de la Recherche, DG/DI CERN, Geneva) touring ISIS with Tim Broome (ISIS) (99RC4730). Centre left: ISIS users are frequently accommodated at local bed and breakfast hotels. Landlords and landladies were invited to visit ISIS earlier in the year to see what their guests get up to! (00RC3066). Centre right: Attendees at a particle physics masterclass visiting the facility (99RC1944). Lower left: A delegation from the French parliament with Heidi Heron and David Hull (OST) considering the virtues of siting the New Synchrotron alongside ISIS (00RC1531).

Introduction to ISIS

ISIS is the world's most powerful pulsed spallation neutron source. The facility provides beams of neutrons and muons that enable scientists to probe the structure and dynamics of condensed matter on scales ranging from the sub-atomic to the macro-molecular. ISIS is a multi-disciplinary research centre used by a wide range of scientists from the Physics, Earth Science, Chemistry, Materials Science, Engineering and Biology communities. ISIS is also a powerful source of neutrinos, used for fundamental Physics investigations.

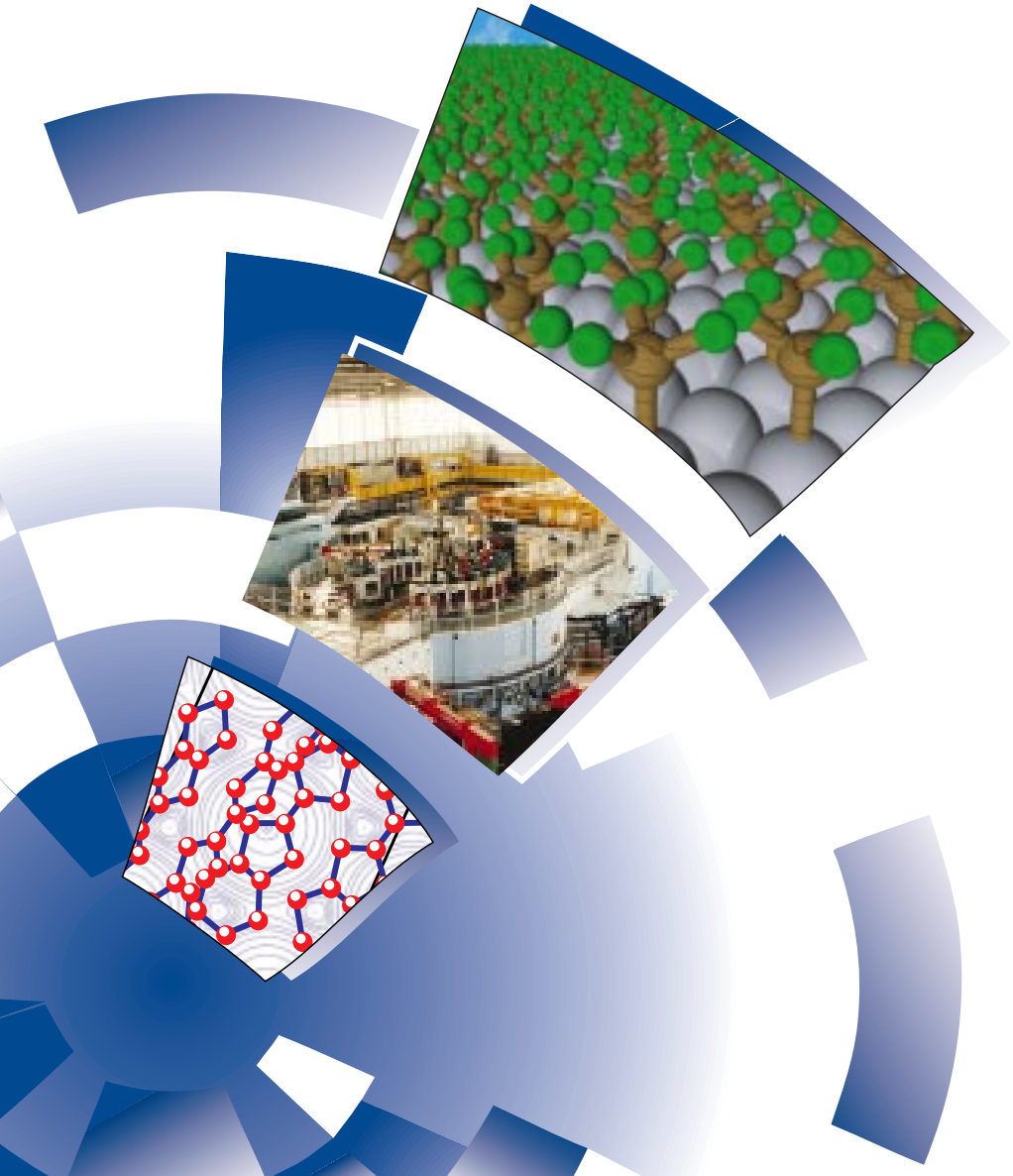

ISIS

Introduction to ISIS

ISIS is the world's most intense pulsed neutron and muon source and the major facility at CLRC's Rutherford Appleton Laboratory. The source was approved in 1977, first neutrons were produced in 1984 and in October 1985 ISIS was officially inaugurated. Over the past fifteen years, the facility has attracted substantial international investment and has developed into a major international force in condensed matter research.

The ISIS Facility (99RC4241).

Why neutrons and muons?

The neutron is a powerful probe for the study of the microscopic structure and dynamics of condensed matter, having significant advantages over other forms of radiation. Detailed information obtained from neutron scattering has had a major impact on our understanding of the microscopic nature of materials, from magnetism and superconductivity to chemical surfaces and interfaces. Muons are an alternative probe of condensed matter, giving complementary information on local structure and dynamics.

Producing neutrons at ISIS

Neutrons are produced at ISIS by the spallation process. A heavy metal target is bombarded with pulses of highly energetic protons from a powerful accelerator, driving neutrons from the nuclei of the target atoms. This results in an extremely intense neutron pulse, delivered with only modest heat production in the neutron target. In contrast, traditional reactor sources of neutrons suffer from intense heat production in the reactor core, pushing the current limits of materials technology.

Proton acceleration

Proton acceleration at ISIS begins with the H^- ion source of -665 kV. The extracted H^- beam is accelerated to ground and injected into a linear accelerator (linac). This accelerates the beam to 70 MeV, providing a 200 μs long, 22 mA H^- pulse. Final acceleration of the beam occurs in the synchrotron. On entry, the H^- beam is stripped of its electrons by a 0.3 μm thick alumina foil. The resulting protons are accumulated over many revolutions, and then trapped by the RF harmonic system into two bunches. They are accelerated to 800 MeV, 'surfing' on the rising edge of the sinusoidal magnetic field. Just prior to extraction, the pulses are 100 ns long, and are separated by 230 ns. The proton beam makes around 10,000 revolutions of the synchrotron as it is accelerated,

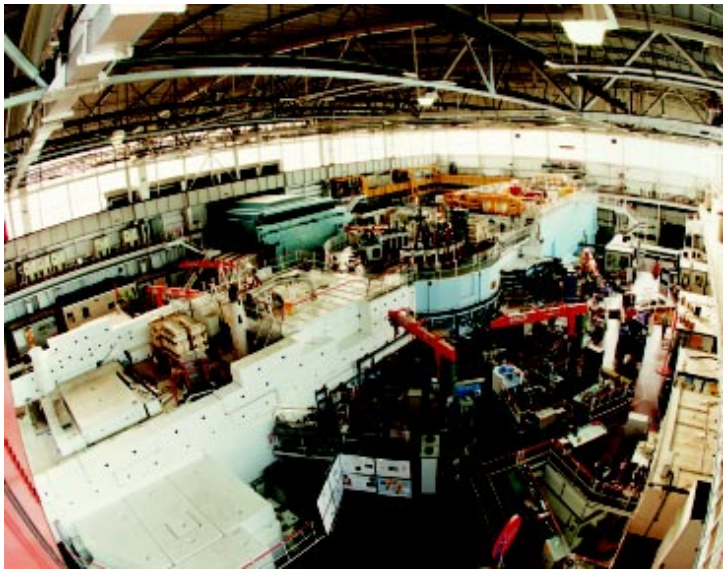

The ISIS experimental hall (99RC5419).

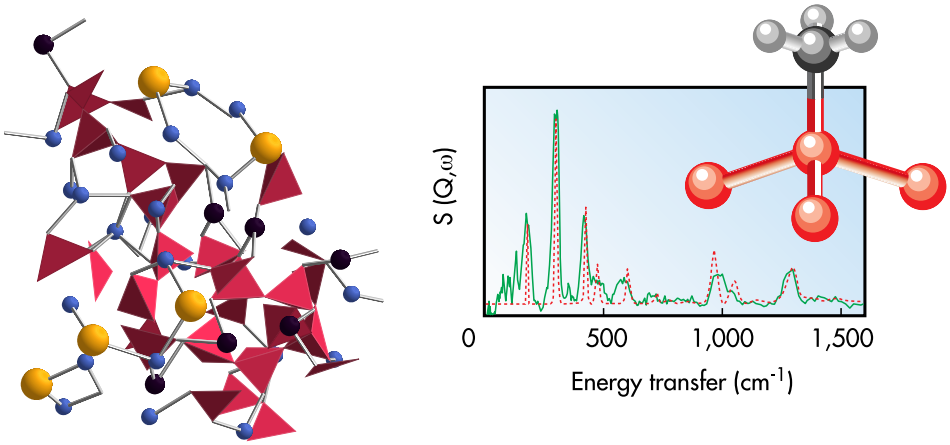

Left: Structural configuration of the ion conducting glass $(PbI_2)_{0.2}$-$(AgI)_{0.1}$-$(AgPO_3)_{0.8}$. Right: Inelastic neutron scattering spectrum from the surface of an industrial catalyst. Inset: schematic of a methyl group bound to the topmost atomic layer of the catalyst.
Thermal neutrons provide an ideal probe of both the structure and dynamics of matter.

before being 'kicked' into the extracted proton beam line and transported to the neutron target. This entire process is repeated 50 times a second.

The spallation process

The spallation target is made from a heavy metal - tantalum at ISIS. Protons hitting nuclei in the target material trigger an intranuclear cascade, putting the individual nuclei into a highly excited state. These nuclei then release this energy by 'evaporating' nucleons - mainly neutrons - some of which will leave the target while others go on to trigger further reactions. Each high energy proton delivered to the target results in the production of approximately 15 neutrons. These neutrons generally have very high energies, and must be slowed to speeds (wavelengths) useful for condensed matter studies. This is achieved using an array of small hydrogenous moderators around the target. The moderator temperature determines the spectral distribution of neutrons produced and this can be tailored for specific experiments.

Other radiation

ISIS also produces intense pulsed beams of muons, via the insertion of a thin graphite intermediate target into the extracted proton beam. High energy nuclear reactions produce pions, which decay into muons. In addition, pion and muon production at the main target also creates a rich flux of neutrinos; the KARMEN experiment is designed to exploit the pulsed structure of their production to investigate problems in fundamental Physics.

Science programme

ISIS is a User Facility, providing pulsed neutrons and muons together with a dedicated, fully supported instrument suite to enable visiting teams to exploit these techniques. The experiments carried out at ISIS typically complement work programs performed at home laboratories. ISIS science encompasses both basic and strategic research, with much collaboration between academia and industry. Experiments are selected by a peer review process. In the last year, some 613 user experiments were performed at the facility by some 1600 visiting researchers. ISIS also proves an excellent training ground for young researchers, with a large fraction of visiting scientists being aged 30 or under.

James Holt (Reading University) using the twin plate shear cell, originally developed for SAXS, for the first time on LOQ (99RC5733).

The ISIS Instrument Suite

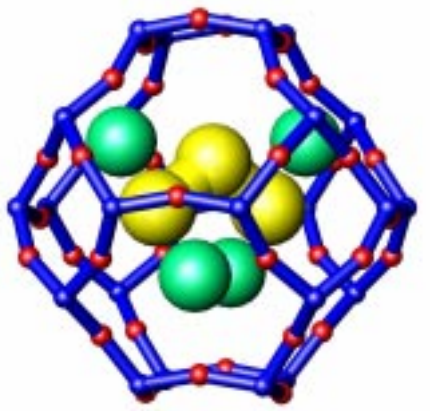

Crystallography

The core of the crystallography instruments at ISIS comprises the two powder diffractometers, **HRPD** and **POLARIS**, and a single crystal diffractometer **SXD**. **HRPD** is the highest resolution neutron powder diffractometer in the world offering a $\Delta d/d$ of approximately $5x10^{-4}$ which is effectively constant over a wide d-spacing range. This high resolution is ideal for the study of subtle structural details and small unit cell changes, and in allowing peaks to be resolved from complex materials at low d-spacings. **POLARIS** is a high flux instrument, well suited for the rapid characterisation of structures, the study of small amounts of sample and use of difficult sample environments such as high pressures. **SXD** uses the time-of-flight Laue technique to survey simultaneously a large volume of reciprocal space, making it particularly well suited to diffuse scattering investigations as well as routine structural studies of a range of organic and pharmaceutical materials. **PEARL** is used for stress measurements on engineering components and materials (**ENGIN**) and to develop diffraction at high pressures (**HiPr**). A programme of high resolution, long wavelength diffraction exists on **IRIS** and **OSIRIS**, covering magnetism and large molecular structures. **ROTAX** is operated by the University of Bonn as a multi-purpose diffractometer for powder, single crystal and texture measurements, and studies in high magnetic fields. The construction work of the new **GEM** instrument is now complete. **GEM**'s high flux, high resolution and large detector angular coverage have already proved extremely useful for a range of applications in both crystallography and disordered materials.

Disordered Materials

The study of disordered materials at ISIS is performed on the small angle liquids diffractometer **SANDALS**. **SANDALS** is optimised for the study of disordered systems with a significant number of light atoms. The low angle detector arrangement permits the inelasticity corrections for such atoms to be minimised, yielding unprecedented detail in the extraction of liquids structure. The newly commissioned **GEM** instrument will provide further opportunities in the study of disordered materials.

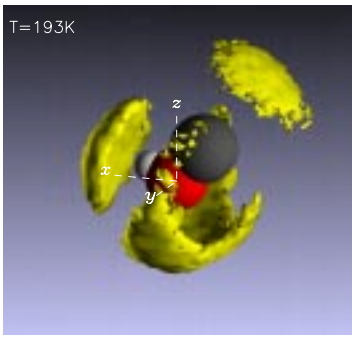

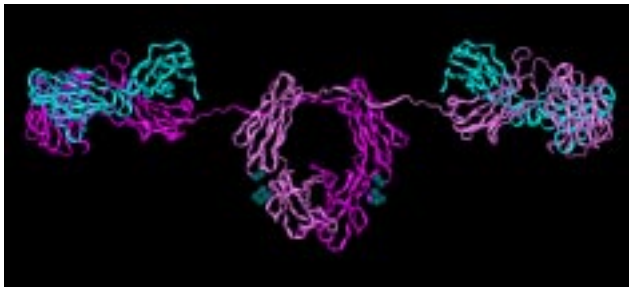

Large Scale Structures

Large scale structures are principally studied at ISIS using surface reflection and small angle neutron scattering techniques. ISIS has two reflectometers, **CRISP** and **SURF**. A glancing-angle incident beam is used to probe details of the structure perpendicular to a surface via the interference pattern of the scattered beam. Neutron reflectometry is a powerful technique for surface science which has many applications such as the study of surfactant absorption, for example in detergency, the adsorption of polymers and proteins, the nature of thin polymer films, Langmuir Blodgett films, and in the study of magnetism in thin films and multilayers. **LOQ**, the small angle scattering diffractometer, uses forward scattering of neutrons to allow large scale structures in the region 10-500 Å to be studied. Applications include investigation of voids, defects and segregation of atoms, the study of micelles and microemulsions in solution, and of polymer structures in solution, the melt and in the solid state.

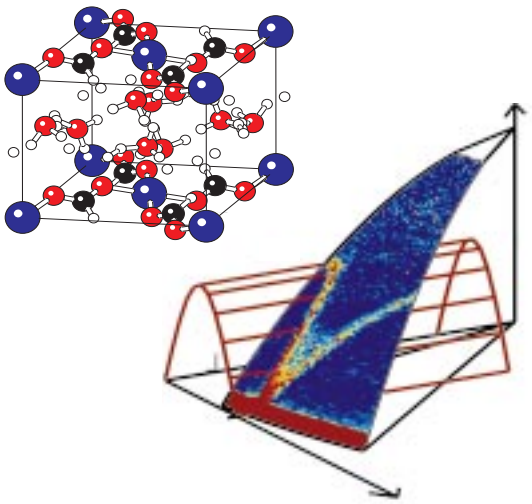

Excitations

The Excitations suite of instruments comprises two chopper spectrometers, **HET** and **MARI**, and the multi analyser spectrometer, **PRISMA**. **HET** is optimised for scattering at low momentum transfers over a wide energy range, making it particularly well suited to studies of magnetic phenomena in polycrystalline and single crystal samples. **MARI**, like **HET,** is a direct geometry spectrometer, but it offers continuous detector coverage from 3° to 138° allowing simultaneous measurement of large areas of (Q,ω) space - ideal for studies of the dynamics of amorphous materials, the vibrational spectroscopy of protonic systems and magnetic phenomena. **PRISMA** is an indirect geometry spectrometer, used to survey phonon and magnon dispersion curves. It also offers great potential for the studies of diffuse and critical scattering. **ALF** utilises the ROTAX beamline for single crystal alignment and sample characterisation. The **MAPS** spectrometer, a chopper spectrometer optimised for single crystal measurements, is now well into its scientific commissioning phase.

Molecular Spectroscopy

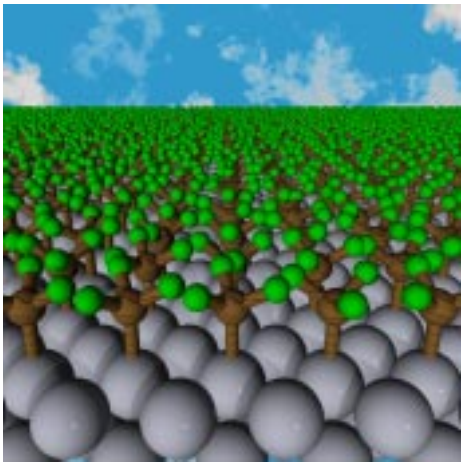

The study of molecular dynamics at ISIS is principally carried out on three dedicated instruments. **IRIS**, the high resolution inelastic spectrometer, provides energy resolutions from 50 μeV to 1 μeV with energy transfers up to 10 meV. It is well suited to studies of translational and rotational diffusion effects in a wide range of materials, quantum excitations, such as the tunnelling of the methyl group in simple organic molecules, and crystal field effects. **TOSCA** is an indirect geometry spectrometer optimised for the examination of molecular vibrations in complex chemical systems. Examples include studies of catalyst materials, hydrogen bonded materials, polymeric model materials and complex organics such as drugs. The electron volt spectrometer, **eVS**, is designed to measure atomic momentum distributions by exploiting the high flux of epithermal neutrons available at ISIS. **eVS** is finding applications in the study of hydrogen bonded systems, giving a direct probe of the atomic potentials, and in the study of quantum fluids such as the He liquids. The first stage of the OSIRIS project - the construction of a long wavelength diffractometer - is now complete. The next stage, development of the OSIRIS spectrometer, is well underway. OSIRIS also serves as a test bed for the development of polarised neutron techniques at ISIS.

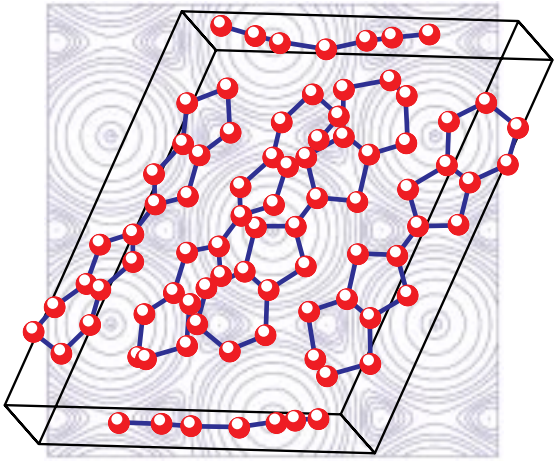

Muon Spectroscopy

The muon spectroscopy programme at ISIS currently boasts three spectrometers, **MuSR**, **EMU** and **ARGUS**, and a development facility **DEVA**. The muon is effectively a sensitive microscopic magnetometer. Implanted into virtually any material, its spin polarisation and relaxation rate can be monitored to provide information about the local structure and dynamics. The muon technique has applications in a wide variety of systems including studies of spin dynamics in magnetic systems, penetration depth and flux line lattice measurements in superconductors, muonium chemistry, light-particle diffusion processes, and hydrogen interactions in, for example, semiconductors.

Introduction

MAPS
Single Crystal Excitations
Toby Perring, ext. 5428, T.G.Perring@rl.ac.uk

eVS
Electron Volt Spectroscopy
Jerry Mayers, ext. 5882, J.Mayers@rl.ac.uk

SXD
Single Crystal Diffraction
Dave Keen, ext. 6556, D.A.Keen@rl.ac.uk

KARMEN
Neutrino Facility
Peter Plischke, ext. 5738, peter@karm6.nd.rl.ac.uk

MARI
S(Q,ω) Vibrational
& Magnetic Spectroscopy
Steve Bennington, ext. 5193
S.M.Bennington@rl.ac.uk

GEM
General Purpose
Diffraction, Liquids and
Amorphous Structures
Paolo Radaelli, ext. 5685
P.G.Radaelli@rl.ac.uk
Alex Hannon, ext. 5358,
A.C.Hannon@rl.ac.uk

HRPD
High Resolution Powder
Diffraction
Richard Ibberson, ext. 5871,
R.M.Ibberson@rl.ac.uk

PEARL
Engineering & High Pressure Instrument
Mark Daymond & Bill Marshall, ext. 5414,
M.R.Daymond@rl.ac.uk, W.G.Marshall@rl.ac.uk

DEVA
Muon Development Beam
Philip King, ext. 6117, P.J.C.King@rl.ac.uk

MuSR, EMU
Implanted Muon Spectroscopy
Philip King, ext. 6117, P.J.C.King@rl.ac.uk
Stephen Cottrell, ext. 5352, S.P.Cottrell@rl.ac.uk

Moderators

liquid hydrogen, 20K

liquid methane, 100K

water, 316K

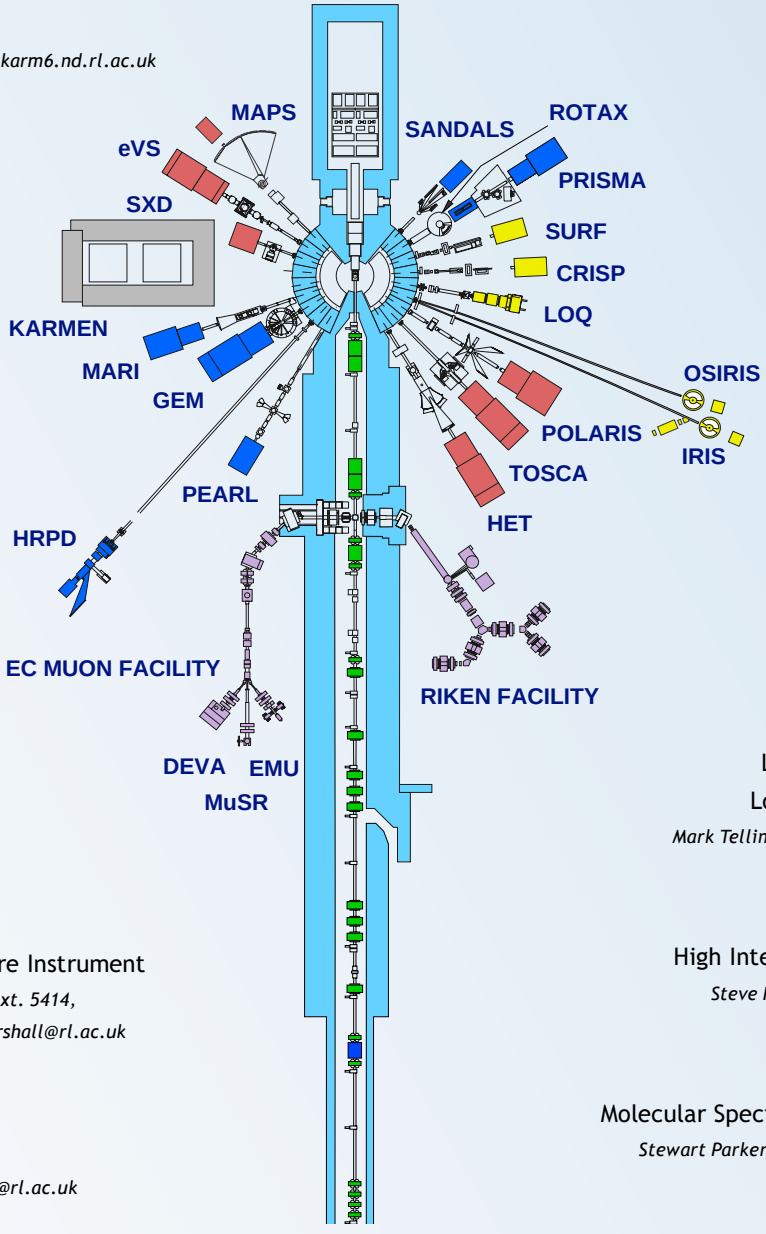

SANDALS
Small Angle Liquids & Amorphous Diffraction
Alan Soper, ext. 5543, A.K.Soper@rl.ac.uk

PRISMA
Coherent Excitations & Critical Scattering
Martyn Bull, ext. 5805 M.Bull@rl.ac.uk

ROTAX
Multiple Purpose Diffractometer
Winfried Kockelmann, ext. 6731
W.Kockelmann@rl.ac.uk

CRISP, SURF
Neutron Reflectometry
Sean Langridge ext. 5269
s.langridge@rl.ac.uk
John Webster, ext. 6381,
J.R.P.Webster@rl.ac.uk

LOQ
Small Angle Scattering
Richard Heenan, ext. 6744,
R.K.Heenan@rl.ac.uk

OSIRIS
Polarisation Analysis
Spectroscopy &
Diffraction
Ken Andersen, ext. 6731,
K.H.Andersen@rl.ac.uk

IRIS
Low Energy Spectroscopy
Long d-spacing Diffraction
Mark Telling ext. 5529, M.Telling@rl.ac.uk

POLARIS
High Intensity Powder Diffraction
Steve Hull, ext. 6628, S.Hull@rl.ac.uk

TOSCA
Molecular Spectroscopy & Crystal Fields
Stewart Parker, ext. 5797, S.F.Parker@rl.ac.uk

HET
Excitations at Low
Momentum Transfer
Rob Bewley, ext. 5797,
R.I.Bewley@rl.ac.uk

RIKEN
Surface & Decay
Line Muon Facility
Katsu Ishida ext. 6802, K.Ishida@rl.ac.uk

Science at ISIS

The scientific programme at ISIS centres on the use of neutron and muon beams for condensed matter research. A review of some of the scientific work performed on the ISIS instruments is presented in this chapter. More detailed descriptions of scientific highlights are presented in chapter 3. Reports describing experiments performed at ISIS in the last year are contained on the CD inside the back cover of this report in PDF format.

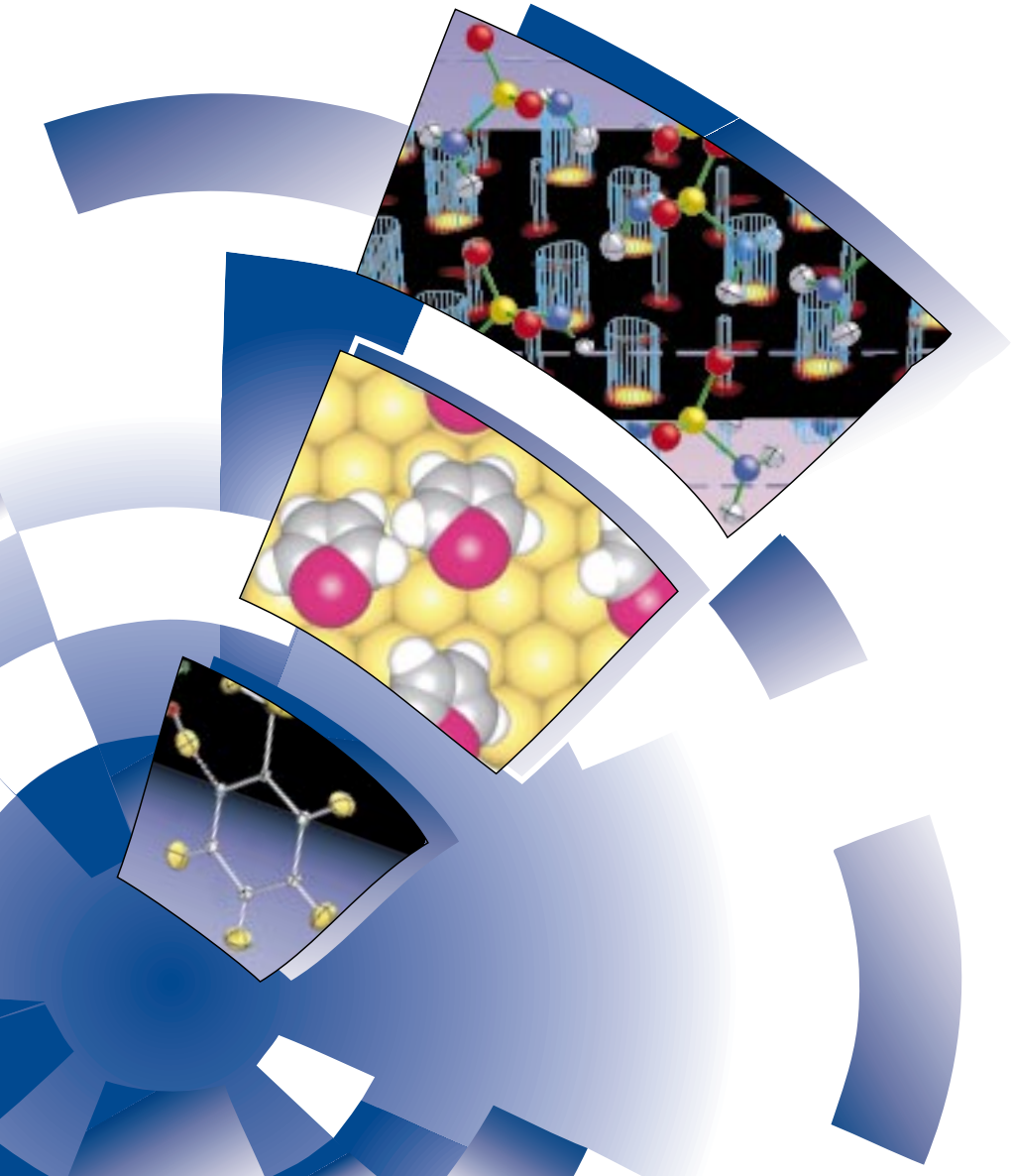

ISIS

Crystallography

The ISIS Crystallography instruments comprise a world-leading suite. The POLARIS, HRPD, SXD and PEARL/HiPr instruments continue to operate busy and diverse user programmes in powder and single crystal diffraction, straddling the areas of Chemistry, Materials, Physics and Earth Sciences. The commissioning phase of GEM has progressed extremely well and the first set of user-led commissioning experiments have been carried out (see page 71). Demand for the high pressure component on PEARL/HiPr remains at a very high level, with Paris-Edinburgh (P-E) cell developments in parallel with a busy user programme; the PEARL/HiPr detector array offers a very powerful tool for high pressure studies. Demand for SXD is also at a notably high level, particularly in the area of chemical crystallography. The re-sited and upgraded POLARIS is performing well in a wide range of studies.

The EPSRC-funded projects to upgrade the 90° detector bank for HRPD and the SXD detectors are advancing well (see page 72). These improvements, together with the new GEM instrument, have provided a high quality instrument suite offering possibilities for more innovative experiments. Examples include the possibility of growing single crystals directly in the beam and the opportunity to deliver reactive, non-robust gases into the powder diffractometers for structure solution and refinement. Extending the existing highly successful high pressure powder diffraction programme to single crystal studies is also being pursued. Developments such as these will have significant benefits for the user community.

The crystallography programme stimulates continual improvements in sample environments. The construction of the ISIS chemical reaction cell, funded under the advanced sample environment grant, has been completed and a call for proposals for its use on POLARIS issued. Future possibilities for enhancement of the POLARIS instrument, notably the backscattering and low angle detector banks, are being considered, along with the possibilities of further optimising the instrument for studying chemical reactions. The high pressure user programme on PEARL/HiPr has benefited from the availability of state-of-the-art dedicated P-E pressure cells, offering routine pressures of 0-10 GPa using tungsten carbide anvils, or up to 25 GPa with user-supplied sintered diamond anvils, in the temperature range ~90-350 K.

The scientific programme remains rich and varied and there are strong strands in advanced materials, materials processing and reaction chemistry, structure/property relationships, structural solution, mineralogical and geological structures, phase transitions and organic and supramolecular chemistry.

In particular this year the area of reaction chemistry has been a highlight. In addition to the work carried out by the Oxford group on developing and using a hydrothermal reaction cell (see Highlight on page 30), there have been several other 'in-situ' measurements. These have included studies of gel decomposition as a synthesis route to single phase manganate materials, studies of controlled recrystallisation of Li-inserted materials for anode applications and the initiation of a programme aimed at understanding the processing of dielectric BZT ceramics. Along the same lines, structural systematics have been explored as a function of temperature and pressure in several experiments, for example in studies of the structural properties

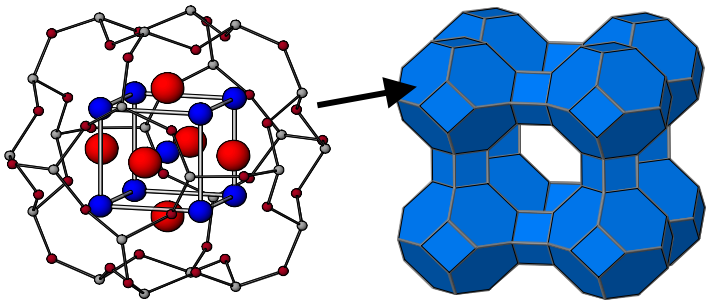

Figure 2.1. Structure of Zn-loaded zeolite A showing the arrangement of zinc oxide clusters (Anderson et al).

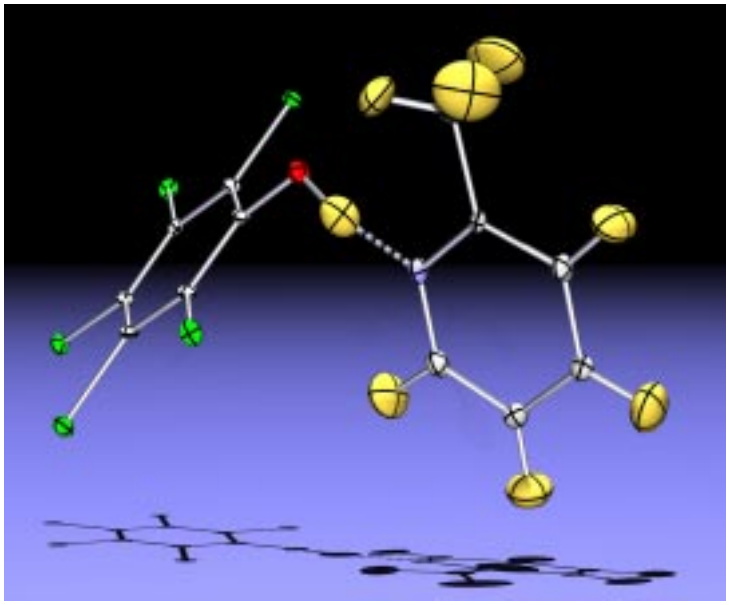

Figure 2.2. The O-H...N hydrogen bond in the crystalline aduct of 2-methylpyridine and pentachlorophenol is the shortest such bond studied to date using neutron diffraction. The O...N distance is 2.588(3) Å, and the SXD study clearly showed the hydrogen-bonded proton to be localised on the oxygen atom in this complex, at an O-H distance of 1.068(7) Å.

of silver-based superionic materials, where the pattern of phase transitions and structural order/disorder are important in understanding conducting properties.

There has been a revitalisation of interest in the use of HRPD to study the fine detail of phase transitions; the ability of the instrument to scan parameter space rapidly at very high resolution offering unique possibilities in this area. In the traditional area of perovskite oxides, there has been a renewed effort to study the pattern of phase transitions in $SrZrO_3$ and $SrHfO_3$, following preliminary studies at Oak Ridge. The results have allowed significant new insights into these processes, and have identified hitherto unsuspected phase transitions. The ferroelectric phase transitions in $SrTeO_3$ were also studied, to try to resolve an ongoing controversy regarding the correct structure at high temperature - the high symmetry space group was confirmed as C2/m. The pattern of phase transitions in lead aluminium fluoride was studied with a view to understanding, for example, the second harmonic generation properties of this material. Mineral structures have also been subject to detailed temperature-dependent studies, for example the possible effect of H/D exchange on the transitions in lawsonite and the detailed thermal evolution of the lattice parameters in gibbsite.

In the area of advanced and complex materials, the study of loaded zeolites has once again featured. These have potential applications in catalysis, optics, electronics and sensors. Studies have been carried out of the inclusion of both alkali metal and zinc ions into zeolites (see figure 2.1), examining the spatial localisation of these ions or clusters of ions in the structure. More recently, studies have been initiated of the inclusion of metal-organic complexes into the zeolite framework, where the particular interest is in the potential optical activity. Such studies are a challenge, but the combination of high flux and high resolution available on the ISIS powder instruments is making these tenable. The use of neutron diffraction in studying a variety of novel materials for potential use in fuel cells has continued, along with many studies of the structural and magnetic characteristics of the CMR manganates. The study of materials under high pressure has also continued. This includes fundamental systems such as ice and other simple molecular materials (see Highlight on page 34), clathrates, minerals (see Highlight on page 32) and studies of the effect of pressure on, for example, magnetic ordering in manganese perovskites. Studies of single crystals of the decagonal quasicrystal AlNiCo have also featured.

The strong programme of studies of molecular and supramolecular systems has continued, with investigation of materials displaying non-linear-optical activity such as substituted urea compounds and the nitroanilines (see Highlight on page 36) where the aim is to correlate molecular structure, hydrogen bonding and molecular packing with optical properties. Among other highlights in this area have been the commencement of studies of methylpyridine: pentachlorophenol complexes, which contain some of the shortest O-H...N hydrogen bonds known (see figure 2.2), and the first successful neutron diffraction structure determination of an icosahedral fragment *nido*-carborane, studied using a natural-boron single crystal.

Disordered Materials

The Disordered Materials Group supports neutron diffraction research into the structure of liquids and disordered materials. The Group operates the recently commissioned GEM diffractometer and the SANDALS diffractometer.

The number of completed disordered materials experiments on GEM is still small due to the time devoted to commissioning and the lack of low angle detectors. Skipper *et al* performed some preliminary experiments on the Li-ammonia system to compare with data taken on SANDALS and at the ILL. A useful commissioning experiment on liquid carbon tetrachloride was also completed and produced a radial distribution function exactly in accord with that obtained in previous experiments on this material (see figure 2.3). These data serve to demonstrate that the full ATLAS suite of analysis programmes can now be applied to GEM data.

At this early stage the performance of the GEM detectors appears outstanding, both in terms of their stability and their uniformity: detector fluctuations appear much smaller than 0.1% over a 24 hr time period. In an experiment to investigate the presence of disordered magnetic structures, Newport *et al* have used GEM to study terbium metaphosphate glass, $Tb_2O_3.3P_2O_5$. The particular interest was to determine the likely separation between the rare earth ions, Tb^{3+}, but this is an extremely difficult and challenging experiment. The aim of the experiment was to measure the correlations between Tb^{3+} ions by comparing data taken with a high magnetic field turned on and off. A previous attempt to do this

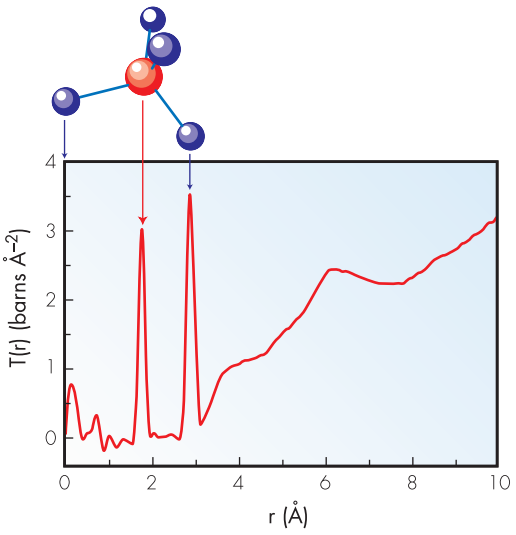

Figure 2.3. Radial distribution function for liquid carbon tetrachloride, used as a commissioning experiment on GEM. The data indicate the excellent spatial resolution obtainable with GEM data, and show that the full ATLAS data analysis package is available on GEM.

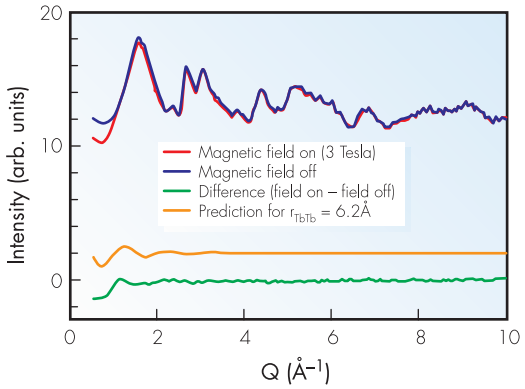

Figure 2.4. Diffraction pattern for a terbium metaphosphate glass, with (red) and without (blue) the magnetic field applied. The small difference between these signals is readily discernible with the excellent GEM stability, and indicates a Tb-Tb distance of about 6.2 Å.

Alex Hannon at the helm of GEM (00RC5039).

experiment on POLARIS had failed due to inadequate data quality. However, the experiment was successfully performed on GEM due to the higher count rate and excellent detector stability. A clear difference in the diffraction pattern was observed when the 3 Tesla magnetic field was turned on and off (see figure 2.4). The data indicate that the Tb-Tb distance is a little over 6 Å.

On SANDALS there has once again been a very diverse programme of research. Neilson has initiated a series of studies of the water environment around increasingly large and complex molecules in solution, with the ultimate goal of understanding the solvent properties which cause large macromolecules to fold or unfold in solution. Skipper has continued his series of experiments on metal-ammonia and metal-amine solutions, investigating changes of structure through the metal to non-metal transition, and in due course perhaps determining the liquid structure around the solvated electron. Poon has investigated a series of methanol-water solutions,

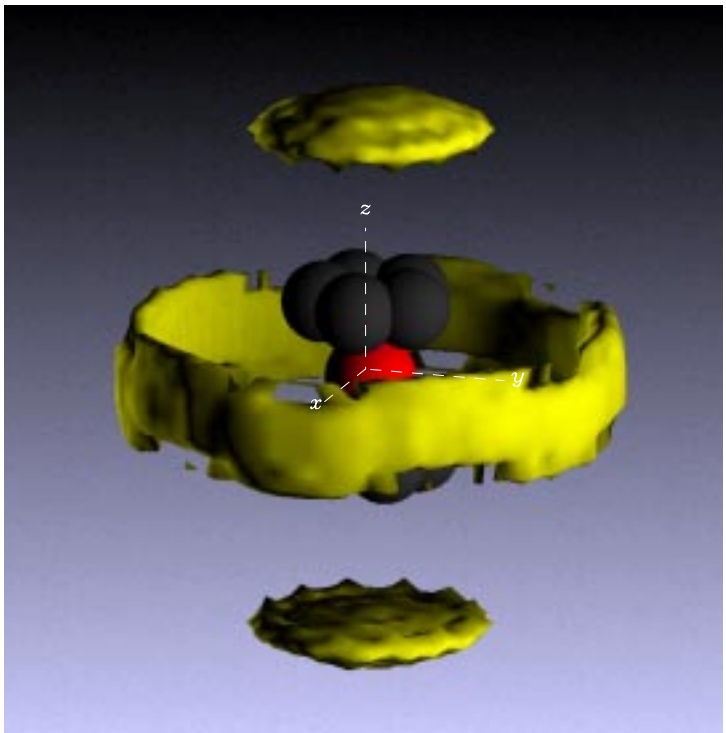

Figure 2.5. Spatial density distribution of toluene around a ferrocene molecule (shown at centre) in solution. The toluene prefers to lie either in the polar regions or the equatorial regions of the central ferrocene molecule. Orientational plots not shown here indicate that there is a strong preference for the plane of the toluene molecule to point directly towards the centre of the ferrocene molecule in both regions.

Piers Buchannan (Bristol University) preparing the SANDALS multi-sample changer (00RC1268).

looking for changes in the methanol-methanol and methanol-water configurations to interpret trends seen in Raman scattering data on the same system. Ricci has started to investigate the structure of supercritical water in the presence of hydrophobic solutes, although at the present time the data are only preliminary. Turner has pioneered the investigation of non-aqueous solutions with an investigation of ferrocene dissolved in toluene, using hydrogen isotope substitution on the ferrocene molecule (see figure 2.5). Adya has continued his work on non-aqueous liquid mixtures.

On the disordered materials front, Barnes has performed some successful furnace experiments on SANDALS, and Greaves returned with another successful levitator experiment to investigate the structure of liquid alumina for the first time with neutrons (See Highlight article on page 40). Dahlborg investigated short and medium range order in molten alloys, Borjesson studied molten PEO-$LiAsF_6$ and Swenson analysed PPO-$LiClO_4$ and PPO-$Mg(ClO_4)_2$ glasses. Other glass studies have been performed by Hoppe, Cormier, Lamparter and Newport.

Large Scale Structures

Neutron reflectometry and small angle neutron scattering, SANS, are key techniques for the study of a wide range of important and technologically relevant phenomena in Soft Matter, Advanced Materials and Bio-molecular Sciences. Whilst neutron reflectometry provides access to the structure of surfaces and interfaces, SANS probes structures on the mesoscale, in the range 20 to 1000 Å. The SANS (LOQ) and reflectometry (SURF, CRISP) instruments at ISIS effectively exploit the features of a pulsed neutron source: a wide dynamic range and good resolution. These features, coupled with the selectivity offered by H/D isotopic substitution and neutron polarisation, make a wide range of complex phenomena experimentally accessible.

Neutron Reflectometry on CRISP and SURF

Developments in the unique polarised neutron capability of CRISP have resulted in an increased use of polarised neutron reflectometry, PNR, in the study of a wide range of magnetic thin films. The technique gives access to an absolute vector measurement of magnetic coupling perpendicular to the sample surface. Recently, there has been much interest in exploiting the giant magneto-resistance, GMR, effect in magnetic storage media. The sign of the GMR effect can be controlled by introducing a rare earth, RE, in proximity with a transition metal layer. The differing exchange interactions between the rare earth and transition metal layers (ferromagnetic or anti-ferromagnetic) give rise to either a positive or negative GMR effect. The ability to determine magnetic coupling mechanisms has been used to study systems such as $[Co/Cu/Co/RE/Co/Cu]_{25}$, where RE corresponds to Dy, Gd, and Nd (Hickey et al). Figure 2.6 shows the spin polarised reflectivity for an anti-ferromagnetic Nd layer at T=3.5K. Detailed analysis allows quantitative modelling of the exchange coupling.

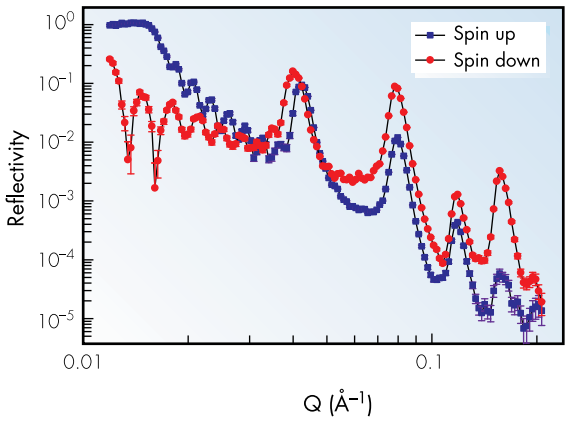

Figure 2.6. Polarised neutron reflectivity at T=3.5K for the Nd multilayer described in the text.

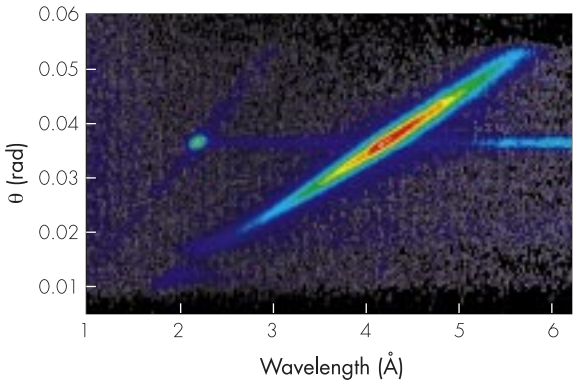

Figure 2.7. The scattering from an annealed Fe/Cr multilayer. The scattering at 4.3 Å corresponds to anti-ferromangetic coupling of the Fe. The magnetic roughness is revealed as the strong scattering away from the specular direction in contrast to the nuclear Bragg peak at 2.1Å.

Use of the multi-detector on CRISP gives access to the off-specular scattering and the in-plane structure of the sample. In the magnetic case this can take the form of magnetic roughness or magnetic domain correlations. Studies of Fe/Cr multi-layers (Takeda et al) deposited on MgO substrates show strong anti-ferromagnetic coupling between the Fe layers, but in the presence of interfacial structural roughness the magnetic coupling is disordered and off-specular scattering is observed (figure 2.7). The level of magnetic disorder can be quantified and correlated with the magnitude of the GMR.

Polymer-surfactant mixtures are examples of complex, multi-component systems that can be effectively studied using neutron 'contrast variation' techniques. Polymers are added to surfactant mixtures as viscosity modifiers, stabilisers and deposition aids, and such mixtures

represent closely the formulation of products such as shower gels and hair shampoos. Although in many cases the bulk phase behaviour of such mixtures is well characterised, their surface or interfacial behaviour (vital in the understanding of aspects of their product functionality) is not. Specular neutron reflectivity, in combination with H/D isotopic substitution, is an ideal technique for the investigation of the surface composition and structure of such mixtures. Recent measurements by Thomas et al on a mixture of polystyrene sulphonate, PSS, and the cationic surfactant dodecyl trimethyl ammonium bromide (C_{12}TAB) have revealed a surprising pattern of behaviour in the adsorption of the mixture at the air-water interface ranging from a thin adsorbed layer comprised of surfactant and polymer at low surfactant concentrations to a highly ordered structure (see figure 2.8) at higher concentrations. Measurements with differently isotopically labelled combinations of surfactant, polymer, and solvent provide the opportunity to determine the detailed structure of the mixed surface layer (see inset in figure 2.8).

Random graft co-polymers exhibit novel surface visco-elastic properties as a function of concentration of the spread film at the air-water interface. To determine the role of the amount of hydrophilic poly-ethylene oxide, PEO, present on the grafting density (to the hydrophobic norbornene backbone) Richards et al have used neutron reflectometry to determine the molecular organisation of these co-polymers at the air-water interface. The results show that the distribution of co-polymer is best described as a uniform layer with a parabolic decay. The hydrophobic backbone is located at the uppermost surface, and the PEO

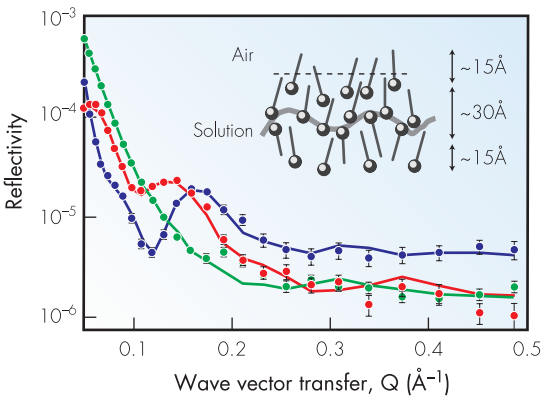

Figure 2.8. Specular reflectivity for 2.3x10⁻² M C_{12}TAB/140 ppm NaPSS in water. Green: d-C_{12}TAB/h-NaPSS; blue: h-C_{12}TAB/h-NaPS/D_2O; red d-C_{12}TAB/h-NaPSS/nrw.

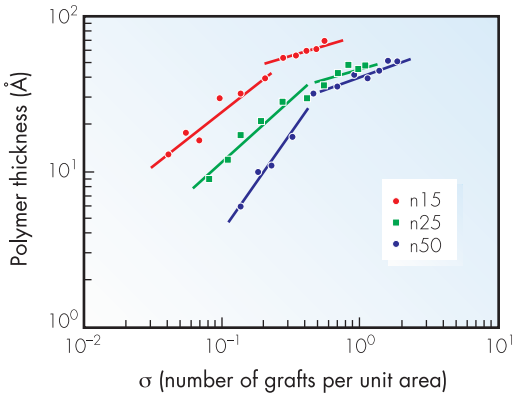

Figure 2.9. PEO graft length verses grafting density for n15 (blue), n25 (green) and n50 (red), where n is the degree of polymerisation of the PEO graft (ie n=15, 25, 50 ethylene oxide units).

grafts extend into the sub-phase. Plotting the PEO graft length as a function of grafting density (figure 2.9) reveals a phase change at a surface concentration that coincides with the onset of the plateaux region of the surface pressure isotherm. At the higher surface concentrations the behaviour is consistent with stretched wet brushes.

The applications of surfactants all occur under non-equilibrium conditions, whereas most academic studies, such as for example surface tension, are made at equilibrium. The kinetics of surfactant adsorption remains relatively poorly understood. In particular there is uncertainty about the role of micelles and whether the mechanism is pure or activated diffusion. Bain and Eastoe are using the complementary techniques of surface light scattering, SLS, and neutron reflectometry to address this problem. An overflowing cylinder (OFC) cell generates a continuously expanding liquid surface with a 'surface age' of 0.1 to 1.0 second, a time scale range of practical relevance. The initial study has used a well-characterised anionic surfactant bis (1H, 1H perfluoropentyl) sulfosuccinate (di-CF4), a fluorinated analogue of Aerosol-OT. Figure 2.10 shows the surface tension results for di-CF4: the equilibrium data were obtained by drop volume tensiometry, and the dynamic values were measured on the OFC using SLS. A significant perturbation under dynamic conditions is observed in comparison to the equilibrium results. Results from the neutron reflection measurements are also shown in figure 2.10, where equilibrium

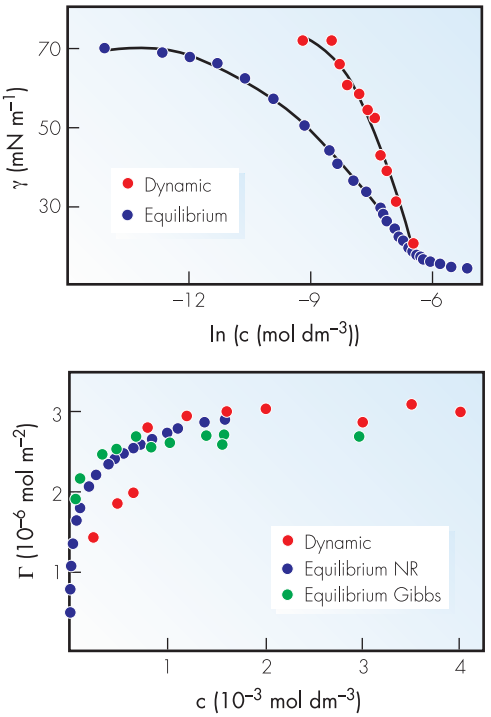

Figure 2.10. Equilibrium dynamic surface tensions (top) and adsorption isotherms (bottom) for di-CF4

surface excesses, as measured by reflection and inferred from tension data using the Gibbs equation, are compared with those measured directly for samples off-equilibrium in the OFC cell. The equilibrium and dynamic surface coverages are essentially the same at higher surfactant concentrations, down to about 0.5 *x* cmc, and at concentrations below this there are significant deviations. The off-equilibrium adsorption can only be directly measured using neutron reflection, and is essential for an understanding of the dynamical processes.

Non-ionic surfactants are frequently used as emulsifiers in a variety of food and pharmaceutical products. A range of interactions exist between proteins and surfactants, resulting in dramatic differences in the stability and rheological properties of food and pharmaceutical formulations. Lu and co-workers have used specular neutron reflection to investigate the competitive adsorption of lysozyme and the non-ionic surfactant $C_{12}E_5$ at the air / solution interface. The neutron reflection measurements quantify the predominant lysozyme occupation of the surface at low surfactant concentration. With increasing $C_{12}E_5$ concentration the lysozyme is eventually completely replaced by $C_{12}E_5$. Structural measurements show that the surfactant causes a partial breakdown of the globular structure of the protein at the interface.

Small Angle Scattering on LOQ

SANS, and the evident advantages of H/D isotopic substitution, is extensively used in the determination of the structure of surfactant mesophases. Eastoe and co-workers have been exploring the production of controlled colloidal particle architectures using surfactants with polymerisable vinyl groups. A range of micelle geometries was investigated using a mixture of single and di-chain surfactants with vinyl groups in the tails which are polymerisable by UV. Once cross-linked the structures should be more stable

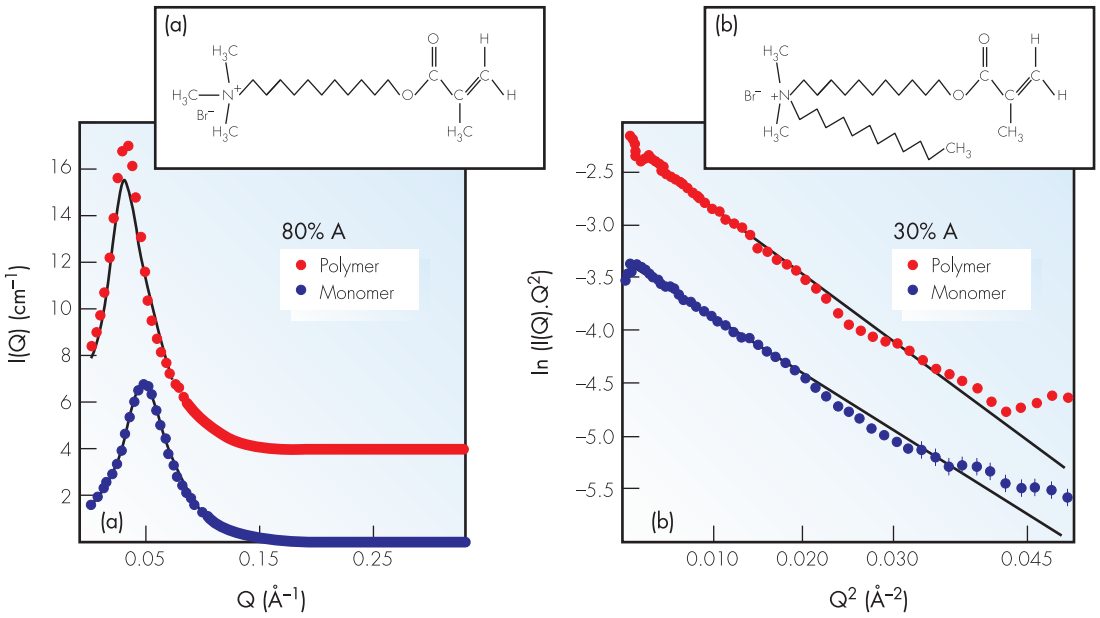

Figure 2.11. SANS data and model fits for 0.15M mixture of single and di-chain surfactants at mixing ratios of (a) 30% and (b) 80%. Insets (a) and (b) show the structures of the single and di-chain surfactants.

to both dilution and temperature than normal surfactant based colloids. Figure 2.11 shows the SANS data for such a mixture of single and di-chain surfactants in both monomer and polymerised form, and for two different compositions. The data show that the micelle structure is broadly retained after polymerisation, and that the variation of structure from spherical to lamellar with composition is consistent with packing arguments.

Concentrated surfactant mesophases are fundamental constituents of detergent-based products in manufacture and use. Formulations, such as fabric conditioners, frequently contain concentrated mixtures of di-chain cationic surfactants and non-ionic surfactants, and have a complex phase behaviour from liposomes to micelles. Penfold and co-workers at Unilever have used SANS measurements to study the microstructure of the di-chain cationic / non-ionic mixture HEQ/$C_{12}E_{12}$. At high HEQ/$C_{12}E_{12}$ composition ratios the system can be described as a defective lamellar phase. At higher surfactant concentrations anisotropic scattering, consistent with an aligned lamellar phase, is observed, whereas the scattering becomes isotropic at lower surfactant concentrations. The structure is more pronounced and ordered at temperatures above the Lα/Lβ phase transition temperature. At lower HEQ/$C_{12}E_{12}$ compositions (see figure 2.12) there is an increased tendency to form small spherical micelles with increasing temperature, such that the solution is completely micellar before the Lα/Lβ phase transition temperature is reached.

The effect of chain branching in polymers is an important area of investigation; small changes in branching can have dramatic effects on processing properties (such as drawability in films and fibres) and on the final physical properties. Although the effect is well documented and extensively used, the underlying molecular mechanisms are not clearly established. Using SANS, Spells has shown clear differences in structure on stretching poly-ethylene (PE) chains with C4 or C6 side chains included every ~200 carbon atoms in the PE chain. A clear correlation was established between the initial draw ratio and the 'permanent' molecular deformation.

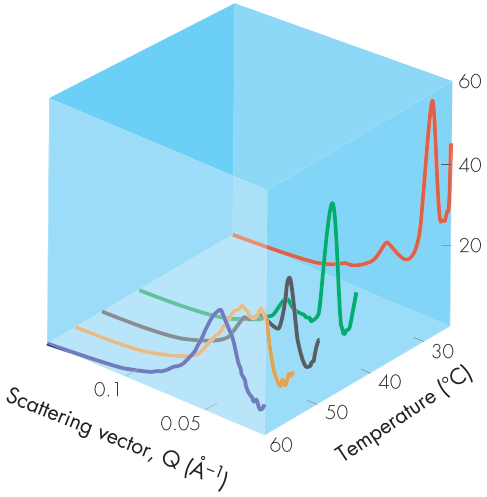

Figure 2.12. Scattering data for 4% HEQ/4% $C_{12}E_{12}$ as a function of temperature.

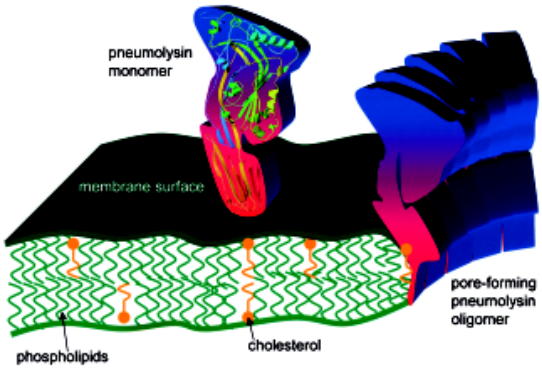

Figure 2.13. Schematic representation of pore formation in membranes by the toxin pneumolysin.

Gilbert *et al* have used SANS measurements at ISIS and the ILL to study the interaction of the toxin pneumolysin, produced from pneumonia bacteria, with synthetic model cell membrane vesicles. Pneumolysin binds to cholesterol in cell membrane surfaces as a prelude to pore formation, which involves the oligomerisation of the protein (see figure 2.13). SANS measurements at different neutron contrasts of the solvent were obtained from liposomes used as model cell membranes with different concentrations of pneumolysin. The overall trend in the structure was a thinning of the liposome surface on toxin attack followed by the formation of localised structures thicker than the liposome bilayer itself. With the liposome index matched to the solvent the pneumolysin oligomers were observed directly. Inactive toxin appeared to bind to the liposome, but did not result in a change to the membrane structure. Subsequent activation of the pneumolysin in-situ brought about changes in the liposome structure similar to that observed from direct toxin attack.

Excitations

The Excitations Group operates the three chopper spectrometers HET, MARI and MAPS, the single crystal coherent excitations spectrometer PRISMA, and the ROTAX diffractometer. The Group is also responsible for the single crystal alignment facility, ALF. The scientific programme of the Group is dominated by research in hard-condensed matter physics ranging from investigations of model magnetic systems to the dynamics of glasses.

HET

The science program on HET this year has been very broad. In addition to the continuation of many strong programmes such as GMR materials, spin ladders and high temperature superconductors, several novel experiments have been performed - for example, the search for quantum entanglement in the correlation dynamics of OH and OD vibration modes in H_2O-D_2O mixtures.

On the powder side, there were many excellent crystal field studies as well as a number of experiments looking at non-fermi liquid (NFL) behaviour. One particular study of $Ce(Rh_{0.8}Pd_{0.2})Sb$ managed to combine the two fields. This sample is at a critical point dividing magnetic and non-magnetic ground states. The temperature dependence of the quasi-elastic contribution to the scattering showed NFL behaviour at low energies. However, crystal field peaks at 18 meV and 34 meV provided convincing evidence of a cross-over from NFL behaviour to a more conventional localised moment at higher energies.

Another very exciting experiment performed recently aimed to determine the spin state of the so-called resonance peak in $YBa_2Cu_3O_{6+\delta}$. This peak is believed to be directly related to the superconductivity. A key issue concerns the spin symmetry of the excited state since a possible interpretation is that the resonance represents a triplet (S=1) excitation of a bound quasi-particle state. The ambitious aim of the experiment was to determine the spin state from the Zeeman splitting of the resonance in an applied magnetic field. The size of the splitting in the maximum field available (7.5T on HET) is only 0.9 meV, beyond the resolution of triple axis spectrometers for these high energy transfers. Initial results taken on a single crystal of $YBa_2Cu_3O_{6+\delta}$ shows that the resonance peak changes shape with the application of a field. However, a more detailed analysis of the peak is currently under way.

MARI

The science program on MARI is as diverse as ever with work spanning low-dimensional magnetism, quantum fluids and solids, phonons in quasi-crystals and the dynamics of amorphous materials.

Historically MARI has played an important role in the understanding of the dynamics of low dimensional magnetic systems. Originally interest was focused on the S=1/2 systems, and attempting to verifying the Haldane conjecture, but during the last year we have seen experiments looking at the quantum effects in the spin 3/2 system $CsVCl_3$ and the S=1 system $CsNiCl_3$ (figure 2.14). The low temperature spectrum of the integer spin system measured is dominated by well-defined single particle excitations. These form a spin triplet with an energy gap consistent with field theoretical descriptions. Measurements on MARI

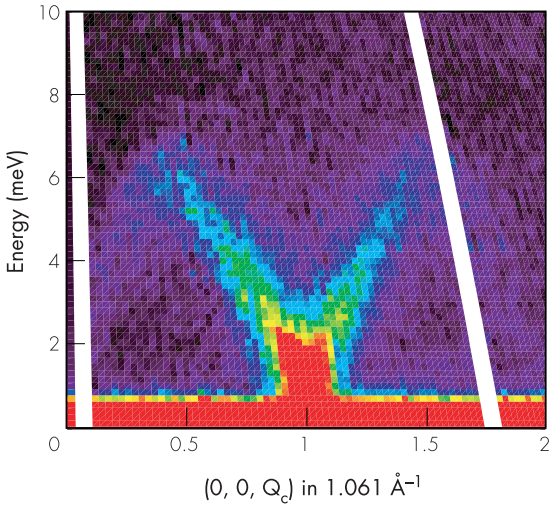

Figure 2.14. Dispersion of magnetic excitations in the spin 1 Haldane chain $CsNiCl_3$ measured using MARI.

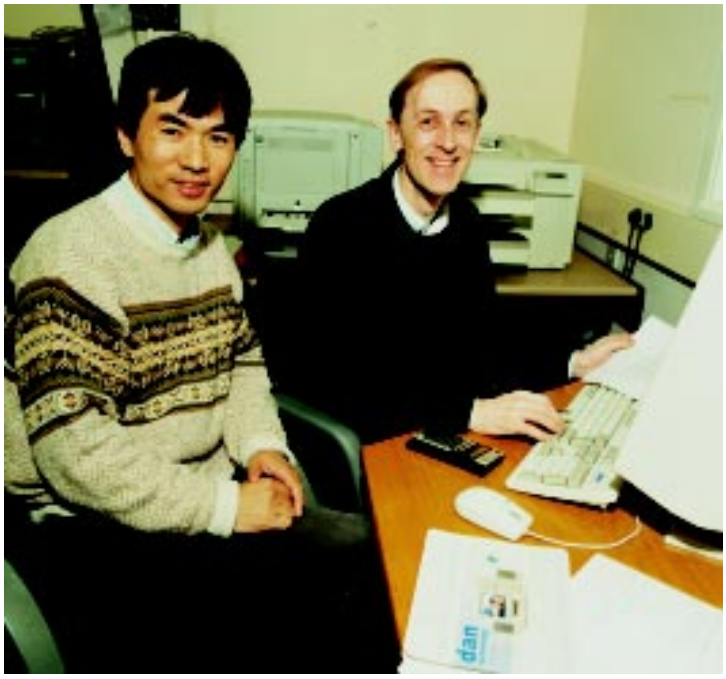

Pencheng Dai (ORNL) and Andrew Boothroyd (Oxford) investigating the field dependence of the resonance peak in YBCO on HET (00RC1266).

were able to see the continuum scattering, and from the temperature dependence it was also possible to test for the predicted scaling behaviour.

The current interest in helium is focused around its confinement in small pores. In vycor (pore sizes of 70 Å) the superfluid transition is considerably suppressed but still has the same critical exponent indicating the universality class is the same. In aerogel, which has much larger pore sizes, the change in the superfluid transition is only small, but the critical exponent, and hence the universality class, looks very different.

Work has continued looking at various aspects of amorphous materials including intermediate range ordering in B_2O_3, rapidly quenched metallic glasses and amorphous DKDP.

PRISMA

Demand for PRISMA beamtime in both inelastic and diffraction modes continues to increase, with the last proposal round showing a significant oversubscription factor. Experiments carried out on PRISMA during the year covered a wide range of science, one of which (by Coldea, Tennant et al) has claimed the ISIS record for low temperatures in a magnetic field: 50 mK in 7 T! Cs_2CuCl_4 is a quasi-1D spin-1/2 Heisenberg antiferromagnet in which frustrated interchain coupling causes cycloidal ordering below T_N = 0.62 K. Quantum fluctuations are thought to renormalise the incommensurate wavevector significantly from its mean field value, and it is conjectured that this can lead to the formation of a gapped spin-liquid state. Applying a magnetic field perpendicular to the cycloidal spin structure should quench the fluctuations and reduce quantum renormalisation effects. The PRISMA diffraction measurements observe directly the change in the quantum renormalization of the incommensurate spiral pitch upon applying a magnetic field that gradually quenches the quantum fluctuations and drives the system from the quantum limit (B = 0) towards the classical limit (B_c = 8.4 T) above which all spins are ferromagnetically aligned. See the Highlight article on page 52 for more details.

An emerging technique on PRISMA is the use of the inelastic detector for the measurement of dynamical correlation lengths in low-dimensional magnetic materials. The standard 2-axis S(Q) measurement technique integrates over all energy transfers and is only valid when the distribution of excitation energies is smaller than the neutron energy. When this is not the case the measured S(Q) can deviate markedly from the actual values. The PRISMA technique utilises the fact that for a particular scattering angle, the measured time-of-flight trajectory is always parallel to k_i. By placing the magnetic chains of a 1-d material perpendicular to k_i, a range of constant q-scans can be collected around the magnetic zone centre, from which an accurate S(Q) can be obtained through correction of the $S(Q,\omega)$ data for kinematical and temperature factors before integration. The technique has been successfully applied to $CsCrCl_3$, $CuGeO_3$ and $RbNiCl_3$.

The scientific commissioning of MAPS is now underway (see page 70). Demand for beamtime is high. Next year's report will be bursting with new and exciting science coming from MAPS.

Molecular Spectroscopy

The Molecular Sciences Group supports the work of Biologists, Chemists and Physicists interested in the dynamics of atoms and molecules. To this end the group operates four spectrometers; eVS, TOSCA, OSIRIS and IRIS, with characteristic time-scales ranging from short (with respect to atomic vibrations) to long (with respect to molecular diffusion).

The rejuvenation programme started about three years ago is almost complete and apart from the new spectrometer, OSIRIS, the group now operates an improved IRIS and the recently completed Phase II of TOSCA. The installation of the VESUVIO hardware will take place towards the end of the year.

IRIS

The science program on IRIS remains topical and diverse, with the quality of experimental data collected being reflected by the spectrometer's high publication record. As ever, the scientific backbone of IRIS remains predominantly that of quasi-elastic neutron scattering from polymeric systems. However, there continues a steady and growing interest towards low energy magnetic excitations and biological systems, in addition to high accuracy studies of the roton dispersion curve in superfluid helium. Indeed, biological studies on IRIS have been greatly assisted by the investment in, and modifications made to, the existing IRIS sample changer and water bath (-50 to +100 ^{o}C) sample environment equipment.

More importantly, however, to improve further the sensitivity of the spectrometer a new IRIS pyrolytic graphite analyser bank has been installed. The new array not only achieves a 3-fold increase in count rate but also a significant improvement in the ratio of signal to background. Future effort on IRIS is focused towards fully exploiting the increase in surface area of the new pyrolytic analyser array by considering improved collimator and detector geometries.

OSIRIS

OSIRIS is a 50% scheduled instrument, presently used for diffraction experiments, and this allows sufficient time to develop the required polarised-neutron techniques for full polarisation analysis to be installed starting in 2001. Determination of long d-spacing magnetic structures makes up the majority of OSIRIS experiments. A wide variety of magnetic materials have been studied, including CMR, high-T_c and rare-earth intermetallics. These measurements benefit from the long wavelengths and high resolution available. Structure determination of crystalline polymers and proteins has also been a major field, pushing long d-spacing diffraction to new limits. The high counting rate at long wavelengths has benefited new measurements on in-situ chemical reactions, e.g. in zeolites and new battery materials. In short, the unique ability to measure long d-spacings with high resolution and high counting rate is building a strong user community spanning a wide range of topical subjects.

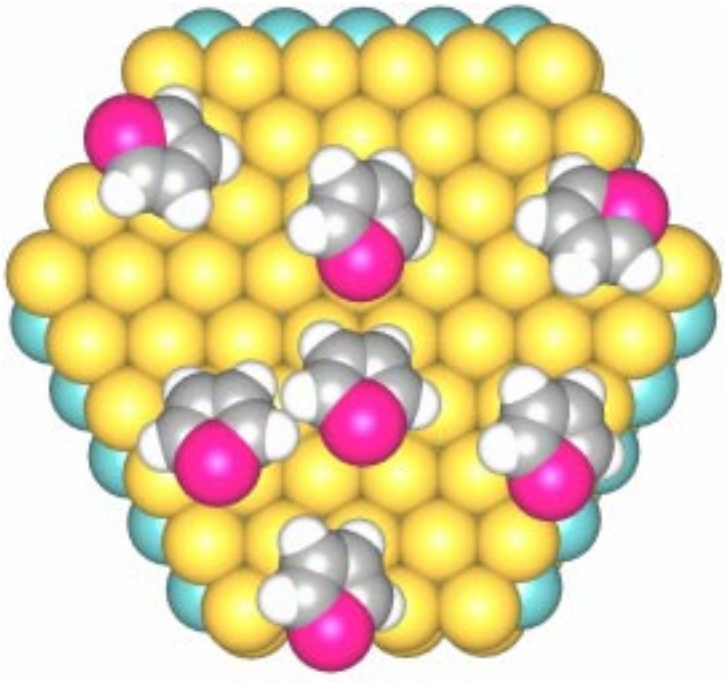

Figure 2.16. Studies of catalysts such as Co-Mo Al_2O_3 used for thiophene hydrodesulphurisation are carried out on all the instruments within the Molecular Spectroscopy Group.

Fabrizio Cavatorta and Nicola Augelini investigating water in amylose using TOSCA (00RC1290).

TOSCA

TOSCA has had a highly successful year. With any new instrument, one of the priorities is to reduce the background and this has been achieved. The background is smooth, stable and almost as low as that of its forefather, TFXA. This is no mean feat in view of the much more open geometry of TOSCA. The science has been as varied as ever, ranging from fundamental investigations of solid and liquid H_2 and H_2S, where the link with work carried out on eVS on the same systems is particularly clear, to studies of small molecules. These include biogenic amines and their salts as well as exotic cage structures like dodecahedrane (see figure 2.17). For such systems, where the intermolecular interactions can be neglected, the use of *ab initio* calculations to analyse the data is rapidly becoming the method of choice. At the end of March, TOSCA was closed to allow the final upgrade to be completed. This is on target and the first users are expected in November. The new TOSCA will offer the spectroscopist's dream: better resolution and more flux simultaneously!

eVS

The scientific program on eVS has included measurements on water below and at the supercritical temperature, where comparison with a harmonic model suggested that half the hydrogen bonds in water are broken at 400 °C. Experimental work on the anomalous cross sections measured on eVS in hydrogen-deuterium mixtures has continued and has recently been given a theoretical explanation in terms of conventional quantum mechanics. A strong area of interest is the kinetic energy in liquid and solid ^{3}He and mixtures of ^{3}He and ^{4}He. eVS is particularly advantageous for these studies as the high incident neutron energies much reduce the strong absorption cross section in ^{3}He. eVS is about to undergo a major upgrade, with the installation of the EU funded VESUVIO modifications, which will considerably improve the instrumental resolution.

Over 30 UK and international participants gathered at the Cosener's House, Abingdon, UK for a workshop organised as part of the VESUVIO project. Current and potential users of eVS had the opportunity to express their needs for the next generation spectrometer. The speakers covered a broad area of science from the pure physics of liquid and solid helium and molecular hydrogen, to the applied physics of glasses and high T_c superconductors, to the chemistry of hydrogen on catalysts and hydrogen bonding in chemical compounds.

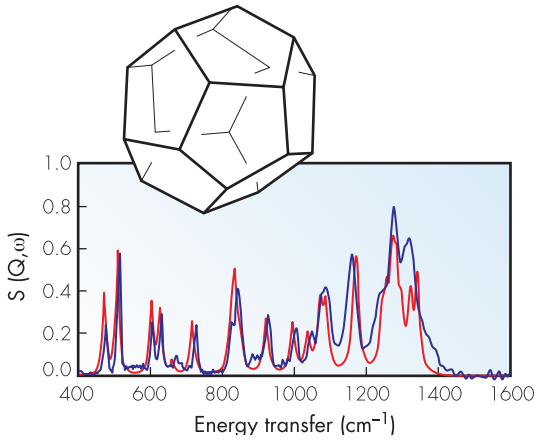

Figure 2.17. Comparison of observed (blue) and calculated (red) by ab-initio methods INS spectra of dodecahedrane.

Muons

The instruments MuSR, EMU and DEVA offer polarized positive muons as magnetic probes of superconducting and magnetic materials, as proton analogues for chemical physics and as spin labels for molecular dynamics. The muons are implanted into the materials to be studied and they relay information on local structure and dynamics via their decay to individually detected positrons. For many experiments MuSR and EMU instrument performance is equivalent, although MuSR, with its greater range of transverse fields and option of a dilution refrigerator, is especially popular for magnetic studies. EMU is optimized for studies in higher longitudinal field and is preferred for measurements involving the decoupling of local spin interactions, e.g. for characterisation of muonium — the light pseudo-isotope of hydrogen — and of muoniated organic radicals. Much use of EMU in so-called fly-past mode has been made this year, improving its performance for small samples. Some experiments are scheduled on the RIKEN-RAL instrument ARGUS, which is capable of high data rates. The DEVA instrument is reserved for unusual or developmental projects — this year for radio-frequency resonance and the testing of new data acquisition electronics.

Experiments on novel and high-temperature superconductors include investigations of mechanism, of the competition or coexistence with magnetism, of flux penetration and characterization of flux line lattices. Investigations of mechanisms cover the high-T_c cuprates, as well as superconducting carbides, silicides and fullerides. The muon response helps assess the nature of both static and dynamic correlations which survive suppression of the antiferromagnetic order by doping and which coexist with superconductivity. In cuprates the results support the picture of electronic phase separation, i.e. the presence of static and dynamic charge-ordered stripes. Indirectly they support models of superconductivity based on this picture. Evidence for phase separation and the coexistence of nanodomains with very different local properties likewise arises from studies of spin and charge ordering in manganites and in the related cobaltites. Muon detection of magnetism in $NH_3K_3C_{60}$ poses the question of its relationship with the unusual superconductivity in $NH_3NaK_2C_{60}$ and gives superconductivity in fullerides a new impulse. MuSR measurements of flux penetration in type-II superconductors are particularly powerful and continue to be popular. This year they include studies of the vortex field distribution in the low critical-current material PbIn and in the heavy-fermion material UPt_3. The results in PbIn achieve a longstanding objective of detecting motional narrowing of the field distribution as the flux line lattice moves in the Lorentz force of an electric current.

Magnetic studies this year concentrated on low-dimensional, layered and geometrically frustrated systems on the one hand and on nano-scale magnetic particles and high-spin molecules on the other. Both categories of experiment use the muon probe to sense magnetic fluctuations

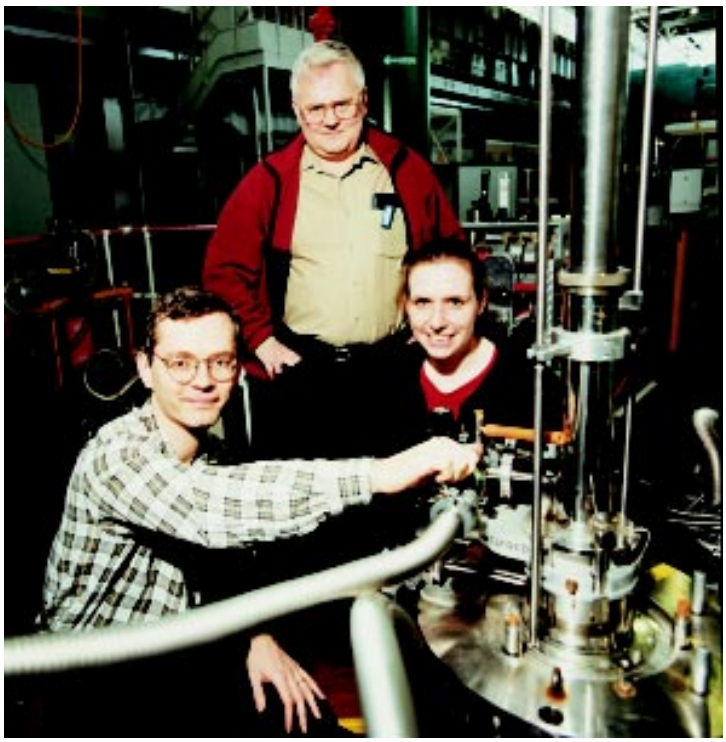

Steve Blundell and Ishbell Marshall (Oxford) preparing the MuSR dilution fridge for studies of the two-dimensional spin gap system CaV_4O_9 under the watchful eye of Chris Scott (ISIS) (00RC1870).

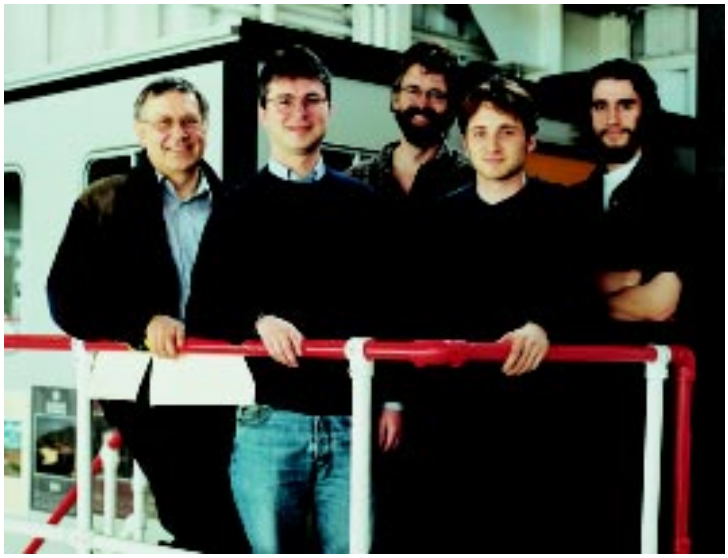

Migg Roduner (Stuttgart), Laurens Siebelles (Delft), Steve Cox (ISIS), Philip Donnelly (UCL) and colleague investigating muonium formation in hexane (00RC1701).

and reveal correlations of the host spins over wide temperature ranges, especially in the vicinity of magnetic phase transitions. The influence of structure is studied in triangular, tetrahedral and ladder-like structures, as well as in molecular magnets exhibiting spin-Peierls transitions. Quantum magnetic tunnelling is seen relaxing magnetization in high-spin molecules. Magnetic grain nucleation is seen in manganites. The influence of size is studied in superparamagnetic clusters, single-domain granules and in colloidal magnetic particles — this latter with a view to application as a contrast agent in medical magnetic resonance imaging.

The study of spin transport (soliton motion) and of charge transport with spin (polarons) in conjugated molecules and polymers exploits the muon as a magnetic probe together with its proton-like chemical properties of adopting specific sites in organic molecules. This year the topic is approached from both ends of the length scale, with systematic studies of the minimum chain-length required to support soliton motion and with explorations on biophysical systems, namely synthetic polypeptide chains mimicking simple proteins and on DNA itself.

The best examples of positive muons behaving like protons are the way they pick up electrons to form muonium, the pseudo-isotope of hydrogen, and the way muonium atoms can then react with organic molecules, labelling the product radical with the muon spin. Molecular reorientation rates and their Arrhenius parameters are determined for organic radicals both in bulk liquids and confined to zeolite cages. The spin-labelling of liquid crystals and the photo-excitation of molecular vibrations are explored. The process of muonium formation, i.e. electron capture by the positive muon, is itself of interest: it is studied in such disparate systems as nano-scale particulate surfaces, bulk semiconductors, hydrocarbons and molecular cryocrystals. Development of a pulsed field method of final state analysis should benefit these studies. On surfaces, e.g. of SiO_2 granules, the behaviour should be relevant to the phenomenon of hydrogen spillover in catalysis; an influence of monolayers of adsorbed inert gas is demonstrated. In the semiconductors and insulators (liquid and solid) the muonium yield reflects excess electron mobility and the mechanism of electron transport. The missing yield in hexane is recovered by decoupling the muonium hyperfine interaction or suppressing depolarization mechanisms in high magnetic field. The yield in Si and the molecular cryocrystals is manipulated with electric fields. In frozen CH_4 and N_2, with and without admixture of Ar, it is strongly influenced by the orientational dynamics of the host molecules: localization of the excess electron wavefunction due to orientational disorder is demonstrated.

In ionic conductors, the implanted muons witness the onset of ionic mobility, e.g. of Li^+ in simple materials such as Li_2SO_4 and in the more complex mixed oxides of Li and Mn which are used as battery cathode materials (see Highlight article on page 60). Transfer from interstitial to substitutional proton sites is probed in water of crystallization and in ice. In insulators and semiconductors, muonium can model all possible charge states of hydrogen defect centres. The influence on these states of oxygen impurity in Czochralski silicon and of the random-network structure of amorphous carbon are investigated. The influence of doping is studied by RF resonance in germanium. Particularly successful this year are measurements on the wide-gap semiconductors CdS, GaN and related compounds - these are described in more detail on page 62.

RIKEN Muon Facility

Labelled-electron method for electron transfer studies in proteins

The RIKEN-KEK-Oxford group has carried out extensive life-science applications of the μSR technique at the RIKEN-RAL Muon Facility. Polarized positive muons (μ^+) can be injected into a biological substance. During the slowing-down process, the injected μ^+ picks up one electron to form a neutral atomic state, muonium. The muonium thermalises and chemically bonds to a molecule of the substance. Then, depending upon the nature of the molecule, the excess electron brought into the molecule by the μ^+ can behave in various ways such as localization or linear motion along the chain. In the latter case, spin relaxation of the injected muon is caused by magnetic interaction between the muon's spin and that of the moving electron; the electron is 'labelled' by the muon. These processes are depicted in figure 2.18. Theoretical modelling of the relaxation process due to 1D (on-chain) diffusing electrons predicts a relaxation parameter proportional to $1/B_{ext}$. Deviations from the $1/B_{ext}$-law in a weak B_{ext} region demonstrate 3D (off-chain) diffusion of the electrons. Rates for the electron diffusion in either case can be estimated by using a hyperfine coupling constant between the moving electron spin and the muon spin.

Microscopic behaviour of electron-transfer in cytochrome-c (with Fe(III)) and myoglobin has been studied in comparison with cytochrome with Fe(III), lysozyme, etc. Measurements between 5K and 300K show that the inter-site diffusion rate for the 1D motion along the polypeptide chain is only weakly dependent on temperature. Evidence for an increase in higher-dimensional motion is seen around 200K in cytochrome-c, apparently reflecting a structural change. The temperature variation for myoglobin differs due to the different protein dynamics of this molecule, representing the difference between 'natural' and 'artificial' electron transfer. The obtained 1D as well 3D diffusion rates are summarized in figure 2.19. For cytochrome-c oxidase (work in collaboration with IT Himeji and U Osaka) it was found that at room temperature, rapid electron transfer along the chain is not dominant, but becomes dominant below 150K.

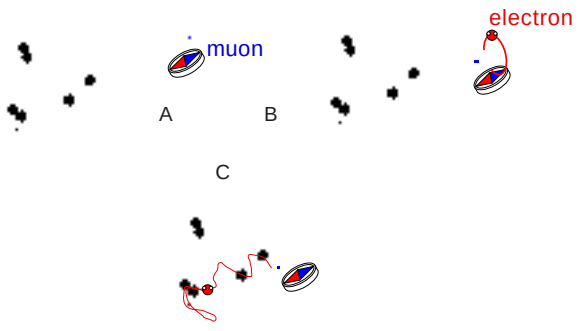

Figure 2.18. A representation of the positive muon implantation process into cytochrome-c.

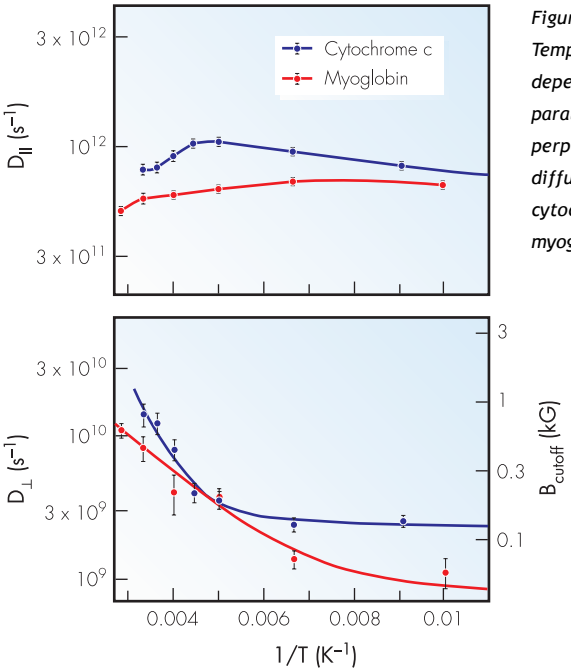

Figure 2.19. Temperature dependence of the parallel (upper) and perpendicular (lower) diffusion rates in cytochrome-c and myoglobin.

The 1/8 problem in high-T_c superconductors

The stripe structure or the 1/8 problem is now attracting much attention in the field of high-T_c superconductivity. The effect has been consistently observed in LaSrCuO and LaBaCuO at the hole concentration of 1/8, with a supression of T_c as well as an occurrence of the magnetic ordering as mostly found by the μSR method. Recent μSR studies by Tohoku University and the RIKEN-KEK group have furthered this work by revealing that the magnetic ordering also exists in Zn-doped Bi2212 as well as Zn-doped YBaCuO.

KARMEN

The neutrino experiment KARMEN is exploiting the unique features of the ISIS beam for a high-sensitivity search for flavour oscillations of neutrinos. KARMEN also investigates neutrino interactions with nuclei which are of particular interest to particle astrophysics, especially with regard to the evolution and the nucleosynthesis processes of core collapse supernovae.

ISIS is providing the world's most intense pulsed source of low energy neutrinos from the consecutive decays of stopped pions and muons produced by interactions of the 800 MeV proton beam in the spallation target. A high resolution 56 tonne liquid scintillator calorimeter, located at a mean distance of 17.7 m from the beam stop, allows identification of neutrino induced reactions with spectroscopic quality. Cosmic ray induced as well as accelerator associated backgrounds are strongly suppressed by a 7000 tonne steel shielding blockhouse and three layers of active veto counter systems, allowing the study of neutrino reactions almost free of background.

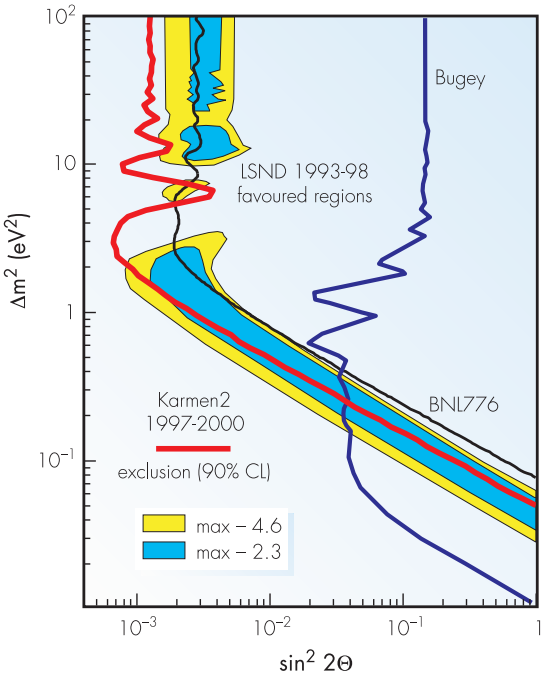

Figure 2.20. Three years of KARMEN measurements at ISIS (1997-2000) yield the world's most stringent limits on flavour oscillations between muon and electron type neutrinos (solid line). The KARMEN exclusion curve (90% confidence interval) excludes almost the entire parameter space for the oscillation parameters $\sin^2 2\Theta$ and Δm^2 favoured by the LSND experiment.

The primary goal of KARMEN is to look for flavour transitions of muon anti-neutrinos (from μ-decay) to electron anti-neutrinos. Oscillations would be signalled by detection of the inverse ß-decay reaction on the free protons of the liquid scintillator, giving rise to a delayed coincidence of a prompt positron followed by a sequential (n,gamma)-capture signal. Taking full advantage of the significant reduction of cosmic ray induced background after the 1996/97 experimental upgrade, KARMEN now has accumulated and analysed data taken from February 1997 to March 2000, corresponding to 7160 Coulombs of protons-on-target.

After applying various well-defined software cuts to the data-set, only 11 oscillation candidate events survive. This number is fully consistent with the background expectation of (12.3±0.6) events, arising largely due to conventional neutrino interactions on carbon-12. Thus, there is no hint for an oscillation signal. This is further strengthened by a more detailed and sensitive maximum likelihood analysis, which takes into account the full experimental information of single events to separate possible oscillation events from background. Again no oscillation signal is observed, leading to a stringent upper limit for the oscillation probability $P < 6.5 \times 10^{-4}$ (90% confidence interval). The corresponding excluded parameter regions of the neutrino-flavour mixing amplitude $\sin^2 2\Theta$ and mass scale Δm^2 are shown in figure 2.20.

Three years of measurements with the upgraded KARMEN experiment have thus yielded the most stringent oscillation limit so far for this oscillation channel. In particular, the KARMEN results now exclude almost the entire parameter space favoured by the positive evidence for oscillations claimed by the LSND experiment in Los Alamos.

Engineering

The Engineering team at ISIS has been increasing its level of activity this year. Whilst maintaining a thriving and expanding user program, a final physics design for the new ENGIN-X diffractometer (see page 75) has been completed, in collaboration with the user community.

At present Engineering is based on the world-leading instrument, ENGIN, utilising approximately half the available time on the PEARL beamline. Bragg diffraction measurements yield information on the distortion of the atomic lattice, typically as a function of position, or applied thermal or mechanical loads. This is used to throw light on deformation mechanisms, processing routes and failure mechanisms in real components or test samples.

Experiments over the last year have demonstrated a varied program of research with strain measurements in materials from steel to minerals such as olivine. A number of real industrial problems have been addressed in collaboration with UK academic groups (see Highlight article on page 64), and through European funded access mechanisms. Industrial partners in work carried out in the last year have included Rolls Royce Engines, British Aerospace Airbus, Nuclear Electric, Mercedes and AEA Technology.

The new stress rig continues to be highly popular, allowing *in-situ* deformation studies. This has recently been improved through the addition of high temperature capabilities.

Despite the heavy over-subscription of ENGIN there has been a healthy growth in the number of academic groups applying for time.

The Engineering team has also expanded this year with the welcome arrival of Carlos Borlado, a postdoc working for the Open University but based at ISIS, and Judith Dann, a new instrument scientist. They will both be heavily involved in the build and commissioning of ENGIN-X, as well as in support of ENGIN.

This year ISIS was host to the final meeting of the Versaille Project on Advanced Materials and Standards (VAMAS) Technical Working Area 20. This group of experts from facilities and academia from Europe, North America, Japan and South Africa have been working, with industrial input, to define an international standard for strain measurement using neutrons, ensuring compatibility and uniformity in achievable results across laboratories. The final draft of the standard is now in preparation, and will go forward for consideration by ASTM in 2001.

Condensed Matter Theory

The Born-Oppenheimer (BO) or adiabatic separation of the electronic and nuclear motions forms the basis of almost any quantum mechanical study of molecules and solids. The method is based on the large difference of the electronic and nuclear masses, which implies that the light electrons adapt almost instantaneously to the nuclear configuration. Each electronic level, in fact, acts as a nuclear potential surface and corresponds to a set of nuclear vibrational and rotational excitations calculated on that surface, but does not couple itself to any nuclear state of this set. For many physical systems and phenomena this separation is extremely successful, at least whenever degeneracy or near degeneracy of the electronic levels is not involved. There are, however, phenomena which crucially depend on the coupling between the electronic and the nuclear wavefunctions and where the adiabatic or BO approximation breaks down.

An elegant and accurate description of such phenomena, preserving the notion of the nuclear

potential surface, has been given. The idea is that the surface is not exactly independent of the nuclear state being studied, but it depends on it self-consistently. The possibility of probing non-BO effects with muon spectroscopic methods is explored by studying molecules, with a positive muon in the role of a light nucleus. One naturally expects that, reducing the nuclear mass enhances the departure from the BO behaviour.

Density functional theory (DFT) has proven a valuable tool for practical electronic calculations in physics and chemistry. The success of ground state DFT, however, is not shared by the excited state version of it, because of the lack of an accurate and simple exchange and correlation energy functional, appropriate for the excited state theory.

For the first time in the literature, it has been shown that the traditional definition (in excited state DFT) of the direct Coulomb interaction term introduces unphysical interactions between electronic orbitals, which are not simultaneously occupied together either in the ground or in the excited states. This ghost interaction has been successfully accounted for by introducing a correction term in the exchange and correlation energy functional. Calculations incorporating this correction prove an order of magnitude more accurate than previously.

Several recent experiments on liquid and solid samples containing protons and deuterons have shown an interesting anomaly, which is apparently absent when the hydrogen isotopes are replaced by heavier particles. The anomaly is a shortfall in the intensity of fast neutrons scattered by the samples. Short-lived correlations in the spatial and spin degrees of freedom of the hydrogen isotopes are proposed as an explanation of the anomaly. The cross-section for scattering by two identical nuclei occupying nonequivalent states embodies entangled degrees of freedom and it is the basis of a compelling explanation of all the observations. In the model calculation, no remnant of the initial entangled state exists in the final state, in which one of the particles carries away a large fraction of the energy from an impinging fast neutron. The reaction event is incoherent and inelastic and akin to Compton scattering, also known as deep inelastic scattering.

In 3d transition-metal compounds orbital moments contribute to many properties, including anisotropy, magnetoelastic relaxation and canted antiferromagnetism. Over the past few years investigations of 3d oxides, especially perovskite-type manganites, have shown that the configuration of orbital moments plays a vital role in their properties, e.g. colossal magneto-resistance. Fortunately, orbital moments are significant in the diffraction of X-rays, because of the **A.p** interaction between photons and electrons.

A unified explanation has been given to resonant X-ray Bragg diffraction from α-Fe_2O_3 and V_2O_3, observed at charge-forbidden reflections. It is argued that resonance at the K edge and an electric quadrupole event engages the orbital magnetism in the 3d valence shell, to a very good approximation. Analysis of the experiments reveals the ordering, symmetry and magnitude of orbital moments carried by the valence shell. In the case of haematite the experiments probe the electron correlations responsible for the Dzyaloshinsky-Moriya interaction.

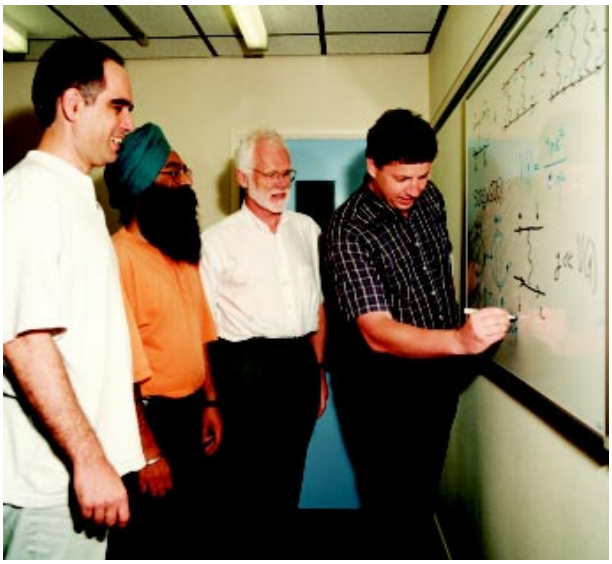

Mike Zhitomirsky (ETH, Zurich) talking theory with Stephen Lovesey, Devinda Sivia and Nikitas Gidopoulos (ISIS) (00RC3946).

Data Analysis

The Data Analysis and Visualisation Group has continued to provide broad support for getting the most out of neutron and muon data at ISIS, and experimental measurements in general. This endeavour entails aspects of software development to test and implement new theoretical ideas principally within a Bayesian probability theory context. The Group is also involved with the upgrade of existing computer programs and the delivery of a consultative and tutorial service on data analysis.

Software developments within the Group have continued to focus on the areas of structure solution and structure refinement. August 99 saw the first public unveiling at the IUCr meeting in Glasgow of the Group's 'DASH' structure solution from powder diffraction data package. A rigorous program of testing, development and documentation performed in collaboration with the Cambridge Crystallographic Data Centre has since resulted in a package that is currently undergoing alpha testing at industrial and academic sites prior to commercial release. The research aspect of the structure solution process has recently been further strengthened by the formulation of a probabilistic approach to the space group determination stage. Effort has also begun into harnessing the high cold neutron flux for structure solution of pharmaceutical compounds from neutron powder diffraction data where the presence of both positive and negative scattering is being utilised for the first time (see figure 2.21).

The ISIX profile refinement package has developed to the stage where TOF powder diffraction patterns can be simulated quickly and efficiently. The conversion of legacy Fortran code to object orientated C++ has proved to be a considerable challenge, but the benefits of this approach to programming the ISIX library are becoming clearer, particularly in the underlying symmetry code, which makes extensive use of templates. Likewise, the gains to be found in employing industry standard libraries as the foundation of the ISIX system have been realised in their utilisation as a key component of other group projects. In the interim, existing CCSL based refinement code has continued to be developed, bringing advantages such as improved performance, better peak shape fitting and interactivity.

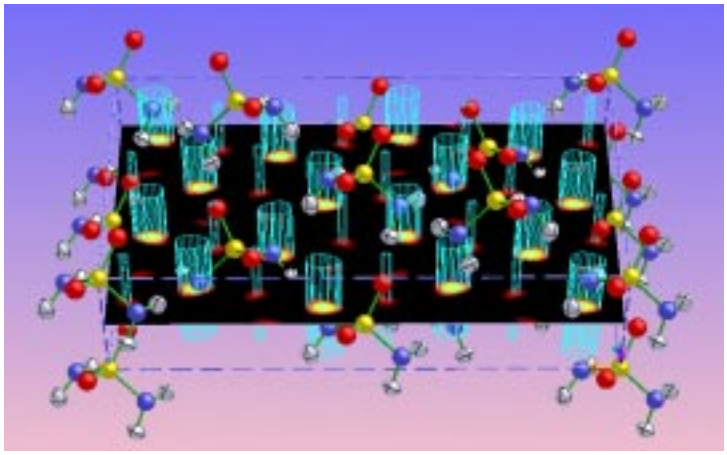

Figure 2.21. With only three phased strong reflections and five unphased weak reflections, all the non-hydrogen atoms of the crystal structure of sulphamide are visible in projection in a MaxEnt map. The light blue 'stovepipes' represent high areas of scattering density; blue, red and yellow respectively represent nitrogen, oxygen and sulphur.

The Group has had strong interaction with other members of ISIS, providing help with the analysis of reflectivity data, quasielastic analysis, residual stress and theoretical studies of muon spin relaxation. An efficient Winteracter driver for PGPLOT has been written, which opens up a fairly effortless route for porting the great wealth of existing analysis and visualisation programs developed on VMS/UNIX workstations onto a PC platform. An investigation of the use of Markov Chain Monte Carlo methods, and the Massive Inference technique, for parameter and density estimation respectively, has begun, and will be incorporated into our analysis suite as appropriate.

In the field of visualisation, a collaboration with ITD has resulted in a prototype virtual reality system for visualising crystal structures and associated nuclear / electron density maps. Further GRID related collaborations are planned. On a lighter note, images produced within the group formed the bulk of the widely distributed ISIS 2000 calendar, and the images have since been used in many publications, one even making the front cover of Neutron News.

ISIS Scheduling Panel Meetings

The quality and timeliness of the science to be performed at ISIS is assessed by the 70 international scientists who form the 7 ISIS Scheduling Panels. These panels meet twice per year to review all the proposals that have been submitted and to allocate beamtime. Full details of the panels can be found on page 86. Shown here are photos from the December 1999 panel lunch.

Above: John Tomkinson (ISIS) and Jane Nicholson (EPSRC) talk about things neutron and muon (99RC5467). Centre: David Smith (Bristol) and Philip Holdaway (DERA) discuss engineering research at ISIS (99RC5650). Below: Uschi Steigenberger (ISIS) with Kazu Kakurai (99RC5666).

Above: Prof. Tony Cosgrove (Bristol) talking with Franz Leermakers (Wageningen) (99RC5651). Below Bob Jones (Exeter) and Roger Lichti (Texas Tech) discussing muons in semiconductors (99RC5664).

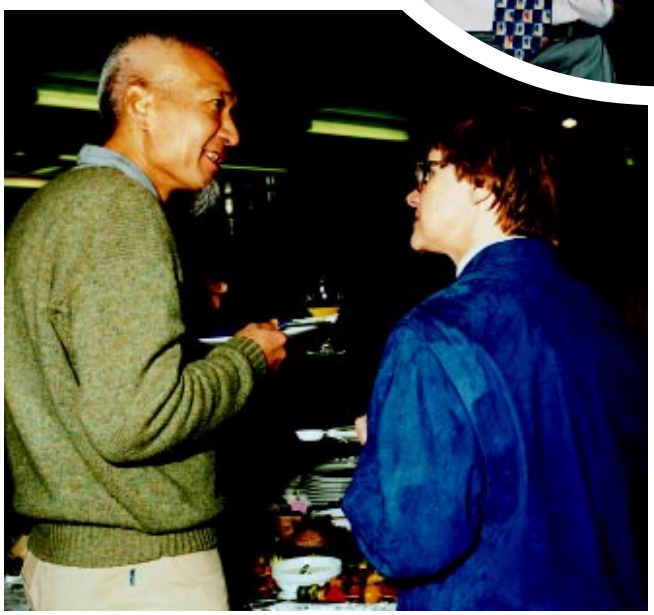

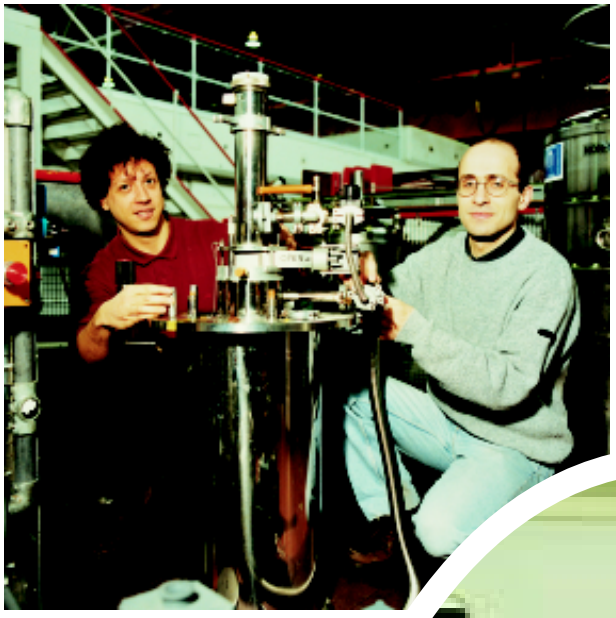

Above left: Filippo Cintolesi (Pavia, Italy) and Alessandro Lascialfari (Oxford) preparing the dilution fridge for an experiment on MuSR (00RC1257). Main Picture: Tessa Brennan and Rob Dalgliesh (Bristol) investigating glass corrosion on SURF (00RC1435). Below left: Yuri Taran (JINR, Dubna) using the new in-situ stress rig on ENGIN (00RC1259).

Above right: Mark Ellerby and Jonathan Allen (UCL) investigating Er at high pressure on PRISMA (00RC1890). Below right: Astrid Schneidewind (TU Dresden) measuring RCu_2 intermetallic compounds on ROTAX (00RC1888).

Following hydrothermal crystallisations using in-situ neutron diffraction

Hydrothermal chemistry is currently one of the principal methods of synthesis for the preparation of new inorganic materials. These materials are used in a number of diverse areas including catalysis, electrochemistry, separation science and as ceramics. There is a pressing need to understand the formation mechanisms of inorganic materials under hydrothermal conditions, aiding preparation of new materials in a rational manner and optimisation of synthesis conditions for efficient production. Studies of the hydrothermal formation of tetragonal barium titanate have been recently used to commission a specially designed hydrothermal cell on the POLARIS diffractometer.

The hydrothermal method involves the heating of solid and liquid reagents with a suitable solvent (usually water) in a sealed vessel at temperatures of up to 250 °C. Although elevated temperatures are used and pressure is generated in the sealed container, the conditions are much less severe than the traditional ceramic methods of solid-state chemistry. These mild, solvent-mediated, reaction conditions have allowed access to many novel materials with important applications. Good examples include zeolites and other microporous materials used in gas separation and shape-selective catalysis, and layered cathode materials for use in efficient rechargeable batteries.

Hydrothermal chemistry is performed in a sealed reaction container with thick-walls to contain the pressures generated; following the course of reactions as they take place is thus difficult. Our recently constructed hydrothermal reaction cell (figure H1.1) allows neutron diffraction from reacting mixtures of solids and liquids. This apparatus exploits certain advantages offered by neutron diffraction for following chemical processes in-situ, but which to date have been little explored. In particular, reaction cells can be constructed from materials with very low neutron scattering and absorption cross-sections, producing very little background scatter in a diffraction experiment. The vessel is of similar volume to the hydrothermal reaction vessels widely used in chemical laboratories (25 ml), so we can mimic real reaction conditions, while obtaining diffraction data only from material within the cell. The hydrothermal cell differs in construction from laboratory vessels only in the attachment of safety pressure devices, and can safely operate at pressures of 20 atms and at temperatures of up to 250 °C, typical conditions for hydrothermal synthesis.

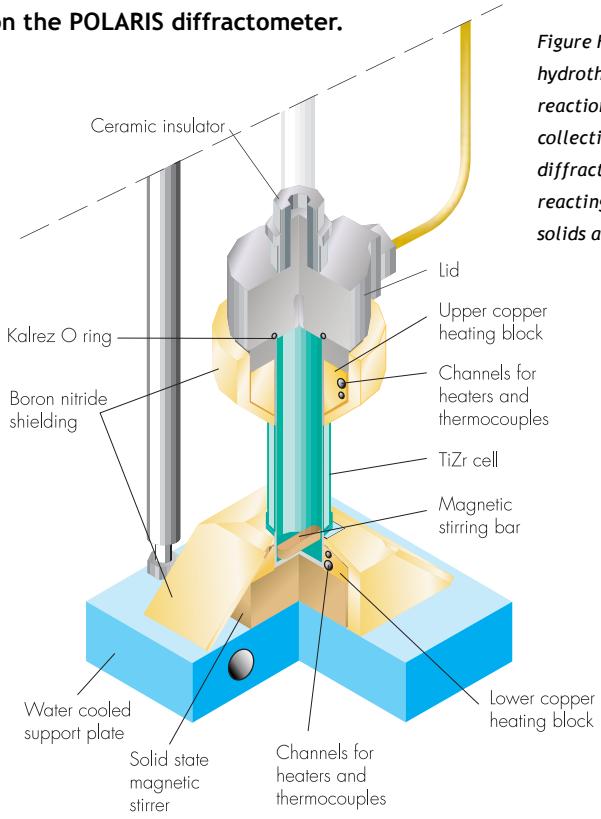

Figure H1.1. A hydrothermal reaction cell, for the collection of neutron diffraction data from reacting mixtures of solids and liquids.

We have recently commissioned the Oxford/ISIS hydrothermal reaction cell studying the hydrothermal formation of tetragonal barium titanate, an important ferroelectric material used as an electroceramic in capacitors, thermistors and electro-optic devices. Although barium titanate can be prepared using high temperature ceramic methods (~ 1000 °C), a hydrothermal route at temperatures as low as 80 °C allows the

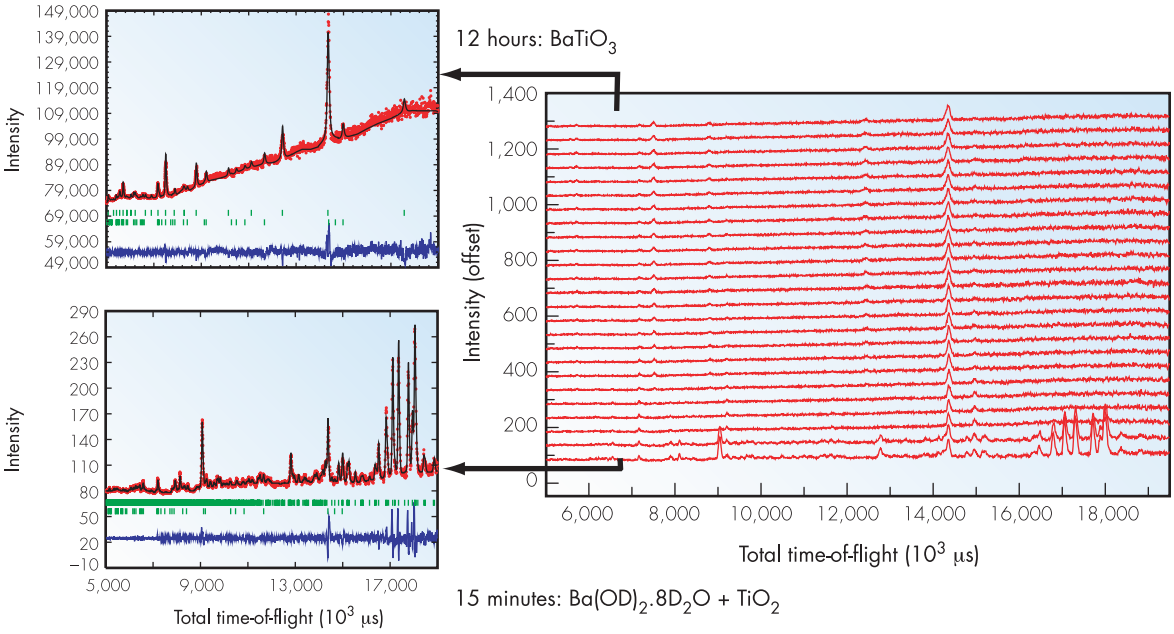

Figure H1.2. Diffraction patterns recorded every 15 minutes as a mixture of $Ba(OD)_2.8D_2O$ and TiO_2 in 10 mL D_2O was heated at 125 °C

production of small particles of the material. This is highly desirable for the production of fine-grained ceramics and, potentially, for device miniaturisation. Figure H1.2 shows diffraction patterns recorded on the POLARIS diffractometer at ISIS every 15 minutes as a mixture of $Ba(OD)_2.8D_2O$ and TiO_2 in 10 mL D_2O was heated at 125 °C. The diffraction data are of sufficient quality to allow the identification of crystalline material present at each stage of the reaction. The resolution of the data is also of sufficient quality to allow the area under closely separated Bragg reflections to be determined as a function of time. This allows the course of the reaction to be followed and quantitative kinetic information to be deduced. Figure H1.3 shows the decay of TiO_2 and the appearance of $BaTiO_3$. The decay of $Ba(OD)_2.8D_2O$ is not shown as it was found to be very rapid with complete dissolution of the barium source occurring within 30 minutes. It is particularly noteworthy that a large amount of TiO_2 is observed to dissolve before the onset of crystallisation of $BaTiO_3$. This strongly suggests that the reaction takes place by a dissolution-precipitation mechanism involving dissolution of the starting materials and crystallisation of the product from solution. Such mechanistic insight has only been made possible by continuous in-situ monitoring of the reaction.

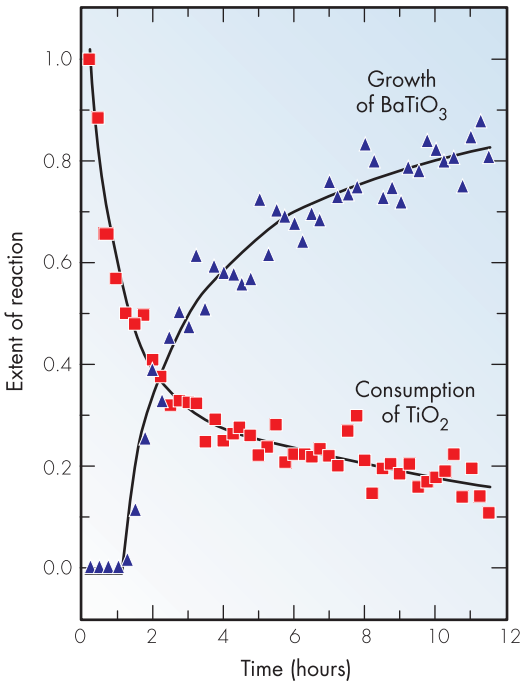

Figure H1.3. Quantitative kinetic data showing the decay of TiO_2 and the appearance of $BaTiO_3$.

Our studies demonstrate the great potential use of neutron diffraction in studying chemical processes under real reaction conditions. The cell we have constructed can be used to study the preparation of a wide range of materials, from microporous zeolites to dense oxides with electronic properties. With ongoing developments in neutron instrumentation, such as the GEM diffractometer, it should be possible to extend the method to collect data of higher quality in even shorter periods of time.

RI Walton, D O'Hare (University of Oxford), **RI Smith** (ISIS)

High-pressure studies of cristobalite

The crystal structure of the high-pressure phase of cristobalite, a form of silica, has been solved through a use of both neutron diffraction on HiPr and atomistic modelling. This study demonstrates the combination of diffraction and modelling methods to determine relatively complex crystal structures.

Silica, SiO_2, is one of the most important materials known to man. It has many technological applications, such as quartz oscillators, silica glass ceramics and as sand in construction. Silica is also important in geology as one of the most significant rock-forming minerals. Silica exists in many different crystalline phases, as well as in its glass phase, and there is considerable interest in understanding the structures of the different phases and the processes that lead to the stabilisation of different phases under different conditions of temperature and pressure.

One of the important phases of silica is cristobalite. At high temperature and ambient pressure the structure of this phase is cubic and can be described as being similar to that of silicon, with oxygen atoms lying half-way between neighbouring pairs of silicon atoms. This description gives the average structure, but only tells part of the story because the linear Si-O-Si bonds would prefer to have an angle closer to 145°. How this is accomplished through dynamic reorientations of the SiO_4 tetrahedra was discussed in a feature article of ISIS'98 (pp 44-45). On cooling the bond-angle problem is resolved by a displacive phase transition to a tetragonal structure, which can be accomplished by the SiO_4 tetrahedra adopting specific orientations without distorting.

Recently it was reported that the tetragonal phase undergoes an additional phase transition to a monoclinic phase on increasing pressure, but its structure could not be solved. The intuitive approach, based on our understanding of the usual processes of displacive phase transitions, would be to suppose that the phase transition involves a distortion that breaks the symmetry of the tetragonal structure. However, using a theoretical approach developed in our group, the 'Rigid Unit Model', it appears that such a mechanism would not be likely. Instead, we proposed that the phase transition could arise from another distortion of the cubic phase. This proposition is represented schematically in figure H2.1. In this scheme, both the tetragonal and monoclinic phases are obtained as separate distortions of the parent cubic phase. The phase fields contain tetrahedral representations of the respective structures viewed down a common direction that corresponds to [111] in the cubic phase. The cubic structure has linear Si-O-Si bonds, which are bent in different ways in the tetragonal and monoclinic structures through rotations of the SiO_4 tetrahedra and buckling of the framework. Taking this idea as our starting point, we began a fresh assault on the structure of the high-pressure monoclinic phase using neutron high-pressure diffraction.

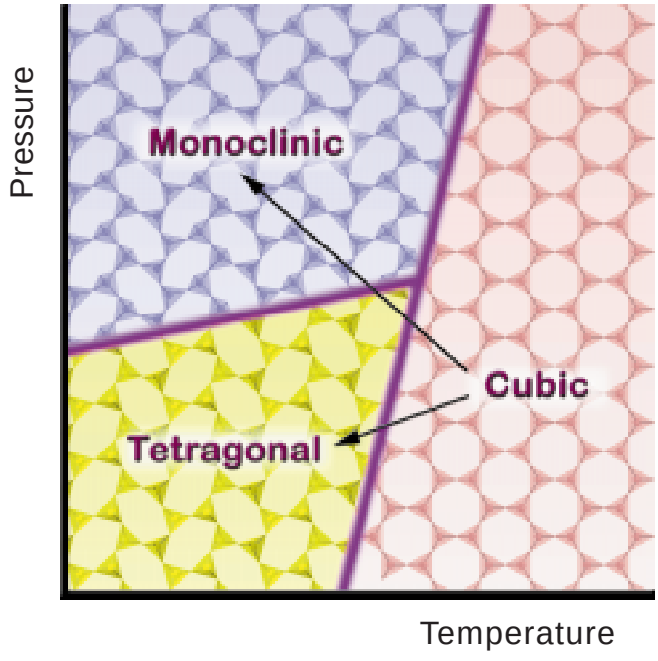

Figure H2.1. Proposed symmetry transformations of cristobalite mapped onto a schematic pressure-temperature phase diagram.

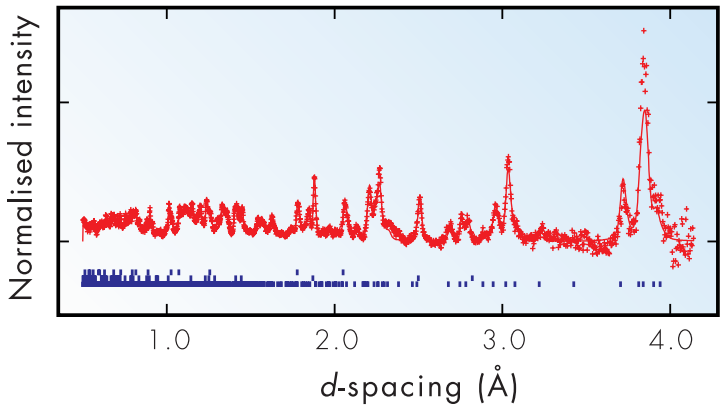

Figure H2.2. Diffraction pattern of the high-pressure monoclinic phase of cristobalite (3.5 GPa) obtained on the HiPr/PEARL beam line at ISIS.

The experiment was performed using the Paris-Edinburgh high-pressure cell on the HiPr/Pearl beam line at ISIS. The diffraction pattern at a pressure of 3.5 GPa is shown in figure H2.2. It could be indexed from the earlier results, but it is not at all straightforward to deduce the structure from a complex, albeit indexed, powder diffraction pattern. Our approach was to use a variety of modelling methods to propose a trial structure for the data analysis. We started from the atomic coordinates of the cubic phase with the lattice parameters of the monoclinic phase, and allowed the atoms to relax to a new equilibrium structure using both lattice energy minimisation and molecular dynamics methods with two different empirical potential energy functions. The different approaches gave the same structure which was subsequently checked using quantum mechanics calculations. This trial structure was used as the starting model in the Rietveld refinement; the refinement locked into it straight away and gave a good refined structure. We were able to conclude that we had obtained the correct crystal structure of the high-pressure monoclinic phase using the combination of modelling and high-pressure neutron diffraction methods.

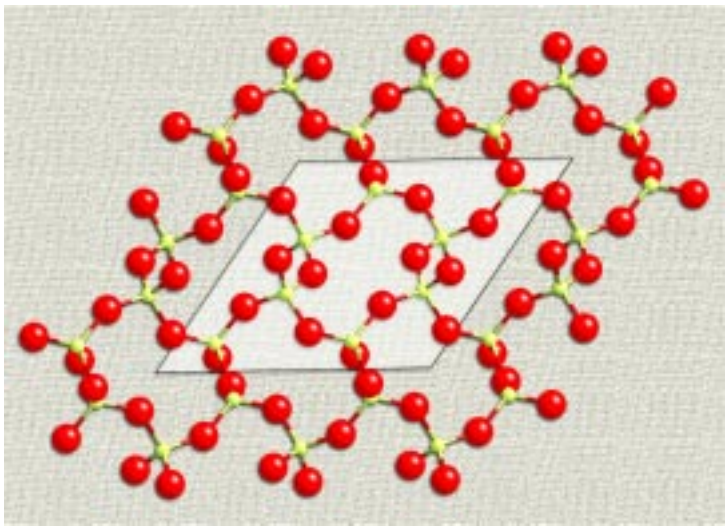

Figure H2.3. Projection of the crystal structure of the high-pressure monoclinic phase of cristobalite (3.5 GPa) viewed down [010].

The crystal structure of the high-pressure monoclinic phase is shown in figure H2.3. In figure H2.1 we show this structure with the SiO_4 tetrahedra highlighted, and compared with the corresponding projections of the cubic and tetragonal phases. The rotations of the SiO_4 tetrahedra, leading to a buckling of the network of connected tetrahedra, are clearly seen. The new structure is a distortion of the cubic structure, and is not directly related to the structure of the tetragonal phase although there are superficial similarities. In fact, the transition mechanism consistent with the new structure is fully compatible with the predictions of the Rigid Unit Mode analysis.

This study has demonstrated two main points. First, it has highlighted the value of combining neutron diffraction with modelling methods to determine relatively complex crystal structures. Secondly, it has shown that high-pressure phase transitions may have more complex group-subgroup symmetry transformations than we usually find in phase transitions caused by changes in temperature. It appears that pressure-induced changes in the free-energy surfaces can give rise to cases, such as in cristobalite, where phases at different pressures have common high-temperature parent phases instead of there being a progressive continuous change in symmetry through the sequence of phase transitions.

M Dove, M Tucker, S Redfern, M Craig, K Trachenko (University of Cambridge),
W Marshall, D Keen (ISIS)

Neutron diffraction probes the interior of Titan

The outer planets and some of their large satellites contain significant proportions of ices and ice mixtures. High-pressure studies, such as those presented here from HiPr, are needed to provide basic information on these systems to underpin models of planetary evolution.

The Paris-Edinburgh cell on the HiPr station of PEARL has a P-T range particularly well suited to studies of Saturn's largest moon, Titan. This satellite is of considerable current interest because of the Cassini-Huygens mission due to arrive there in 2004.

Figure H3.1 shows predictions from current models for the internal structure of Titan at the end of accretion of the satellite from the nebula around Saturn. The core is believed to have formed from a mixture of mainly ammonia monohydrate, methane clathrate and rock. Estimates of the initial accretion temperature vary from 100K to 130K. Various sources of heating will have raised the temperature from this initial value, particularly at the outer surface, until the ices in further deposits would melt at some 180K. From there on the rock would accrete around the core mixture, with the co-deposited ice fraction melting on impact and migrating to the surface, initially as liquid phases. In due course much of the liquid would refreeze as the depth of outer ices increased. At the end of accretion there would thus be a mixed core, surrounded by a rocky 'carapace', outside which would be a layer of ices, with probably a liquid 'ocean' under an ice sheet forming the outermost layer. Further warming in the core would then eventually bring about some core melting, resulting in rupture of the carapace and then 'core overturn', in which the rocks of the carapace would fall towards the centre of the satellite to form its final core.

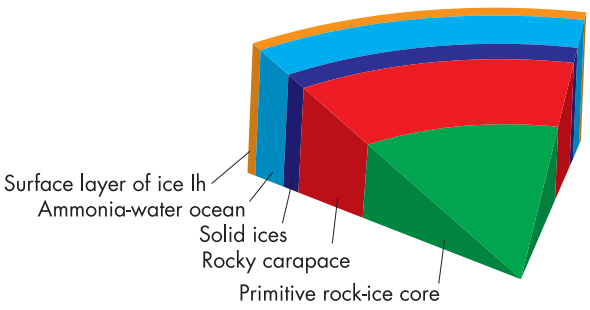

Figure H3.1. Internal structure of Titan after accretion according to current models.

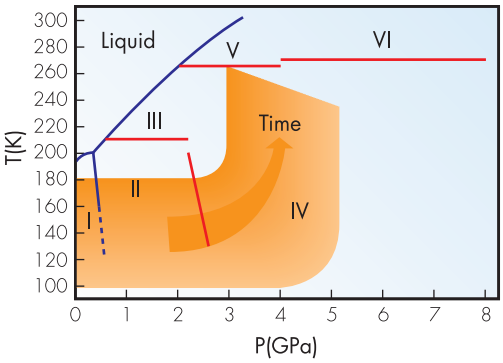

Figure H3.2. Phase diagram of ammonia monohydrate showing approximate transition lines. The dotted extension of the boundary between phases I and II indicates that this transition is not observed below 150K. Phases I and II were known previously; III, IV, V and VI have been found in these studies. The shaded area shows the estimated range of pressures and temperatures followed by Titan's core with time, from accretion to core overturn.

Hitherto, very little has been known about the detailed P-T behaviour of the two key components, ammonia monohydrate (AMH) and methane clathrate. Our studies have focused first on AMH, in which only one high-pressure phase had previously been identified. Studies on HiPR have revealed the existence of four new phases in the P-T range relevant to Titan, as shown in figure H3.2. This figure also shows the estimated range of pressure and temperature through accretion to core overturn. The phase transitions

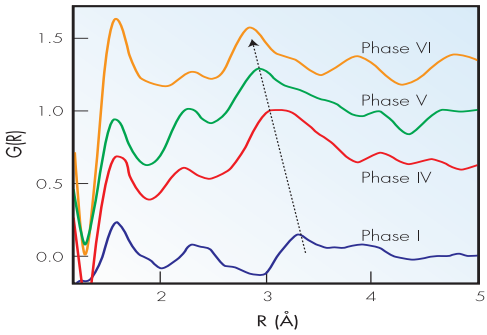

Figure H3.3. 1-D Fourier transforms of the diffraction patterns of phases I, IV, V and VI. The peak highlighted with an arrow corresponds to D..D distances between nearest neighbour molecules and its movement to lower R from phase I to phase VI indicates increasing co-ordination from pseudo-fourfold co-ordinated AMH-I to eightfold co-ordinated AMH-VI.

are very relevant, as current models assume no phase transitions and negligible density changes. We have measured the equation of state up to ~6 GPa at 130K. The structure of phase I is known; the transition to phase II is suppressed at 130K; and phase IV gives a very complex diffraction pattern and its structure has yet to be solved. However, we can determine the phase-IV unit cell volume and hence obtain its density for a given number of formula units per cell. Comparison with the known structures of phases I and VI (see below) indicates a ~10% density increase from phase I to phase IV. This is supported by the radial distribution functions shown in figure H3.3; the main nearest-neighbour peak of phase IV is closer to that of phases V and VI than of phase I. Such a significant densification of the core during formation could shrink and 'seal' the carapace, requiring much more melting (i.e. higher temperatures) to effect core overturn.

A key discovery of this work has been the structure of phase VI. The diffraction pattern of the deuterated profile (upper part of figure H3.4) is remarkably simple, and at first appeared to have only one peak! The body-centred cubic structure shown in the inset gives an excellent fit, but the complete substitutional disorder of ammonia and water and the form of the H-bonding is surprising. Data were therefore collected from hydrogenous AMH-VI. The good fit to the very different relative intensities (lower part of figure H3.4) — despite the very high incoherent background — not only provided a strong test of the structure solution, but also confirmed that naturally occurring (i.e. hydrogenous) AMH forms the same unexpected structure. The bcc arrangement of molecular centres in this structure is likely to be stable over a wide range of pressures and the substitutional disorder raises the possibility that this phase may accommodate non-stoichiometric ammonia/water compositions. Both of these considerations are also interesting and important for modelling of ammonia/water phases at higher pressures in planets such as Uranus and Neptune.

Work has also now commenced on the other major ice phase in Titan, methane clathrate, in a collaboration with Dr D.D.Klug and Dr J.S. Tse of the National Research Council of Canada, in Ottawa. First results promise some further very significant insights into Titan's evolution.

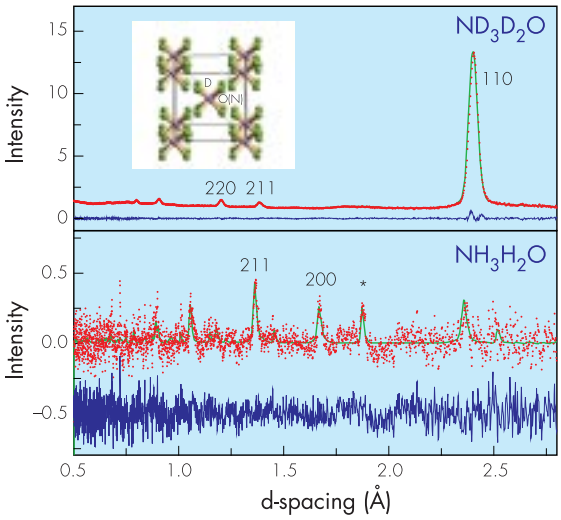

Figure H3.4. Diffraction patterns collected from deuterated and hydrogenous AMH-VI at ~6 GPa. The data are shown in red, the green line shows the result of a Rietveld least-squares profile refinement and the difference between observed and calculated patterns is shown in blue. The asterisked peak in the lower plot is the strongest reflection from the tungsten carbide anvils. The inset shows the structure of phase VI.

JS Loveday, M Guthrie, RJ Nelmes (The University of Edinburgh)

Hydrogen bonding in nitroanilines

Much effort has been devoted in the last decade to the understanding of the aggregation of organic molecules. The considerable interest in the field has been based on the fact that the ability to predict and/or direct the three-dimensional molecular arrangement can be used to tailor materials of biological or technological importance. In this context, intermolecular hydrogen bonds (HB) have been proven to be an effective tool for organising organic molecules. This is well typified by nitroaniline compounds, important due to their recognized second harmonic generation capability and large microscopic hyperpolarizabilities. These molecules are found to associate via intermolecular HB between the amino and nitro groups. SXD has been used to investigate role of the hydrogen bonds in nitroaniline molecular organization.

A common structural feature in nitroanilines is the presence of polar chains of molecules, even in the few cases where the crystal structures are centrosymmetric. This has been interpreted as an indication that the N-H…O(nitro) synthons (intermolecular association motifs) are so strong that they overcome other interactions, inducing molecules to assemble in polar chains as the first aggregation step in solution. This in turn would induce the formation of acentric structures during the crystal nucleation. X-ray data from a series of nitroanilines also indicated that the hydrogen bonding forming these chains will have an asymmetric bifurcated motif. Nonetheless, several semi-empirical and *ab-initio* calculations on aniline derivative aggregates, performed with the aim of rationalising this assumption and to examine the validity of the oriented-gas model, have failed. This failure has been partially ascribed to the omission of the non-planarity of the amino group.

In this context single crystal neutron diffraction experiments on 2-methyl-5-nitroaniline (2M5NA) and *m*-nitroaniline (mNA) were carried out on SXD. The aim of these studies has been to tackle some outstanding structural issues in this system, to establish the degree of planarity of the amino group, and to add to the understanding of the role of the hydrogen bonds in the molecular organization of nitroanilines.

The planarity of the amino group was mainly analyzed through the examination of an internal coordinate χ_N, a function of the torsion angles involving the hydrogen atoms, which is a measure of the degree of the nitrogen atom pyramidalisation (P_N). The extreme values for χ_N, 0° and 60°, correspond to a planar sp^2 and a regular tetrahedral sp^3 hybridised nitrogen respectively. The values obtained for 2M5NA (χ_N= 25.8(4)°) and mNA (χ_N= 41.3(5)°) indicate in both cases a significant P_N, especially for the latter. Intermolecular distances for 2M5NA show that the H12 aminic hydrogen is connected with the two oxygens of a nitro group through an asymmetric bifurcated HB (figure H4.1). This N-H…O(nitro) interaction links molecules related by a glide

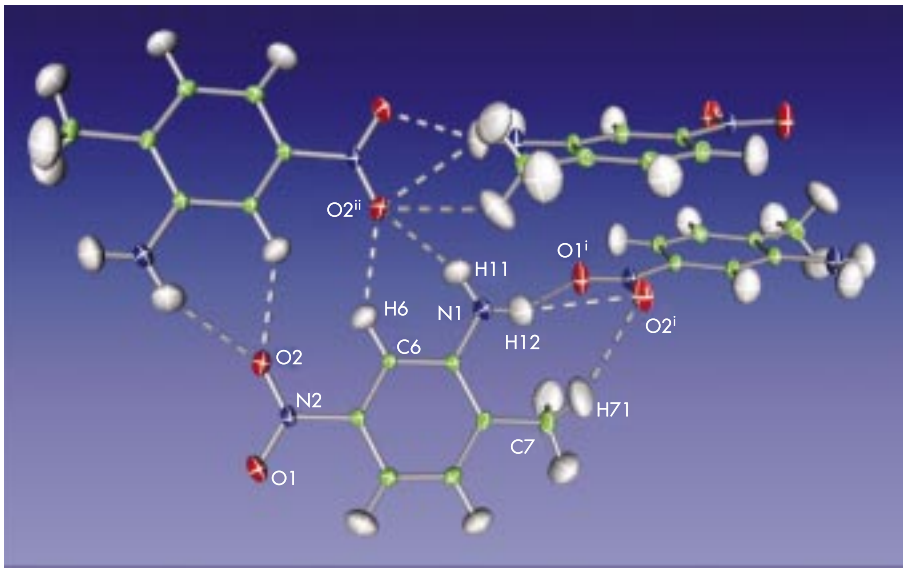

Figure H4.1. The main hydrogen bonds in 2-methyl-5-nitroaniline.

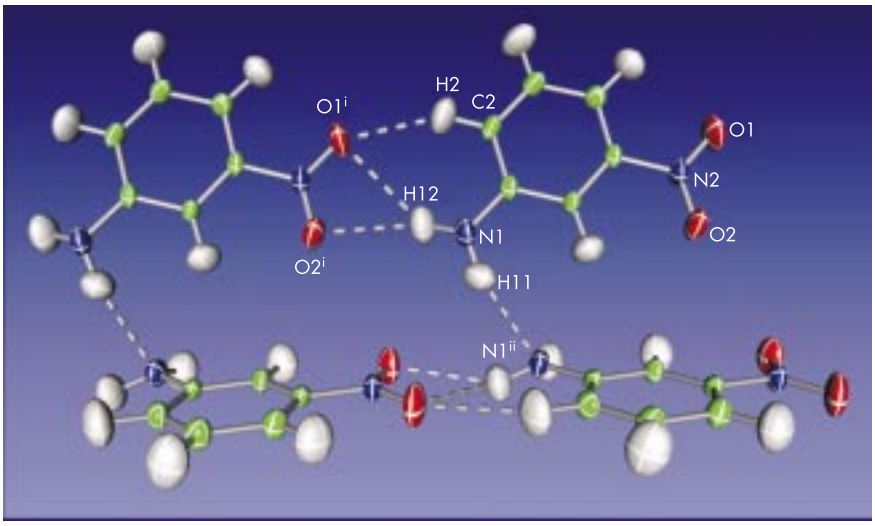

Figure H4. 2. The main hydrogen bonds in m*-nitroaniline.*

plane and induces the formation of infinite polar chains along [10$\bar{1}$] where consecutive molecules are rotated 60.15(4)°. Molecules in the chain are also joined by a weak C(methyl)-H.....O interaction as shown in figure H4.1. It can also be seen that molecules related by an inversion centre are linked by four HB, which causes the generation of centrosymmetric dimers (figure H4.1). As a result, two adjacent antiparallel chains are alternately joined by the centrosymmetric dimer interactions. This gives rise to non-polar ribbons that inhibit the macroscopic second order non-linear optical response of 2M5NA. Ribbons along the [10$\bar{1}$] direction are interlinked, via the centrosymmetric dimer interaction and two weak C(methyl)-H…O interactions, with equivalent ribbons along the *b* axis, forming (101) layers. A less conventional C-H…π (centre of aromatic ring) HB was also found. The comparison of the interactions that induce chain formation with those that induce the dimeric arrangement would suggest that in 2M5NA the short range ordering (dimer formation) is energetically more stable than the long range ordering (chain development). This is supported by the melting point of 2M5NA, 378K, being lower than that for 2M4NA, 405K. In the latter compound long range ordering prevails, chains are connected head-to-head and dimeric units are not observed.

In mNA, the H12 aminic hydrogen is connected again with the oxygens of a nitro group through an asymmetric bifurcated HB, although more symmetric than in 2M5NA (figure H4.2). This N-H…O(nitro) interaction connects molecules related by a translation operation and induces the formation of infinite polar chains along [01$\bar{1}$] and [0$\bar{1}\bar{1}$] where consecutive molecules are parallel to each other. Molecules in the chain are also joined by a C(ar)-H…O interaction, shown in figure H4.2. Contrary to the case of 2M5NA, dimers are not formed here; instead chains associate in pairs to form polar ribbons. The association is induced by a significant N-H…N interaction, not reported previously, which links molecules with their mean planes forming an angle of 66.70(6)° between them and related by a glide operation (figure H4.2). The ribbons stack to originate a polar layer with chains either along [01$\bar{1}$] or [0$\bar{1}\bar{1}$] and the three dimensional structure can be described as polar layers piled along *a*. Adjacent layers, alternately comprising chains oriented along [01$\bar{1}$] and [0$\bar{1}\bar{1}$], are connected via a weak C(ar)-H…O bond and all in all a polar supermolecule along the [00$\bar{1}$] direction is formed. The melting point of mNA, 386K, is also higher than that in 2M5NA, again supporting the contention that in 2M5NA short order prevails while in 2M4NA and mNA long order prevails.

The results presented here show that nitroanilines may not assemble in chains as the first aggregation step in solution as previously proposed. They also provide conclusive evidence that the amino group is far from planar and that the amino nitrogen can work as a HB acceptor in these systems. These last two facts have not been considered until now, when we have obtained the first detailed accurate neutron structures of this series. Clearly, however, they should be considered in the future when performing calculations on aggregation in such systems.

AE Goeta (Durham), **G Punte, JC Autino** (Universidad Nacional de La Plata, Argentina), **J Ellena** (Universidade de São Paulo, Brazil), **CC Wilson** (ISIS)

Structure and dynamics of polymer electrolytes

The relationship between mechanical and electrical relaxation in polymer-lithium salt complexes is a fascinating problem in condensed matter physics, with important bearing on the viability of such materials for use as electrolytes in lithium batteries. Despite a large body of work on the electrical and chemical properties of these materials, surprisingly little is known about the microscopic basis of their behaviour. We have used SANDALS and IRIS to explore the structure and dynamics of polymer electrolyte materials.

At room temperature polymer electrolyte materials are biphasic, consisting of fluid amorphous regions along with salt enriched crystalline regions. Ionic conduction is known to occur predominantly in the former, via mechanisms not yet fully understood. This provides an ideal opportunity to exploit the present state-of-the-art of neutron diffraction and quasielastic scattering to probe the structure and dynamics at an atomic level.

We have used SANDALS to determine the structure of $P(EO)_{7.5}LiTFSI$ (TFSI= $LiN(SO_2CF_3)_2$), a polymer electrolyte whose conductivity, phase diagram and chemical safety and stability make it a promising candidate for battery applications. Neutron diffraction with isotopic substitution allows a direct determination of the structure around the isotopically substituted element, in this case Li, and provides information about longer-range structural correlations. The *S(Q)* measured for the ^6Li and ^7Li samples (figure H5.1) have identical features but there is a small intensity variation arising from the different Li scattering lengths for the two samples. The strong peak at Q =1.5 $Å^{-1}$, highlighted in the inset to figure H5.1, reflects the intermediate-range order of the polymer network; it is similar to the first sharp diffraction peaks observed in many network and molecular liquids. The peak at Q = 0.57 $Å^{-1}$, reflects the extended-range order (ERO) that appears when the salt is added.

The structural environment about a Li^+ ion is obtained from the first-order difference pair

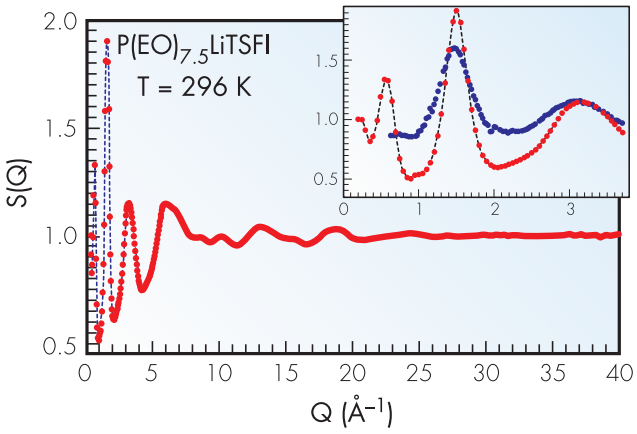

Figure H5.1. Neutron weighted average structure factor S(Q) *for liquid* $P(EO)_{7.5}LiTFSI$ *at T=296 K. Inset: Low-Q region of* S(Q) *for the electrolyte and liquid PEO at T=363K.*

distribution function $T_{Li}(r)$, shown in figure H5.2. Making use of *ab initio* quantum chemistry results, we can assign the peaks to various pair correlations and allocate the distribution of coordination numbers among them. This has led us to a structural representation for the polymer electrolyte where the Li^+ ions are bonded on average to five ether oxygens belonging to pairs of PEO coils which interlock to form cylinders arranged in a 2-D dense random packing, with the $TFSI^-$ anions occupying the spaces between them. This picture implies a retention into the liquid state of a high degree of ERO, similar to that reported by Bruce and coworkers in crystalline $P(EO)_6LiAsF_6$ (results obtained on IRIS), and explains the relatively high conductivity of this electrolyte. Li conduction must occur by

breaking and remaking of the five Li-O bonds, as observed in molecular dynamics studies of polymer electrolytes, accompanied by fast relaxation of the local polymer chain structure.

The dynamics of these systems can be explored with quasielastic neutron scattering, which provides a powerful probe on the nanosecond time scale which appears to be relevant for the lithium motions and associated relaxation of the polymer chains. We have used IRIS to study pure PEO and two electrolytes, $P(EO)_{7.5}LiCLO_4$ and the $P(EO)_{7.5}$LiTFSI discussed above. The scattering intensities $I(Q,\omega)$ exhibited quite different behaviour for each of the samples examined. For the pure polymer, $I(Q,\omega)$ could be represented by a spectral function $\varphi_{\beta\tau}(\omega)$, the Fourier transform of the stretched exponential function $\phi_{\beta\tau}(t) = exp[-(t/\tau)^{\beta}]$, commonly used to describe relaxation effects in polymers. The rapidly increasing value of τ^{-1} (figure H5.3) indicates that the relaxation is related to the translational diffusion of the chain segments.

For the polymer electrolytes, the scattering showed a quite different behaviour and was best fitted by the sum of two terms, one describing a slow relaxation that appears static on the IRIS time scale (0.09 ns) and the other a fast process with a spectral function $\varphi_{\tau}(\omega)$, the Fourier transform of a pure exponential. We have recently extended our investigations to longer times with neutron spin-echo spectrometry at ILL and confirmed that the slow process reflects a drastic slowing down of the translational motions of the chain segments due to the addition of the salt. The form of $\varphi_{\beta\tau}(t)$ and $\varphi_{\tau}(t)$, shown in the inset to figure H5.3, illustrates the very different behaviour of the fast process. The fact that τ^{-1} is almost independent of Q indicates a rotational character for this process, which must arise from rapid conformal fluctuations of the chain segments between cross-links, presumably associated with the making and breaking of the coordination bonds that enhances the Li^+ ion transport in the amorphous phases.

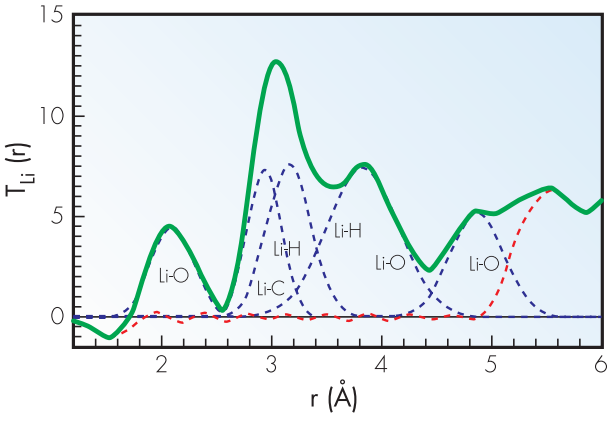

Figure H5.2. Lithium difference pair distribution function for liquid $P(EO)_{7.5}$LiTFSI: Green line: data; blue lines: fitted Gaussians; red line: residual.

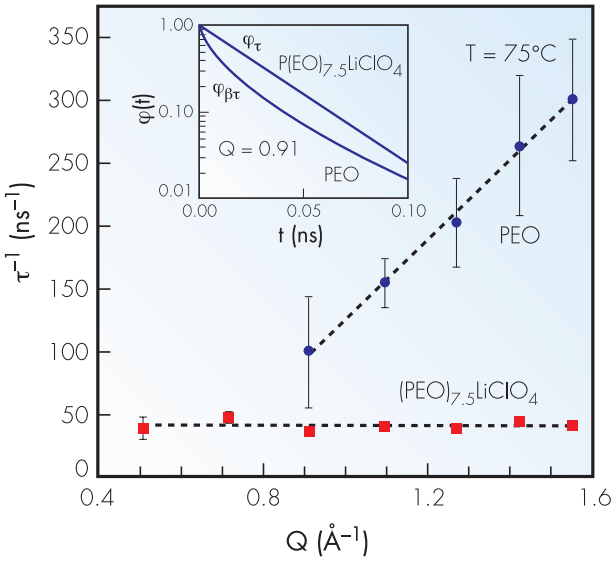

Figure H5.3. Variations of the inverse relaxation times τ^{-1} for pure PEO and $P(EO)_{7.5}LiClO_4$ electrolyte at 75°C. Inset: behaviour of $\varphi_{\beta\tau}(t)$ and $\varphi_{\tau}(t)$ for the two systems at Q = 0.91 Å^{-1} (dashed lines are a guide to the eye).

DL Price, M-L Saboungi, G Mao, RF Perea (Argonne National Laboratory, USA), **WS Howells** (ISIS)

Neutron diffraction study of molten alumina

We report the first measurements by neutron diffraction of the structure factor and radial distribution function of liquid alumina at temperatures up 2400K, using the SANDALS instrument. A continuous wave CO_2 laser is used to heat and melt a 3 mm diameter alumina sphere, levitated in the neutron beam by a jet of argon gas. The data are interpreted using a computer simulation structure refinement process. The results are entirely in accord with an earlier X-ray diffraction study of liquid alumina, with an average coordination of about 4.5 oxygens around aluminium. Contrary to this earlier experiment however, which claimed that *Al* is predominantly 4-fold coordinated by oxygen in the liquid, the present results indicate significant numbers of 5- and 6-fold coordinated *Al* are present as well.

There has recently been much interest in exploring the use of gas levitation techniques to simplify the examination of high temperature molten ionic oxides. These materials typically have melting points in excess of 2000K which, combined with their generally high reactivity, precludes the use of a container in a conventional furnace. Levitation, using a laser to heat the material, avoids the possibility of chemical contamination by the container, and therefore presents a real opportunity for synthesis and *in-situ* characterization of liquids or solids at highly elevated temperatures. The possibility of using aerodynamic levitation in association with CO_2 laser heating to look at the structure of a melt has been demonstrated in earlier investigations of refractory oxides, including alumina, using X-ray scattering as the structural probe. The levitation technique however presents a major challenge for a diffraction experiment since the amount of material that can be supported by the levitator is in the region of 20-50 mg, that is around 1/20th to 1/100th of the amount of material used in a conventional diffraction experiment on a liquid. Intense X-ray sources have allowed the first determination of the structure factor of molten aluminium oxide, but the interpretation of those data in terms of there being predominantly tetrahedral coordinations of oxygen about aluminium in the melt is not fully consistent with earlier NMR data and subsequent

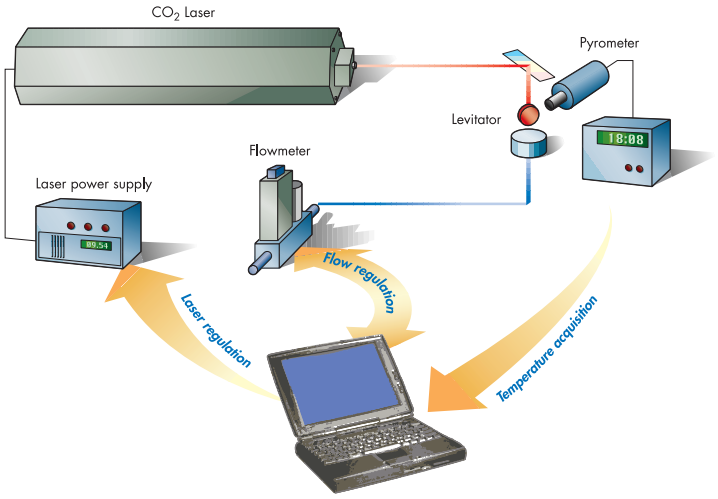

Figure H6.1. Experimental set-up of the levitation chamber for measuring the neutron diffraction pattern from molten alumina at 2300°C.

computer simulations, where a range of coordinations, in the region of 4 – 6, were found. We present here the first structural data of molten alumina obtained in a neutron diffraction study using contactless conditions. The strong scattering of neutrons by oxygen compared to aluminium serves to accentuate the essential structural features of molten aluminium oxide and so complements the existing X-ray data.

The neutron experiments were carried out on SANDALS. The starting material was a high-purity powder of alumina pressed under isostatic pressure to 250 MPa. The specimens were spherical with a nominal diameter of 2.7 mm,

corresponding to a weight of ~40 mg. On the diffractometer the laser beam was incident horizontally to the sample (figure H6.1). The spherical sample rotated around a vertical axis in the argon flow, so that the temperature of the sample was stable and uniform. Any crystallinity in the sample was readily detectable as sharp Bragg peaks in the diffraction pattern, the absence of which was the indication that the sample was fully molten. The argon flow, measured by a thermal mass flowmeter, was precisely adjusted versus temperature by a remote control computer in order to optimize the stability of the sample. Contactless temperature measurement was performed by optical pyrometry.

Figure H6.2(a) shows the diffraction pattern from molten aluminium oxide obtained in this experiment, after subtracting the scattering from the boron nitride levitator nozzle. The data shown were aggregated from about 5 separate scans on molten alumina, each one requiring about 20 minutes of neutron beam time. Obviously the statistical quality of these data is not ideal, but the fact that data from such small samples are obtainable at all attests to the great power of modern neutron diffractometers.

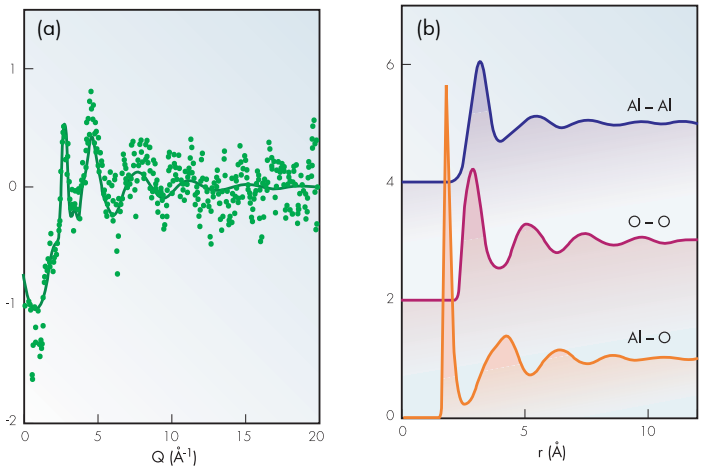

Figure H6.2. (a) Measured neutron structure factor for molten alumina (circles). The line shows the computer simulation fit to these data. (b) Estimated Al-Al, Al-O and O-O site-site radial distribution functions for molten alumina as estimated from the computer simulation of the diffraction data. Note the strong charge ordering present in this system (Al-O correlations out of phase with Al-Al and O-O), and that the Al-Al near neighbour distance is slightly larger than the O-O near neighbour distance.

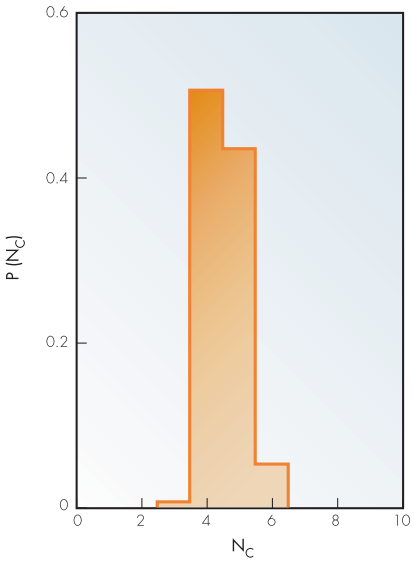

Figure H6.3. Relative numbers of aluminium atoms in molten alumina with 3, 4, 5 and 6 oxygens at the near neighbour distance of 1.8 Å.

The neutron structure factor obtained here is in fact a weighted sum of Al-Al, Al-O and O-O partial structure factors:

$S_N(Q)=0.081S_{AlAl}(Q)+0.406S_{AlO}(Q)+0.513S_{OO}(Q)$

which shows that the measured data are dominated by the important *AlO* and *OO* correlations. To interpret these data a computer simulation procedure was invoked to set up model ensembles of *Al* and *O* ions whose calculated structure factor reproduced the measured structure factor as close as possible. This produced the set of site-site radial distribution functions shown in figure H6.2(b), which can be shown to be also perfectly consistent with the previous X-ray data. The coordination number of oxygen about aluminium in this simulation turned out to be 4.5. What the previous experiments did not reveal was the precise distribution of these coordination numbers, between 3 and 6, as shown in figure H6.3, where it is seen that there are almost as many 5- and 6-fold coordinated aluminium atoms combined as 4-fold coordinated aluminium atoms. Thus the true picture of molten alumina must be one where the octahedral coordination of aluminium in the crystalline form becomes highly defective in the liquid state. However molten alumina certainly cannot be described as a 'tetrahedral liquid'.

C Landron, L Hennet (CRMHT, Orleans and LURE, Orsay, France), **TE Jenkins, GN Greaves** (University of Wales, Aberystwyth), **G Derbyshire** (ISIS), **JP Coutures** (CRMHT, Orleans, France), **AK Soper** (ISIS)

In-situ real time reflectivity studies of polymer/polymer spinodal dewetting at ISIS

The process of dewetting, in which liquid films break up into droplets, is of importance in many areas of technology including coatings, microelectronics fabrication and surface patterning. The subject has also been the focus of attention from a more fundamental point of view. Much of this work has involved polymer films, both because of their technological importance and because their high viscosity means that experiments can be carried out on convenient time scales. We have performed in-situ, real-time neutron reflection experiments to study the dynamics of the spinodal dewetting process in thin polymer films using the SURF reflectometer at ISIS.

The behaviour of polymeric fluids at surfaces, interfaces and in thin films, is of importance in many areas of technology such as coatings and microelectronics fabrication. Our attention here is focused on dewetting, in which an initially uniform film becomes unstable and breaks up into an array of droplets or holes. One mechanism of dewetting involves the nucleation and growth of isolated holes. The initial distribution of these holes is random and hence there is no particular length scale that characterises the morphology. Another possibility is that the initial stages of dewetting consist of the unstable growth of capillary waves driven by attractive dispersion forces across the film. This process is known as spinodal dewetting and is an important mechanism of dewetting for ultra-thin polymer films. In this case the morphology is characterized by one particular length scale.

The study of the kinetics of dewetting, while being of interest in its own right, is also a potentially useful tool for probing the dynamics of polymers in confined situations.

We have shown recently, with a series of experiments using the reflectometers CRISP and SURF, that the interface of two immiscible polymers sustains a spectrum of thermally excited fluctuations - capillary waves. The signature of such capillary waves is a logarithmic dependence of the interfacial width on the thickness of the films. In the original experiments, the system studied was a thin polystyrene (PS) layer on a thick poly(methyl methacrylate) (PMMA) film deposited on a silicon substrate. This system has

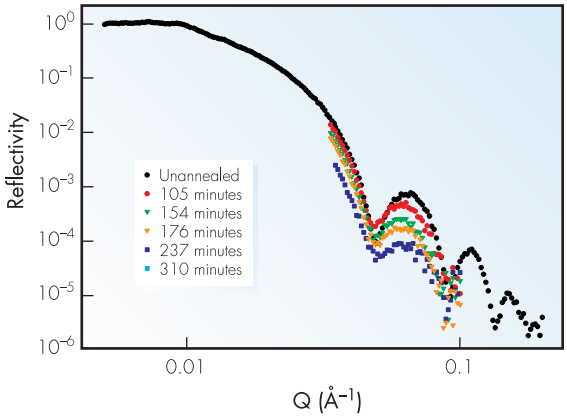

Figure H7.1. Typical reflectivity curves of a sample with a thickness of the top d-PMMA layer of around 140 Å and a thickness of the bottom h-PS layer of 1400 Å during annealing time at a temperature of 170 °C.

a positive Hamaker constant that describes the dispersion forces acting across the thin PS layer between air and the PMMA polymer substrate. Subsequent work using neutron reflectometers at both ILL and ISIS showed that by inverting the order of the two polymers, the system was destabilised and dewetting took place. The Hamaker constant for the inverted system is negative, and theory predicts the growth of long wavelength capillary waves leading to dewetting. The linear theory of spinodal dewetting predicts that the fastest wave depends on the square of the thickness of the top thin layer. The characteristic rise time of the instability depends on the viscosity, interfacial tension, thickness of the film and the Hamaker constant. The rise time depends on a power law on the top film thickness, with a power that varies from 4 to 6. Preliminary

observations were made on the silicon/PS/deuterated-PMMA system by using specular and off-specular neutron reflection to probe both the length scale and the dynamics of dewetting, as a function of the top d-PMMA layer.

To follow in detail the dynamics of dewetting, we have now concentrated on the specular neutron reflectivity. In particular by using a narrow *q* range combined with a suitable choice of molecular weights and annealing temperature we were able to perform reflectivity measurements in situ at ISIS as dewetting proceeded. Neutron reflectivity profiles collected at ISIS have the advantage of using a white beam that gives a full reflectivity profile at a fixed incident angle. Data collection times are then limited only to the time required to gain enough statistics. Using CRISP and SURF, the full reflectivity profile of limited *q* range for a single incident angle can be collected in a few minutes to provide sufficient statistics for extracting the interfacial widths from the data.

We have investigated how the time scale of dewetting depends on the molecular weight of the two polymers. By performing experiments in the regime where the dynamics are independent of the substrate PS polymer molecular weight, we have investigated the possibility of using dewetting to probe the viscosity dependence of the PMMA thin film as a function of temperature and molecular weight.

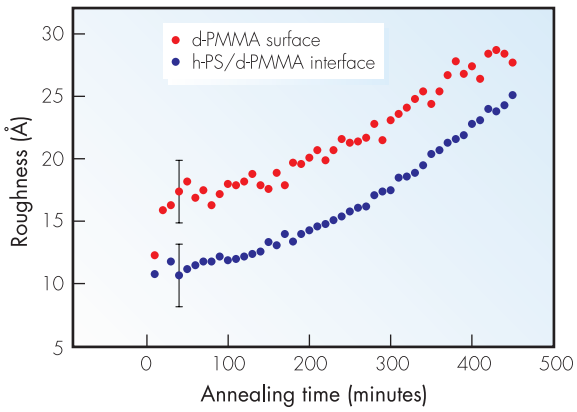

Figure H7.2. Surface roughness and interface roughness as extracted from the fitting of the reflectivity curves of figure H7.1 using a 2-layer model.

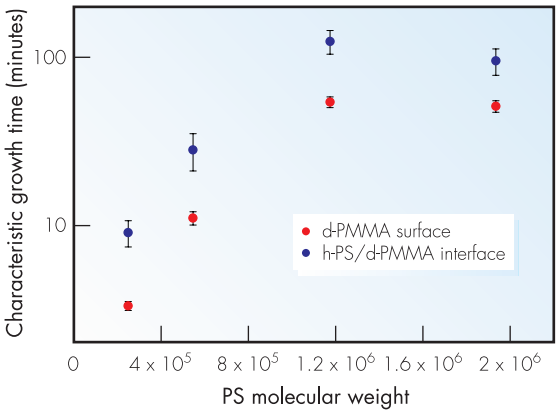

Figure H7.3. Characteristic growth time as a function of the PS molecular weight extracted from data as in figure H7.2.

Bilayers of PMMA on PS were prepared on silicon disk. A thickness of around 1500 Å was used for the bottom PS layer, and a thickness of around 140 Å was used for the top d-PMMA layer. The annealing temperature was around 170 °C, well above the glass transition of the polymers. Figure H7.1 shows typical in-situ reflectivity curves for the system. From the model fitting the surface roughness and interface roughness were extracted. Figure H7.2 shows typical data for the development of both surface and interface roughnesses during annealing, revealing that after an initial stage there was a gradual increase in both roughnesses due to the dewetting. Figure H7.3 shows the rise time for the growth of both surface and interface roughness extracted from figure H7.2 as a function of the PS molecular weight. The rise time initially increases as the substrate viscosity changes from a low value, compared to the top PMMA viscosity (liquid substrate regime), to a high value (solid substrate regime) and then plateaus. From the analyses of these data one can determine the crossover from a liquid substrate regime to a solid substrate regime and compare this with theoretical predictions. These experiments also show the potential of white beam at ISIS to explore the initial process of spinodal dewetting of liquid/liquid systems, opening the possibility of new and exciting experiments in this field.

M Sferrazza (ISIS), **AM Higgins, RAL Jones** (University of Sheffield)

Probing liquid/liquid interfaces

The liquid/liquid interface remains an important area of chemistry due to its widespread application in practical systems in which the formation, stability and breakdown of liquid/liquid dispersions (emulsions) are involved. Furthermore, liquid/liquid interfaces are essential constituents of biological systems as well as being involved in many chemical separation processes. Recently, progress has been made in developing the methodology for routine investigations of liquid/liquid interfaces using specular neutron reflection on CRISP and SURF.

Overcoming the drastic attenuation of a neutron beam upon transmission through a liquid medium remains the major obstacle in the routine investigation of liquid/liquid interfaces using neutron reflection. The advances made in the past have revolved around the ability to form and maintain a thin oil film through which the neutron beam is transmitted. This can be achieved in two ways. One is the established method whereby an oil film is condensed on to the surface of an aqueous subphase. The second method is to support an oil film on a solid substrate and then bring this into contact with the water surface. Both methods are complementary since together they offer means of studying volatile and non-volatile oils and water-soluble, oil-soluble and insoluble polymers and surfactants. It is the second of these methods which has seen significant development over the last year.

The sample environment used in these studies is shown in figure H8.1. The silicon surface is modified by a hydrophobic moiety chemisorbed onto the block's native oxide layer. Hexadecane with the desired scattering length density is spread on to the modified surface. The block is then spun until an oil film of several thousand Ångströms is produced, which can be monitored by visually observing the formation of Newton rings produced by the film. The coated block is cooled to $T<T_m$=16 ºC to freeze the oil film and then maintained at that temperature. This is achieved by using a Peltier cooling device housed in the upper part of the sample cell. The spread or adsorbed film can be prepared in the trough part of the sample cell. The frozen oil surface is then brought into contact with the aqueous phase and after some adjustments the oil film is allowed

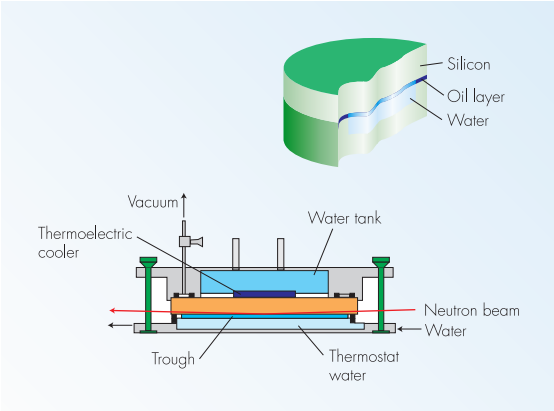

Figure H8.1. Schematic diagram, and section through, the liquid/liquid reflectivity cell.

to warm up to $T>T_m$. Reflectivity spectra (R_{tot}) are then measured at several angles of incidence, as in a typical solid/liquid interface experiment, transmitting the incident neutron beam through the silicon substrate. Some further measurements are also required: the linear absorption coefficient of the oil contrast used needs to be known and, for convenience, the reflectivity spectrum (R_1) from the silicon/oil interface is also measured independently.

The next stage is to extract the reflectivity (R_2) from the buried oil/water (o/w) interface from the measured R_{tot}. This then allows direct analysis of R_2 to determine the structure at the o/w interface. A convenient starting point for the analysis is the thick film approximation for the calculation of the overall reflectivity, R_{tot}. It is assumed that the overall reflectivity arises from the reflections from two interfaces (with reflectivities R_1 and R_2) separated by a thick absorbing layer and contributing incoherently to the total signal. The direct measurement of R_1 removes the model dependence of the silicon/oil

interface. R_2 can be determined by incorporating an attenuation factor $A(\lambda)$ which accounts for the absorption by the intervening oil film; if the absorption coefficient is known this factor depends only on the film thickness.

The film thickness can be readily determined if two critical reflection edges are present in the spectrum. The decrease in reflectivity between the two edges is a measure of the attenuation and hence optical path length. For conditions where a double edge doesn't occur the thickness can be determined by use of a known scale factor or by relying upon the reproducibility of oil film thickness based on the spinning process. In either case, negligible errors are incurred. The work presented here is for refractive index contrasts for which there is, at the very least, a total reflection from the buried o/w interface.

Figure H8.2 shows the reflectivity spectrum measured from a hexadecane/water interface (T=25°C) based on this measurement procedure, and the inset shows an example of a double critical edge, from which the film thickness can be determined. The spectrum can be analysed in terms of a r.m.s. roughness, which has contributions from both the (thermal) roughening of the interface by capillary waves and the intrinsic width of the interface. In this case it is found that the intrinsic width of the interface is ~15 Å indicating that molecular shape is a dominant contributing factor.

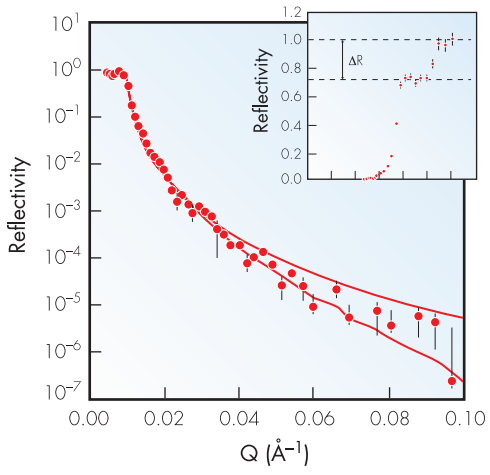

Figure H8.2. Net reflectivity from the hexadecane/water interface, with simulations of 3 Å and 17 Å roughness. The inset shows the original double critical edge (in wavelength).

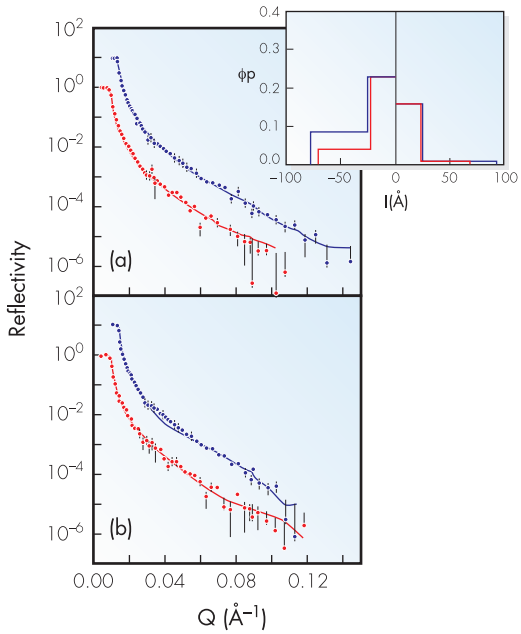

Figure H8.3. Measured and modeled reflectivity spectra a) Γ≈4 mg m⁻²; b) Γ≈10 mg m⁻². H-H copolymer at CM4/D2O interface (red) and D-H copolymer at CMSi/D2O interface (blue). Inset shows the corresponding volume fraction profiles.

Amphiphilic copolymers of poly(butadiene) and poly(ethylene oxide) with molecular weight of ~60,000 g mol^{-1} have been spread at the hexadecane/water interface with concentrations of 4 mgm^{-2} and 10 mgm^{-2}. Reflectivity spectra and the derived volume fraction profiles through the interface are shown in figure H8.3. For the contrasts shown, the reflectivity is most sensitive to changes in the conformation of the hydrophobic poly(butadiene) block. In contrast to the air/water interface the hydrophobic block exhibits a more extended dilute region in addition to a concentrated 'collapsed' region close to the interface.

The results presented here indicate that the approach described to measure neutron reflectivity from a buried oil/water interface is both practical and suitable, and show the potential for future investigations of polymeric, surfactant and biological systems.

J Bowers, A Zarbakhsh (QMW), **J Webster** (ISIS), **R Richards** (Durham)

Towards improved drug delivery

Colloids, materials which have been dispersed into particles or droplets less than a micrometre in size, form an indispensable component of modern technology and are used in fields as disparate as foodstuffs, surface coatings, and pharmaceuticals. A detailed understanding of their production and behaviour is not only important for their technical applications, but contributes much to our understanding of organised microscopic systems. The length scales of interest in these materials, and the ability to selectively 'highlight' regions of interest with contrast variation studies, make them amenable to study by small-angle neutron scattering (SANS) on the LOQ diffractometer.

Perhaps the most fundamental property of colloids is that they experience an attractive Van der Waals force, which causes them to aggregate into a single mass. In order to produce useful colloidal materials it is necessary to overcome this, by providing a more dominant repulsive force that will then allow the particles to remain dispersed. One of the most widely used methods of accomplishing this is to cover the particle surface with a layer of polymer that prevents the particles coming into contact.

One class of polymers that have been widely utilised for the steric stabilisation of colloids are the Pluronic™ or Poloxamer™ block copolymers illustrated in figure H9.1. Here a central mass of poly(oxypropylene), or POP (in red), is linked to two or four terminal blocks of poly(oxyethylene), or POE (in green). The POE in these polymers is rather more hydrophilic (water-soluble) than the POP and this leads to a rich variety of phase behaviour. These polymers have been used to stabilise pharmaceutical colloids and, in the process, found to influence the biodistribution of the colloid after intravenous injection. Adsorbed layers of structurally (and chemically) similar polymers, differing only in the values of *n* and *m*, targeted the colloidal particles to different

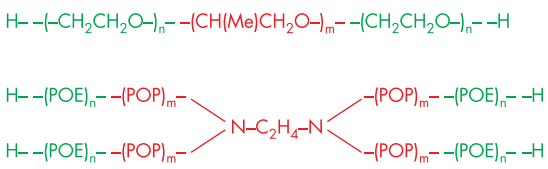

Figure H9.1. The chemical structures of Pluronic™ (top) and Tetronic™ (bottom) block copolymers; n and m represent numbers used to describe the block lengths.

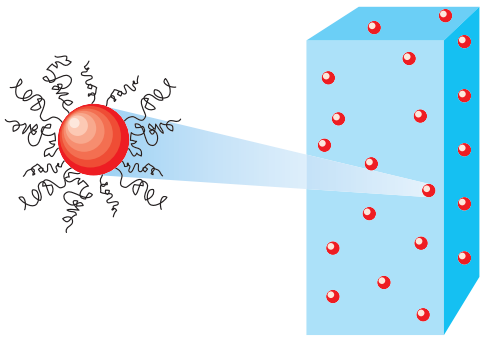

Figure H9.2. Schematic representation of the emulsion system investigated on LOQ. The pink fluorocarbon oil droplets with their adsorbed polymer layers are dispersed in an aqueous bulk phase (shown in blue).

organs. The only explanation for these observations is that the adsorbed layers are mediating the biological response in different ways. To be able to understand and control the relationship between the adsorbed polymer layer structure and the *in vivo* fate of the particle is evidently of potential importance. To learn about the adsorbed layer structure one can study them in a model colloid and the system that has been used here consists of an emulsion of perfluorodecalin (a water-immiscible oil) droplets dispersed in water (figure H9.2).

Since the density of perfluorodecalin is greater than that of water, the oil droplets could be easily manipulated by centrifugation, thereby allowing the bulk phase to be washed free of unadsorbed polymer, which would otherwise have complicated the data analysis. Furthermore, because perfluorocarbons can be readily contrast-matched by a deuterium-rich H_2O / D_2O mixture, the only scattering that is measured is that from the adsorbed layer. This is a huge advantage, and the principle reason for using neutrons for this type of investigation. Using inversion or minimisation methods it is possible to extract the concentration distribution function of the adsorbed polymer

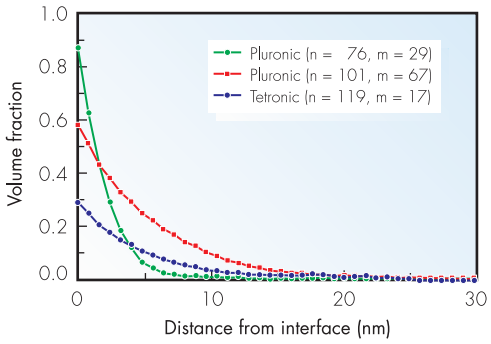

Figure H9.3. Volume fraction profiles derived from the SANS data for three different adsorbed polymers.

layer from the SANS scattering data (figure H9.3). This describes how the volume fraction of polymer segments varies with distance from the interface, and thus provides a very detailed view of the adsorbed layer structure which can be correlated with predictions from molecular modelling.

The volume fraction profiles are consistent with a picture in which the POP segments are mostly adsorbed at the oil/water interface and where the POE blocks extend into the surrounding water phase. However the shape of the profiles indicates that the chains are not all extended to the same length (which would yield a step profile) and there are also clear differences in the amount of each polymer at the interface. With this information it has been possible to build up a picture of the comparative arrangement of the polymers at the oil/water interface (figure H9.4).

Further experiments have allowed an understanding of the interactions between electrolytes and the adsorbed polymers that had not previously been studied in any great detail. The hydrophilic POE blocks are normally heavily hydrated (experimental evidence suggests around 3 molecules of water for each POE segment; i.e. 3 per n) and the hydration shells of dissolved electrolyte ions compete for this water. Figure H9.5 shows what the effect of this is on an adsorbed polymer layer. It is evident that, although the polymer chains collapse back toward the interface at high electrolyte concentrations the adsorbed layer actually becomes more extended at intermediate ionic strength.

The most likely explanation for this effect is that the lower electrolyte concentrations disrupt a polar interaction between the POE blocks and the surface. This reduces the number of loops in the POE chains, allowing the whole chain to move further from the interface despite the fact that the POE blocks are becoming dehydrated. As the electrolyte concentration is increased further the segment-segment interactions in the polymer become increasingly important and the adsorbed layer collapses.

POE-based surfactants are among the most widely used in pharmacy due to their reasonable biocompatibility, ease of synthesis and low cost. They are formulated into products as diverse as oral medicines, skin creams and intravenous injections. Until recently the refinement of these formulations has been performed on a largely empirical basis. Detailed structural studies of this type are providing a better understanding of the behaviour of PEO surfactants in such complex mixtures, and thus allowing the pharmacist to devise more effective medicines for the new millennium.

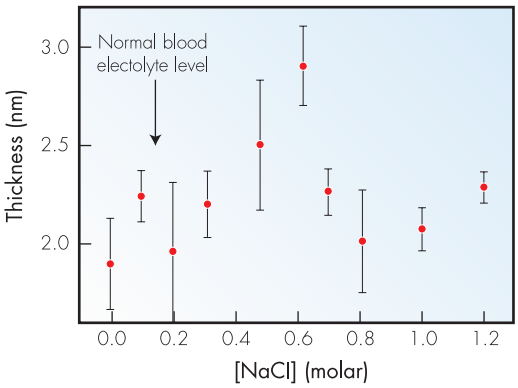

Figure H9.5. The variation of the mean thickness of the adsorbed layer with electrolyte concentration for the Pluronic copolymer with n=76.

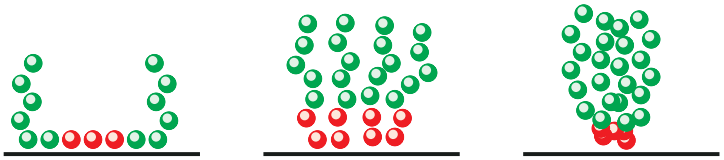

Figure H9.4. Schematic illustration of the arrangement of three different polymers at the emulsion interface; left: Pluronic (n=76, m=29); centre: Pluronic (n=101, m=67) which has the most adsorbed; right: Tetronic (n=119, m=17).

C Washington (University of Nottingham), **SM King** (ISIS)

Glass corrosion: chemistry of the water-glass interface

Flat glass produced by the Pilkington float process is of major economic importance in a wide range of industrial applications. Float glass surfaces are often coated with thin films to give them enhanced properties; for instance, indium tin oxide coatings are applied to the glass surface to produce optically transparent electrodes and silica gel materials are commercially important as water repellent coatings e.g. for the windscreen of aeroplanes. It has been suggested that atmospheric water (liquid and vapour) can lead to degradation of the glass surface, which results in poor adhesion and/or performance of the coatings. Specular neutron reflection on SURF and CRISP has been used to investigate the interaction of water with untreated float glass surfaces and the effect of adding fluorocarbon doped coatings.

The effect of prolonged exposure of float glass to atmospheric conditions can be seen in the atomic force microscopy (AFM) images in figure H10.1. The deposits formed on the surface of the stored sample are a type of sodium bicarbonate.

The incorporation of water into the glass surface as a function of immersion time has been investigated on SURF and CRISP. Four pairs of float glass samples were prepared by immersing one in H_2O and its 'twin' in D_2O. The soak time was varied from 1 week to 6 months, at ambient temperature. The neutron scattering lengths of H_2O and D_2O are very different (b_{D2O}=19.15x10^{-5} Å and b_{H2O}=-1.68x10^{-5} Å), hence the difference in reflectivity between a pair of glasses soaked for the same time in H_2O and D_2O gives information on the water penetration into the surface.

The number density N(z) profiles for water and glass, which fit the reflectivity data, are shown for all samples (including untreated float glass) in figure H10.2. The data were fitted using

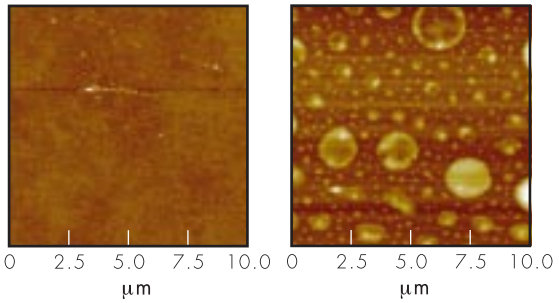

Figure H10.1. AFM height image of the surface of float glass. Left: fresh sample; right: a sample which has been stored under atmospheric conditions for a prolonged period. Height range (z) of the image is 50 nm.

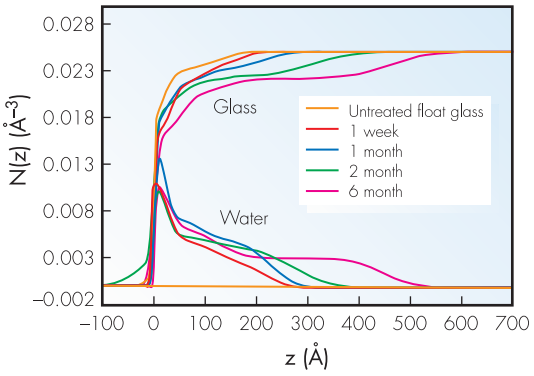

Figure H10.2. Number density profiles N(z) versus penetration depth z into the sample for float glass immersed in water for different periods.

a modification of a standard slab model. The glass and water number density profiles and their relative origins are varied to obtain the best fit. Two distinct regions can be observed. The first layer starts at the origin, and has a thickness of approximately 30 Å, which appears almost constant with immersion time. The second region extends further into the glass; the water penetration distance increases systematically with immersion time, and after 6 months this can be seen to extend to ~500 Å.

The most likely explanation for the trends in number density profile is that as the water penetrates the glass surface, the mobile Na^+ ions are leached out of the glass network and replaced by H_3O^+. Two mechanisms have been suggested for this process: either the H_3O^+ ions diffuse in from the surface and exchange with the sodium atoms, or molecular water diffuses in from the surface and reacts to replace the sodium ions with H_3O^+ so that Na^+ and OH^- diffuse out of the glass.

In the deeper layer, our results indicate that the sodium atoms are only partially replaced by water (or H_3O^+), hence it is unlikely that there is disruption of the Si-O network to accommodate interstitial water.

Analogous measurements have been made on float glasses coated with perfluoroalkylsilane doped silica gel. The thin films were produced by co-condensation using the sol gel process, which results in a silica layer (~50 nm) on the glass surface upon which a bound monolayer of fluorocarbon chains form. The fluorocarbon layer is very hydrophobic, producing the water repellent surface utilised in the aeronautical industry. Two samples were produced; float glass coated with non-fluorinated silica gel (2.40wt% tetraethoxysilane (TEOS)), and a fluoroalkysilane (FAS) doped version (2.40wt% TEOS + 0.08wt% FAS). Once again the samples have been cut into pairs; one was immersed in D_2O for two weeks and the other in H_2O for the same period. The sol gel coatings have a degree of porosity, which will affect the water absorption properties of the film, however they do not contain the alkali ions which were present in the float glass, so leaching is not expected to occur.

The neutron reflectivity data for the silica gel coated float glass for H_2O and D_20 are displayed in figure H10.3. The difference between them indicates that water has penetrated the coating. The interference fringes present in both data sets, with a periodicity of ~0.027 $Å^{-1}$, correspond to the existence of a silica layer with a thickness of

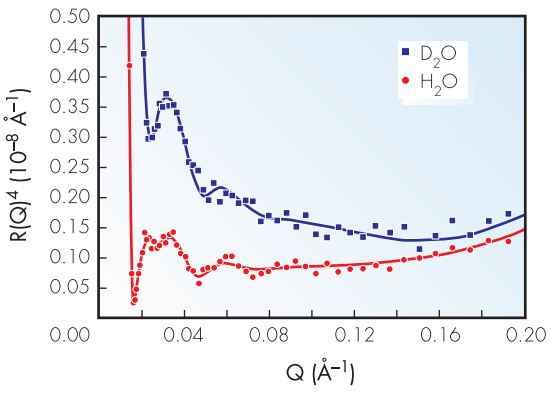

Figure H10.3. Reflectivity data for float glass coated with silica gel, immersed in H_2O or D_2O for 2 weeks. The lines are the fits modeled to the reflectivity data.

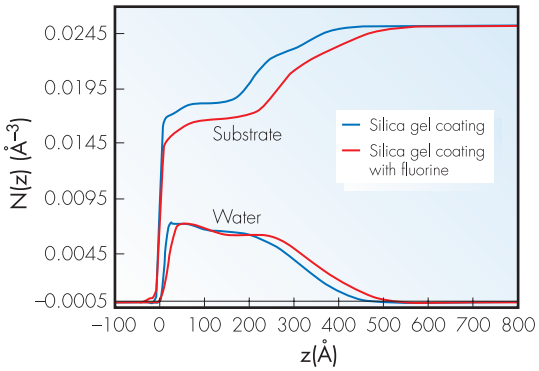

Figure H10.4. The number density profiles N(z) as a function of penetration depth z into the sample for float glass coated with silica gel (black), and fluorinated silica gel (red).

approximately 230 Å. The effect of fluorine content on the hydrophobic nature of the silica coating is shown in figure H10.4.

The number density of the fluorocarbon doped coating, in the region 0-500 Å, is lower than that of its non-fluorinated counterpart, suggesting that the film layer is thicker in this sample. Consequently the water profile of the fluorinated film extends fractionally deeper into the surface than in the float glass coated with silica gel. In both samples the water penetrates the surface to a depth of 500 Å; the amount of water which is incorporated into the coated glasses is approximately the same. This is surprising as the fluorine doped silica gel coating appears to be very hydrophobic having a large contact angle with water.

The non-invasive nature of neutron reflection techniques, coupled with the fact that the investigations can be performed under normal atmospheric conditions, has meant that the effect of aqueous solutions on the structure of the surface of glass can be investigated in-situ. Water was found to penetrate the surface of float glass, both untreated and coated with a hydrophobic perfluoroalkylsilane doped silica gel. The reaction of float glass with water is very important, commercially and scientifically, as it will effect both the chemical durability and fracture strength of the glass, as well as potentially modifying the performance of coating films.

RM Richardson, T Brennan, RM Dalgliesh, MR Lovell, AC Barnes, JE Enderby (University of Bristol), **JRP Webster** (ISIS), **S Sergeant, D Wood** (Pilkington Technology Centre)

Spin waves and electronic interactions in La_2CuO_4

The magnetic excitations of the square-lattice spin-1/2 antiferromagnet and high-T_c parent La_2CuO_4 are determined using high-resolution inelastic neutron scattering. Sharp spin waves with absolute amplitudes in agreement with theory including quantum corrections are found throughout the Brillouin zone. The observed dispersion relation shows evidence for substantial interactions beyond the nearest-neighbour Heisenberg term, which are best understood in terms of a cyclic or ring exchange due to the strong hybridization path around the Cu_4O_4 square plaquettes. CuO_2 planes are thus the second example of an important Fermi system (^{3}He is the other) where strong cyclic exchange terms have been measured. The technological advance enabling the present investigation is the use of position-sensitive detectors for the scattered neutrons on HET, which increases the wavevector resolution by an order of magnitude.

Magnetic interactions are revealed through the dispersion of the magnetic excitations. The CuO_2 planes and calculated excitations are shown in figure H11.1. Figure H11.1(a) shows the atomic orbitals involved in the magnetic interactions, where J, J' and J'' are the first-, second- and third-nearest neighbour exchanges and J_c is the cyclic interaction which couples all four spins at the corners of a square plaquette. Arrows indicate the spins of the valence electrons involved in the exchange.

The effect of turning on interactions beyond the nearest neighbour interaction is show in figure H11.1(b) where the lower frame shows the spin-wave dispersion surface for a square-lattice antiferromagnet with nearest neighbour exchange J (=136 meV) only. Spin waves emerge from the antiferromagnetic zone centre (1/2,1/2) and disperse to reach a maximum energy 2J that is a constant along the antiferromagnetic zone boundary marked by dashed squares. The upper frame of figure H11.1(b) shows the same dispersion calculated but now with modest interactions between next nearest neighbours. Virtually the only visible effect of the additional interactions is the dispersion along the zone boundary.

The magnetic scattering throughout the Brillouin zone as measured on a 48.6 g 7-crystal

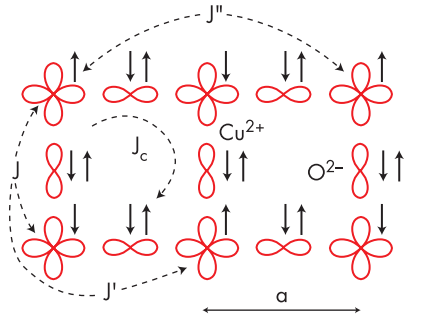

Figure H11.11(a). Diagram of the CuO_2 planes, showing the first, second and third nearest neighbour magnetic interactions involved, J, J', J'' and the cyclic interaction J_c.

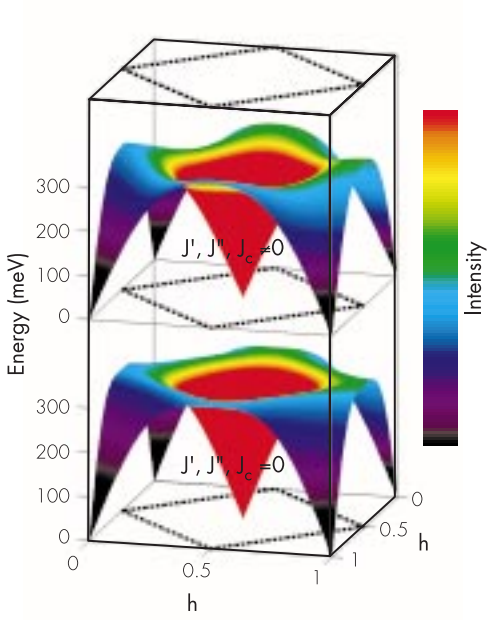

Figure H11.1(b). Calculated dispersion relations for the CuO_2 planes. The lower figure has J=136 meV with no higher order couplings or quantum corrections whilst the upper figure shows the effect if higher order interactions are turned on.

multicrystal using HET are show in figure H11.2. Data obtained by taking cuts through the dispersion at constant energy transfers near the antiferromagnetic zone centre are shown in figure H11.2(a). The solid lines are fits to the one-magnon cross-section convolved with the instrumental resolution.

Figure H11.2(b) shows a series of constant-Q scans collected at various points along the zone boundary. The spin waves have a clearly noticeable dispersion, from a minimum of 282±7 meV near Q=(3/4,1/4) to a maximum of 318±8 meV near (1/2,0). This is in obvious contrast to the dispersion-less behaviour of spin waves for the nearest-neighbour model (quantum corrections predict a zone-boundary dispersion, but of opposite sign from that observed).

Figure H11.3(a) shows the dispersion relation along major symmetry directions in the Brillouin zone and figure H11.3(b) displays the corresponding spin wave amplitudes, in absolute units calibrated using acoustic phonon scattering from the sample.

The results can be explained by adding a small second-neighbour exchange J'=-13.6 meV, however its sign is in contradiction with

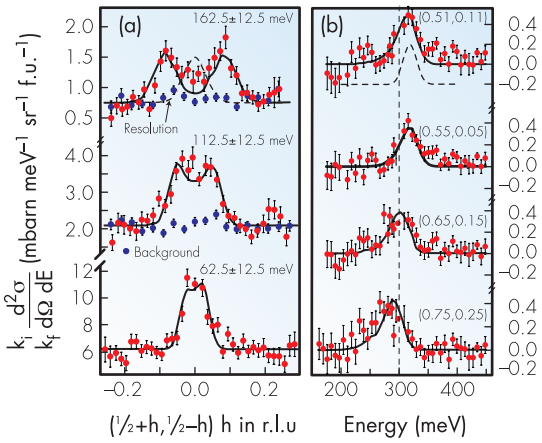

Figure H11.2. (a) Constant energy transfer cuts near the antiferromagnetic zone centre (E_f=250 meV). (b) Constant Q cuts measuring the dispersion along the antiferromagnetic zone boundary (E_i =750 meV). The vertical dotted line at E=300 meV is a guide to the eye. A background measured near the nuclear zone centre (1,0) has been subtracted.

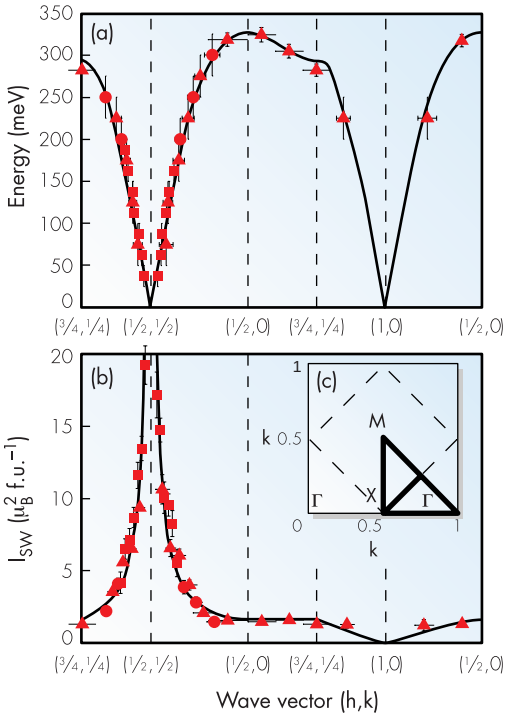

Figure H11.3. (a) Measured dispersion relation fitted to a spin-wave model including higher order couplings. (b) Wavevector-dependence of the spin-wave intensity compared with predictions of spin wave theory (solid line) with an intensity-lowering renormalization factor of 0.52±0.13 in agreement with the theoretical prediction of 0.61.

superexchange theory and experiments on $Sr_2Cu_3O_4Cl_2$. The data can also be explained by including a ring exchange interaction coupling quartets of spins at the corners of a square plaquette. A significant cyclic interaction is in fact predicted by expansions of the electronic Hubbard model to higher orders in (t/U) where t is the nearest-neighbour hopping energy and U is the on-site Coulomb repulsion. The extracted values t=0.32(2) eV and U=2.6(3) eV are consistent with values obtained from photoemission. The exchanges J=143.3±5 meV and J_c=48.4±9 meV are also in agreement with numerical simulations for finite clusters. We conclude that the dominant further neighbour coupling is the cyclic interaction favoured by the strong orbital hybridization in the CuO_2 planes.

R Coldea (ORNL and ISIS), **SM Hayden** (University of Bristol), **G Aeppli** (NEC Princeton), **TG Perring , CD Frost** (ISIS), **TE Mason** (ORNL), **S-W Cheong** (Lucent Technologies), **and Z Fisk** (University of Florida)

Experimental realization of a 2D fractional quantum spin liquid

The ground-state ordering and excitations of the two-dimensional (2D) *S*=1/2 frustrated Heisenberg antiferromagnet Cs_2CuCl_4 have been explored using neutron scattering in high magnetic fields. We find that the dynamic correlations show a highly dispersive continuum of excited states, characteristic of a 'resonating valence bond' (RVB) state, arising from pairs of *S*=1/2 spinons. Large quantum renormalizations of the excitation energies and incommensuration are observed.

The concept of fractional quantum states is central to the modern theory of strongly correlated systems. In magnetism, the most famous example is the 1D spin-1/2 Heisenberg antiferromagnetic chain where locally allowed *S*=1 states are de-confined into pairs of *S*=1/2 spinons identified with quantum domain walls. A 2D generalization of a fractional quantum spin liquid has been proposed to take the form of an RVB state comprising singlet spin pairings in the ground state, and with pairs of excited *S*=1/2 spinons separating via rearrangement of these bonds. To date no experimental realization of such a state has been found; in the case of the *S*=1/2 Heisenberg square lattice (HSL) mean-field confining effects lead to *S*=1 magnons and a renormalized classical picture emerges. However, frustrating interactions can counteract the staggered fields responsible for confinement, and they may provide a route to generating fractional phases in 2D. We explore such a scenario in the anisotropic triangular antiferromagnet Cs_2CuCl_4 using high-field diffraction on PRISMA and cold-neutron spectroscopy on IRIS.

In Cs_2CuCl_4 magnetic interactions are mostly restricted between Cu^{2+} *S*=1/2 spin-sites in the (*b*,*c*) plane, see figure H12.1(a), with coupling *J* along *b* ('chains') and zig-zag 'interchain' coupling *J*' along *c*. A small interlayer coupling stabilizes 3D order below T_N=0.62 K into an incommensurate structure along *b* due to the frustrated couplings; weak anisotropies confine the ordered moments to rotate in cycloids nearly coincident with the (*b*,*c*) plane (figure H12.1(c)).

Diffraction measurements were made on a single crystal of Cs_2CuCl_4 in magnetic fields up to 7 T using PRISMA. For fields along *a* (near perpendicular to the ordering planes) the 3D incommensurate 'cone' order is stable up to full ferromagnetic (F) alignment (B_c=8.44 T at *T*=0.03 K), see figure H12.1(b). At 0.2 K magnetic Bragg peaks move from ε_0=0.030(2) in zero field to ε=0.047(2) at 7 T, where ε is the incommensuration relative to Néel order, see figure H12.1(c). Mean field theory predicts no change with field, and the large renormalization observed is a purely quantum effect. The value at saturation ε_c=0.064 (estimated by extrapolating a quadratic fit) and the critical field B_c determine the couplings as

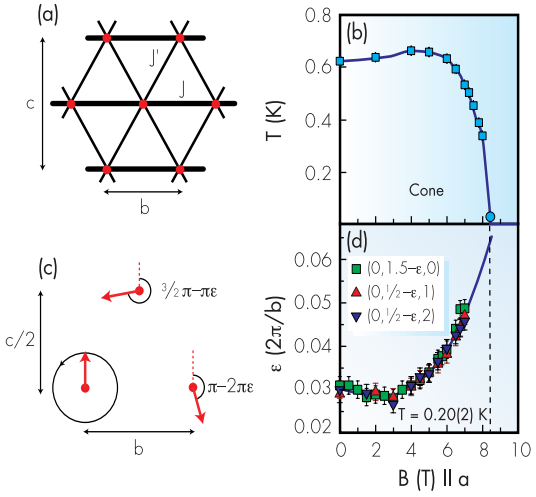

Figure H12.1. (a) 2D couplings in Cs_2CuCl_4. (b) Magnetic phase diagram in a field along a. *(c) Spin rotation in the* (b,c) *plane upon translation along the* b*-axis. (d) Incommensuration ε vs. field along* a.

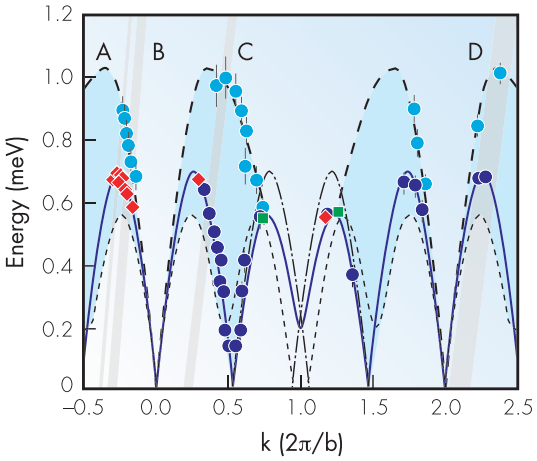

Figure H12.2. Dispersion of the magnetic excitations along b at T=0.1K, zero field. A, B, C, and D are typical scan trajectories with data shown in figure H12.3.*

J=0.37 meV, J'=0.15 meV and the quantum renormalization $\varepsilon_0/\varepsilon_c$=0.47.

Dynamical correlations in a 2.5 cm^3 single crystal of Cs_2CuCl_4 were probed using IRIS. The sample was mounted with the (a,b) scattering plane horizontal.

Figure H12.2 shows the dispersion along the b* direction; no measurable dispersion could be detected along a* confirming negligible coupling between layers. The solid symbols show the position of the main peak in the lineshape and the solid line is a fit to the principal spin-wave mode for a cycloid (dashed and dash-dotted lines show the calculated dispersions of the other two secondary modes). Light blue circles show the experimentally estimated upper boundary of the continuum and the upper (heavy) dashed line is a guide to the eye. The dispersion can be described by a spin-wave model with J_{sw}=0.62(1) meV and $J'_{sw}=2J_{sw}\sin\pi\varepsilon_0$. The quantum renormalization of the excitation energy J_{sw}/J=1.67 is similar to the exact result $\pi/2$ for the 1D chain.

A remarkable feature of the measured lineshapes is that they do not show single particle poles, but rather extended continua as shown in figure H12.3(a)-(d). Because in a neutron scattering process the total spin changes by ΔS_{total}=0, ±1 the absence of single-particle poles and the presence of excitation continua implies that the underlying excitations carry fractional quantum numbers. For J'=0, these are rigorously known to be S=1/2 spinons and two-spinon production is the principal neutron scattering process. The measured scattering can be well described by the Müller ansatz lineshape appropriate to the 1D J'=0 limit generalised to 2D such as to include the incommensurate dispersion relations and a modified upper boundary (dashed upper line in figure H12.2). We conclude that Cs_2CuCl_4 has fractional spin quasiparticles with a dispersion modified by the two-dimensionality at all energy scales.

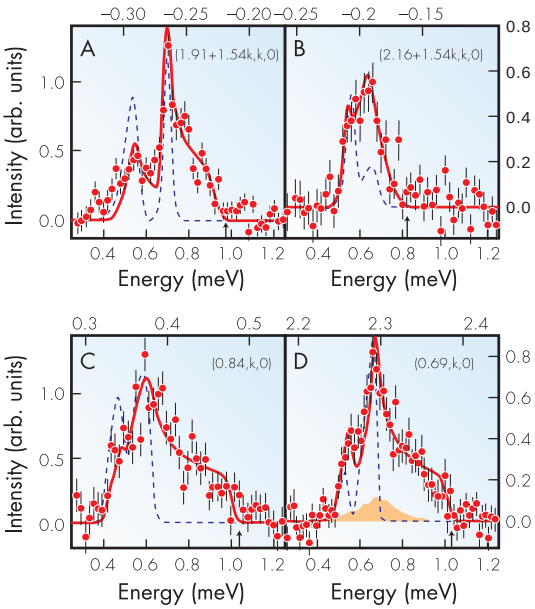

Figure H12.3. Magnetic inelastic spectra along the shaded regions A-D in figure H12.2. Solid lines are fits to a modified two-spinon cross-section. Dashed lines show predicted lineshape for polarised cycloidal spin waves and the dark shaded region (shown only in (d) for clarity) indicates the estimated two-magnon scattering continuum. All calculations include the magnetic form factor and instrument resolution effects.

R Coldea (ORNL and ISIS), **DA Tennant** (ISIS and Oxford), **AM Tsvelik** (Oxford), **MJ Bull**, **MA Adams** (ISIS), **Z Tylczynski** (Institute of Physics, Poland)

Structure and magnetism of doped ruthenium oxide superconductors

In recent years there has been considerable interest in the physics of transition metal oxide perovskites. This has been due to the discovery of colossal magnetoresistance in manganites, charge and spin stripes in nickelates and high T_c cuprate superconductors. The coexistence of superconductivity and magnetic order has proved particularly intriguing, since in conventional *s*-wave superconductors the local moment breaks up the spin singlet Cooper pairs and strongly suppresses superconductivity. Much research has focused on finding an explanation for the mechanism of superconductivity in high T_c materials and the interplay with magnetism. We have used time-of-flight neutron powder diffraction at OSIRIS at ISIS to enable us to probe the magnetic structure of a series of recently discovered ruthenium oxide superconductors. The ability of OSIRIS to observe magnetic reflections at long *d*-spacings with high resolution provides the key to the successful determination of the magnetic structure of these systems.

A recent systematic study has demonstrated the coexistence of superconductivity and magnetic ordering at lower temperatures in the double perovskite $Sr_2Y(Ru_{1-x}Cu_x)O_6$. The observation of a superconducting transition, by both magnetic and electrical measurements, with T_c as high as ~50K, in a system that contains no CuO_2 planes, is quite remarkable. Similar behaviour is also observed in samples in which the yttrium is replaced by holmium. Magnetic susceptibility measurements show the Ho compound to display similar behaviour but with an additional transition, presumably due to Ho-order, at ~15K while the sample remains superconducting. The observed magnetic and electrical features can be explained in terms of a plausible theoretical model based on the double exchange mechanism, which predicts the existence of canting order at a temperature lower than the magnetic ordering temperature.

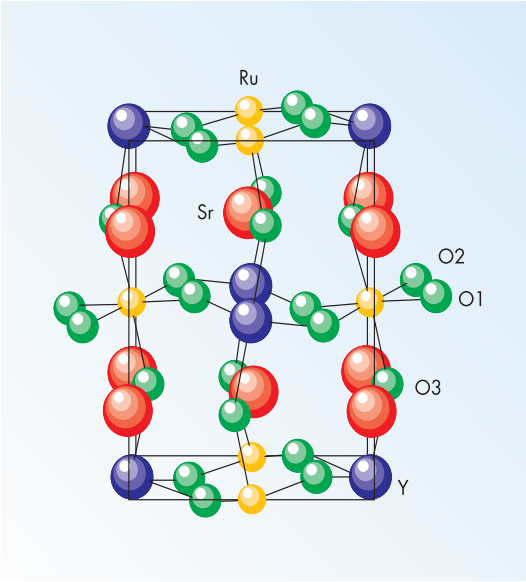

Figure H13.1. The crystal structure of $Sr_2Y(Ru_{1-x}Cu_x)O_6$

The $Sr_2Y(Ru_{1-x}Cu_x)O_6$ series was studied using high-resolution neutron diffraction at D2B at the ILL. The structure (figure H13.1) is that of the parent compound Sr_2YRuO_6 with copper atoms occupying the Ru-site rather than Y-site In addition to the structural peaks, antiferromagnetic peaks were observed at low scattering angles at temperatures below 28K confirming the magnetic order in a Type I spin arrangement of Ru ions. The requisite canting was not observed in these experiments due to insufficient resolution of the magnetic peaks. It was hoped that experiments at OSIRIS, with the extra intensity and higher resolution, particularly at high *d* spacing, would provide definitive answers on the existence of a second magnetic transition to a canted state and its relationship to the observed superconductivity.

The magnetic structure of $Sr_2YRu_{0.9}Cu_{0.1}O_6$ was shown to be more complicated than a simple Type I antiferromagnet. Preliminary analysis of the OSIRIS data strongly suggests that for the

$Sr_2YRu_{0.9}Cu_{0.1}O_6$, the Ru moments have a canted magnetic structure with the copper moments acting as a balance. Thus, although individual Ru and Cu moments are canted, the overall magnetic structure is one of ferromagnetic (001) planes, antiferromagnetically stacked. This observation is important in determining the superconducting mechanism in these materials.

More intriguing is the $Sr_2HoRu_{0.95}Cu_{0.05}O_6$ sample with the huge magnetic moment of the Ho^{3+} ion. Such a large magnetic moment is expected to have a tremendous impact on the magnetic structure and implications for the superconductivity in the sample.

The powder diffraction pattern is shown for this sample at 1.6 K in figure H13.2 and clearly the largest peaks in the pattern are the (100) and (010) magnetic peaks. Previous neutron studies had not been able to resolve these two peaks due to the similarity of the *a* and *b* lattice parameters (5.7692 Å and 5.7812 Å respectively) but due to the high intensity of OSIRIS at this wavelength and the good resolution, this was achieved. The closeness of the *a* and *b* values and the similar intensity of the magnetic peaks indicate that the moments are at 45° in the *a*-*b* plane. The Ru moments were similarly refined and the components of the moments in the *a*-*b* plane are shown in figure H13.3. Similarly, the same refinements determined the canting of the structure in the *a*-*c* plane as shown in figure H13.4.

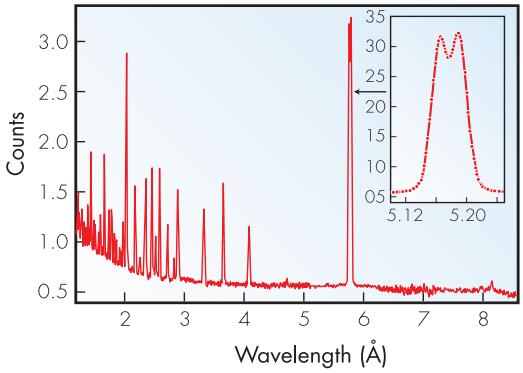

Figure H13.2. Neutron powder diffraction pattern of $Sr_2HoRu_{0.95}Cu_{0.05}O_6$ at 1.6 K from d = 1.5 Å to 8.5 Å. The inset shows the two magnetic peaks (100) and (010) resolved at ~5.77 Å and ~5.78 Å respectively.

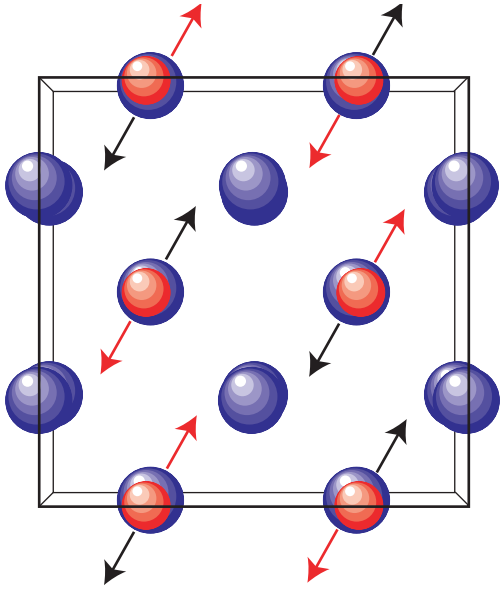

Figure H13.3. Magnetic structure projection in a-b plane of $Sr_2HoRu_{0.95}Cu_{0.05}O_6$. The Ho ions are represented by blue circles, the Ru ions red circles. The Ru moments are just shown in the c = 0 layer in black. The Ho moments are just shown in the c = ½ layer in red.

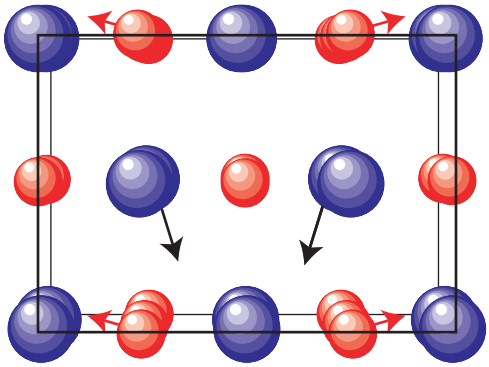

Figure H13.4. Magnetic structure projection in a-c plane of $Sr_2HoRu_{0.95}Cu_{0.05}O_6$. The Ho ions are represented by blue circles, the Ru ions red circles.

The observation of the two peaks was critical in terms of determining the canted magnetic structure of these materials and will have a profound impact on the proposed models of high temperature superconductivity in these systems.

Further studies of mixed ruthenium-copper oxide superconducting materials are planned to determine both their crystal and magnetic structures, and also the local magnetic environment with experiments on HET.

NG Parkinson, PD Hatton (University of Durham), **MK Wu** (National Tsing Hua University, Hsinchu, Taiwan), **KH Andersen** (ISIS)

Inelastic neutron scattering of bone

Inelastic neutron scattering (INS) spectroscopy is especially sensitive to vibrations of groups with hydrogen and has been used on TFXA and TOSCA to resolve the extent of substitutions at the hydroxyl group site in bone. Bone is a complex material consisting of a mineral apatite, $(Ca_5(PO_4)_3OH)$ in an extracellular protein matrix. Many aspects concerning the composition of the mineral are controversial. It has been suggested that there is complete substitution by carbonate at the hydroxyl site. We show, by INS, that in ox femur bone 40% of the hydroxyl groups are not substituted. The INS experiment opens up new opportunities to monitor changes in bone composition which are important in bone ageing and some pathological conditions.

The combination of strength and toughness of bone derives from its construction as a composite. Bone consists of a mineral, hydroxyapatite ($Ca_5(PO_4)_3OH$), in a matrix that is mainly collagen protein. The structure of hydroxyapatite viewed down the c-axis is shown in figure H14.1. The hydroxyl ions reside in channels, so that substitution by other ions, particularly carbonate, is facile. Changes in the spatial and temporal properties of bone are significant in the ageing process and in some pathological conditions caused by the incorporation of foreign ions.

There have been many studies on the composition and structure of bone mineral. Infrared and Raman spectroscopies provide information on carbonate substitution sites and on the presence of hydrogen phosphate. Despite this, the extent of carbonate substitution at the hydroxyl sites remains unresolved. Hydroxyl groups were not detected by resolution enhanced Fourier transform infrared spectroscopy of bone nor by proton magnetic resonance, leading to the suggestion that complete replacement of the hydroxyls had occurred.

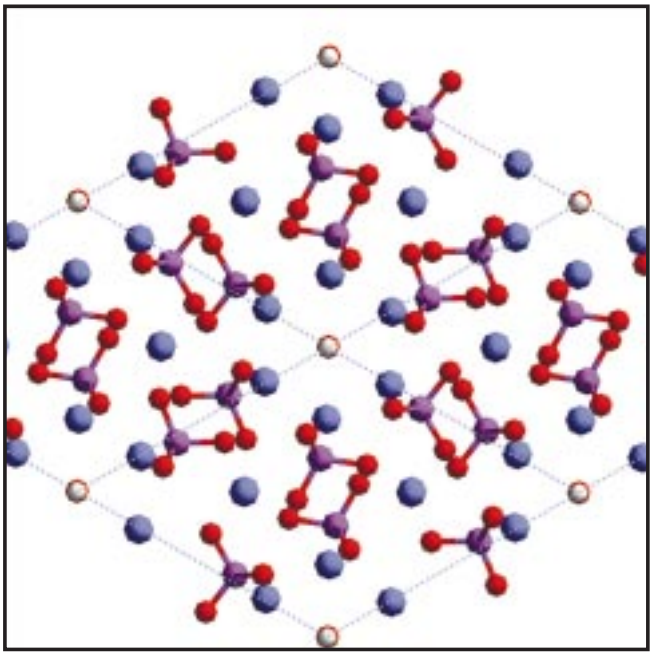

Figure H14.1. Crystal structure of hydroxyapatite in the ab-plane viewed down the c-axis. The hydroxyl ions lie in the channel formed by the calcium ions at the intersection of the four unit cells shown. (Hydrogen: white, oxygen: red, calcium: blue, phosphorous: purple).

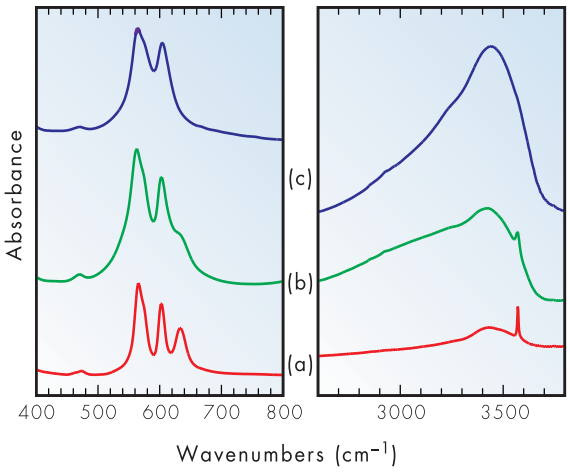

Figure H14.2. Comparison of the infrared spectra of (a) highly crystalline hydroxyapatite (b) poorly crystalline hydroxyapatite and (c) defatted, deproteinated, dried bone showing the regions of the hydroxyl stretching vibration on the right and the hydroxyl libration on the left.

INS spectra using TFXA and TOSCA, as well as infrared and Raman spectra of ox femur and two standard hydroxyapatite samples of different degrees of crystallinity, were recorded. The bone was successively defatted and then deproteinated and spectra were obtained at each stage before and after drying.

Figure H14.2 shows the infrared spectra of a highly crystalline hydroxyapatite, a poorly crystalline hydroxyapatite and the defatted, deproteinated, dried bone. The hydroxyl group has two characteristic vibrations; the stretching mode at 3572 cm^{-1} and the librational mode at 650 cm^{-1}. In the highly crystalline hydroxyapatite both bands are clearly resolved, in the poorly crystalline material, the 650 cm^{-1} band is only apparent as a shoulder and in the bone, there is no evidence for hydroxyls at all. Concurrent with the disappearance of the hydroxyl modes, bands due to carbonate (broad feature at ~1400 cm^{-1}) grow in, consistent with replacement of hydroxyl by carbonate.

INS spectra of the same three samples are shown in figure H14.3. In agreement with the infrared spectra, the highly crystalline hydroxyapatite shows an intense librational mode at 650 cm^{-1}, the poorly crystalline material shows a band at the same frequency but significantly broader. However, the spectrum of bone shows a broad but distinct feature at the same frequency, indicating the presence of hydroxyl. This is in marked contrast to the infrared results. The width of the feature explains why it is not observed in the infrared spectra.

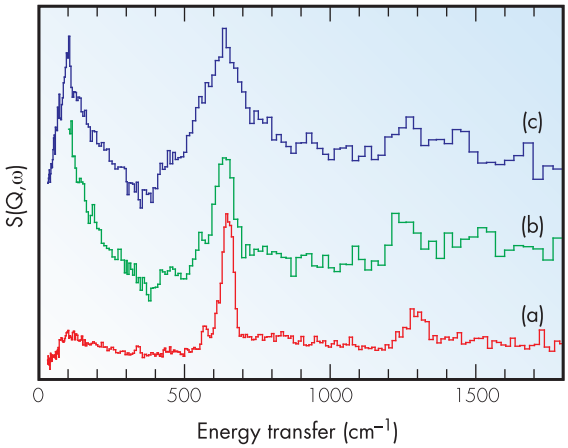

Figure H14.3. Comparison of INS spectra in the region of the OH librational mode of the same samples shown in figure H14.2. (a) Highly crystalline hydroxyapatite, (b) poorly crystalline hydroxyapatite and (c) defatted, deproteinated, dried bone.

To determine the relative hydroxyl concentration in the bone compared with the highly crystalline hydroxyapatite, we integrated the peaks between 500 and 750 cm^{-1} normalising the relative intensities to 1 gm of material. The hydroxyl concentration in the bone was 42% of that in the highly crystalline hydroxyapatite, thus a significant fraction of the hydroxyl groups remain in the bone.

The INS studies of bone mineral have shown how the question of the extent of carbonate substitutions at the hydroxyl sites in bone can be resolved and have also allowed us to demonstrate why the OH libration mode is not always seen in the infrared spectra. This work opens up opportunities of exploiting INS to monitor changes in the composition of bone at various stages in its growth and maturity and in pathological conditions.

MG Taylor (University of Reading), **SF Parker** (ISIS), **K Simkiss, PCH Mitchell** (University of Reading)

Dynamics of H_2O in confined 2D geometry

The diffusion of water molecules or hydrogen atoms in confined geometries has a large variety of applications, such as in biology, food and soil science. It is therefore important to elucidate the nature of the diffusive dynamics of confined water. In this work we have used a hydrated Na-vermiculite clay as an ideal model system for water in a confined 2D geometry. The water dynamics has been studied at ambient temperature, as well as in its supercooled regime, by quasi-elastic neutron scattering (QENS) and dielectric spectroscopy. The experimental results suggest that the temperature dependence of the relaxational dynamics of the confined supercooled water changes from a highly fragile behaviour at high temperatures to an Arrhenius behaviour at low temperatures, in accordance with a proposed fragile-strong transition around 228 K for supercooled bulk water.

The behaviour of water in confined geometries and near solid surfaces is of central importance in nature since most of the water in, for instance, living organisms is closely associated (within approximately 5 Å) with different kinds of biomolecules. Since this associated water is necessary for all living organisms it is essential to elucidate its microscopic properties and functional role. A comprehensive description of the structure and dynamics of biomolecules hydration water is however a difficult task and therefore we have used a geometrically more well-defined model system for such a study. The Na-vermiculite clay chosen was studied with three hydration levels, corresponding to zero, one and two molecular layers of water between the regularly spaced clay platelets.

The QENS experiments were carried out at T=265 and 300 K in two different scattering geometries; the clay platelets being at angles of 45° and 135° to the incident beam in order to make the elastic Q-vector perpendicular and parallel, respectively, to the clay platelets for a scattering angle of 90° (Q ~1.33 $Å^{-1}$). In the case of the one-H_2O layer Na-vermiculite the data were satisfactorily fitted with a single Lorentzian convoluted with the resolution function, whereas two Lorentzians were needed to fit the spectra of the two-H_2O layer system. From the directional dependencies of the quasi-elastic intensities it is evident that almost no water dynamics occurs perpendicular to the clay platelets on the experimental time-scale (about 2-40 ps).

Figure H15.1 shows that the two-H_2O layer vermiculite exhibits a planar rotational motion

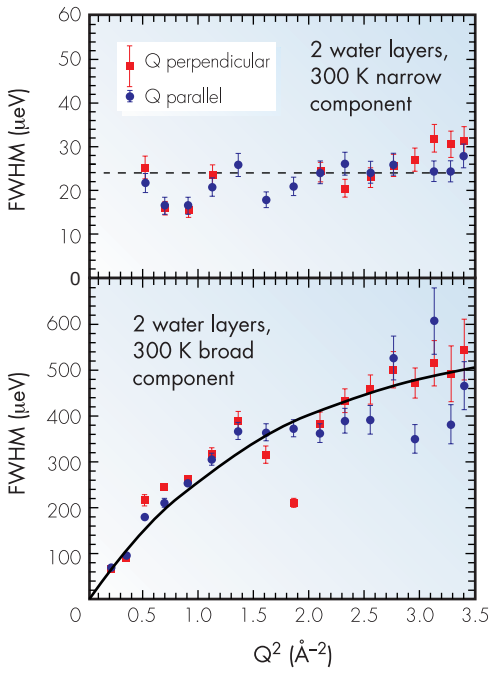

Figure H15.1. FWHM values of the two quasi-elastic components as a function of Q^2 for the fully hydrated Na-vermiculite clay at 300 K. Red squares and blue circles correspond to sample orientations where the clay platelets are aligned perpendicular and parallel, respectively, to the Q-vector at a scattering angle of 90°.

of water molecules and a basically two-dimensional translational jump diffusion motion on the experimental time-scale. Since the correlation time of the rotational motion was estimated to be as long as 27 ps the motion is interpreted as arising from rotating hydration shells around the intercalated Na ions. The translational motion was modelled using the Gaussian jump-length distribution model, resulting in a mean jump length (1.1 Å) and an average residence time (2.3 ps) similar to the corresponding values for bulk water. This suggests that the short range hydrogen bonding interactions are mainly determining the water dynamics.

In the case of the one-H_2O layer vermiculite we were only able to observe a planar rotational motion with a rotational correlation time of 16 ps, i.e. faster than in the two-H_2O layer vermiculite. This suggests that a smaller number of water molecules are involved in the rotational process in the one-H_2O layer vermiculite, and furthermore that the translational motion, if existent, is too slow to be observed on the experimental time-scale.

The dielectric data of the two-H_2O layer vermiculite shows a strong dielectric loss peak (absent in the one-H_2O layer vermiculite), corresponding to the main α-relaxation process of the interlayer water not interacting with the clay surfaces. It has an Arrhenius temperature dependence and a relaxation time of 100 s at T=127K (glass-transition temperatures in the range 124-136K have been reported for bulk water).

The combination of high temperature (265K-300K) QENS data and low temperature (125K-215K) dielectric data of the 'free' water molecules in the two-H_2O layer vermiculite suggests that the temperature dependence of the relaxational dynamics changes from a highly fragile behaviour at high temperatures to an Arrhenius behaviour at low temperatures, in accordance with a proposed fragile-strong transition around 228 K for supercooled bulk water.

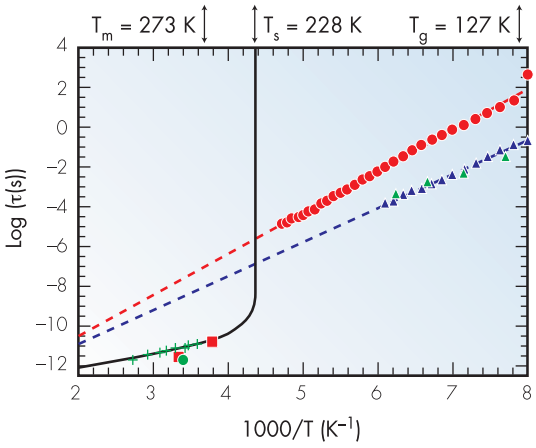

Figure H15.2. Relaxation times obtained from fits of the dielectric and neutron scattering spectra from the fully hydrated Na-vermiculite clay together with literature data. The red circles denote the relaxation times for the main dielectric relaxation and the blue triangles show the relaxation time of the second process observed at low temperatures. The green triangles, coinciding with the relaxation times of the second process, are from Cole-Cole fits of dielectric spectra of bulk ice. The dashed straight lines are fits to the Arrhenius equation, $\tau = \tau_0 exp(E/RT)$. Also included are new literature data (green crosses) of the dielectric relaxation time of bulk water at higher temperatures. The full line through the data is a power-law fit diverging at T_s = 228 K. The residence times of the neutron scattering data of our system (red squares) coincides with the neutron scattering data (green circle) and the dielectric relaxation data of bulk water.

J Swenson and R Bergman (Chalmers University of Technology) **W S Howells** (ISIS)

Li mobility in the battery cathode material $Li_x[Mn_{1.96}Li_{0.04}]O_4$: a technological application of μSR

The common use of rechargeable batteries as power supplies means that it is important for them to be cheap, light and environmental friendly, properties shown by the newly developed battery which uses $Li_x[Mn_{1.96}Li_{0.04}]O_4$ as the cathode material. We have characterized the Li^+ mobility in $Li_x[Mn_{1.96}Li_{0.04}]O_4$ with the zero-field muon spin depolarization technique. The results suggest that the battery could be recharged more efficiently above room temperature than at room temperature as is usually done.

For several decades batteries have been used in consumer electronics such as cameras, multimeters and radios, and more recently they have become common in laptop computers and cellular phones. There is still a demand for new batteries with good rechargeable properties, and research into materials which are harmless to the environment is ongoing. A primary objective is to use light metals, instead of heavy metals which are a source of pollution. Additionally, for some applications, batteries have to be stable at high temperature. They must also be inexpensive to produce.

Materials of the composition $Li_x[Mn_{2-z}Li_z]O_4$ with the spinel cubic structure are very promising as cathodes for Li batteries. In combination with boriumphosphate as the intermediate solid electrolyte and carbon or B_2CN as the anode, these materials form excellent solid state rechargeable batteries, fulfilling all the requirements mentioned above. They are based on the transport of Li ions, which are light and give a high power density per unit. Since compounds of the type $Li_x[Mn_{2-z}Li_z]O_4$ are ceramics, they give access to an interesting temperature range from 320K up to at least 380K. This explains why Li batteries are found in sensors on drilling heads in the oil industry.

As shown in figure H16.1 the flow of Li^+ ions induces a voltage difference between the anode and cathode of the battery when it is used as a power supply. The battery operates between the x = 0.2 ('charged') and x = 1 ('empty') states. The x refers to the degree of occupation of the regular Li sites.

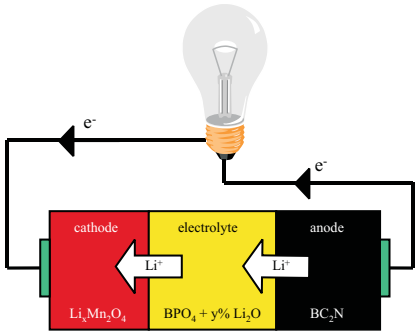

Figure H16.1. Principle of a battery based on the cathode material $Li_xMn_{1.96}Li_{0.04}O_4$ working as a power supply.

Pure $LiMn_2O_4$ (x = 1, z = 0) contains equal amounts of Mn^{3+} and Mn^{4+} ions. It undergoes a phase transition at ≈ 290K attributed to a cubic to tetragonal structural transition driven by a cooperative Jahn-Teller distortion mechanism around the Mn^{3+} cation sites, and this makes it unsuitable as a cathode because of the bad cycling performance. Small Li substitution on to Mn sites gives rise to an increase in Mn^{4+} concentration and subsequently a small decrease in Mn^{3+} concentration, leading to an increased stability of the cubic spinel structure.

$Li[Mn_{1.96}Li_{0.04}]O_4$ does not exhibit a structural phase transition, and this makes it very suitable as a cathode material. On the other hand, for efficient operation of the cathode, the amount of Li substitution, i.e. the amount of Mn^{4+} ions, must be restricted. Optimal battery prototypes work with $0.04 \leq z \leq 0.06$.

To optimize $Li_x[Mn_{2-z}Liz]O_4$ for use as a cathode material, the Li^+ mobility ion for different x and z values needs to be known. Therefore we have performed a detailed investigation of the Li^+ ions behaviour with the zero-field muon spin relaxation (μSR) technique for x=1 and x=0.2 with z=0.04.

The μSR measurements were done at the EMU

and MuSR spectrometers of the ISIS facility. Above 100K, the muon depolarisation function could be fitted by the product of an exponential relaxation function with the so-called dynamical Kubo-Toyabe function. The exponential component is due to the relaxation on the Mn magnetic moments; it is relatively small and temperature independent. The depolarization is mainly due to the quasi-static field distribution induced at the muon site by the nuclear magnetic moments of Li and Mn. The distribution is characterized by its variance Δ^2.

As shown in figure H16.2, Δ drops by $\approx$ 35% between 230K and 300K for $Li[Mn_{1.96}Li_{0.04}]O_4$. For $Li_{0.2}[Mn_{1.96}Li_{0.04}]O_4$ the drop of Δ is even larger but starts at $\approx$ 300K. This thermal dependence of Δ cannot be a muon diffusion effect; in fact the muon is quasi-static for both compounds in the whole temperature range investigated. The decrease of Δ can only be understood if we suppose that some of the Li^+ ions do not contribute any longer to the depolarization. This means that, as the temperature is raised, some of the Li^+ ions diffuse and their contribution to the muon depolarisation is motionally narrowed. A quantitative discussion of the magnitude of Δ supports our interpretation.

We performed some measurements up to 600K. In figure H16.3 we compare two spectra recorded at 300 K on $Li_{0.2}[Mn_{1.96}Li_{0.04}]O_4$. One spectrum was taken before heating the compound above 300K.

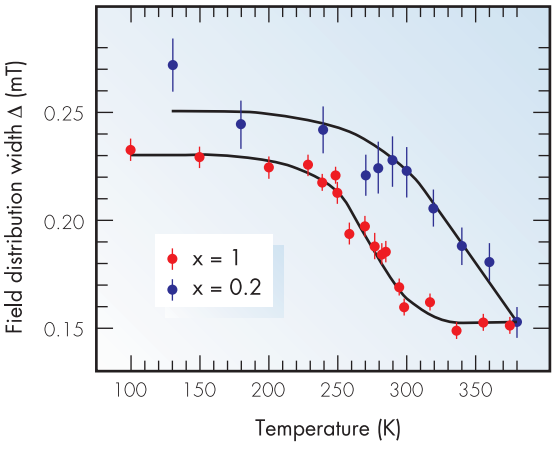

Figure H16.2. Kubo-Toyabe linewidth Δ measured up to 380K for $Li[Mn_{1.96}Li_{0.04}]O_4$ and $Li_{0.2}[Mn_{1.96}Li_{0.04}]O_4$. The solid lines are guide to the eye.

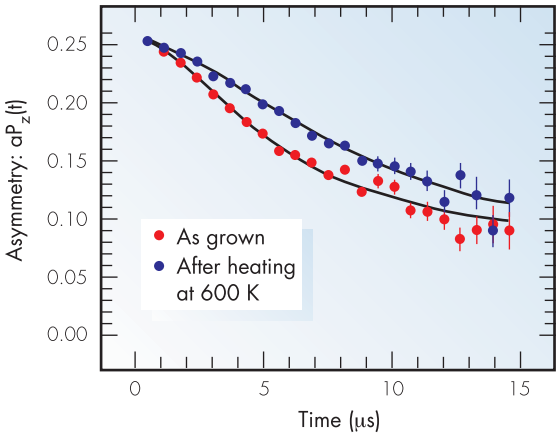

Figure H16.3. Comparison of two μSR spectra of $Li_{0.2}[Mn_{1.96}Li_{0.04}]O_4$ measured in zero field at 300K. The solid lines are fits to the data.

The other spectrum was recorded after measurements done up to 600K. Clearly the two spectra are different. The observed irreversibility is not surprising since it is known that a phase transition occurs at $\approx$ 490K. We have checked that no irreversibility effect occurs if the two compounds (x = 0.2 and x = 1) are heated only up to 380K.

In contrast to the Li^+ ion behaviour, the muon is quasi-static in the whole temperature range investigated. This rather surprising result is understood if the diffusing particle passes through a bottle neck in the transition state as for example if it has to squeeze through the lattice from one interstitial state to the next. Then the lighter particle has the higher activation energy and so may not diffuse as fast as the heavier particle.

In conclusion we have discovered that the onset of Li^+ diffusion in $Li[Mn_{1.96}Li_{0.04}]O_4$ occurs at 230 K and for $Li_{0.2}[Mn_{0.96}Li_{0.04}]O_4$ at 300 K, i.e. just above room temperature. This latter result suggests that the battery could be recharged more efficiently above 340 K than at room temperature as usually done since, according to figure H16.2, the Li^+ ions start to diffuse above 300 K. However, the temperature should not be too high to avoid irreversibility effects. Quite remarkably, for our study we did not need a single crystal sample. In fact our sample was quite close to the cathode material which will be used in commercial batteries.

CT Kaiser, VWJ Verhoeven, PCM Gubbens (IRI, TUDelft, The Netherlands)
P Dalmas de Réotier, A Yaouanc (CEA-Grenoble, France), **SP Cottrell** (ISIS)

Muonium models for hydrogen defect centres in CdS and GaN

A novel muonium state discovered by μSR studies of CdS implies that interstitial hydrogen forms a shallow-donor state in this and perhaps other II-VI compound semiconductors. This result is without precedence, the various muonium and hydrogen defect centres known in Group IV semiconductors (Si, Ge) and in III-V compounds (GaAs, etc) all having energy levels which lie deep in the semiconducting energy gap. In GaN, μSR data are likewise clarifying the structure and dynamics of muonium states which mimic the behaviour of hydride ions. In all of these new wide-gap materials currently being developed for solar cells and for blue light emitters, hydrogen impurity influences fabrication processes and can also alter final electrical properties. The μSR studies are providing a unique atomistic picture of hydrogen behaviour and are now extending our understanding of its site preferences and dynamics from covalent to ionic semiconductors.

With applications in photovoltaics and optoelectronics in mind, ionic semiconductors with wide bandgaps are the subject of intensive R&D efforts worldwide. CdS and other II-VI compounds, together with the related chalcopyrites, are the most promising materials for the fast-developing thin-film solar cell industry. GaN and its alloys with other Group-III nitrides are being developed for blue light emitting diodes and lasers. Hydrogen impurity, incorporated during the processing of these materials, can have a profound influence on electronic properties even in trace quantities. Yet atomistic pictures of its crystallographic sites and dynamical behaviour are lacking.

We need to understand what sites are occupied by the various charge states — the interstitial proton, the neutral trapped atom and the hydride ion — together with the mobilities of each state, their relative stabilities as a function of temperature and doping, and the possible processes of interconversion caused by capture and loss of charge carriers. This is exactly the sort of information provided by studies, not of the hydrogen states themselves, but of their muonium counterparts. Here, muonium is the light pseudo-isotope of hydrogen in which the proton is replaced by a positive muon. Suitable sources of muons are available at ISIS and at a few other facilities worldwide (PSI, TRIUMF and KEK). The muons are stopped (not scattered) in the sample, so that in semiconductors an individual muon can either remain as the positive ion, mimicking the interstitial proton, or pick up an electron to mimic atomic hydrogen. Occasionally a muon can pick up two electrons to form the hydride-ion analogue. μSR spectroscopy has the sensitivity and selectivity to detect muonium in all its different charge states and to characterise their structure and dynamics.

Cadmium sulphide

Neutral muonium centres are recognizable by the distinctive hyperfine coupling between the muon and the single unpaired electron; a slow beating in the muon spin rotation signal shows

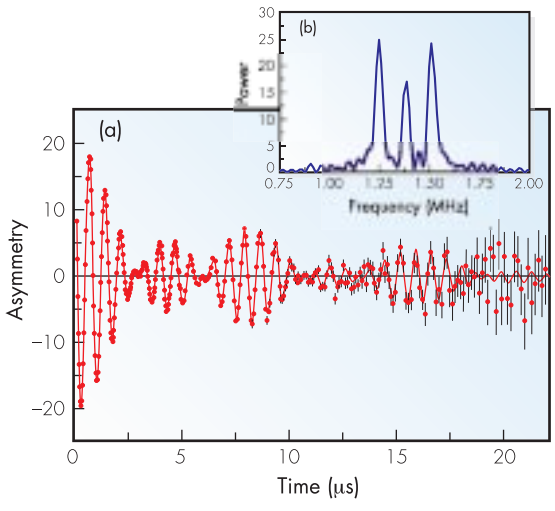

Figure H17.1. Muon spin rotation signal in CdS recorded on EMU at 3.7K and its Fourier transform.

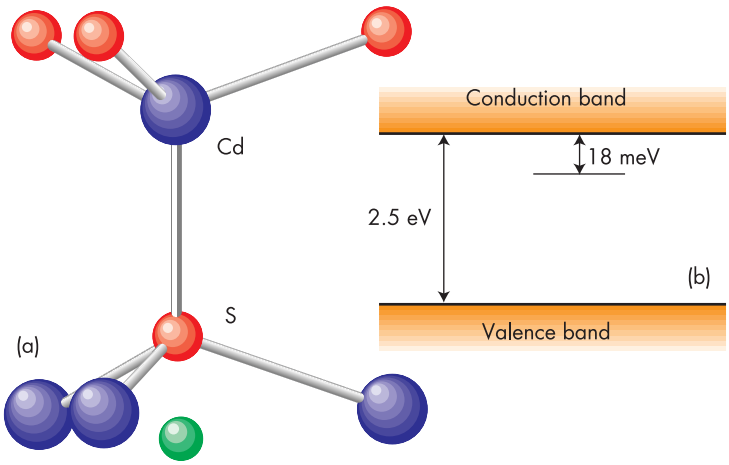

Figure H17.2. Antibonding site (a) and energy level scheme (b) for the novel shallow donor state of muonium or hydrogen in CdS.

this in CdS, figure H17.1. The corresponding frequency-domain signal exhibits satellite lines on either side of the muon Larmor precession frequency: the frequency splittings are a measure of the muon-electron hyperfine interaction. Spectra of this sort require a particularly low background; those from PSI have recently been improved in this respect by the MORE (Muons On REquest) development but the pulsed muon source at ISIS still offers the cleaner spectra — in figure H17.1 out to almost 10 muon lifetimes.

The muonium hyperfine interaction in CdS is just 50 ppm of the free-atom value, indicating that the electron wavefunction is highly dilated. It corresponds to a shallow, rather than a deep-level defect with the ionization or binding energy deduced to be 18 meV. This finding is without precedent, since no shallow state was known previously for hydrogen or muonium in any semiconductor. In figure H17.2 we assign the muon to a site which is antibonding to sulphur (as would also be expected for the positive ion or interstitial proton in this ionic material).

A unified picture

Our work on a variety of covalent and ionic materials allows proposal of the following general description, to be tested by future experiments. The stable states are the positive (in p-type material) and negative (in n-type) ions. Whereas the positive ion adopts the bond-centre site in covalent materials it prefers an antibonding site in ionic materials. The negative ion invariably prefers an antibonding or cage-like site in all materials - in GaN we find it antibonding to Ga. Neutral centres can be formed from each without site change, leading to metastability or choice of site for the neutral states. In Si, Ge and GaAs the neutral states associated with the positive ions are bond-centred, forming a donor level quite deep in the gap, and with electronic spin density localised on the two nearest neighbour host atoms. In CdS, the neutral state associated with positive ion proves instead to be shallow, with the electron wavefunction distributed over many host atoms. In all materials, the neutral centres associated with negative ions have their electron wavefunctions tightly localized on the muon or proton and the corresponding acceptor levels lie deep in the energy gap.

At normal temperatures, the neutral states are short-lived but transitions in and out of them control the capture and loss of conduction electrons or the dynamic exchange of charge with other nearby defects. At cryogenic temperatures, on the other hand, where no such exchange is possible, the neutral states can be relatively long lived and they are naturally formed when an implanted positive muon comes to rest bringing an electron with it; they are then particularly informative on local structure via their hyperfine and superhyperfine interactions. Their stability against conversion to other states likewise defines the influence of real material properties, notably doping, temperature and the presence of other defects or impurities. As a guide to the behaviour of hydrogen impurity in these materials, the new muonium data are virtually unique. Local geometric and electronic structures are essentially identical for muonium and hydrogen, subject only to small zero—point corrections; the dynamical behaviour can exhibit significant isotope effects but all this information should carry over, mutatis mutandis, to the properties and behaviour of hydrogen itself.

SFJ Cox (ISIS), **J Gil** (University of Coimbra), **A Weidinger** (HMI Berlin), **R Lichti** (Texas Tech University, Lubbock)

Lighter, stiffer, stronger . . . engineering aeroengines for the 21st century

Innovative aeroengine designs demand combinations of properties unavailable in conventional advanced alloys. In principle, metals reinforced with ceramic fibres can meet the need, but in practice thermal stresses caused by differences in thermal expansion between the phases need to be monitored and intelligently managed through the manufacturing process. The challenge is to measure the stresses in the fibres and matrix in prototype components at depths of many millimetres non-destructively. Neutron strain scanning on ENGIN is providing the solutions.

The drive toward improving the thrust - weight performance of modern aeroengines places ever increasing demands on the materials from which they are made, with the present challenge to develop lighter, stiffer, stronger materials (figure H18.1). Composites are attractive in this respect, and the combination of ceramic fibres within a titanium alloy as a Ti Metal Matrix Composite (TiMMC) offers the designer the potential to save weight in highly loaded rotating structures, enabling integrally bladed ring structures (blings) to be considered as an alternative to traditional bladed discs. Such structures are, of course,

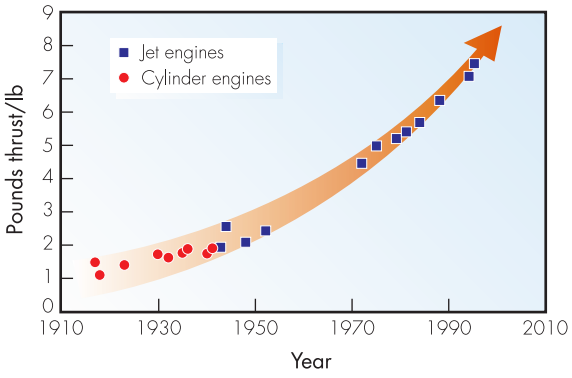

Figure H18.1. New aeroengine designs require new materials, the use of Ti/SiC composite reinforced components would lead to significant improvement in thrust-to-weight ratio.

predominantly hoop loaded, with stresses much higher than their conventional counterparts, and hence composite rings are constructed as hoop reinforced structures to take advantage of the high strength and stiffness along the fibre axis,

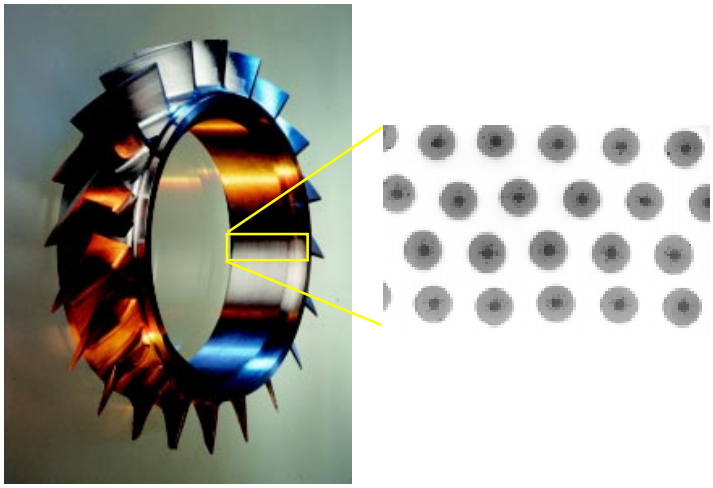

Figure H18.2. A prototype Ti/SiC reinforced bling, courtesy of Rolls-Royce plc.

in much the same way that a tennis racket is hoop wound to resist hoop compression. A prototype structure is shown in figure H18.2.

The production of integrally bladed rings presents considerable manufacturing challenges. They are first produced as a cylindrical blank by hot isostatic pressing at temperatures in excess of 900°C prior to substantial machining to form the final shape. While it has been shown on laboratory composite test-pieces that considerable thermal stresses are generated between the cladding, matrix and fibre constituents, until recently it has not been possible to measure the stresses in real components. Furthermore, as machining modifies the residual stress state, a non-destructive technique is required if one is to monitor the evolution of stress through the complete

processing route. Neutron strain scanning is perhaps the only method capable of measuring the elastic strains non-destructively at the depths required for this component. Furthermore, because Bragg diffraction is phase selective, the technique provides an atomic strain gauge for each phase of the composite separately.

ENGIN, the purpose built neutron strain scanning instrument on the PEARL beam line, is well suited to this type of measurement. The focusing collimators mean that detectors occupy large areas of diffraction space around $2\theta=90^\circ$ to give good data collection rates with low levels of background. This is essential for the long path lengths (up to 20 mm) required to locate and monitor the SiC fibres since they are clad in Ti-6%Al-4%V alloy (titanium is a strong attenuator and both Ti and V are strong incoherent scatterers). Strains have been mapped to 1.5 mm spatial resolution. Furthermore, the fact that complete diffraction profiles are collected as a function of time of flight means that it is simple to identify when the reinforced region is reached.

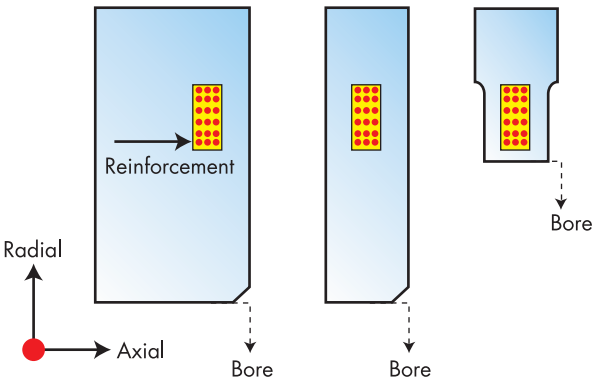

Figure H18.3. Schematic of the machining steps required to form the bling.

In a collaboration between Rolls-Royce plc. and the University of Manchester, funded as a joint EPSRC/MOD project, the strain evolution is being monitored on a single component through the various stages of manufacture shown in figure H18.3. At the same time a finite element model

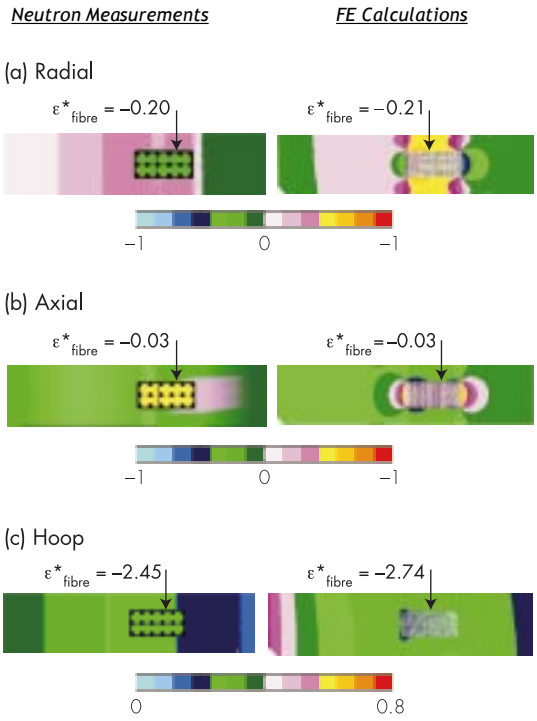

Figure H18.4. A side by side comparison of the strain field measured on ENGIN and predicted by finite element modelling (in normalised units). ε^*_{fibre} is the normalised strain of the SiC fibres.

has been constructed to predict the measured strains in the initial bling blank and after each subsequent manufacturing stage. It is clear that the volume fraction of the composite region becomes successively greater as more and more cladding is removed. As a result the fibre strains decrease and cladding strains increase through the stages. Measurements on stages I and II show excellent agreement with the manufacturing FE model. This is exemplified by the agreement between the predicted and measured strain maps in figure H18.4. As might be expected, large compressive hoop strains are observed in the SiC fibres with correspondingly lower hoop tension in the Ti-6Al-4V cladding. As with any material, the understanding of residual stress is an important element of safe life prediction.

JWL Pang, G Rauchs, PJ Withers (Manchester Materials Science Centre, University of Manchester) **NW Bonner, ES Twigg** (Rolls-Royce Plc., Derby)

Megawatt upgrades for ISIS

ISIS beam power is presently 160 kW, and is set to increase to 240 kW on installation of a dual harmonic RF (DHRF) system now under development. Here we describe upgrade options for higher beam powers, between 0.5 and 5.0 MW. A summary is given of options for a scheme of staged upgrades which exploit the existing accelerators and infrastructure, and provide long term flexibility.

The dual harmonic RF upgrade

Presently, ISIS is based on a 50 Hz high intensity proton synchrotron which accelerates 2.5×10^{13} protons per pulse (ppp) to 800 MeV, providing two 100 ns pulses spaced by 220 ns to the spallation target. Installation of the DHRF system, adding four new RF cavities operating at the 4th harmonic to the six existing 2nd harmonic devices, is expected to increase the intensity to 3.75×10^{13} ppp which is equivalent to 0.24 MW.

Upgrade options

Power levels above 0.24 MW require substantial increases in beam current or energy or both. The requirements of machine protection and 'hands on' maintenance mean beam loss is a critical issue in any upgrade and should be limited to present ISIS levels at most.

Increasing the injection energy into the existing ring would reduce space charge related losses and provide increases in current. However, losses associated with a larger extracted emittance, the problems of injecting higher energy beam in limited space, and the practicalities of upgrading the injector with minimal interruption to operations, do not make this a favoured option.

The scheme with the most potential is the addition of further rapid cycling synchrotrons (RCS's), raising the energy of the existing beam to 3.5 GeV.

Principal concerns for the 3.5 GeV RCS are provision of space for the required RF systems, and keeping beam losses below 0.1%. This has influenced the selection of a repetition rate of 25 Hz and a circumference twice that of the existing ring. The RF system provides four RF buckets, matched to the structure of the 0.8 GeV fast injected bunches, for near lossless capture.

Upgrades to 1 MW

There are a number of possible schemes for operating 25 Hz high energy rings, with a 50 Hz 'injector', to achieve upgrades to 1.0 MW.

The preferred option, which is more expensive but has much potential, uses two 25 Hz, 3.5 GeV RCS's filled on alternate 50 Hz cycles, with two out of four RF buckets being occupied during acceleration.

The other, cheaper option uses a 25 Hz, 3.5 GeV RCS plus a 0.8 GeV storage ring (SR). Here, two 0.8 GeV bunches are stored for 20 ms, until the next two bunches emerge from the 50 Hz RCS, and all four are then injected into the high energy ring. Following the 20 ms acceleration interval the beam is extracted in a single turn and transported to the appropriate targets.

To provide convenient, manageable stages for the upgrade, a single 25 Hz RCS could be added initially, providing 0.5 MW to a new target and leaving the remaining 25 Hz, 0.12 MW beam going

	Description	*Power (MW)*
0	Present status	0.160
1	Current DHRF upgrade	0.240
2	Add 1x3.5 Gev RCS, 25 Hz	0.645
3	Add 2x3.5 GeV RCS, 25 Hz	1.05
3(a)	Add 1.3.5 GeV RCS + SR	1.05
4	Add 2x3.5 GeV RCS + 800 MeV Linac	5.0
4(a)	Add 2x3.5 GeV RCS + 0.8 GeV RCS	2.0

Table H19.1. Summary of upgrade routes for ISIS.

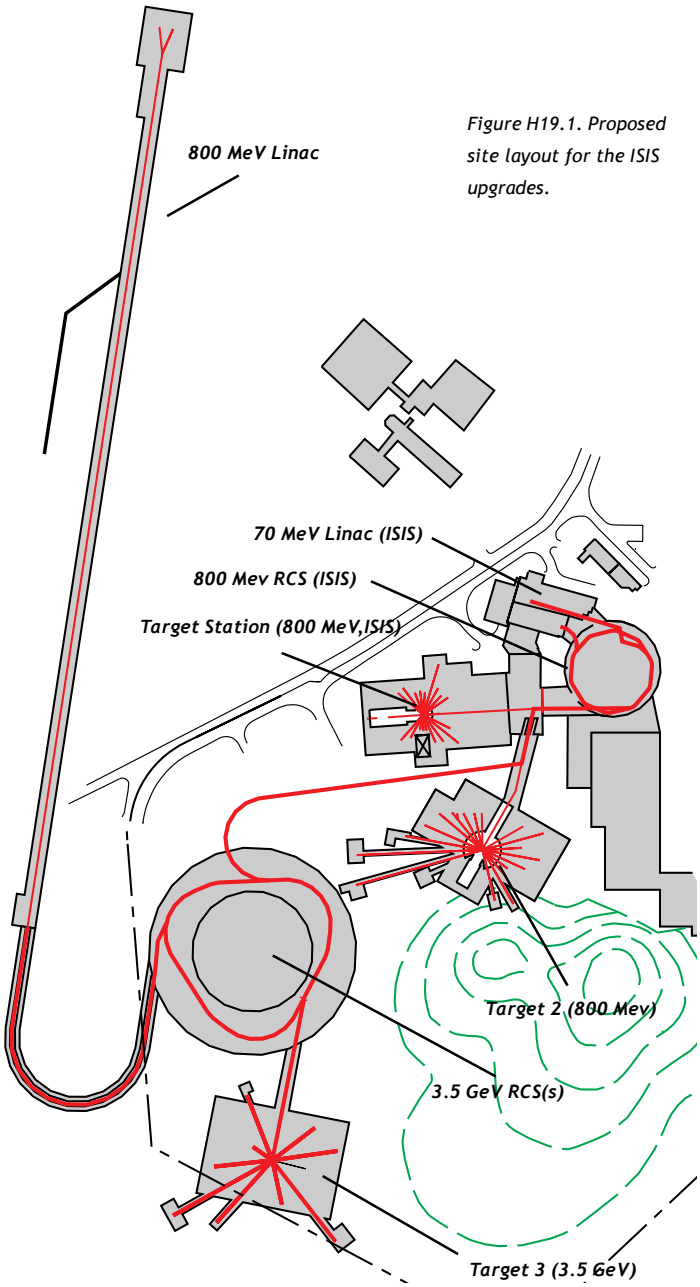

Figure H19.1. Proposed site layout for the ISIS upgrades.

to the existing target. Beam could also be directed to the planned new low power second ISIS target station. At a later stage, a second RCS or storage ring would be added, taking the power to 1.0 MW.

These upgrades should all be possible with minimal interruption to the ISIS operational programme.

Beyond 1 MW

The addition of a second 800 MeV RCS, fed from the present 70 MeV injector, could be used to fill the two free RF buckets in each new 3.5 GeV RCS. In this scheme all four RF buckets of each 3.5 GEV RCS would be occupied on each 25 Hz cycle, taking the power to 2.0 MW.

To take beam power to 5.0 MW levels, the most promising route would involve converting the two 3.5 GeV RCS's to multi-turn charge-exchange injection, and adding an 800 MeV linac. This is similar to a scheme already studied for the European Spallation Source. It would require some careful ring lattice design to allow conversion to the highly optimised multi-turn injection scheme.

Site Layout

The 0.5 to 5 MW upgrade paths detailed above require the siting of a new 800 MeV RCS, one or two vertically stacked 3.5 GeV RCS's, a new 800 MeV linac, a target station and the associated injection/extraction beam lines. A possible layout is shown in figure H19.1.

Upgrades to 1 MW use the existing ISIS infrastructure as an injector. An 800 MeV beam could feed the new 3.5 GeV ring(s) using a beam line which extracts from the existing 800 MeV beamline or the proposed Second Target Station beam line. This would have minimal effect on the ISIS user run schedule since the extraction point could be built within a scheduled maintenance period.

A 2 MW upgrade uses a new 'ISIS like' 800 MeV ring. This would probably be stacked on top of the existing ring to make optimal use of the 800 MeV beam lines. The impact on the ISIS user schedule would have to be carefully considered.

The 5 MW upgrade requires a new 800 MeV linac and injection collimation line and could be sited as shown.

DJ Adams, ISK Gardner, GH Rees, CM Warsop (ISIS)

New Developments

Development at ISIS is a continuous process, driven both in response to the changing needs of the user community and to maintain the facility as a world-leading neutron and muon source. Evolution and development of existing instruments, and design and construction of new ones, open up fresh areas of research. Some of the major improvements over the past year are described here.

10 year development programme

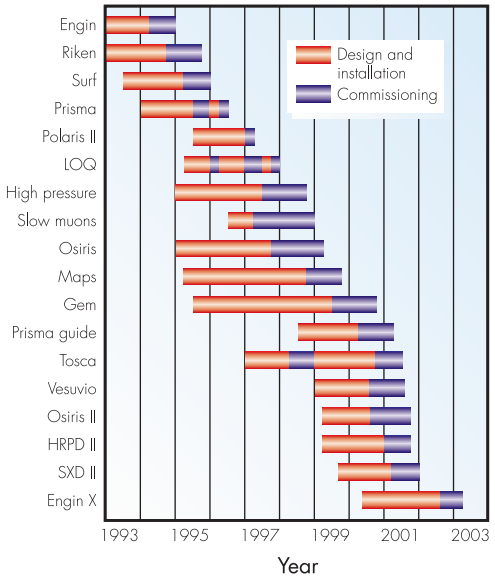

Figure 4.1. The ISIS instrument development programme.

Since ISIS began operations in 1985, the complement of scheduled neutron and muon instruments has increased from 4 to 20. Figure 4.1 shows the ISIS instrument development programme. This investment, worth over £30M, has come from collaborations with international partners (Australia, the EC, France, Germany, Italy, India, Japan, the Netherlands, Spain, Sweden, Switzerland and the USA) together with applications through the Research Council grant system by UK university-led consortia. Some of the ongoing instrument developments and upgrades are described in this chapter.

MAPS

MAPS is the first chopper spectrometer optimised to measure magnetic excitations in single crystals. At the time of the ISIS 99 annual report, it had just received its first neutrons. Since then the spectrometer has been in its commissioning phase, during which various beamline components have been commissioned and the first inelastic data has been taken. The new-design background suppressing chopper has been running routinely at 50 Hz, monochromatic beam has been produced, and numerous photographs have been taken along the primary beamline to check the alignment of the components.

The full complement of MAPS detectors has now been installed. Tests of the detectors reveal uniformity of response along their length, resolution typically 14 mm FWHH along the tubes, and there is no loss of efficiency compared to equivalent length non-PSD ^{3}He tubes. Background count rates are the same per unit area as for the non-PSD tubes on HET and MARI. Figure 4.2 shows the first inelastic scattering data taken on MAPS.

All the detector electronics are now installed and tested. At the time of writing, commissioning on MAPS of the new generation data acquisition system, DAE-II, is nearing completion. Accordingly, the spectrometer has now been opened up to the user community. The first experiments are due to start in the July 2000 cycle.

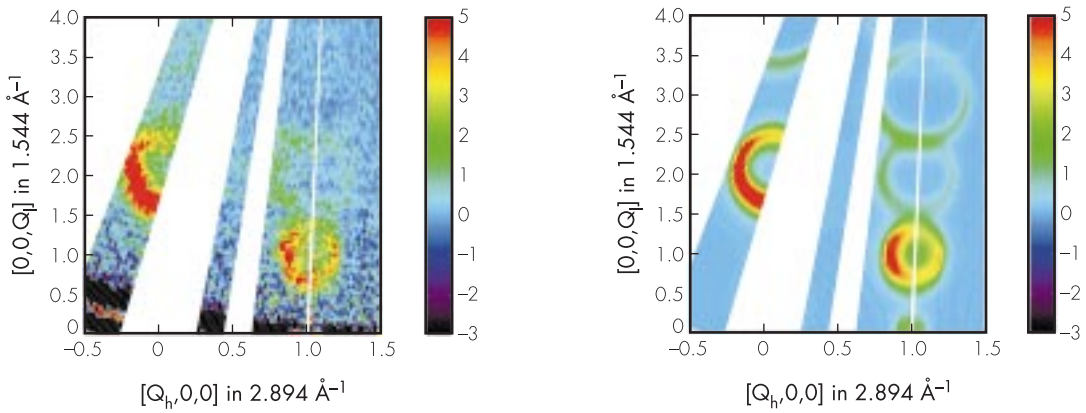

Figure 4.2. (Left) scattering data and (right) corresponding simulation of scattering from a single crystal of cobalt, taken on MAPS with incident energy E_i = 450 meV. The data are taken in the (h0l) scattering plane. Rings of intensity are visible around the (101) and (002) reciprocal lattice points. A weaker ring is also visible around (102). The rings of intensity correspond to the intersection of the ferromagnetic spin wave dispersion with the neutron phase space surface probed by the spectrometer.

GEM

The first opening of the GEM shutter on October 12, 1999 was undoubtedly a momentous event. After four years of planning and construction by the members of the Collaborative Research Group (under the leadership of Peter Day (The Royal Institution) and including several leading UK universities, the Japanese RIKEN Institute and ISIS), the new, high-intensity, high-resolution diffractometer for crystalline, liquid and amorphous materials was about to see its first neutrons. GEM was expected not only to meet high performance expectations, such as a peak resolution of 0.2% and a detector stability better than 0.1%, but also to be able to handle extremely high data rates (in excess of 100 Mbytes/min) in a user-friendly manner. It is fair to say that GEM passed its first exams with flying colours. For example, the first high-quality, multi-bank Rietveld refinement of GEM data was produced only 48 hours after the first shutter opening.

The initial 5 months of operation, which were devoted to scientific commissioning, enabled exploration of the envelope of the instrument performances and its interactions with the many pieces of sample environment equipment available. Also, commissioning experiments produced a number of high-quality pieces of science. An example is presented in figure 4.3, which shows the temperature evolution of the 90-degree scattering from the fast-ion conductor Ag_3SI (work performed by S Hull and D Keen). Clearly seen is a dramatic phase transition in the Bragg peak intensities arising from the ordering of the silver ions. At the same time, the order-disorder transition is reflected in changes of the

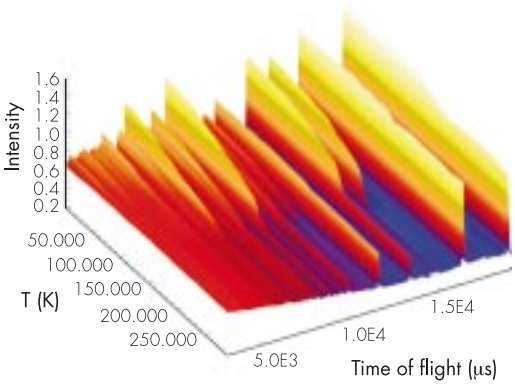

Figure 4.3. Temperature evolution of the 90-degree scattering from the fast-ion conductor Ag_3SI.

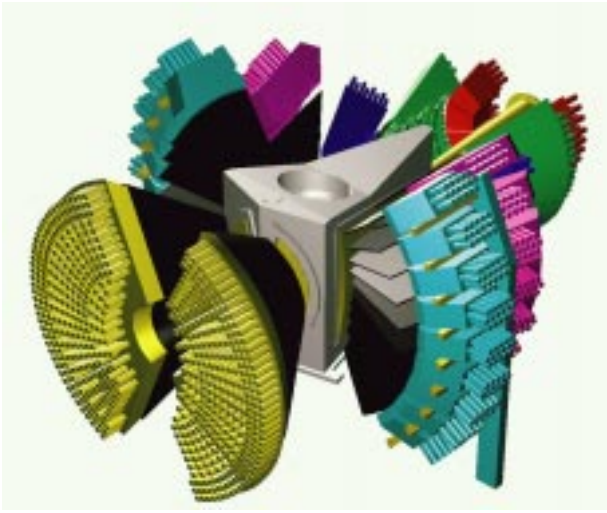

Figure 4.2. The GEM instrument.

diffuse scattering. The collection time for each of the 50 data sets, which are suitable for both Rietveld refinement and Radial Distribution Function calculation, was 30 min. Very recently, we have managed to collect Rietveld-quality data sets on Ni superalloys at a rate of one every 30 seconds, including the on-line data reduction.

GEM has now 4 complete detector banks (20 degrees, 90 degrees, 140 degrees and 160 degrees) and a portion of the 65-degree bank, for a total of 4200 elements and a solid angle of 2.85 sterad. Further work to continue the instrument development continues, including

- Detector completion: the improvement of the low-angle coverage is an essential prerequisite to maximise the impact of GEM in the fields of non-crystalline materials and magnetism.
- Advanced sample environment: during next winter we will install an innovative oscillating radial collimator, which will enable the study of small samples (~2 mg) inside cryostats and other pieces of sample environment. There are also plans for a new 10 Tesla cryomagnet, and fast sample changers are also in the advanced testing phase.
- Ultra-fast and stroboscopic measurements: it is hoped to improve the data transfer rate to allow sub-second measurements on transient phenomena and stroboscopic measurements on cyclic processes.

HRPD

The EPSRC-funded project to upgrade the 90° detector bank for HRPD is advancing well. This development will provide an order-of-magnitude enhancement of the 90° bank count-rate, matching it to the existing backscattering detector bank. This will have significant benefits by substantially improving the count rate for longer d-spacings and by offering in many cases the possibility of measuring all parts of the pattern of interest in a single shot. The improvement will lead to better data for larger unit cell systems and in studies using bulky sample environment apparatus such as reaction vessels and pressure cells. The transfer of the technology used to produce the detector modules for GEM has been important in keeping both the costs and the timescales for this upgrade to a minimum. The manufacture of the fourteen detector modules is now complete, and the programme is ahead of schedule with the new bank due for installation in the second half of 2000. The possibilities offered on HRPD by replacing sections of the 15-year-old neutron guide, using new supermirror components, are being assessed.

SXD

The EPSRC-funded project to upgrade SXD is also advancing well. This complete reconfiguring of the diffractometer has been planned based on the increased understanding gained at ISIS of the capabilities of single crystal diffraction on a pulsed source. The new instrument will have an integrated sample and detector support, which will contain 11 PSD modules and together with some improvements in the scintillator material will offer an overall count rate increase of around an order of magnitude. The motivation is towards better science by allowing structural work to be carried faster, on larger unit cells, and on smaller crystals. The design of the array of 11 detector modules is complete, and manufacture has begun. The projected installation date for the reconfigured instrument is mid-2001, with a commissioning period to follow.

TOSCA

At the end of March 2000, TOSCA was closed to allow the upgrade from TFXA to be completed. For the 'mid-infrared' energy range (0 – 4000 cm^{-1}) TOSCA is already the best instrument in the world. The new TOSCA will build on this and will simultaneously provide still better resolution and greater sensitivity, while retaining the ease of use that made TFXA so popular. Figure 4.4 shows an exploded view of the instrument; there will be analyser modules for both forward and backscattering with the detectors sandwiched between them.

TOSCA II will be at 17 m from the source rather than the 12 m of TFXA and TOSCA I. To compensate for the reduced flux (from a smaller solid angle), the beam size will be increased by 60%. In addition, a Nimonic chopper is required to prevent frame overlap. As a consequence, it was necessary to rebuild the beamline from the shutter onwards. The new position of the beamstop meant that the TOSCA cabin had to be removed, to be replaced by a new one on the mezzanine. At the same time, TOSCA was shipped back to Italy for the installation of the new analyser modules. The instrument returned on time and

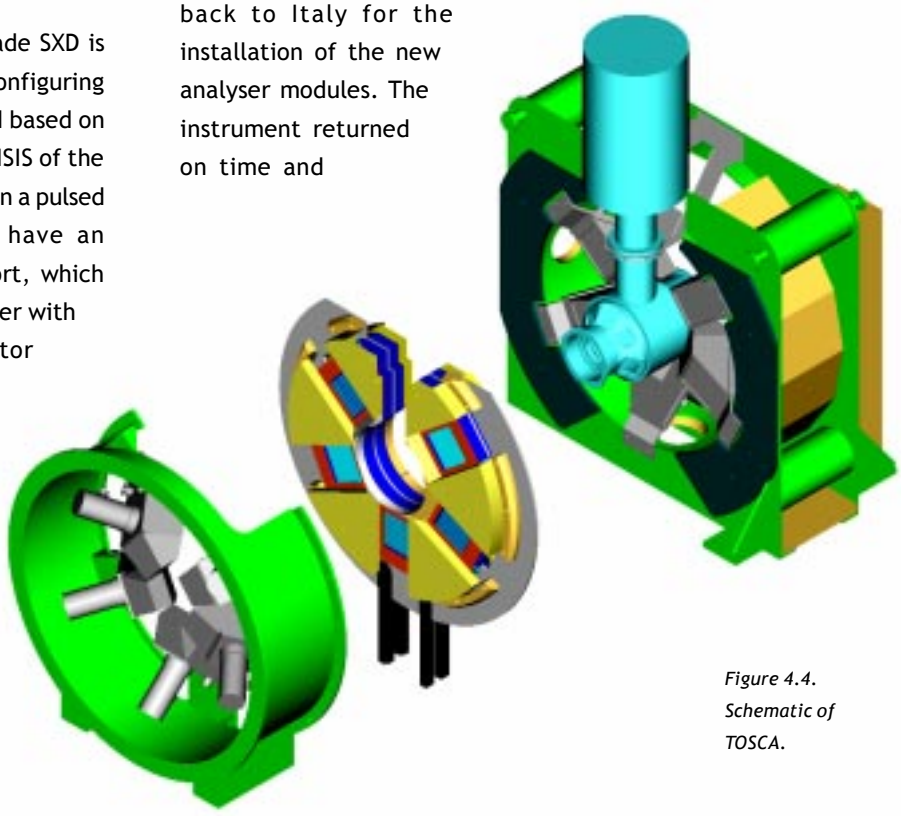

Figure 4.4. Schematic of TOSCA.

Dennis Abbley and Howard Vizor installing guide field coils on OSIRIS (99RC1109).

the detectors are being installed. Overall the project is both on-time and on-budget. First neutrons are expected in cycle 00/2, the remainder of the cycle being used for calibration and commissioning. The first users are scheduled for the start of cycle 00/3 in November.

OSIRIS

OSIRIS is 50% scheduled for diffraction experiments to allow sufficient time to develop the required polarised-neutron techniques for full polarisation analysis. The diffractometer section of the instrument has recently been completed. The final diffraction detector modules were installed during the May 2000 shutdown, bringing the total up to 8 modules, covering 0.7 steradians of solid angle.

The spectroscopy section will be installed during the first half of 2001. This involves a 40 cm high array of graphite crystals in near-backscattering, cooled to liquid helium temperatures, providing an energy resolution of 25 μeV.

Polarisation analysis will be performed using a ^{3}He spin-filter. A 10 Watt fibre laser will be used for the metastable pumping of the low-pressure ^{3}He gas, which is then compressed by a peristaltic pump. OSIRIS will use a novel continuously circulating system, which is expected to improve the polarisation level and avoid the problems associated with time-dependence of the beam polarisation. This system is expected to be available for first on-line tests by 2002.

IRIS

The pyrolytic graphite (PG) analyser bank on IRIS has been upgraded. While the original design utilised a 6 row by 225 column array of 1 cm^2 (2 mm thick) graphite crystals, the new design comprises of 4212 crystal pieces (1 mm thick, 18 rows by 234 columns). Installation of the new analyser is now complete and commissioning measurements highlight a 3-fold increase in the number of detected neutrons. In addition, a significant improvement in the ratio of signal to background is achieved; a consequence of cooling the graphite crystals from the previously achieved 25K to liquid helium temperature. More importantly, however, only minimal broadening of the instruments resolution for both PG002 (from 15 μeV to 17 μeV) and PG004 (from 50 μeV to 54 μeV) spectrometer configurations is observed despite the increased vertical extension of the new analyser out of the horizontal scattering plane.

Future effort on IRIS is focused toward fully exploiting the increase in surface area of the new pyrolytic analyser array by considering improved collimator and detector geometries.

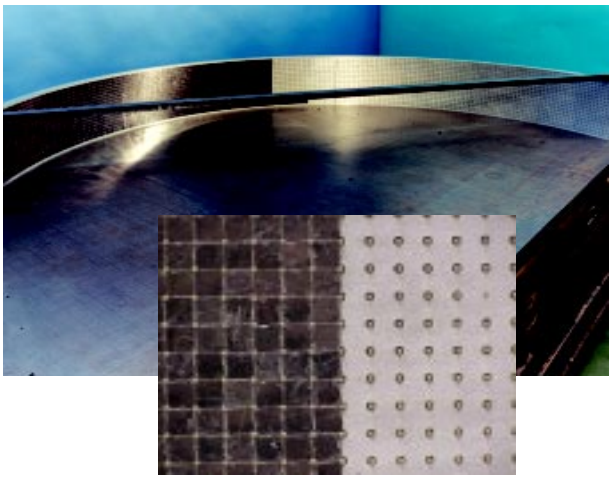

The new IRIS analyser being built (00RC1511). The inset shows a close-up of the individual graphite crystals mounted on the analyser support structure.

Muon developments

The ability to measure small samples by suspending them in the muon beam has undergone considerable development during the past year. Of particular note were measurements carried out by a team from the University of Coimbra: muonium states in a small sample of CdS were studied with an almost total absence of background signal (see the Highlight article on page 64 for further details). Our present sample environment equipment allows these 'flypast' measurements, which can be made on samples as small as 4 mm across, to be carried out between 4K and 400K; further developments are planned, however, to extend this temperature range down to 350 mK.

The development of radio-frequency (RF) μSR techniques has continued using the new spectrometer on the DEVA beamline, work being focused on applying novel pulsed RF methods to muon measurements. The recent demonstration of continuous wave decoupling to cancel the dipolar interaction between the muon and neighbouring nuclei (figure 4.5) is a particularly exciting development that promises to become an important tool in future μSR investigations.

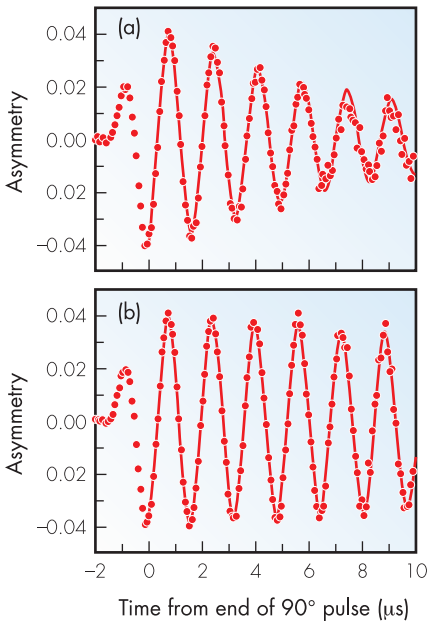

Figure 4.5. (a) Muon precession signal in $Ca(OH)_2$ following a 90° pulse. (b) Signal recorded with an RF pulse simultaneously applied at the proton resonance frequency to decouple the dipolar interaction between the muons and the protons.

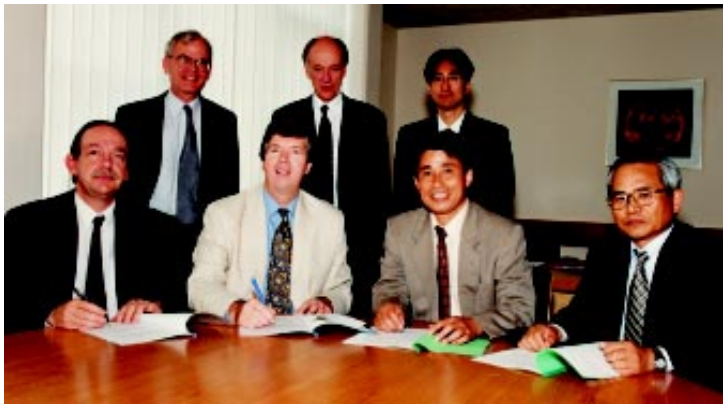

H Yabuki, M Hazama and H Itoh (RIKEN) with R Lawrency-Wilson, A Taylor, WG Williams and G Stirling (CLRC) at the signing of the agreement enabling a new muon beamline to be constructed on the existing RIKEN muon facility at ISIS (00RC3742).

The method works by applying a decoupling field at the nuclear resonance frequency while simultaneously measuring the muon free precession signal following a 90° pulse.

PRISMA

Phase 1 of the Prisma neutron guide project was completed during the April shutdown and initial results look promising with flux gain factors of 2.5 already realised for cold neutrons. The short, straight, tapered design of the guide is unique to ISIS instruments, and the system incorporates many features to reduce the background from fast neutrons and to tailor the beam characteristics to the required experimental conditions.

Other measures incorporated to reduce background include regular sintered B_4C absorbing irises, a modified nimonic chopper, a GEM-type variable aperture disc chopper, interchangeable Soller collimation and a set of beam defining jaws. A set of supermirror-on-silicon frame overlap filters will remove very cold neutrons (< 0.6 meV) from the beam.

During phase 1, supermirrors have been installed in the Prisma shutter, the chopper and sample pits have been reconfigured, and the choppers and frame overlap filters have been set up. In the sample pit, a new nose section has been constructed to replace the existing collimation, containing two sliding collimator changers, monitors and a set of beam defining jaws.

In the October 2000 shutdown, the remainder of the guide system will be installed. Once this has been completed, Prisma will receive the full benefit of the neutron guide with cold neutron fluxes increased by factors of up to 10.

ENGIN-X

The physics design of the new ENGIN-X has been completed. ENGIN-X is a departure from the philosophy of previous diffractometer designs. Unlike the majority of neutron diffractometers which are generally built as 'all-purpose' instruments, with designs that are compromises balancing the competing requirements to measure the intensities, positions and widths of diffraction peaks simultaneously, for ENGIN-X the overriding requirement of the instrument is the accurate measurement of a lattice parameter, at a precisely known location within the component under study.

Through the design of its neutron optics, ENGIN-X will provide an order of magnitude improvement in performance over the existing ENGIN diffractometer. With the design of the 50 m flight path instrument now complete, building is expected to begin in the autumn of 2000, with first neutron expected by mid 2002.

A lens for neutrons

The development of effective thermal neutron lenses would offer considerable advantages to neutron instrumentation by adding to the tools available for new instrument designs. This is particularly true for time-of-flight instrumentation – which up to now has not had a method, apart from neutron guides, of de-coupling the divergence of the neutron beam from its flight path, and allowing optimised design of instruments.

Mike Johnson and Mark Daymond of the Engineering group at ISIS have come up with an adaptation of the X-ray 'lobster eye' lens for neutrons. The 'lobster eye' works by having multiple 2D layers of reflective material, but the new ISIS design incorporates a number of improvements. By restricting the focusing to a single dimension, better exploitation of super-mirror optics is possible. Secondly, by designing the layer thicknesses and separations such that every neutron makes one, and only one, reflection in its path through the lens, all neutrons incident on the lens will be reflected towards the focal point. The simplest design of 140 sheets of single crystal silicon coated with super-mirror has been constructed and has been successfully tested on OSIRIS. Results are promising and presently being analysed.

Prof. Masayoshi Ono (Kyoto University), Dr. Lyndon Edwards (The Open University) and Prof. George Webster (Imperial College) examine the ENGIN stress rig during a recent Versaille Project on Advanced Materials and Standards, Technical Working Area 20 meeting held at ISIS to discuss international standardisation of the neutron stress measurement technique (00RC3537).

VESUVIO

eVS is about to undergo a major upgrade, with the installation of the EU funded VESUVIO modifications, which will considerably improve the resolution for quantum fluid studies. These improvements will be obtained by cooling uranium foils to 77K and by using a double difference measurement, rather than the single difference technique used at present. The construction of the new sample tank and filter-cooling device is complete and the system is being tested in Italy. Installation is planned for November 2000. The design for a new back scattering bank of ^{6}Li doped glass scintillator detectors, with a geometry opimised for the new filter, has also been finalised.

New Developments

Above: Uschi Steigenberger and Zoe Bowden inspecting MAPS during its installation (98RC5889). Centre: the GEM installation team (99RC5316). Below: Chris Frost (ISIS) shows attendees of the Sixth Oxford Neutron Summer School the new MAPS instrument (99RC4551).

Above: Paolo Radaelli (ISIS) oversees the mounting of GEM's top-loading 4K CCR, watched by Simon Hibble and Simon Cheyne (Reading University) (99RC5755). Below: Careful sample mounting for a GEM experiment by Richard Walton (Oxford University) (00RC3808).

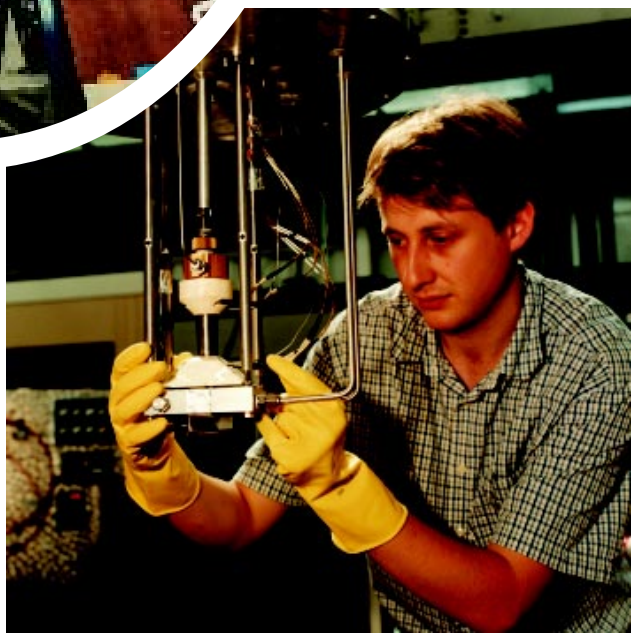

Accelerator and Target Station

5

Studies of the accelerator and target characteristics, and modifications to the accelerator equipment, enable continual improvements to be made to the beam intensity and stability. This chapter details the performance of the accelerator and target over the past year along with an outline of new developments.

ISIS

ISIS Beam Statistics 1999-2000

ISIS continues to be the world's most intense pulsed spallation neutron source. For the period of this report and during scheduled operating cycles, ISIS delivered a total of 687 mA.hrs of user proton beam to the muon and neutron targets at an average current >171 μA. Table 5.1 gives beam statistics for the individual cycles in the year 1999-2000. Year-on-year statistics for ISIS performance are given in table 5.2. Figure 5.1 indicates the improvement in operational efficiency obtained since 1987 and figure 5.2 shows the total integrated current for each year also since 1987.

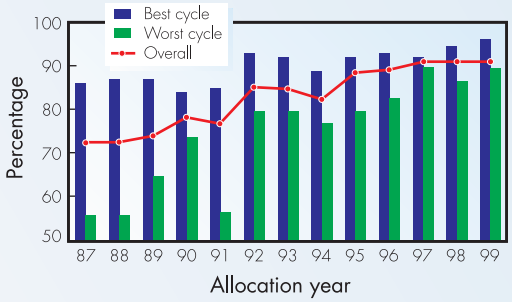

Figure 5.1. Year-on-year operational efficiency improvements.

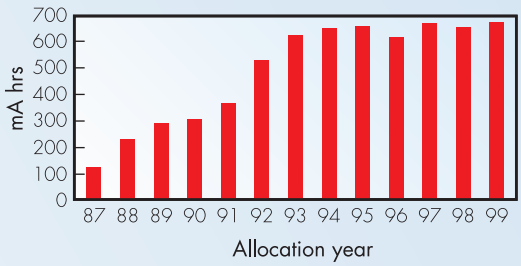

Figure 5.2. Total integrated ISIS current.

Cycle	99/1	99/2	99/3	99/4	99/5
Beam on target (hrs)	869	854	667	778	508
Total beam current (mA.hrs)	159	158	128	150	92
Average beam current on target(μA)	183	185	192	193	181
Peak beam current (μA, averaged over 24 hrs)	186	188	198	195	183
Current averaged over cycle (μA)	164	167	183	173	174
Average beam trips per day	64	39	37	28	12

Table 5.1. ISIS operational statistics for year 1999-2000.

Year	1993	1994	1995	1996	1997	1998	1999
Total scheduled user time (days)	168	168	168	168	168	175	168
Total time on target (days)	152	155	151	152	153	160	153
Total integrated current (mA.hrs)	623	653	661	621	672	656	687
Average current on target (μA)	171	176	182	171	183	171	187
Peak current averaged over 24 hours (μA)	187	184	201	204	197	193	198
Current averaged over year (μA)	145	145	162	153	167	156	171
μA.hrs per trip	59	59	80	115	81	72	106
Total power consumption (GWh)	45	50	46	47	47	42	52
Energy efficiency (mA.hr/GWh)	13.8	13.1	14.4	13.1	14.9	14.9	13.2

Table 5.2. Year-on-year ISIS performance summary.

Accelerator and Target Developments

The Accelerator and Target Station have had a very good year, surpassing the Service Level Agreement with EPSRC and providing an availability of 92%. To maintain this performance, considerable effort has been made to increase machine reliability by replacing obsolete equipment and developing new systems - the major projects are described in this chapter.

Injector

The 70 MeV drift tube linear accelerator (linac), the 665 keV Cockcroft-Walton preinjector, and the H^- ion source have yet again maintained good availabilities during the year.

Major refurbishment work was completed on Tank 3 of the linac this year (Tank 3 accelerates the H^- particles from 30 to 50 MeV). Several weeks were also spent replacing all the water-to-vacuum O-rings on Tank 2, again with major efforts to avoid disturbing the alignments of the drift tubes. During the Tank 3 work, the plant supplying temperature-controlled water to the linac was refurbished. Other work carried out this year includes procurement of new pulsed power supplies for the drift tube quadrupole magnets in Tank 1.

During the year the 665 keV RFQ accelerator built at the University of Frankfurt and intended as a replacement for the present ISIS Cockcroft-Walton preinjector was delivered to RAL and installed in the RFQ Test Stand. Following a successful review of safety arrangements, conditioning was carried out, and the RFQ has been run with the full design input RF power (200 kW at 202.5 MHz). Equipment to measure X-ray spectra during operation has been installed and is delivering key diagnostic information on the peak voltages achieved between the (modulated) rods.

The ion source development rig is nearing completion. An ion source has been run on the rig with a new form of arc driver which promises well for the programme to upgrade ion source performance towards levels appropriate for the European Spallation Source (ESS).

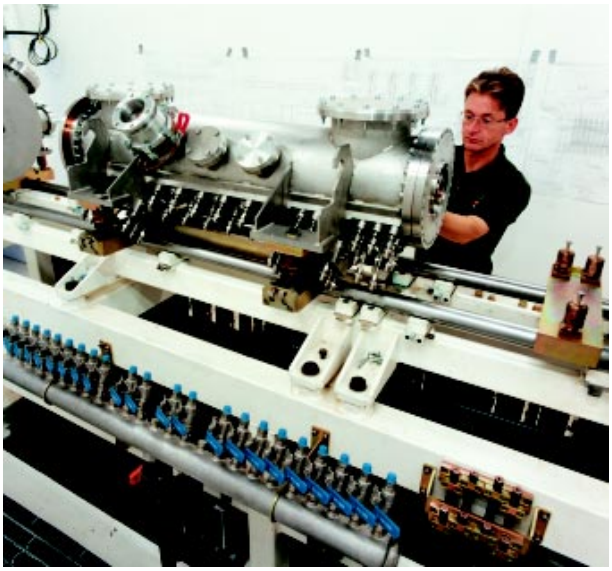

Jim Loughrey assembling the ISIS RFQ (99RC4375).

Synchrotron and electrical engineering

Continual assessment of the synchrotron performance has ensured safe and effective operation.

Work continues on upgrading the extract kicker power supplies. New switching thyratrons have been installed in system two after the success of the 1998 installation in system three. Studies on the kicker power supply pulse forming networks (PFN's) show that upgrading the capacitors to a higher maximum voltage and the addition of clamping diodes will improve operational reliability.

A study has started to look at the future operation of the main magnet power supply (MMPS) and in particular the large storage choke and capacitor banks. The choke is 30 years old and was installed on ISIS after many year's service

on the NINA facility at Daresbury. Being a large item (120 tons) the study is looking at ways of replacing it with 5 smaller chokes.

A number of tests were completed on a spare synchrotron RF shield, to determine why some shields have failed in operation causing a reduction to the beam aperture. A greater understanding of the failure mechanism is now known and the importance of accurate assembly of vital coupling capacitors recognised.

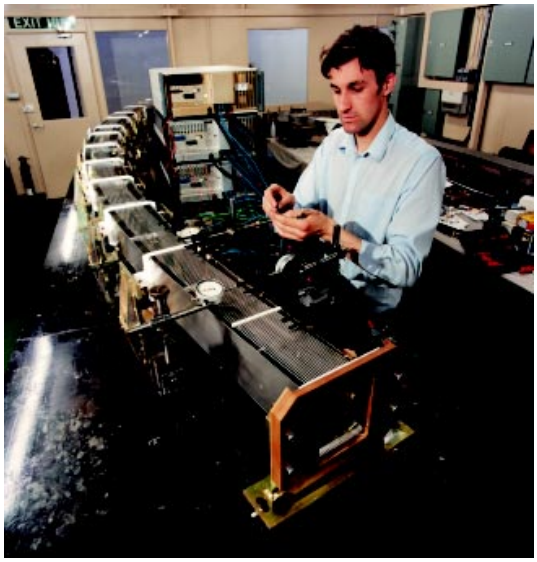

Kevin Tilley measures the thermal expansion of a synchrotron dipole RF screen (99RC3433).

A programme of work is underway to replace ageing components in the straight 1 section (SP1) of the synchrotron. The components located in SP1 experience high radioactivity levels from collectors, used for collecting non-trapped low energy beam, and induced activity from the occasional malfunction of extraction equipment used for diverting the beam to target. The programme includes replacement and upgrading of the extract septum and the collector system. It is planned to install the new components in 2002.

Work towards the 300 μA ISIS upgrade continues where the intention is to install four RF cavities operating at twice the harmonic frequency of the existing cavities. Initial measurements on a test cavity have been completed, and equipment is now being manufactured to test the cavity at high power RF. A space in straight 5 of the synchrotron has been cleared for the installation of a cavity. Collaboration with KEK, Japan and ANL, USA is progressing well with ISIS supplying KEK with a cavity and other equipment for testing in Japan by the end of 2000.

The group continues to give electrical engineering support to many projects on ISIS, for example design of the electrical systems of the MAPS and GEM neutron beam lines and for the RIKEN muon beamline laser.

Target Station

The conceptual design for a Second Target Station has been completed and a detailed costing made for the proposal - see also page

Explorations continue of ways to overcome the constraints on ISIS running imposed by the current methane moderator lifetime. Measurements of the neutron energy and time spectra using ethane as a moderator material instead have been completed and show that ethane would be acceptable. Irradiation experiments have also continued at the CARE reactor of Imperial College London to assess the effect of chemical scavengers in reducing the build-up of high mass hydrocarbons in moderator material. Measurements have been made with methane and methane with 1% ethylene and 1% propylene. The production of hydrogen gas from all three is essentially the same. A feature of all irradiations has been the low measured production of higher mass hydrocarbons (wax). Whether the production of hydrocarbons is lower than expected or they are not being efficiently extracted is an open question at present. More measurements are planned with higher concentrations of additives, and also with ethane. However, initial results are not encouraging from the point of view of providing a longer operational lifetime for the methane moderator. As an alternative the mechanical design of the moderator system and the remote handling procedures are being examined to find a way of reducing the time to change a moderator from three weeks to one.

The decision has been taken that uranium targets will not be used on the target station in future and all spent uranium targets have been sent for disposal. A new tungsten target has been manufactured and this will be installed at the end of life of the current tantalum target.

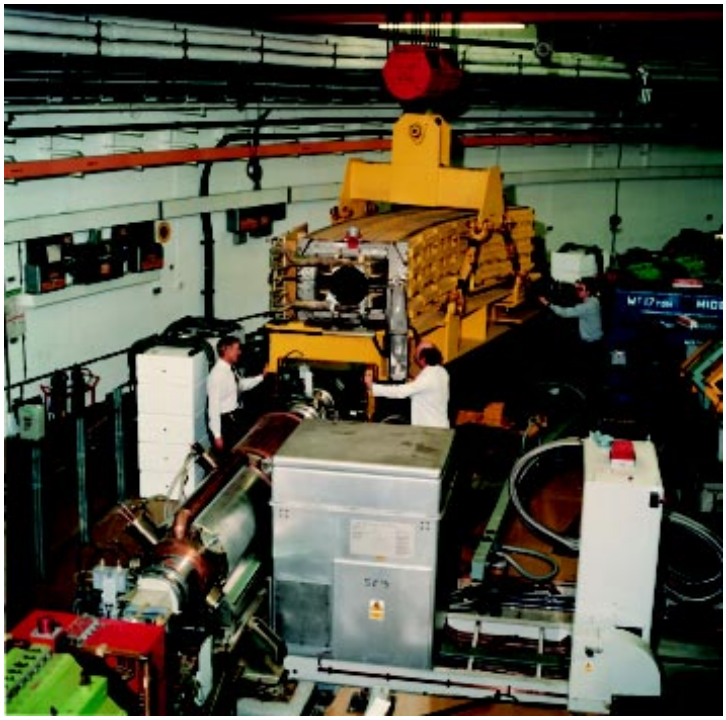

Ken Louch Supervises the installation of a dipole (96RC2021).

Controls Group

Controls Standard STEbus (CSS) control and acquisition systems have been developed for the RFQ and ion source projects, and their respective test areas have been included in the ISIS Controls network and ISIS distributed timing system. In addition, a temporary CSS system for unattended RFQ running was provided. As part of the project to replace all the LINAC Tank 1 quadrupole power supplies, their control has been transferred to the new control system.

Transfer of the synchrotron correction magnet control to the new control system is complete and the task of transferring the synchrotron RF control will be complete before the year end.

Transferred application programs for filling and draining operations on the ISIS target have completed initial tests successfully on the new control system. The conversion of control software for the target control (Fisher) valves is the last task to be done before the old target control computer can be removed.

Analogue Waveform Switching (AWS) control has now been transferred to the new control system – replacement commercial hardware for the AWS system is being evaluated. PLC and PXI/PCI based control and acquisition systems are now being integrated into the new control system.

The group continues to provide a divisional resource for CAD/CAE system and expertise for the type of electronics (both conventional and surface mount) prevalent on the accelerator and target. We are now expanding this to include an EMC evaluation capability.

Future developments will include migration of parts of the new control system to NT. A fully functional ISIS controls NT domain has already been created and Vsystem (the commercial package used for ISIS controls) for NT is under test. The machine physics computer node will be the first to be moved to an NT machine. The upgrade of the ISIS controls graphics library to a multi-platform X-version is well under way.

Operations

The Operations Group have dealt with a variety of equipment faults and problems during the year, such as the failure of a support insulator in one of the four high power RF drive systems of the linac. These systems provide the ~ 2 MW of pulsed RF power to each of the four RF cavities that make up the linac. The resultant high power breakdown within the drive system caused severe damage (and a small fire) requiring several days of work by skilled craftsmen and RF engineers to strip down and refurbish failed components before successful reassembly and testing.

Mick Mills repairs a damaged Muon Target (00RC1645).

Above left: Mohammed Kemali (Salford) inserting the Orange Cryostat into eVS during an experiment on a single crystal of palladium deuteride (00RC1879). Main Picture: Simon Cheyne (Reading) preparing samples for an experiment on GEM (99RC5036). Below left: Rebecca Green and Louise Peel (Surrey) cleaning up their surfactant samples after an experiment on CRISP (00RC1715).

Above right: David Bucknall (Oxford) and Ian Gentle (Brisbane Univ) preparing Langmuir-Blodgett films in the CRISP blockhouse (00RC1432). Below right: Umpali Jayasooriay, Susan Hall and Penny Hubbard preparing a cryostat for the RIKEN ARGUS muon spectrometetr (00RC1291).

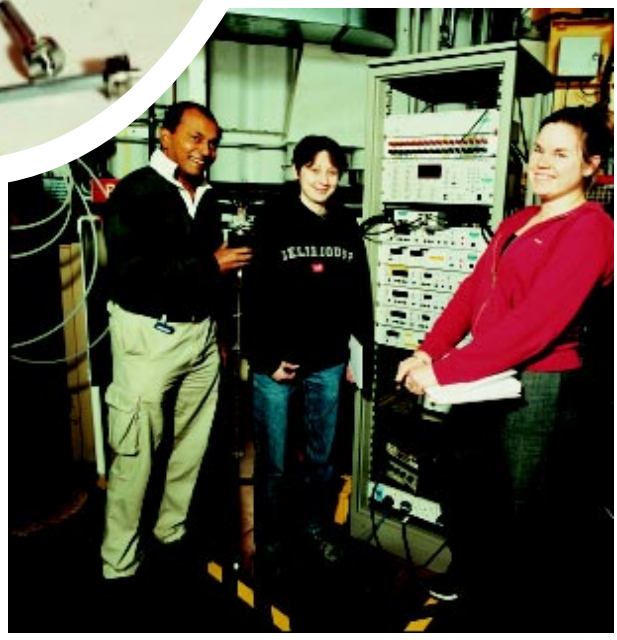

User Interaction and Support

Essential for the successful operation of ISIS experiments are the specialised teams responsible for maintaining and developing experimental and computing facilities. The technical support given by these groups is complemented by the organisational and administrative services provided by the User Office, which oversees the arrangements for the 1600 scientists who visit ISIS annually.

ISIS

Organisation and User Interaction

There are two calls for experimental proposals each year in April and October, and these are followed in June and December by meetings of the Instrument Scheduling Panels (ISPs). The seven ISPs comprise 70 international scientists (see table 6.1) who have the job of assessing the scientific quality and timeliness of submitted proposals, and to advise on the allocation of beamtime.

User Liaison

The User Office (UO) plays a central role in user reception and programme organisation. More than 1000 proposals are received each year for the use of ISIS instruments, and these are collated and recorded by the UO for the ISP meetings. The information entered into the ISIS integrated data base system forms the first stage in the scheduling of the instruments and the sample environment equipment which is carried out by the instrument scientists and the user support group. The UO is also responsible for travel and accommodation arrangements for the 1600 researchers who visit the facility annually.

Information about ISIS, the ISIS instruments and how to apply for beamtime at ISIS is available on the World Wide Web (http://www.isis.rl.ac.uk), including electronic versions of the ISIS beamtime application forms. Some 75% of the applications during the year were by electronic submission.

ISIS User Committee

The ISIS user community is represented by the ISIS User Committee (IUC). The Committee draws its membership from the seven ISIS Instrument User Groups. The chairman from each group plus an elected representative attend, together with the Division Heads of the ISIS Science Divisions and the Leader of the User Support Group. The Committee reports to the Director of ISIS. The present committee membership is shown in table 6.2. The group meets twice a year following the ISIS Scheduling Panel meetings. Its terms of reference are:

- To address all aspects of user satisfaction at the facility, including scientific and technical support, source reliability, instruments and sample environment, detectors, electronics, data acquisition and control, computing and data analysis, safety and security, food, accommodation, and transport and claims;
- To provide input and advice on development of instruments, and sample environment and associated equipment;
- To coordinate user groups and user meetings;
- To recommend specific training courses for the community.

ISP-1 Diffraction	ISP-2 Liquids	ISP-3 Large Scale Structures	ISP-4 Excitations	ISP-5 Molecular Spectroscopy	ISP-6 Muons	ISP-7 Engineering
P Attfield	P Madden	RK Thomas	KA McEwen	D Jones	R De Renzi	P Withers
W Clegg	MC Bellissent-Funel	N Clarke	AT Boothroyd	JP Bradshaw	P Carretta	ME Fitzpatrick
M Davidson	H Fisher	T Cosgrove	ME Hagen	RG Delaplane	P Dalmas De Reotier	P Holdway
MA Estermann	GN Greaves	P Grundy	K Kakurai	JZ Larese	R Jones	T Lorentzen
I Gameson	D Holland	CC Jones	M Loewenhaupt	LC Li	RL Lichti	DJ Smith
C Henderson	U Hoppe	J Lawrence	T Mason	A Navarro	SL Lee	
T Kamiyama	P Lamparter	FAM Leermakers	D McMorrow	W Petry	N Nishida	
A Powell	G Neilson	RM Richarson	R Reynolds	K Prassides	I Reid	
MT Weller	T Ottomo			D Timms		
S Zochowski	DH Powell			B Winkler		
	N Skipper					
RM Ibberson	AC Hannon	JRP Webster	TG Perring	J Mayers	SP Cottrell	M Daymond
CC Wilson	AK Soper	J Penfold	RS Eccleston	J Tomkinson	PJC King	MW Johnson

Table 6.1 Instrument Scheduling Panel membership.

Chairman	**RJ Stewart (IUG 3)**	**University of Reading**
IUG1 Crystallography	P Attfield RJ Nelmes	University of Cambridge University of Edinburgh
IUG2 Liquids and Amorphous	P Salmon AC Wright	University of East Anglia University of Reading
IUG3 Large Scale Structures	RK Thomas	University of Oxford
IUG4 Excitations	D McK Paul SM Hayden	University of Warwick University of Bristol
IUG5 Molecular Science	V Arrighi DK Ross	Herriot Watt University University of Salford
IUG6 Muons	EA Davis S Blundell	University of Leicester University of Oxford
IUG7 Engineering	L Edwards M Fitzpatrick	Open University Open University

Dr AD Taylor	Director, ISIS
Dr U Steigenberger	ISIS Spectroscopy and Support Division Head
Dr J Tomkinson	ISIS User Office Co-ordinator
Dr MW Johnson	ISIS Instrumentation Division Head
Dr WG Williams	ISIS Diffraction and Muon Division Head
Ms Z A Bowden	ISIS User Support Group Leader
Ms C Wadley	ISIS IUC Secretary
Dr J Green	EPSRC

Table 6.2. ISIS User Committee membership.

User satisfaction

ISIS values the opinions of its users, and all visiting scientists are asked to complete a satisfaction survey after each experiment. As can be seen from the survey results (figure 6.1), the facility scores consistently highly in areas such as scientific and technical support, and instrument performance. Areas where improvements are needed are noted and appropriate action taken - a good example is the processing of claims, which is now handled by ISIS and which has seen a marked improvement over the past couple of years.

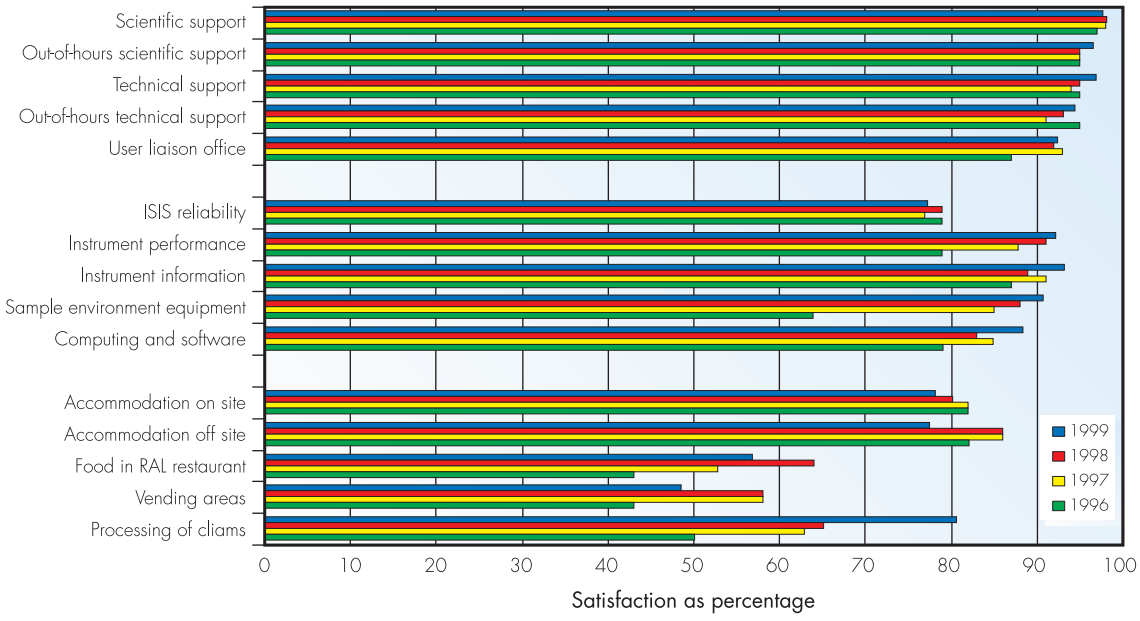

Figure 6.1. ISIS User survey results 1996-1999.

News and Events

A Second Target Station for ISIS

The proposed Second Target Station on the ISIS pulsed neutron facility represents a new generation of neutron production target and instrument suite. It will offer unique instrumentation and unrivalled potential for structural and dynamical studies of matter, using cold neutrons and high resolution spectroscopy. Such studies will be inter-disciplinary, with applications predominantly in Soft Condensed Matter, Bio-molecular Sciences and Advanced Materials.

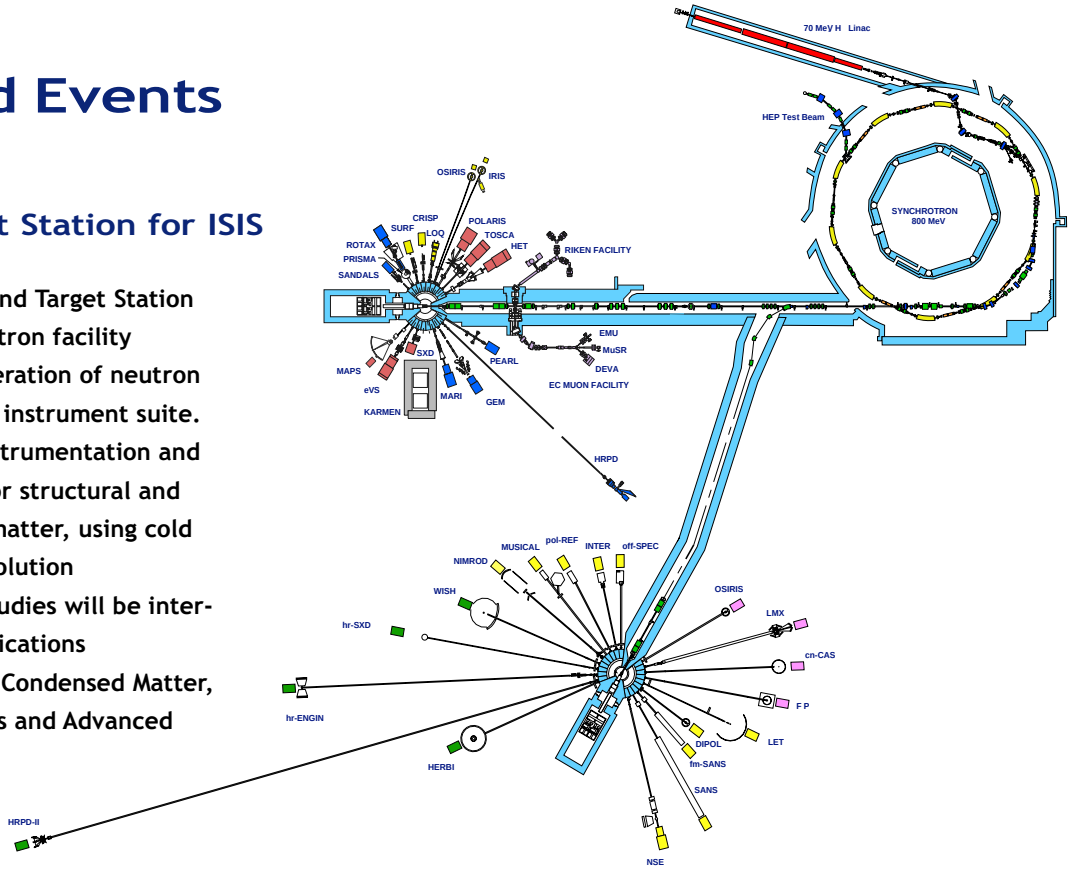

A User Consultation Meeting was held at RAL in May 2000 to discuss the scientific possibilities offered by the proposed Second Target Station. The meeting, attended by around 120 potential users and chaired by Bob Thomas (Oxford) provided information on the potential performance on the target station and the possible instrument suite, and offered a forum for users and to discuss the scientific opportunities that will accrue.

The morning consisted of a plenary session including technical accounts of the possibilities offered by the Second Target Station (Andrew Taylor and Jeff Penfold, ISIS) and four wide-ranging talks on the scientific opportunities and challenges, given by Tom McLeish (Leeds; 'Soft Condensed Matter', Chris Dobson (Oxford; 'Bio-molecular Sciences', Steve Mann (Bath; 'Nano-scale Materials') and John White (ANU Canberra; 'Advanced Materials'). These themes were then picked up in a series of afternoon discussion sessions with feedback from these forming the focus of the final session.

The meeting enthusiastically endorsed the proposal and it is clear there are many exciting scientific opportunities which will be offered by the proposed new Target Station, for which funding is now being sought. The science case for the Second Target Station can be found on the CD accompanying this report, and on the ISIS web at http://www.isis.rl.ac.uk/targetstation2/case.

Right: Participants at the User Consultation Meeting listen to presentations of Science for the Millennium (00RC2809). Left: John White (ANU), Tom McLeish (Leeds) and Bob Thomas (Oxford) discuss future science prospects (00RC2787).

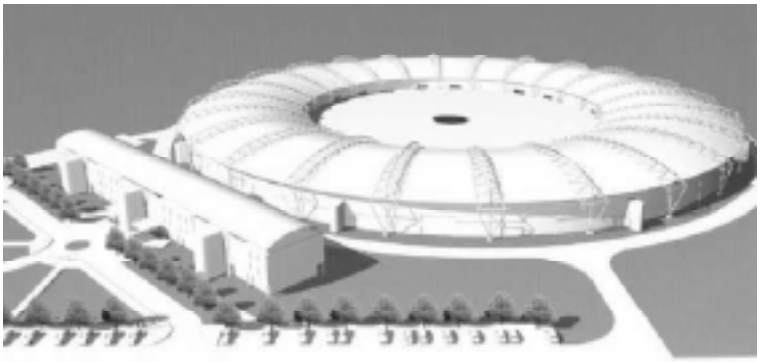

ISIS and the New Synchrotron

Synchrotron radiation and neutron scattering have together provided much of what we know at the microscopic level about the nature of the material world around us. Synchrotron radiation has been the diffraction tool of choice for large, complex systems such as protein structures, while neutron diffraction is the preferred tool for simpler systems. There is, however, considerable overlap in the use of both techniques in Materials Science, Physics, Chemistry and Engineering. Furthermore, significant advances have been made in the past decade in the study of more complex systems such as polymers, surfactants and catalysts by neutron scattering. The proposed Second Target Station at ISIS, optimised for the study of complex systems, Soft Condensed Matter, Advanced Materials and Bio-molecular Sciences, will give a breadth of new research possibilities using neutron scattering that will complement the science performed at synchrotron sources. The fact that this next step in neutron scattering is planned to take place on the same campus as the New Synchrotron provides unique opportunities for complementary and combined research programmes that optimise the use of both facilities and which will give UK researchers a once-in-a-generation opportunity to command a leading role in many aspects of condensed matter science.

Progress with the ESS

With the appointment of Peter Tindemans as new Chairman of the ESS Council, the ESS project has entered a new phase of concerted activities. A Central Team has been set up at the Research Center in Jülich, headed by Kurt Clausen as new Project Director. The Central Team have overall responsibility for the progress of the project and will provide the link between the three technical R&D tasks: accelerator, target systems and instrumentation.

These three tasks are managed by lead laboratories: ISIS for the accelerator, the Forschungszentrum Jülich and the Paul Scherrer Institut for the target, and the Hahn Meitner Institute and ISIS for instrumentation. A detailed workplan with clearly defined milestones is in preparation which will guide the work of the individual teams for the next three years. A Science Advisory Committee under Dieter Richter's stewardship is acting as a focus for the users' points of view and will guide the project towards the optimal solution for the next generation Neutron Source in Europe.

In parallel to the ESS R&D work, the French CEA has proposed a feasibility study for a multipurpose accelerator driven facility. Potential applications include a neutron spallation target, a high power irradiation station, a demonstrator for transmutation of nuclear waste, radioactive beams, neutrino production, etc. This study will explore possible synergies of such a facility compared with a stand alone solution for the ESS and will address issues like reliability, R&D needs, construction and operating costs.

ISIS users and staff continue to play an active part in the ESS project, as members of the newly formed Scientific Advisory Committee, in the R&D activities and through their active involvement in many associated projects, in particular instrumentation issues.

ISIS is fully committed to supporting the R&D efforts to realise a 5 MW ESS on a green field site. In the meantime ISIS continues to evolve: the first step of the upgrade to 300 μA has been approved and will be completed by 2002. The Scientific Case for the Second Target Station has been endorsed by the User Community and further upgrade options have been identified to take ISIS to 1 MW and beyond. This evolutionary approach will allow the science programme to continue to develop and progress as new experimental opportunities become available.

Neutron and Muon Beam Users Meeting (NMUM)

The 1999 Neutron and Muon Beam Users' Meeting was held at Collingwood College, University of Durham from September 9th - 10th. The objective of the meeting, organised and funded by the Engineering and Physical Sciences Research Council (EPSRC), was to provide an informal forum for researchers to discuss the current operations and future opportunities at ISIS and the ILL. The meeting was attended by 135 participants from 32 different institutions, both academic and industrial, and was chaired by Professor Andrew Harrison (Edinburgh University).

The international Review Panel of UK Physics visited ISIS in April. Their report commented that '. . . outstanding work is being performed at RAL on the neutron spallation source ISIS . . . ' (00RC2215).

Scientific Meetings

In August, the International Union of Crystallography Satellite Meeting on Structural and Dynamical Aspects of Molecular and Ionic Solids Using Neutrons was held at Merton College, Oxford and was attended by over 40 delegates from 10 countries. Twenty-four short talks were given in a wide range of sessions from model organic structures and intercalates and composites to the future impact of computers, and the informal atmosphere provided for much discussion.

Steve King (centre) and Sam Foster (second from right) from ISIS presenting copies of the ISIS calendar to poster prize winners at a reception for young chemists held at the House of Lords at the beginning of the year.

September saw the third 'New Perspectives in Neutron and Muon Science' meeting, organised by ISIS staff and held as a satellite to the NMUM in Durham. The meeting provided an opportunity for the 30 or so PhD students and post-docs who attended to present their work in a friendly atmosphere, and consisted of three keynote lectures and nine contributed talks.

To mark the occasion of the retirement of Professor Alan Leadbetter CBE as Associate Director of the Institut Laue Langevin, and to celebrate his research career in physical chemistry and neutron scattering, the joint Neutron

The TECHNI Network at their first meeting at the Cosener's House in Abingdon. TECHNI (Technology for Neutron Instrumentation) draws together expertise from 12 European laboratories with the aim of developing new detectors and optical devices for neutron instruments (00RC2115).

Members of the Sixth Oxford Neutron Scattering Summer School visiting ISIS in September (99RC4553).

Scattering Group of the Institute of Physics and the Faraday Division of the Royal Society of Chemistry held a scientific meeting entitled 'Science, Facilities and Facilitating Science' at the Cosenor's House, Abingdon on 22 and 23 October 1999. The meeting focused upon recent progress in those areas of physical chemistry with which Professor Leadbetter has been most closely associated, and also upon the developments and future prospects at the major international research facilities that he has both used and managed during the course of his scientific career.

The VESUVIO project is a collaboration between ISIS, INFM, Italy and Liverpool University under the EU TMR Programme to redesign the eVS instrument for improved resolution and higher count rate. A workshop was held in November at the Cosener's House, Abingdon, to introduce potential new users to the applications of eVS, to outline the developments planned under the VESUVIO project and allow users to input their requirements, and to discuss future applications of the technique.

Members of the London International Youth Science Forum touring ISIS with Andrew Taylor (99RC4012).

November also saw the British Crystallographic Association Physical Crystallography Group Autumn Meeting 'Pushing the Limits of Powder Diffraction' held at RAL and organised by Chick Wilson. Fifty participants heard 17 contributions on instruments, techniques and software, opportunities and challenges presented to powder diffraction, and disorder and conditions. The meeting allowed a free-flowing exchange of ideas, showing the strength of the area and the way in which powder diffraction is developing to meet current and future challenges posed by structural scientists.

ISIS People

ISIS has welcomed several new faces this year: Ken Andersen (OSIRIS), Bjørn Fåk (PRISMA), Oleg Petrenko (MARI), Daniel Bowron (SANDALS), Carlos Borlado (ENGIN), Alan Tennant (Excitations Group) Sam Foster (Large Scale Structures Group) and Matthew Dickson (Laboratories Manager). ISIS has bid a fond farewell during the year to Chris Scott who has retired from things muon, Michele Sferraza leaving for Surrey University, and Chris Benmore who is now at the IPNS in Chicago. Brian Boland has retired as Leader of the ISIS User Support Group, a role now taken on by Zoe Bowden. On the accelerator side Brain Fail, Ken Louch and Tony Borden have retired. The ISIS User Office has seen a productive year, with Rachael, Jackie and Paula giving birth to Alex, Elodie and Adam respectively.

Congratulations to Sean Langridge who has been awarded this year's Philips Physical Crystallography Prize by the Physical Crystallography Group of the British Crystallographic Association. Sean joins the illustrious list of previous ISIS winners of this prize: Mark Harris, Chick Wilson and Steve Hull.

Experimental Support

Sample Environment

This was another successful year for the Sample Environment Group with a number of notable achievements, including lost time due to SE problems at less than 0.75%.

More than 100 gas handling and high-pressure experiments were performed during the year, in both furnaces and cryostats, while the total number of helium cryostat days, more than 1200, represent an average of 7 cryostats in use every day. The cryogenics team moved into new territory supporting the first experiments at ISIS combining the 7.5 T cryomagnet with He^3/He^4 dilution fridge and He^3 sorption insert.

Thirteen of the projects supported by the Advanced Sample Environment grant from EPSRC have been completed, with the remaining 3 projects either at an advanced design stage or in-build with external suppliers. One of the projects, a LabVIEW® controlled 15-position variable temperature sample changer, underwent trouble-free commissioning and has been put into regular service. Use was made of commercially available components to simplify and accelerate the design process on this project, and a similar approach has been taken for the 9 position ambient temperature sample changer for GEM.

Sam Foster adjusts a liquid-liquid interface cell on CRISP (99RC5538).

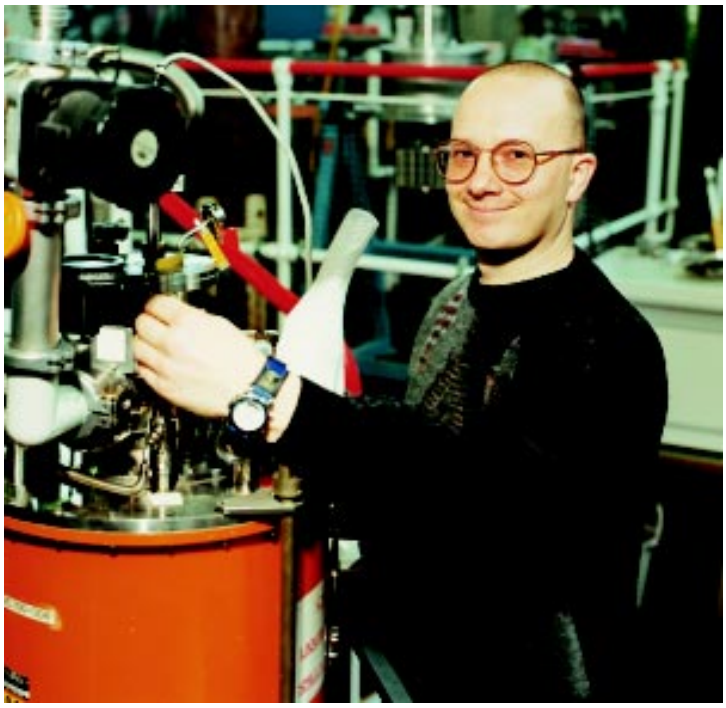

Richard Downs of the Sample Environment Group nursing an orange cryostat (00RC1438).

A full test, at 20K, of the 24-position TOSCA sample changer built at Salford University, was also completed. Sample tracking and identification uses an innovative web-camera based system and character-recognition LabVIEW® software.

In response to an increased demand by diffraction instruments a new vanadium-windowed variable temperature insert has been ordered for the 7.5 T cryomagnet. A replacement for the original MuSR dilution insert has also been ordered which will allow temperatures from 50mK to 300K to be accessed in a single cryostat.

The high-pressure section's major facilities have been upgraded by a purpose-built automated 1.0 GPa Helium gas intensifier. It will be LabVIEW® interfaced allowing users greater flexibility and control of their experiments.

The mechanical hardware of a reflector furnace to mount directly on to the ENGIN extensometer has been completed. This will enable for the first time at ISIS strain measurements at elevated temperatures.

We have also introduced for most instruments a new generation of Eurotherm-based

temperature controllers. Features of the new controllers are the options of one-shot auto-tuning, continuous adaptive tuning of PID values and an auto-ranging cryostat heater voltage.

Electronics

The detector electronics for MAPS has been completed with the manufacture and testing of 80 front-end pre-amps. Regarding the back-end of the detector electronics, a total of 34 16/18 Channel ADC Cards were designed, manufactured and tested. Each card has twelve layers of PCB tracking and over 3000 surface mount components, with over 150000 gates of programmable logic on-board controlling the position encoding process. The whole MAPS detector system represents the biggest single instrument source of work that the Electronics Group has ever undertaken.

The MAPS DAE-II system has been successfully taking data since it was installed in March 2000. Four detector cards each with 64 Mbytes of histogram memory allow data to be taken for over 27000 spectra. This represents more detector elements than the rest of the ISIS instrument detector suite put together. Since then the number of detector elements has risen to over 92000, with the final third of the detector cards currently being tested. Once MAPS has been completed, then work will start on delivering the DAE-II systems for GEM and SXD.

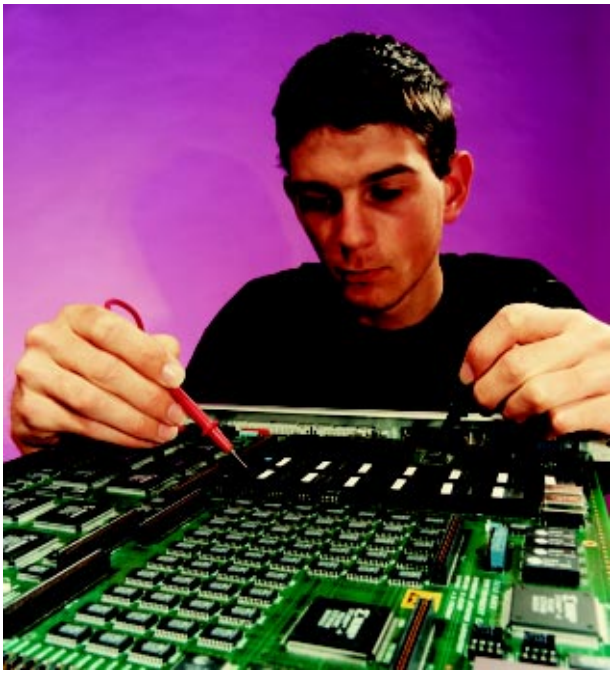

Joe Russell testing a data acquisition board (99RC2981).

The other significant work in the past year has been GEM. For the first GEM neutrons in October, approximately 400 photo-multiplier tube electronic front-end sets, nine power supply distribution boards, thirteen integrator/discriminator cards and two crates were produced. Since then, second phase of bank 6 has also been delivered. The success of the GEM electronics has led to its implementation in the HRPD 90 degree bank upgrade which is currently being manufactured, and the possibility of using GEM detector electronics for SXD-II is being investigated.

On eVS, measures have been taken to resolve the DAE-related data saturation problem at short times. Both HRPD and SANDALS have had 64 Mbyte histogram memory cards installed and electronics supplied to GEM and HRPD to enable evaluation of the ILL Gas MicroStrip detector. Also, as part of the completion of the OSIRIS detector array, five DIM2's were delivered. Currently, the testing of two DIM3's for TOSCA-II and a third Julios detector-to-DAE Interface for ROTAX is underway. Preliminary design of the LOQ Ordela Multi-Wire detector-to-DAE Interface has now started.

Detectors

Three major detector systems, GEM, MAPS and OSRIS, have been delivered this year, while further detector upgrades to other instruments are well advanced.

During cycle 99/2 phase I of the GEM detector installation programme was successfully completed with twenty-three GEM detector modules being brought into operation. One of the great successes of this project has been the transfer of bulk detector manufacture to outside industry, enabling large numbers of detector heads to be delivered in relatively short periods of time. This success was repeated for cycle 00/1 when the backscattering detector array was installed, consisting of a further twenty-four modules.

Assembly, testing and installation of the MAPS resistive wire detectors has progressed well throughout the year and the installation of all

576 detectors comprising of more than 30,000 separate pixels was complete for cycle 00/1.

A fourth OSIRIS backscattering detector has been assembled and tested in house. Benefiting from the experience gained with GEM, the construction of the final four OSIRIS detector heads was transferred to an outside manufacturing company. All five modules were tested and installed on OSIRIS ready for cycle 00/1.

The fourteen detector heads for the HRPD 90° detector upgrade have now been delivered to RAL and are being tested. They will be ready for operation in cycle 00/3. A new detector head has been constructed in house for SXD, with a further eight detector heads of this type now being manufactured for the SXD upgrade scheduled for the spring of 2001.

Design and production of the new transmission detectors for MARI and ENGIN are well advanced. Rebuilding of the TOSCA detector system to provide a factor of three increase in available detector area is progressing. A new detector for VESUVIO with improved light collection and more stable electronics has been designed and successfully tested on eVS. Detailed design of a new scintillation detector system for ENGIN-X with 3 mm resolution is also underway.

Research and development of new detector systems continues, particularly under the umbrella of the TECHNI initiative. Work on a variety of different detector projects involves collaborations with personnel from Perugia, ILL, Delft and Rome. Microstrip gas detector technology continues to be of great interest. The ILL kindly loaned ISIS a D4 detector module which was tested on HRPD with encouraging results. In collaboration with CLRC's Instrumentation Department, a two-dimensional microstrip gas detector with application as a position sensitive beam monitor is in the final stages of completion. In addition, work with MSI on developing a detector based on their new gadolinium borate scintillator with high pulse pair resolution and relatively low gamma sensitivity has progressed well. The option of using fibre coupled readout techniques with this material now seems a real possibility.

Winfried Kockelmann mounting a calcite sample from Syros in Greece on the new ROTAX goniometer (99RC5258).

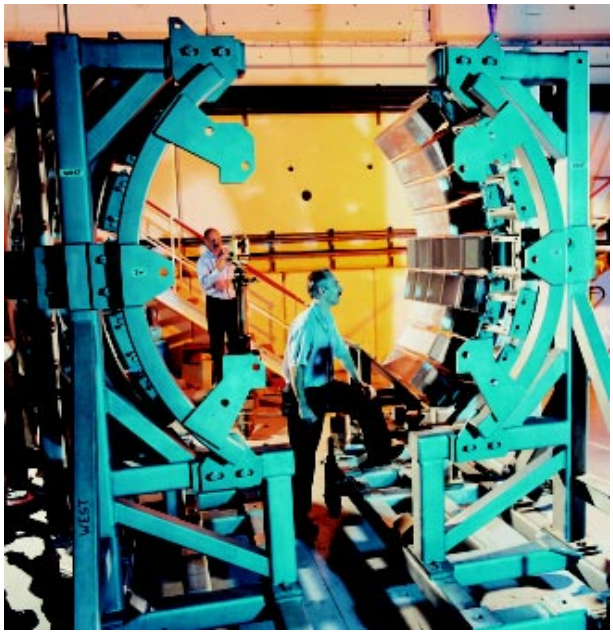

Detector installation on GEM (99RC4802).

Computing

The Computing Group splits its time between managing, supporting and upgrading all aspects of the ISIS computing infrastructure, and developing software for instrument control and data manipulation.

The group spent a significant amount of time this year ensuring that ISIS computer systems were Y2K compliant with a range of tests and upgrades.

John Finney and Frank Gotthardt (UCL) analysing GEM data (00RC1444).

As a consequence the new millennium started with very few problems.

To counter attacks by computer hackers, security has gradually been increased while aiming to minimise the impact on our genuine users. One restriction is that the VMS cluster can now only be accessed through a single node.

On the instrument side the group worked on a number of upgrades. The GEM control system was commissioned, based around a system 200 times more powerful than the LAD computer. As part of MAPS moving towards a full compliment of detectors its computer is now connected to the second generation DAE. So far its control program handles 128 MB of data per run - twice the size of any other instrument and continuing to grow! Computer upgrades to SANDALS, eVS and OSIRIS have resulted in much greater reliability.

Further sample environment and beam line control devices have been integrated into the control system using the Labview®-based Ray-of-Light program including the new MAPS chopper, a dilution fridge and the SANDALS sample changer. Also linked in were the TPG vacuum gauges and OSIRIS TSX1820P power supplies.

ISIS continues to produce an increasing volume of data with the archive growing by 105 GB and 75000 datasets this year. Within the next 2 to 3 years this could rise towards 1 TB/yr! To cope with the demand for more working space an additional 800 GB of disk storage space has been added to the VMS cluster to be split between archive and user space. Faster access has been achieved by ensuring more files are either on-line or accessible through the CLRC's multi-terabyte automated data store. More data also causes a greater network load and a Gigabit backbone has now been installed in the experimental hall.

Movement of software towards running on PCs using NT4 continues. As well as the project to control instruments using the Ray-of-Light program, PC based data analysis is growing. Visitors regularly bring laptops to ISIS and their network connection is now accommodated both in the on-site hostel and around ISIS.

A new version of OpenGENIE is available on VMS, UNIX and NT4 and it has a new reference manual. As part of a move towards greater portability of data ISIS is heavily involved in developing code for NeXus, the standard neutron and X-ray format based on the Hierarchical Data Format. HDF can be read by several standard packages (eg. IDL). OpenGENIE both writes and reads NeXus files.

Stewart Campell of the ISIS Computing Group keeping the VMS cluster in order (00RC3776).

User Interaction and Support

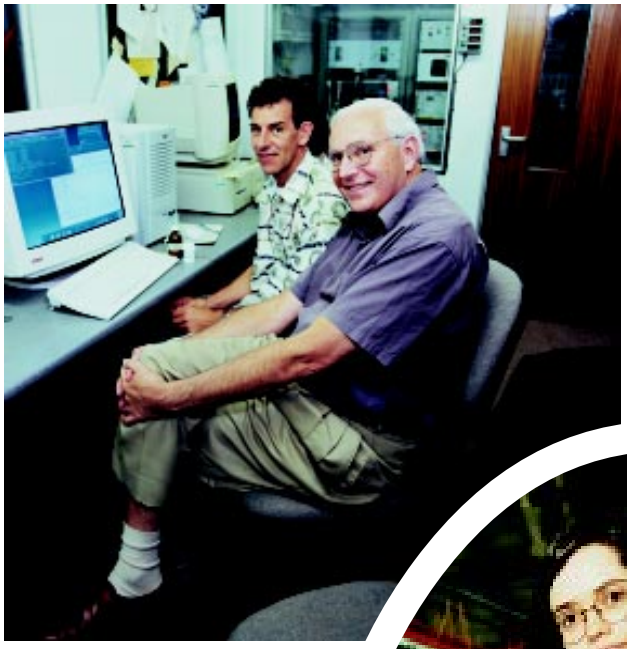

Above left: John White and Jeremy Ruggles (ANU, Canberra), reflecting upon their data in the SURF cabin (00RC1716). Main Picture: Paz Vaqueiro (Heriot-Watt) increasing the pressure on her sample of chromium thiospinel during a high pressure experiment on POLARIS (00RC1284). Below left: Valeria Arrighi and Simona Gagliardi (Heriot-Watt) analysing data from a polymer experiment on IRIS (00RC1705).

Above right: Paolo Radaelli (ISIS) and M Matsuda (RIKEN) inspecting their GEM experiment (00RC1260). Below right: Slava Storchak and Dmitri Eschenko (Kurchatov Institute, Moscow) investigating muon dynamics in solid CO_2 (00RC1872).

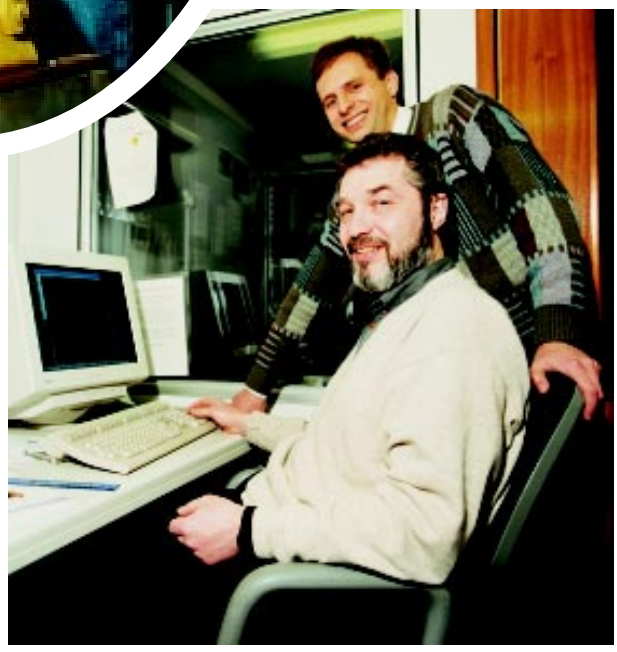

Publications

Publications relate to all work carried out at ISIS. In addition, work performed elsewhere by ISIS staff is included where relevant. 550 publications resulting from ISIS work were reported this year; a further 103 are updated from those which were 'in press' at the time of last year's report.

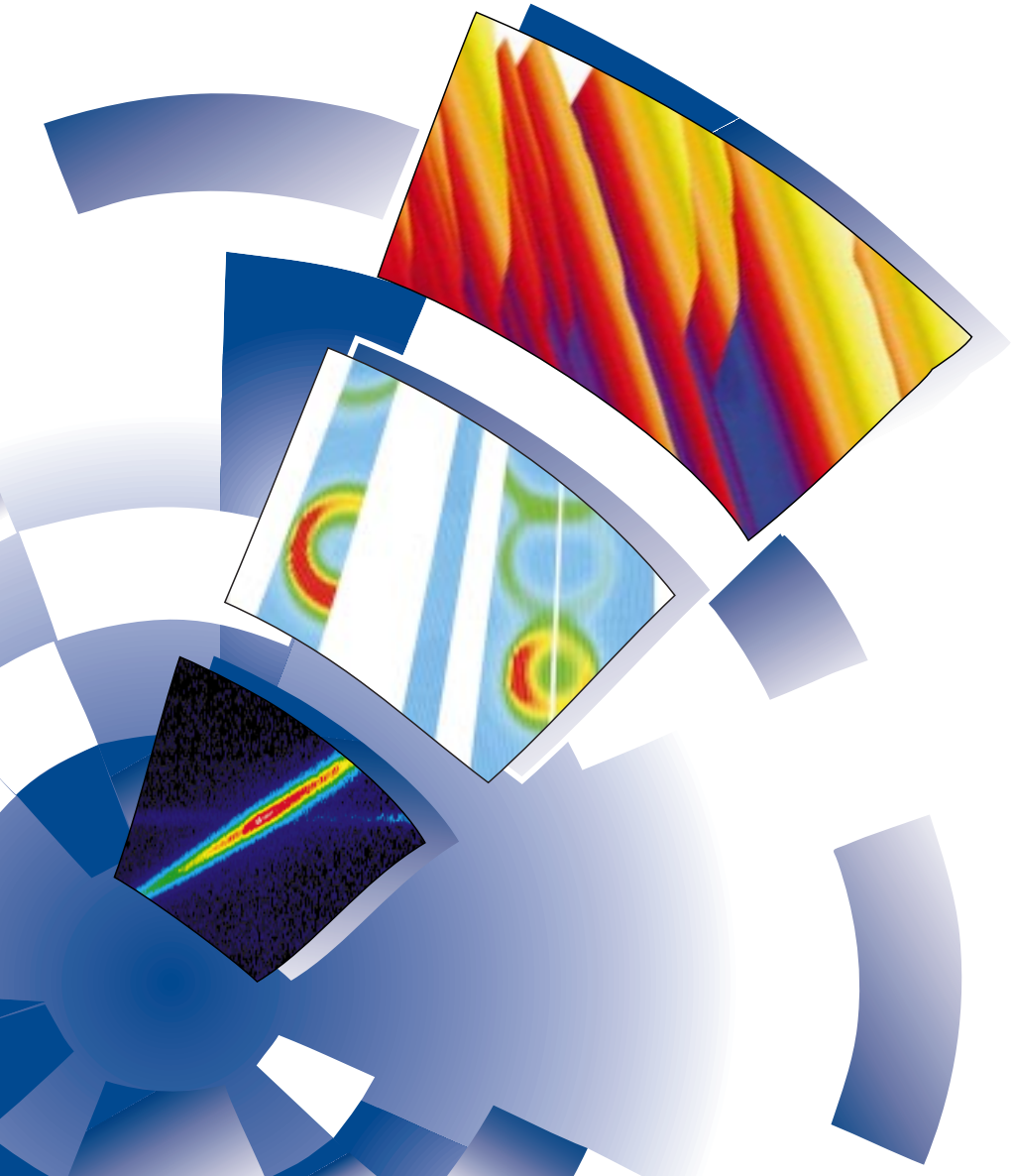

ISIS Publications 1999 - 2000

T Abdul Redah, E B Karlsson, C A Dreismann, R M Streffer, B Hojvardsson, J Uhrmalm, J Mayers
Anomalous neutron Compton scattering in metallic hydrides: new experiments
Physica **B 276-278** 824 (2000)

I Abrahams, A J Bush, G E Hawkes, T Nunes
Structure and oxide ion conductivity mechanism in $Bi_2Al_4O_9$ by combined X-ray and high resolution neutron powder diffraction and ^{27}Al solid state NMR
J Solid State Chem **147** 631 (1999)

St Adams, J Swenson
Determining ionic conductivity from structural models
Phys Rev Lett **84** 4144 (2000)

P Adler, S G Eriksson
Structural properties, Mossbauer spectra and magnetism of perovskite-type oxides $SrFe_{1-x}Ti_xO_{3-y}$
Z Anorg Allg Chem **626** 118 (2000)

D T Adroja, B D Rainford, K S Knight, P C Riede, T Takabatake
Neutron scattering studies of an antiferromagnetic Kondo lattice: $Ce_8Pd_{24}Ga$
J Phys:Condens Matter (in press 2000)

A K Adya, L Bianchi, C J Wormald
The structure of liquid methanol by H/D substitution technique of neutron diffraction
J Chem Phys **112** 4231 (2000)

A K Adya, H Matsuura, R Takagi, L Rycerz, M Gaune-Escard
STructural and thermodynamic properties of molten UCl_3 and UCl_3-MCl (M=Li, Na, K, Cs) systems
Proc 12th Int Symp on Molten Salts, (Electrochemical Society) 99-12 (in press 2000)

A K Adya, H Matsuura, R Takagi, L Rycerz, M Gaune-Escard
The structure of molten UCl_3 by neutron and X-ray diffraction and molecular dynamics simulations
Proc Int George Papatheodorou Symp (ICE/HT Patras) p53 (1999)

G Aeppli, S M Hayden, P Dai, H A Mook, R D Hunt, T G Perring, F Dogan
The weights of various features in the magnetic spectra of cuprates
Physica Status Solidi **B 215** 519 (1999)

G Aeppli, D J Bishop, C Broholm, P Dai, S M Hayedn, T G Perring et al
Neutron scattering and the search for mechanisms of superconductivity
Physica C **318** 9 (1999)

S Affrossman, F T Kiff, S A O'Neill, R A Pethrick, R W Richards
Topography and surface composition of thin films of blends of PMMA and PEO
Macromolecules **32** 2721 (1998)

P Ahlstrom, O Borodin, G Wahnstrom, E J W Wensink, P Carlsson, G D Smith
Molecular dynamics simulation of structural and conformational properties of poly(propylene oxide)
J Chem Phys (in press 2000)

M Ain, S J Blundell, J S Lord, J Jegoudez, A Revcolevschi
Muon spin relaxation in NaV_2O_5
Physica B **284-288** 1633 (2000)

M Ain, S J Blundell, J S Lord, J Jegoudez, A Revcolevschi
Muon spin relaxation in NaV_2O_5 in its spin-Peierls phase
Physica B **281-282** 648 (2000)

P B Aitchison, B Ammundsen, T Bell, D J Jones, J Roziere, G R Burns, H Berg, R Tellgren, J Thomas
Proton insertion in spinel lithium manganates and the effect of manganese substitution
Physica B (in press 2000)

P B Aitchison, B Ammundsen, D J Jones, J Roziere, G R Burns
Long range and local structure on Ti, Cr, Co and Ga-doped lithium manganate spinels
Proc Mat Res Soc, Spring meeting (in press 1999)

R Akagi, K Handa, N Ohtori, A C Hannon, M Tatsumisago, N Umesaki
Structure of K_2O-TeO_2 glasses
Japanese J Applied Physics **38** 160 (1999)

F A Akeroyd, R L Ashworth, S I Campbell, S D Johnston, J M Martin, C M Moreton-Smith, R G Sergeant, D S Sivia
The ISIS Open GENIE User Manual
RAL-TR-2000-002 (2000)

F A Akeroyd, R L Ashworth, S I Campbell, S D Johnston, C M Moreton-Smith, R G Sargeant, D S Sivia
Open GENIE Reference Manual
RAL-TR-1999-031 (1999)

S Al-Heniti, N Cowlam, A R Wildes
A study of the structures of some (FeRu)B metallic glasses by X-ray and neutron scattering
J Phys:Condens Matter **11** 9139 (1999)

P W Albers, H Klein, E S Lox, K Seibold, G Prescher, S F Parker
INS-, SIMS- and XPS-investigations of diesel engine exhaust particles
Phys Chem Chem Phys **2** 1051 (2000)

P W Albers, G Prescher, K Seibold, S F Parker
Applications of inelastic incoherent neutron scattering in technical catalysis
Studies in Surface Science and Catalysis, Eds A Corma, F V Melo, S Mendioroz, J J G Fierro (Elsevier, Amsterdam) **130** 3155 (2000)

P W Albers, H Angert, G Prescher, K Seibold, S F Parker
Catalyst poisoning by methyl groups
J Chem Soc, Chem Comm **17** 1619 (1999)

P W Albers, M Poniatowski, S F Parker, D K Ross
Inelastic neutron scattering study on different grades of palladium of varying pretreatment
J Phys:Condens Matter **12** 4451 (2000)

D R Allan, S J Clarke, R M Ibberson, P Parsons, C R Pulham, L Sawyer
The influence of pressure and temperature on the crystal structure of acetone
J Chem Soc, Chem Comm **751** (1999)

C Andreani, D Colognesi, E Pace
Deep inelastic neutron scattering from fluid hydrogen and deuterium: From vibrational excitations to the impulse approximation
Phys Rev **B60** 10008 (1999)

C Andreani, P Cipriani, D Colognesi, E Pace
Single-particle dynamics in fluid hydrogen and deuterium
J Phys:Condens Matter **12** 139 (2000)

C Andreani, D Colognesi, E Pace
Deep inelastic neutron scattering from fluid and solid H_2 and D_2
Neutron News **11** 21 (2000)

Y G Andreev, P G Bruce
Polymer electrolyte structure and its implications
Electrochimica Acta **45** 1417 (2000)

B K Annis, A Habenschuss, C J Benmore, O Borodin, D Bedrov, G D Smith
Comparison of scattering data and molecular dynamics simulations for liquid poly(ethylene oxide),PEO, and small molecule analogs
Bull American Phys Soc **45** 568 (2000)

M Arai, Y Inamura, T Otomo
Novel dynamics of vitreous silica and metallic glass
Phil Mag **B 79** 1733 (1999)
M Arai, T Nishijima, Y Endoh, S Tajima, K Tomimoto, Y Shiohara, M

Takahashi, A Garrett, S M Bennington
Incommensurate spin dynamics of superconductor $YBa_2Cu_3O_{6+x}$
High Temperature Superconductivity, Eds S E Barnes et al, American Institute of Physics Conference Proceedings **483** p172 (1999)

D N Argyriou, J F Mitchell, P G Radaelli, H N Bordallo, D E Cox, M Medarde, J D Jorgensen
Lattice effects and magnetic structure in the layered colossal magnetoresistance manganite $La_{2-2x}Sr_{1+2x}Mn_2O_7$, x = 0.3
Phys Rev **B59** 8695 (1999)

D N Argyriou, J F Mitchell, J D Jorgensen, J B Goodenough, P G Radaelli, D E Cox, H N Bordallo
Structure and magnetism in the layered CMR manganites $La_{2-2x}Sr_{1+2x}Mn_2O_7$ (x=0.3, 0.4)
Australian J Phys **52** 279 (1999)

A R Armstrong, A D Robertson, P G Bruce
Structural transformation on cycling layered $Li(Mn_{1-y}Co_y)O_2$ cathode materials
Electrochimica Acta **45** 285 (1999)

V Arrighi, W Zajac, S Shenoy, D Martin, B Gabrys, M T Garay, S Gagliardi, K H Andersen
Short range order in blends of polycarbonates with polystyrene
Physica B **276-278** 849 (2000)

G Artioli, C Lamberti, G L Marra
Neutron powder diffraction study of orthorhombic and monoclinic defective silicalite
Acta Cryst **B56** 2 (2000)

J M Baker, I Z Machi, S H Connell, K Bharuth Ram, J E Butler, S F J Cox, C G Fischer, T Jestadt, P Murphy et al
Longitudinal field muon spin relaxation (LF-μSR) measurements and evidence for a new muonium defect site in type Ia diamond
Hyp Inter **121** 579 (1999)

S M Baker, G S Smith, D L Anastassopoulos, C Toprakcioglu, A A Vradis, D G Bucknall
Structure of polymer brushes under shear flow in a good solvent
Macromolecules **33** 1120 (2000)

V I Bakhmutov, J A K Howard, D A Keen, L G Kuzmina, L A Leech, G I Nikonov, E V Vorontsov, C C Wilson
Combined single crystal neutron diffraction and solution NMR relaxation studies of mono- and bis(silyl) substituted niobocene hydrides with nonclassical interligand interactions
Dalton Transactions 1631 (2000)

A M Balagurov, D V Sheptyakov, V L Aksenov, E V Antipov, S N Putlin, P G Radaelli, M Marezio
Structure of $HgBa_2CuO_{4+\delta}$ ($0.06<\delta<0.19$) at ambient and high pressure
Phys Rev **B59** 7209 (1999)

D Barlow, A M Muslim, J R P Webster, J Penfold, C M Hollinshead, M J Lawrence
Molecular modelling of surfactant monolayer under constraints derived from neutron reflectance measurements
Phys Chem Chem Phys (in press 2000)

D J Barlow, M J Lawrence, S Zuberi, T Zuberi, R K Heenan
Small angle neutron studies on the nature of the incorporation of polar oils in aggregates of N,N-dimethyl-dodecylamine-N-oxide
Langmuir (in press 2000)

F Bartolome, J Bartolome, R S Eccleston
Induced and Cooperative Order of Nd ions in $NdNiO_3$
J Appl Phys **87** 7052 (2000)

E S Bates, R L Lichti, S F J Cox, C Schwab
Low temperature diamagnetic muonium states in n-type gallium arsenide
Physica B **289-290** 550 (2000)

P D Battle, W R Branford, A Mihut, M J Rosseinsky, J Singleton, J Sloan, L E Spring, J F Vente
Structural chemistry and electronic properties of the n=3 Ruddlesden-Popper phases $Ca_4Mn_2FeO_{9\cdot75}$ and $Sr_4Mn_2FeO_{9\cdot80}$
Chemistry of Materials **11** 674 (1999)

P D Battle, G R Blake, T C Gibb, J F Vente
Structural chemistry and electronic properties of Sr_2FeIrO_6
J Solid State Chem **145** 541 (1999)

P D Battle, M J Rosseinsky, P G Radaelli
Comment on 'Neutron-diffraction studies on the magnetic ordering process in the layered Mn perovskite $La_{2-2x}Sr_{1+2x}Mn_2O_7$ (x=0.40, 0.45 and 0.48)'
J Phys Soc Japan **68** 1462 (1999)

U Beck, W Freyland
A neutron diffraction study on liquid Rb-Sb alloys
J Non-Cryst Solids **250-252** 250 (1999)

A M T Bell, J N B Smith, J P Attfield, J M Rawson, K Shankland, W I F David
A synchrotron X-ray powder diffraction study of 4-(2,3,4-trifluorophenyl)-1,2,3,5-dithiadiazoyl. Crystal structure determination using a global optimisation method
New Journal of Chemistry **23** 565 (1999)

A V Belushkin
Application of neutron scattering methods to the study of superprotonic conductors
Solid State Ionics **125** 61 (1999)

C J Benmore, Y L Loh
The structure of liquid ethanol: a neutron diffraction and molecular dynamics study
J Chem Phys **112** 5877 (2000)

S M Bennington, N Kitamura, M G Cain, M H Lewis, R A Wood, A Fukumi, K Funakoshi
In-situ diffraction measurements of the polymerisation of C_{60} at high temperatures and pressures
J Phys:Condens Matter **12** L451 (2000)

P Berastegui, S Hull
The crystal structures of thallium(I) fluoride
J Solid State Chem **150** 266 (2000)

F J Bermejo, B Fak, S M Bennington, R Fernandez Perea, C Cabrillo, J Dawidovski, M T Fernandez Diaz, P Verkerk
Microscopic dynamics in liquid para-H_2
Phys Rev **B60** 15154 (1999)

F J Bermejo, K Kinugawa, C Cabrillo, S M Bennington, B Fak, M T Fernandez Diaz, P Verkerk, J Dawidowski, R Fernandez Perea
Quantum effect on liquid dynamics as evidenced by the presence of well-defined collective excitations in liquid para-hydrogen
Phys Rev Lett **84** 5359 (2000)

R I Bewley, R S Eccleston, T Nagata, J Akimitsu
Hole migration in the spin-ladder, dimer chain material $Sr_{2.5}Ca_{11.5}Cu_{24}O_{41}$
Physica **B 276-278** 662 (2000)

R I Bewley, S J Blundell, B W Lovett, T Jestadt, F L Pratt, K H Chow, W Hayes, P D Battle, M A Green et al
μSR studies of magnetic order and dynamics of the n = 2 Ruddlesden-Popper phases $Sr_2RMn_2O_7$ (R = Pr, Nd, Sm, Eu, Gd, Tb, Dy, and Ho)
Phys Rev **B60** 12286 (1999)

L Bianchi, A K Adya, O N Kalugin, C J Worwald
The structure of liquid methanol: a molecular dynamics study using a six-site model
J Phys:Condens Matter **11** 9151 (1999)

L Bianchi, O N Kalugin, A K Adya, C J Wormald
The structure of liquid methanol: a molecular dynamics study using three-site models
Molecular Simulations **23** (in press 2000)

G R Blake, P D Battle, J Sloan, J F Vente, J Darriet, F Weill
Neutron diffraction study of the structures of $Ba_5CuIr_3O_{12}$ and $Ba_{16}Cu_3Ir_{10}O_{39}$
Chemistry of Materials **11** 1551 (1999)

S J Blundell, A Husmann, T Jestadt, F L Pratt, I M Marshall, B W Lovett, M Kurmoo, T Sugano, W Hayes
Muon studies of molecular magnetism
Physica **B** (in press 2000)

Publications

S J Blundell
Spin-polarized muons in condensed matter physics
Contemporary Phys **40** 175 (1999)

S J Blundell
μSR studies of organic magnets
Phil Trans Roy Soc Lond A **357** 2923 (1999)

M Bonin, W G Marshall, H-P Weber, P Toledano
Structure of the high pressure phases of urea
Rev High Pressure Sci Technol (in press 2000)

Z A Bowden, D Colognesi, R J Newport, S F Parker, J Tomkinson, M Zoppi
The TOSCA incoherent inelastic neutron spectrometer: progress and results
Physica B **276-278** 98 (2000)

D A Braden, B S Hudson
Ab initio and DFT studies of structure, vibrations and inelastic neutron scattering spectra
J Phys Chem **104** 982 (2000)

D K Breitinger, J Mohr, H Schukow, R G Schwab, D Colognesi, S F Parker
IR, Raman and neutron spectrometry of florencites $LaAl_3(OH)_6(XO_4)_2$ (X=P and V)
7th Austrian-Hungarian Int Conf on Vibrational Spectroscopy (Balatonfured, Hungary) p40 (1999)

D K Breitinger, J Mohr, H Schukow, S F Parker, D Colognesi, R G Schwab
Vibrational spectra of florencites
Eur Conf on Solid State Chemistry (Madrid) **II** p171 (1999)

D K Breitinger, H Schukow, Th Zeiske, J Mohr, J Tomkinson, R G Schwab
Untersuchung von Struktur und Dynamik von Aluniten mit Neutronenstreuung
Erlanger Beitr. Petr. Min. **9** 19 (1999)

T Brennan, G A Saunders, B D Rainford, R S Eccleston, G Carini, G DAngelo, G Tripodo
Low energy excess magnetic states in terbium metaphosphate glass
Phil Mag B **79** 2121 (1999)

W Bronger, G Auffermann
New alkali-metal-transition-metal hydrides synthesised at high-pressure: characterization and properties
Chemistry of Materials **10** 2723 (1998)

W Bronger, G Auffermann
Rb_3ReH_{10}, ein neues Hydrid des siebenwertigen Rheniums - Hochdrucksynthese
Z anorg allg Chem **625** 1147 (1999)

A S Brown, R W Richards, D M A Buzza, T C B McLeish
Surface visco-elastic modes in a spread film of a block copolymer
Farad Disc **112** 309 (1999)

A S Brunacci, F T Kiff, R W Richards, R I Thompson, S M King
Influence of temperature and composition on the small angle neutron scattering from polydiene star diblock copolymers and mixtures with homopolymers
Polymer **41** 2557 (1999)

D G Bucknall, S A Butler, J S Higgins
Neutron reflectivity of polymer interfaces
J Phys Chem Solids **60** 1273 (1999)

D G Bucknall, S A Butler, J S Higgins
Real-time measurement of polymer diffusion coefficients using neutron reflection
Macromolecules **32** 5453 (1999)

F J Burghart, W Potzel, G M Kalvius, E Schreier, G Frosse, D R Noakes, W Schafer, W Kockelmann, S J Campbell et al
Magnetism of crystalline and nanostructured $ZnFe_2O_4$
Physica B (in press 2000)

C J Burnham, J-C Li, S S Xantheas, M Leslie
The parametrization of a Thole-type all-atom polarizable water model from first principles and its application to the study of water clusters (n=2-21) and the phonon spectrum of ice Ih
J Chem Phys **110** 4566 (1999)

O Byron, R J C Gilbert
Neutron scattering: good news for biotechnology
Current Opinion in Biotechnology **11** 72 (2000)

R Caciuffo, P Schiebel
Rotational tunneling and quantum dynamics of methyl groups in supramolecular complexes
Neutron News **11** 17 (2000)

J M Cadogan, Suharyana, D H Ryan, O Moze, W Kockelmann
Neutron diffraction and Mössbauer Study of the magnetic structure of YFe_6Al_6
J Appl Phys **87** 6046 (2000)

M Calvo-Dahlborg, U Dahlborg, V E Sidorov, P S Popel, S V Chernoborodova
Physical properties of some iron based alloys in liquid and amorphous states
J Mat Sci (in press 2000)

M Calvo-Dahlborg, J M Ruppert
Influence of the production conditions on the quality and mechanical properties of metallic glasses
Mechanical Properties of Metallic Glasses, Eds V Z Bengus, V Ocelik (UEF SAV Kosice) p9 (1998)

S J Campbell, M Hofmann, A Calka
The synthesis of TiN by ball-milling - a neutron diffraction study
Physica B **276-278** 899 (2000)

S J Campbell, J M Cadogan, X L Zhao, M Hofmann, Li Hong-Shuo
Magnetic transitions in $La_{1-x}Y_xMn_2Si_2$ - Mossbauer investigation (4.2 - 520K)
J Phys:Condens Matter **11** 7835 (1999)

S I Campbell, M T F Telling, C J Carlile
The optimisation of analyser geometry for a near back-scattering spectrometer - IRIS on the ISIS Pulsed Source
Physica B **276-278** 206 (2000)

P Carlsson, J Swenson, L Borjesson, R L McGreevy, P Jacobsson, L M Torell, W S Howells
Neutron diffraction investigations of the cation coordination in an amorphous polymer electrolyte, PPO-$LiClO_4$
Electrochimica Acta **45** 1449 (2000)

P Carlsson, J Swenson, D Andersson, L Borjesson, R L McGreevy, P Jacobsson, L M Torell, W S Howells
Structural investigations of polymer electrolyte PPO-$LiClO_4$ using diffraction experiments and reverse Monte Carlo simulation
J Chem Phys (in press 2000)

V J Carter, J P Kujanpaa, F G Riddell, P A Wright, J F C Turner, C R A Catlow, K S Knight
Structure and dynamics of methyl groups in the deuterated microporous organic-inorganic hybrid, aluminium methylphophonate-b
Chem Phys Lett **313** 505 (1999)

G S Case, A L Hector, W Levason, R L Needs, M F Thomas, M T Weller
Synthesis, powder neutron diffraction structures and Mossbauer studies of some complex iron oxyfluorides: $Sr_3Fe_2O_6F_{0.87}$, Sr_2FeO_3F and $Ba_2InFeO_5F_{0.68}$
J Materials Chemistry **9** 2821 (1999)

M A Castro, S M Clarke, A Inaba, R K Thomas, T Arnold
The investigation of mixed monolayers adsorbed from solution: Octane and nonane mixtures on graphite
Phys Chem Chem Phys **1** 5017 (1999)

M Catti, S Stramare, R M Ibberson
Lithium location in NASICON-type Li^+ conductors by neutron diffraction. I. Triclinic α'-$LiZr_2(PO_4)_3$
Solid State Ionics **123** 173 (1999)

M Catti, N Morgante, R M Ibberson
Order-disorder and mobility of Li^+ in the β'-β'-$LiZr_2(PO_4)_3$ ionic conductors: a neutron diffraction study
J Solid State Chem **152** 340 (2000)

M Celli, D Colognesi, M Zoppi
The measurement of the translational kinetic energy of liquid hydrogen using TOSCA
Physica B **276-278** 814 (2000)

M Celli, N Rhodes, A K Soper, M Zoppi
The total neutron cross section of liquid para-hydrogen
J Phys:Condens Matter **11** 10229 (1999)

M Ceretti, S Janssen, D McMorrow, P Radaelli, U Steigenberger
ECNS'99 - Young Scientists Forum
Physica **B 276-278** 45 (2000)

B Charrier, S P Cottrell, D Schmitt
Spin dynamics in i-$R_8Mg_{42}Zn_{50}$ quasicrystals (R = Gd, Tb, Dy)
Physica **B 266** 165 (1999)

B-C Choi, A Samad, W Y Lee, S Langridge, J Penfold, J A C Bland
Layer selective magnetic moment distribution in an epitaxial double spin valve structure
IEEE Trans Mag **35** 3847 (1999)

H Choo, M A M Bourke, P G Nash, M R Daymond
Evolution of thermal residual stress in intermetallic matrix composites during heating
Proc 24th Cocoa Beach meeeting, Am Ceram Soc (in press 2000)

M Chorlton, K Nikbin, G A Webster
Effects of cyclic loading and residual stresses on the early stages of creep crack growth
Lifetime Management and Evaluation of Plant, Structures and Components, Eds J H Edwards et al (EMAS Publishing) p47 (2000)

S J Clarke, C W Michie, M J Rosseinsky
Structure of Zr_2ON_2 by neutron powder diffraction: The absence of nitride-oxide ordering
J Solid State Chem **146** 399 (1999)

K N Clausen, F Bodker, M F Hansen, L Theil Kuhn, K Lefmann, P-A Lindgard, S Morup, M T Telling
Structure and dynamics of magnetic nanoparticles
Physica **B 276-278** 830 (2000)

R Coldea, S M Hayden, G Aeppli, T G Perring, C D Frost, T E Mason, S W Cheong, Z Fisk
Spin excitations and exchange couplings in the cuprate antiferromagnet La_2CuO_4
Physica B **276-278** 592 (2000)

J M Cole, E R H van Eck, G Mountjoy, R J Newport, T Brennan, G A Saunders
A neutron diffraction and ^{27}Al MQMAS NMR study of rare-earth phosphate glasses, $(R_2O_3)_x(P_2O_5)_{1-x}$, x = 0.187-0.263, R = Ce, Nd, Tb containing Al impurities
J Phys:Condens Matter **11** 9165 (1999)

J M Cole, C C Wilson, J A K Howard, F R Cruikshank
Quantitative analysis of hydrogen-bonding and anomalous atomic thermal motion in an organic non-linear optical material using X-ray and neutron diffraction
Acta Cryst B (in press 2000)

S Collins, S K Peace, R W Richards, W A MacDonald, S M King
Transesterification in polyethylene terephthalate. Molecular weight and end group effects
Macromolecules **33** 2981 (2000)

S Collins, A M Kenwright, C Pawson, S K Peace, R W Richards
Transesterification in mixtures of polyethylene terephtalate and polyethylene naphthalene-2,6-dicarboxylate: an NMR study of kinetics and end group effects
Macromolecules (in press 2000)

D Colognesi, E Pace
Deep inelastic neutron scattering from diatomic molecules
Physica **B 266** 267 (1999)

D J Cooke, C C Dong, R K Thomas, A M Howe, E A Simister, J Penfold
The interaction between gelatin and SDS at the air-water interface: a neutron reflection study
J Phys Chem B (in press 2000)

L Cormier, P H Gaskell, S Creux
Comparison of the low-Q features in diffraction data for silicate glasses and crystals containing Sr or Ba
J Non-Cryst Solids **248** 84 (1999)

S P Cottrell, S F J Cox, C A Scott, J S Lord
The commissioning of a spectrometer optimised for radiofrequency measurements at a pulsed muon source
Physica B **289-290** 693 (2000)

S P Cottrell, J S Lord, W G Williams
Muon charge state and dynamics in alkali metal hydrides
Physica B **289-290** 570 (2000)

R A Cowley
The coherence of the magnetic structures of rare-earth superlattices
J Magn Magn Mater **177-181** 1156 (1998)

R A Cowley
The excitations of one-dimensional spin 1/2 antiferromagnets
Dynamical Properties of Unconventional Magnetic Systems, Eds A T Skjeltorp, D Sherrington, NATI ASI Series (Kluwer Academinc) **349** 5 (1998)

R A Cowley
The magnetic structures of rare-earth superlattices
Dynamical Properties of Unconventional Magnetic Systems, Eds A T Skjeltorp, D Sherrington, NATI ASI Series (Kluwer Academinc) **349** 203 (1998)

S F J Cox, S P Cottrell, M Charlton, P Donnelly, S J Blundell, J L Smith, J C Cooley, W L Hults
Muon Korringa relaxation
Physica B **289-290** 594 (2000)

S F J Cox
Muonium states and dynamics
Muon Science: Muons in Physics, Chemistry and Materials, Eds S L Lee, S H Kilcoyne, R Cywinski (I O P Publishing, Bristol) (1999)

S F J Cox, P J C King, W G Williams, K H Chow, T H Jestadt, W Hayes, R L Lichti, C R Schwab, E A Davis
Modelling hydrogen in the III-V nitrides by its pseudo-isotope, muonium
Physica B **289-290** 538 (2000)

S F J Cox, S P Cottrell, J S Lord, C A Scott, U A Jayasooriya, G A Hopkins, N Suleimanov
μSR studies of elemental boron, modelling interstitial protons with implanted positive muons
Mag Res in Chemistry **38** S9 (2000)

A Criado, M Jiménez-Ruiz, C Cabrillo, F J Bermejo, M Grimsditch, H E Fischer, S M Bennington, R S Eccleston
Role of low-frequency vibrations on sound propagation in glasses at intermediate temperature
Phys Rev **B61** 8778 (2000)

T Csoka, K Shankland, C C Wilson, A D Taylor
Neutrons in the material world
CERN Courier **40** no 3 (Apr 2000)

U Dahlborg, W S Howells, M Calvo-Dahlborg, J M Dubois
Diffusive motions in an $Al_{50}Cu_{35}Ni_{15}$ crystalline alloy at high temperature
Mat Sci Eng **A** (in press 2000)

U Dahlborg, W S Howells, M Calvo-Dahlborg, J M Dubois
Atomic motions in the crystalline $Al_{50}Cu_{35}Ni_{15}$ alloy
J Phys:Condens Matter **12** 4021 (2000)

U Dahlborg, M Calvo-Dahlborg, R K Heenan, J M Ruppert, V E Sidorov, P S Popel
Influence of the production conditions on the microstructure of nickel phosphorous metallic glasses studied by small-angle neutron scattering
Phil Mag (in press 2000)

Publications

U Dahlborg, M Calvo-Dahlborg
Influence of the production conditions on the structure and microstructure of metallic glasses
Mechanical Properties of Metallic Glasses, Eds V Z Bengus, V Ocelik (UEF SAV Kosice) p17 (1998)

U Dahlborg, M Calvo-Dahlborg
Influence of the production conditions on the structure and the microstructure of metallic glasses studied by neutron scattering techniques
Mat Sci Eng A (in press 2000)

U Dahlborg, M Calvo-Dahlborg
Structure and properties of some glass-forming liquid alloys
Eur J Phys (in press 2000)

P Dalmas de Reotier, A Yaouanc, R H Heffner, J L Smith, P C M Gubbins, C T Kaiser
Muon spin relaxation and rotation measurements on single crystals of the heavy fermion superconductor UBe_{13}
Phys Rev B (in press 2000)

P Dalmas de Reotier, A Yaouanc, P C M Gubbins, C T Kaiser, A M Mulders, P Bonville, P J C King et al
Magnetism and superconductivity of UPt_3 by muon spin techniques
Physica B (in press 2000)

W I F David, J S O Evans, A W Sleight
Direct evidence for a low frequency phonon mode mechanism in the negative thermal expansion compound ZrW_2O_8
Europhys Lett **46** 661 (1999)

W I F David, K Shankland, T Csoka
Simulated annealing as a tool for structure determination from powder diffraction cata
Acta Cryst **A55** Supplement (1999)

M R Dawdy, R L Lichti, S F J Cox, T L Head, C Schwab
Muonium transitions in n-type gallium nitride
Physica B **289-290** 546 (2000)

M R Daymond, C N Tome, M A M Bourke
Intergranular strains in textured steel
Proc European Conf on Residual Stress **V** (in press 1999)

M R Daymond, C N Tome, M A M Bourke
Measured and predicted intergranular strains in textured austenitic steel
Acta Mat **48** 553 (2000)

M R Daymond, L Edwards
Squeezing the most out of neutrons
Materials World p22 (2000)

S de Brion, F Ciorcas, G Chouteau, P Lejay, P G Radaelli, C Chaillot
Magnetic and electric properties of $La_{1-\delta}MnO_3$
Phys Rev **B59** 1304 (1999)

A V de Siqueira, C Lobban, N T Skipper, G D Williams, A K Soper, R Done, J W Dreyer, R J Humphreys, J A R Bones
The structure of pore fluids in swelling clays at elevated pressures and temperatures
J Phys:Condens Matter **11** 9179 (1999)

A Deriu
Dynamics of proteins probed by inelastic and quasielastic neutron scattering
Neutron News **11** 26 (2000)

R A Dilanian, F Izumi, K Itoh, T Kamiyama
Neutron powder diffraction study of the order-disorder transition in $K_2Mn_2(SO_4)_3$
J Phys Soc Japan **68** 3893 (1999)

R A Dilanian, F Izumi, T Kamiyama, K Itoh
Neutron diffraction study of the phase transition in $K_2Mn_2(SO_4)_3$
J Phys Chem Solids **60** 1423 (1999)

N Diot, R Marchand, J Haines, J M Leger, P Macandiere, S Hull
Crystal structure determination of the oxynitride Sr_2TaO_3N
J Solid State Chem **146** 390 (1999)

S Dong, J-C Li
The test of water potentials by simulating the vibrational dynamics of ice
Physica B **276-278** 469 (2000)

J C Dore, M Sliwinski, A Burian, W S Howells, D Cazorla
Structural studies of activated carbons by pulsed neutron diffraction
J Phys:Condens Matter **11** 9189 (1999)

M T Dove, W G Marshall, D A Keen, S A T Redfern, K Trachenko, M Tucker
Crystal structure of the high-pressure monoclinic phase of cristobalite
Mineralogical Magazine **64** 569 (2000)

M T Dove, D A Keen
Atomic structure of disordered materials
Microscopic Structure of Disordered Materials, Eds K Wright, R Catlow, (Kluwer Academic) p371 (1999)

A Downer, J Eastoe, A R Pitt, E A Simister, J Penfold
Effects of hydrophobic chain structure on the adsorption of fluorocarbon surfactants with either CF_3- or H-CF_2 terminal groups
Langmuir **15** 7591 (1999)

C A C Dreismann, T Abdul Redah, R M F Streffer, B Hessmo
Comment on: Precision neutron interferometric search for evidence of nuclear quantum entanglement in liquid H_20-D_20 mixtures
Phys Rev Lett **84** 2036 (2000)

C A C Dreismann, T Abdul Redah, R M F Streffer
Quantum dynamical correlation of protons in water at T=298K: new Raman light scattering and neutron Compton scattering experiments
Quantum Coherence and Decoherence - ISQM-Tokyo'98, Eds Y A Ono, K Fujikawa (Elsevier) p327 (1999)

G Drexlin, (KARMEN collaboration)
Status of neutrino-oscillation searches
Proc 5th Int WEIN Symposium: A Conference on Physics Beyond the Standard Model, Eds P Herczeg, C Hoffman, H V Klapdor-Kleingrothaus, (World Scientific) p136 (1999)

J Durr, P Lamparter, J Bill, S Steeb, F Aldinger
X-ray and neutron diffraction investigation on amorphous silicon carbonitrides
Precursor-derived ceramics, Eds J Bill, F Wakai, F Aldinger (Wiley-VCH) **214** (1999)

J Eastoe, S Nave, A Downer, A Paul, A Rankin, K Tribe, J Penfold
Adsorption of ionic surfactants at the air-solution interface
Langmuir **16** 4511 (2000)

G H Eaton, S H Kilcoyne
Muon production: past, present and future
Muon Science: Muons in Physics, Chemistry and Materials, Eds S L Lee, S H Kilcoyne, R Cywinski (I O P Publishing, Bristol) Ch **2** p11 (1999)

L Edwards, P J Bouchard, M Dutta, M E Fitzpatrick
Direct measurement of residual stresses at a repair weld in an austenitic steel tube
Integrity of High Temperature Welds (Professional Engineering Publishing, Bury St Edmunds) p181 (1998)

R Edwards, B Derby, J R P Webster, P Xiao
High-temperature neutron reflectometry of liquid metal-ceramic interfaces
J Phys D: Appl Phys **32** 2319 (1999)

K Eitel (KARMEN collaboration)
Update of the KARMEN2 anti-$\nu_\mu \rightarrow$ anti-ν_e oscillation search
Proc Lake Louise Winter Institute, Eds A Astbury et al (World Scientific) p353 (2000)

K Eitel (KARMEN collaboration)
Compatibility analysis of the LSND evidence and the KARMEN exclusion for anti-$\nu_\mu \rightarrow$ anti-ν_e oscillations
New J Physics **2** 1.1 (2000)

K Eitel (KARMEN collaboration)
Results from the KARMEN anti-$\nu_\mu \rightarrow$ anti-ν_e Oscillation Search
Proc INPC 98, Eds B Frois, D Goutte, D Guillemaud-Mueller, (Elsevier) p977 (1999)

K Eitel, B Zeitnitz, (KARMEN collaboration)
The search for neutrino oscillations anti-$\nu_\mu \rightarrow$ anti-ν_e with KARMEN
Proc XVIIIth Int Conf on Neutrino Physics and Astrophysics, Eds Y Suzuki, Y Totsuka (Elsevier) p 212 (1999)

S Enzo, R Frattini, P Canton, G Mulas, P G Radaelli
A study of Al-Mo alloys synthetized by mechanical treatment and annealed *in-situ*
Nanostructured Materials **12** 547 (1999)

S Enzo, G Mulas, F Delogu, R Frattini
A study of $Al_{75}Mo_{25}$ nanocrystalline alloys by X-ray and neutron diffraction
J Metastable and Nanocrystalline Materials **2-6** 417 (1999)

S Enzo, R Frattini, F Delogu, A Primavera, A Trovarelli
Neutron diffraction studies of ceria-zirconia catalysts prepared by high-energy mechanical milling
Nanostructured Materials **12** 673 (1999)

D G Eshchenko, V G Storchak, J H Brewer, G D Morris, S F J Cox, S P Cottrell, J S Lord, V N Gorelkin
Muonium formation in condensed neon and argon
Physica B **289-290** 418 (2000)

D G Eshchenko, V G Storchak, J H Brewer, G D Morris, S F J Cox, J S Lord
The origin of anomalous muonium in semiconductors
Physica B **289-290** 421 (2000)

J S O Evans, J D Jorgensen, S Short, W I F David, R M Ibberson, A W Sleight
Thermal expansion in the orthorhombic gamma phase of ZrW_2O_8
Phys Rev **B60** 14643 (1999)

J S O Evans, W I F David, A W Sleight
Structural investigation of the negative thermal expansion material ZrW_2O_8
Acta Cryst B **55** 333 (1999)

J S O Evans
Negative thermal expansion materials
J Chem Soc, Dalton Trans **3317** (1999)

J S O Evans, T A Mary
Structural phase transitions and negative thermal expansion in $Sc_2(MoO_4)_3$
Int J Inorg Mat (in press 2000)

A N Ezeilo, G A Webster
Advances in neutron diffraction for engineering residual stress measurements
Textures and Microstructures **33** 151 (1999)

A Faraone, C Branca, S Magazu, G Maisano, H D Middendorf, P Migliardo, V Villari
QENS and PCS study of aqueous BSA-PEG 'crowded' solutions
Physica B **276-278** 524 (2000)

J F Fernandez, M Kemali, D K Ross, C Sanchez
An empirical potential for interstitial hydrogen in some C-15 Laves phase compounds from IINS measurements
J Phys:Condens Matter **11** 10353 (1999)

J F Fernandez, M Kemali, D K Ross, C Sandrez
A Born-Mayer approach to the hydrogen potential in C_{15} Laves phase compounds
J Alloys & Comp **293-295** 300 (1999)

A Fielding, J Mayers
Calibration of the Electron Volt Spectrometer at the ISIS Pulsed Neutron Source
RAL- TR-2000-013 (2000)

A L Fielding, D N Timms, J Mayers
The temperature dependence of the momentum distribution of beryllium measured by neutron Compton scattering
Physica B **276-278** 69 (2000)

F Fillaux
New proton dynamics in solids revealed by vibrational spectroscopy with neutrons
Solid State Ionics **125** 69 (1999)

F Fillaux
New proton dynamics in solids revealed by vibrational spectroscopy with neutrons
J Molecular Structure **511-512** 35 (1999)

F Fillaux
The Pauli principle and the vibrational dynamics of protons in solids: a new spin related symmetry
Physica D **113** 172 (1998)

F Fillaux, J P Perchard
Hydrogen bonding. A historical perspective.
J Chim Phys, Hors serie, **91** (2000)

Y Finkelstein, D Nemirovsky, R Moreh, G Kimmel
Study of the papyex structure using neutron Compton scattering
Physica **B** (in press 2000)

J L Finney, D T Bowron, A K Soper
The structure of aqueous solutions of tertiary butanol
J Phys:Condens Matter **12** 123 (2000)

M E Fitzpatrick, M Dutta, L Edwards
Determination by neutron diffraction of effect of plasticity on crack tip strains in a metal matrix composite
Mater Sci Technol **14** 980 (1998)

A M Fogg, V M Green, D O'Hare
Superconducting intercalation compounds of metal nitride halides
J Mater Chem **9** 1547 (1999)

E M Forgan
Vortices in superconductors
J Phys:Condens Matter **11** 7685 (1999)

C Frontera, J L Garcia-Munoz, A Llobet, M Respaud, J M Broto, J S Lord, A Planes
Spin dynamics, phase coexistence, magnetic inhomogeneity and disorder in the charge ordered state of $Pr_{2/3}Ca_{1/3}MnO_3$
Phys Rev B (in press 2000)

C D Frost, B D Rainford, F V Carter, S S Saxena
Inelastic neutron scattering study of $CeNi_2Ge_2$
Physica B **276-278** 290 (2000)

B J Gabrys, W Zajac, M S Kalhoro, K H Andersen, S M King
Neutron and X-ray scattering studies of ionomer blends
Physica B **276-278** 911 (2000)

M P Gaigest, N Leulliot, M Ghomi, H Jobic, O Bouloussa, C Coulombeau
Analysis of the vibrational spectra of RNA building blocks by NIS spectroscopy and density functional calculations
Phys Chem (in press 2000)

J L Garcia-Munoz, A Llobet, C Frontera, J Fontcuberta, X Obradors, C Ritter
Charge localization and magnetic dynamics in manganites
J Magn Magn Mater **196-197** 477 (1999)

J L Garcia-Munoz, A Llobet, C Frontera, C Ritter
Charge localization and magnetic dynamics in ferromagnetic and charge-ordered manganites
J Appl Phys **85** 5639 (1999)

M Geoghegan, F Boué, A Menelle, F Abel, T Russ, H Ermer, R Brenn, D G Bucknall
Surface segregation from polystyrene networks
J Phys:Condens Matter **12** 5129 (2000)

J M Gil, H V Alberto, R C Vilao, J Piroto Duarte, P J Mendes, L P Ferreira, N Ayres de Campos, A Weidinger, S F J Cox
Novel muonium state in CdS
Phys Rev Lett **83** 5294 (1999)

J M Gil, H V Alberto, R C Vilao, J Piroto Duarte, P J Mendes, N Ayres de Campos, A Weidenger, Ch Niedermayer, S F J Cox
High temperature trapping of muons in $CuInSe_2$ and $CuInS_2$
Physica B **289-290** 567 (2000)

J M Gil, H V Alberto, R C Vilao, J Piroto Duarte, P J Mendes, N Ayres de Campos, A Weidinger, J Krauser, Ch Niedermayer, S F J Cox
Shallow level muonium centre in CdS
Physica B **289-290** 563 (2000)

Publications

E P Gilbert, P A Reynolds, P Thiyagarajan, D Wozniak, J W White
Microphase separation kinetics in n-alkane mixtures
Phys Chem Chem Phys **1** 2715 (1999)

H R Glyde, R T Azuah, W G Stirling
Condensate, momentum distribution and final-state effects in liquid ^{4}He
Phys Rev (in press 2000)

H R Glyde, R T Azuah, J R Beamish, M A Adams
Excitations beyond the roton of liquid ^{4}He in aerogel
J Low Temp Phys **117** 113 (1999)

E A Goremychkin, R Osborn, B D Rainford, A P Murani
Evidence for anisotropic Kondo behaviour in $Ce_{0.8}La_{0.2}Al_3$
Phys Rev Lett **84** 2211 (2000)

R J Green, T J Su, J R Lu, J R P Webster, J Penfold
Competetive adsorption of lysozine and $C_{12}E_5$ at the A/L interface
PCCP (in press 2000)

J Grins, S Esmaeilzadeh, P Berastegui, S G Eriksson
Determination of the magnetic structure at 10K of $Mn_3Ta_2O_8$ and a refinement of the crystal structure at 295K using neutron powder diffraction data
J Mater Chem **9** 1575 (1999)

P C M Gubbins, A M Mulders
Magnetic behaviour of systems with a quasi-doublet ground state
Aust J Phys **51** 315 (1998)

F Haarmann, H Jacobs, W Kockelmann
Dynamics of alkali metal hydrogensulfides
Physica B **276-278** 264 (2000)

B Han, G Yang, D C Steytler
Structural and thermodynamic properties of solutions of butane in aqueous sodium dodecyl sulfate: A study using neutron scattering and solubility measurements
J Colloid and Interface Science **218** 145 (1999)

A C Hannon, B G Aitken
Neutron diffraction studies of the structure of Ge-based multicomponent sulphide glasses
J Non-Cryst Solids **256-257** 73 (1999)

A C Hannon (ed)
Proceedings of 'LAD, 1982-1998: The First ISIS Diffractometer'
J Phys:Condens Matter Issue 47 pp **9127**-9302 (1999)

M L Harkam, R F Pettifer
EXAFS calculations using Debye-Waller factors deduced from inelastic neutron scattering
Neutrons and Numerical Methods **479** 167 (1999)

A Harrison, K M Kojima, A S Wills, Y Fudamato, M I Larkin, G M Luke, B Nachumi, Y J Uemara, D Visser, J S Lord
mSR studies of the Kagome antiferromagnet $(H_3O)Fe_3(OH)_6(SO_4)_2$
Physica **B 289-290** 217 (2000)

O Hartmann, R Wappling, M Ekstrom, B Heisel, M Schmelzer, H Natter, R Hempelmann
Positive muons in nanocrystalline transition metals: diffusion and magnetic nanostructure
Nanostruct Mater **12** 943 (1999)

H L M Hatharasinghe, M V Smalley, J Swenson, A C Hannon, S M King
Freezing experiments on clay gels
Langmuir **16** 5562 (2000)

N Hatto, T Cosgrove, M J Snowden
Novel microgel-particle colloids: the detailed characterisation of the layer structure and chain topology of silica:poly(NIPAM) core-shell particles
Polymer **41** 7133 (2000)

U Haussermann, P Viklund, C Scevsson, S G Eriksson, P Berastegui, S Lidin
The Hume-Rothery compound $Mn_8Ga_{27.4}Zn_{13.6}$: separated Zn_{13}-clusters interspersed in a primitive cubic host lattice
Angew Chem Int Ed **38** 488 (1999)

S M Hayden, R Doubble, G Aeppli, T G Perring, E Fawcett
Strongly enhanced magnetic fluctuations near the quantum critical point of $Cr_{(1-x)}V_{(x)}$ and why strong exchange enhancement need not imply heavy fermion behavior
Phys Rev Lett **84** 999 (2000)

A M Healey, P F Henry, G M Johnson, M T Weller, M Webster, A J Genge
Synthesis and single crystal determination of a sodium-rubidium aluminogermanate with the Zeolite JBW topology
Microporous and Mesoporous Materials (in press 2000)

R K Heenan, J Eastoe
Surfactant interfacial structure studied by SANS contrast variation
J Appl Cryst **33** 749 (2000)

R Hempelmann
Hydrogen diffusion in proton conducting oxides and in nanocrystalline metals
Anomalous Diffusion: From Basics to Applications, Eds R Kutner, A Pekalski, K Sznajd-Weron, Lecture Notes in Physics (Springer) **519** 247 (1999)

P F Henry, M T Weller
The synthesis and crystal structure of Ca_3Au_4
J Alloys and Compounds **292** 152 (1999)

C H Hervoches, P Lightfoot
A variable temperature powder neutron diffarction study of ferroelectric $Bi_4Ti_3O_{12}$
Chem Mater **11** 3359 (1999)

S J Hibble, A C Hannon, I D Fawcett
Total neutron diffraction: the correct way to determine the true structure of crystalline materials?
J Phys:Condens Matter **11** 9203 (1999)

S J Hibble, S P Cooper, A C Hannon, I D Fawcett, M Greenblatt
Local distortions in the colossal magnetoresistive manganates $La_{0.70}Ca_{0.30}MnO_3$, $La_{0.80}Ca_{0.20}MnO_3$ and $La_{0.70}Sr_{0.30}MnO_3$ revealed by total neutron diffraction
J Phys:Condens Matter **11** 9221 (1999)

W Higemoto, K Nishiyama, I Watanabe, K Nagamine, A Asamitsu, H Kuwahara, Y Tokura
m^+SR studies on $(Nd_{1-y}Sm_y)_{0.5}Sr_{0.5}MnO_3$
Physica **B 259-261** 822 (1999)

K Hochgesand, R Kurzhofer, R Winter
Neutron diffraction studies of liquid alloys at high temperatures and pressures
Proc 17th AIRAPT Int High Press Conf, in High Press Sci and Tech (in press 2000)

K Hochgesand, R Kurzhofer, O Leichtweiss, R Winter
Polyanionic clustering and electronic properties of the expanded equiatomic liquid alloy cesium-lead
Ber Bunsenges Phys Chem **102** 1259 (1998)

M Hofmann, S J Campbell, S J Kennedy
Competing magnetic interaction in $La_{0.8}Y_{0.2}Mn_2Si_2$ - coexistence of canted ferromagnetism and antiferromagnetism
J Phys:Condens Matter **12** 3241 (2000)

J H E Hone, A M Howe, T Cosgrove
A SANS study of the structure of gelatin/polyelectrolyte complexes
Macromolecules **33** 1206 (2000)

J H E Hone, A M Howe, T Cosgrove
A rheological and SANS study of the structure of gelatin/polyelectrolyte complexes under shear
Macromolecules **33** 1199 (2000)

I Hopkinson, R W Richards
Surface organisation and dynamics in multicomponent polymer systems
Structure and Properties of Multiphase Polymeric Materials, Eds T Araki, Q Tran-Cong, M Shibayama (Marcel Dekker) p269

U Hoppe, G Walter, R Kranold, D Stachel
Structural specifics of phosphate glasses probed by diffraction methods: a review
J Non-Cryst Solids **263-264** 29 (2000)

U Hoppe, R Kranold, D Stachel, J Neuefeind
Oxygen coordination of modifier cations in metaphosphate glasses probed by high-energy X-ray diffraction
Phosphorus Research Bull **10** 546 (1999)

U Hoppe, R Kranold, H-J Weber, J Neuefeind, A C Hannon
The structure of potassium germanate glasses - a combined X-ray and neutron diffraction study
J Non-cryst Solids (in press 2000)

U Hoppe, R Kranold
Improved reverse Monte Carlo approach to the structure of vitreous P_2O_5
Solid State Comm (in press 2000)

W S Howells, A C Hannon
LAD, 1982-1998: the first ISIS diffractometer
J Phys:Condens Matter **11** 9127 (1999)

W S Howells, A C Barnes, M Hamilton
Ion motion in high-temperature solid and liquid silver chalcogenides
Physica B **276-278** 493 (2000)

B S Hudson, D A Braden, S F Parker, H Prinzbach
The vibrational inelastic neutron scattering spectrum of dodecahedrane: experimental and DFT simulation
Angew Chem Int Ed **39** 514 (2000)

E M Hughes, M T Weller
Synthesis and structure of $CsCoPO_4$ an ABW zeotype
Dalton Transactions **4** 555 (2000)

S Hull, D A Keen
Structural characterization of the b>a superionic transition in Ag_2HgI_4 and Cu_2HgI_4
J Phys:Condens Matter **12** 3751 (2000)

L R Hutchings, R W Richards
Synthesis of deuterobutadiene-butadiene AB_2 and AB_3 miktoarm star isotopic copolymers
Polymer Bulletin **41** 283 (1998)

R M Ibberson, W I F David, S Parsons, M Prager, K Shankland
The crystal structures of m-xylene and p-xylene, C_8D_{10}, at 4.5 K
J Mol Struct **524** 121 (2000)

R M Ibberson, C Morrison, M Prager
Neutron powder and *ab initio* structure of ortho-xylene: the influence of crystal packing on phenyl ring geometry
J Chem Soc, Chem Comm 539 (2000)

R M Ibberson, O Yamamuro, T Matsuo
Crystal structures and phase behaviour of acetaldehyde-d_4: A study by high-resolution neutron powder diffraction and calorimetry
J Mol Struct **520** 265 (2000)

M J G Jak, V W J Verhoeven, I M de Schepper, F M Mulder, E M Kelder, J Schoonman
Neutron and X-ray scattering on Li-doped BPO_4
Physica **B 266** 108 (1999)

M R Jakel, C J Carlile, E Jericha, D E Schwab, H Rauch
New measurements with a perfect crystal cavity for neutrons
EUV, X-ray and Neutron Optics and Sources, SPIE **3767** 353 (1999)

T Jannakos (KARMEN collaboration)
The search for neutrino oscillations anti-$\nu_\mu \rightarrow$ anti-ν_e with KARMEN
Proc Les Rencontres de Moriond 1999 (in press 2000)

T Jannakos (KARMEN collaboration)
The KARMEN limit on anti-$\nu_\mu \rightarrow$ anti-ν_e oscillation and its implication for the LSND result
Proc 6th Topical Seminar on Neutrino and Astroparticle Physics 1999 (in press 2000)

E Jericha, D E Schwab, M R Jakel, C J Carlile, H Rauch
Neutron beam tailoring by accumulation between perfect crystal mirrors
Physica **B 283** 414 (2000)

T Jestadt, M Kurmoo, S J Blundell, B W Lovett, F L Pratt, W Hayes
Layered transition metal molecular magnets studied with implanted muons
Synthetic Metals **103** 2325 (1999)

K A Johnson, W S Howells
The liquid-state structure of octafluoropropane and decafluoro-n-butane as determined by neutron diffraction
J Phys:Condens Matter **11** 9239 (1999)

G M Johnson, P J Mead, M T Weller
Synthesis of a range of gallium and germanium containing sodalites
Microporous and Mesoporous Materials (in press 2000)

M W Johnson, M R Daymond
The neutron silicon lens: A new lens design for thermal neutrons
Physica **B 283** 308 (2000)

J A Johnson, C E Johnson, D Holland, A Sears, J F Bent, P G Appleyard, M F Thomas, A C Hannon
Ternary alkali stannosilicate glasses: a Mossbauer and neutron diffraction study
J Phys:Condens Matter **11** 1 (1999)

G M Johnson, P J Mead, M T Weller
Structural trends in the sodalite family
Phys Chem Chem Phys **1** 3709 (1999)

R H Jones, L H Doerrer, S J Teat, C C Wilson
Variable temperature diffraction study of the barrier to rotation and zero point motion in bis(η6-benzene)chromium
Chem Phys Lett **319** 423 (2000)

D E Joyce, S I Campbell, P R T Pugh, P J Grundy
X-Ray and neutron reflectivity investigations of Co/Cu multilayers
Physica B **248** 152 (1998)

R Kadono, W Higemoto, K Nagamine, F L Pratt
An atom in the Bloch state
Phys Rev Lett **83** 987 (1999)

J A Kaduk, S J Maginn, J Cole, K Shankland
Crystal structure of a new polymorph of sulfabenzamide
Advanced Photon Source Report (in press 2000)

M S Kalhoro, B J Gabrys, W Zajac, S M King, D G Peiffer
Small angle neutron scattering study of SPBT/PC blend
Polymer (in press 2000)

O N Kalugin, A K Adya
Microscopic structure of nickel(II) co-ordination shell in $NiCl_2$-methanol solution: neutron diffraction and *ab initio* studies
Phys Chem Chem Phys **2** 11 (2000)

G M Kalvius, D R Noakes, G Grosse, W Schafer, W Kockelmann, S Fredo, I Halevy, J Gal
Magnetism of crystalline and nanostructured $ZnFe_2O_4$
Physica **B** (in press 2000)

K V Kamenev, M R Lees, G Balakrishnan, D McK Paul, W G Marshall, V G Tissen, N V Nefedova
Pressure tuning of magnetic interactions in layered $(La_{0.6}Nd_{0.4})_{1.2}Sr_{1.8}Mn_2O_7$ Manganite
Phys Rev Lett **84** 2710 (2000)

E B Karlsson, C A C Dreismann, T Abdul-Redah, R M F Streffer, B Hjorvarsson, J Ohrmalm, J Mayers
Evidence for anomalous correlations of protons in a metallic hydride
Quantum Coherence and Decoherence - ISQM-Tokyo'98, Eds Y A Ono, K Fujikawa (Elsevier) p331 (1999)

E B Karlsson, S W Lovesey
Neutron Compton scattering by proton and deuteron systems with entangled spatial and spin degrees of freedom
Phys Rev **A61** 062714 (2000)

L Karlsson, R L McGreevy, J D Wicks
The magnetic structure of $Fe_{0.91}Zr_{0.09}$ metallic glass
J Phys:Condens Matter **11** 9249 (1999)

L Karlsson, A Wannberg, R L McGreevy, D A Keen
Modeling the magnetic structure of Dy_7Fe_3 metallic glass
Phys Rev **B61** 487 (2000)

Publications

N Kawanura, K Nagamine, T Matsuzaki, K Ishida, S N Nakamura, S Sakamoto, I Watanabe, M Iwasaki, G H Eaton
Measurements of ^{3}He accumulationeffect on muon catalyzed fusion in the solid/liquid DT mixtures
Phys Lett **B 465** 74 (1999)

D A Keen, M T Dove
Local structures of amorphous and crystalline phases of silica, SiO_2, by neutron total scattering
J Phys:Condens Matter **11** 9263 (1999)

A M Kenwright, S K Peace, R W Richards, A Bunn, W A Macdonald
End group modification in poly(ethylene terephthalate)
Polymer **40** 2035 (1999)

A M Kenwright, S K Peace, R W Richards, A Bunn, W A MacDonald
Transesterificationin poly(ethylene terephthalate) and poly(ethylene naphthalene 2,6 dicarboxylate): the influence of hydroxyl end groups
Polymer **40** 5851 (1999)

A Keren, G Bazalitsky, P Mendels, I Campbell, J S Lord
Magnetic field-time scaling relations and exotic spin correlations: a μSR study of spin glasses
Physica **B 289-290** 202 (2000)

P J C King
Imaging and analysis of crystal defects using transmission channeling
MRS bulletin (in press 2000)

S M King, P C Griffiths, T Cosgrove
Using SANS to study adsorbed layers in colloidal dispersions
Applications of neutrons to soft condensed matter, Ed B J Gabrys (Gordon & Breach) (in press 2000)

S M King, C Washington, S Calpin-Davies, T Cosgrove, R K Heenan, R May
Polyoxyalkylene block copolymers in oil-in-water emulsions
Phys Chem Chem Phys (in press 2000)

S Kister, H-L Keller, W Kockelmann
Hydrogen position, hydrogen bonding and hydroxide dynamics in the Cd(OH)Cl structure type
Physica B **276-278** 262 (2000)

J Kleinfeller (KARMEN collaboration)
KARMEN 2: A new precision in the search for neutrino oscillations
Proc XXIX Int Conf on High Energy Physics (ICHEP98), Eds A Astbury, D Axen and J Robinson (World Scientific) p611 (1999)

C S Knee, R J Crookes, M T Weller
The structures of $Pb_2Ba_2Cu_2TaO_8Cl$ phases
J Solid State Chemistry (in press 2000)

C S Knee, M T Weller
Synthesis and structure of a new family of nickelates: $Tl(Ln_2Sr_2)Ni_2O_9$, Ln=La,Pr,Nd,Sm,Eu and Gd
J Solid State Chem **150** 1 (2000)

K S Knight, K Shankland, N Shankland
Solid state polymorphic transformations induced by variations in temperature and pressure
Acta Cryst **A55** Supplement (1999)

K S Knight, I C Stretton, P F Schofield
Temperature evolution between 50K and 320K of the thermal expansion tensor of gypsum derived from neutron powder diffraction data
Phys and Chem of Minerals **26** 477 (1999)

K S Knight
Oxygen vacancy ordering in neodymium-doped barium cerate
Solid State Communications **112** 73 (1999)

J C Knowles, I R Gibson, I Abrahams
High temperature phase transitions in $Ca_3(PO_4)_2$ measured by neutron diffraction
Bioceramics (in press 2000)

W Kockelmann, W Schafer, A Kirfel, F J Burghart, W Potzel, G M Kalvius, S J Campbell
Nanocrystalline ferromagnetic $ZnFe_2O_4$ spinel studied by neutron diffraction
Z Krist Suppl **16** 165 (1999)

W Kockelmann, U Ruschewitz
Novel ternary alkali metal silver acetylides $M'AgC_2$ (M'=Li, Na, K, Rb, Cs)
Angewandte Chemie, Int Ed **38** 3492 (1999)

W Kockelmann, E Pantos, A Kirfel
Neutron and synchrotron radiation studies of archaeological objects
Radiation in Art and Archaeometry, Eds D C Creagh, D A Bradley (in press 2000)

W Kockelmann, A Kirfel, E Hahnel
Non-destructive phase analysis of archaeologiocal ceramics using TOF neutron diffraction
J Archaeological Science (in press 2000)

H Kockelmann, J Schreiber, Yu V Taran, J S Wright
Investigation of residual stresses in a shape welded steel tube by the time-of-flight neutron diffraction technique
Mat Sci Forum **321-324** 726 (1999)

A I Kolesnikov, J-C Li
Neutron spectroscopy of vapour deposited amorphous ice
Ice Physics and the Natural Environment, Eds J S Wettlanter, J G Dash, N Untersteiner, NATO ASI Series I **56** (Springer-Verlag) p305 (1999)

A I Kolesnikov, O I Barkalov, M Calvo-Dahlborg, U Dahlborg, W S Howells, E G Ponyatovsky
Neutron diffraction study of bulk amorphous $(GaSb)_{38}Ge_{24}$ alloy
Phys Rev B (in press 2000)

A M Korsunsky, M R Daymond, K E Wells
The development of strain anisotropy during plastic deformation of an aluminium polycrystal
Proc ECRS-5, Mat Sci Forum (in press 2000)

A M Korsunsky, K E Wells, B A Shaw
A comparative study of diffraction methods for strain measurement in a particulate MMC
Proc ECRS-5, Mat Sci Forum (in press 2000)

D P Kozlenko, B N Savenko, V P Glazkov, V A Somenkov, S Hull
Structure and dynamics of ammonium halides under high pressure
Physica **B 276-278** 226 (2000)

F Krok, W Bogusz, M Malys, I Abrahams
Crystal structure and electrical properties of the oxygen ion conductor BIMEVOX (in Polish)
Proc VI National Symposium on Fast Ionic Conductors (Academy of Mining and Metallurgy, Poland) p75 (1998)

C Lamonier, E Payen, P C H Mitchell, S F Parker, J Mayers, J Tomkinson
Hydrogen species in cerium-nickel oxide catalysts: inelastic and Compton neutron scattering studies
Studies in Surface Science and Catalysis, Eds A Corma, F V Melo, S Mendioroz, J J G Fierro (Elsevier, Amsterdam) **130** 3161 (2000)

S Langridge, J Schmalian, C H Marrows, D T Dekadjevi, B J Hickey
A neutron study of magnetic domain correlations in antiferromagnetically coupled multilayers
J App Phys **87** 5750 (2000)

A Lanzara, F Natali, N L SAini, A Bianconi, P G Radaelli
Spatial cross-over of polarons across the CMR transition in $La_{0.75}Ca_{0.25}MnO_3$ system
J Synchrotron Radiation **6** 776 (1999)

A Lappas, K Prassides, F N Gygax, A Schenck
Magnetic and structural instabilities in the stripe-phase region of $La_{1.875}Ba_{0.125-y}Sr_yCuO_4$ ($0<=y<=0.1$)
J Phys:Condens Matter **12** 3401 (2000)

A Lascialfari, P Carretta, D Gatteschi, C Sangregorio, J S Lord, C A Scott
μSR study of the superparamagnetic mesoscopic cluster Fe_8
Physica **B 289-290** 110 (2000)

S L Lee, S H Kilcoyne, R Cywinski (Editors)
Muon Science: Muons in Physics, Chemistry and Materials
I O P Publishing, Bristol, ISBN 0-7503-0630-0 (1999)

O Leichtweiss, K Hochgesand, C Biermann, R Winter
Neutron diffraction and computer modelling studies of expanded liquid Cs-Tl
J Chem Phys **110** 497 (1999)

A Leineweber, H Jacobs, W Kockelmann, S Hull
Structural investigations on e-phase type nitrides M_3N_{1+x} (M=Mn,Fe,Ni)
Physica B **276-278** 266 (2000)

A R Lennie, K S Knight, R A Fellows, C M B Henderson, S A T Redfern
Temperature dependent cation ordering of minerals with the pseudobrookite structure observed by *in situ* neutron diffraction
AGU Fall Meeting, Suppl EOS Trans **80** F1155 (1999)

N Leulliot, M Ghomi, H Jobic, V Baumruk, O Bouloussa
Ground state properties of the nucleic acid constituents studied by density functional calculations. IV Comparison between calculated and experimental spectra of adenusine and guanosine
J Phys Chem (in press 2000)

N Leulliot, H Jobic, M Ghomi
Search for reliable nucleic acid force fields using neutron inelastic scattering and quantum mechanical calculations: Bases, nucleosides and nucleotides
Neutrons and Numerical Methods - N2M, Eds M R Johnson, G J Kearley, H G Buttner (AIP, New York) p179 (1999)

N Leulliot, M Ghomi, H Jobic, V Baumruk, O Bouloussa
Ground state properties of the nucleic acid constituents studied by density functional calculations. II. Comparison between calculated and experimental vibrational spectra of uridine and cytidine
J Phys Chem **B 103** 9716 (1999)

J-C Li, J Tomkinson
Simulation of inelastic neutron scattering spectra for water ice - a most effective way of testing water potentials
Neutrons and Numerical Methods - N2M, Eds M R Johnson, G J Kearley, HG Buttner (AIP, New York) p155 (1999)

J-C Li, J Tomkinson
Interpretation of inelastic neutron scattering spectrum by molecular dynamics
Molecular Dynamics - from Classical to Quantum Methods, Eds P B Balbuena, J M Seminario (Elsevier Scientific) p471 (1999)

J-C Li
Simulation of vibrational dynamics by lattice and molecular dynamic simulation
Physica B **263-264** 404 (1999)

R L Lichti
Dynamics of muonium diffusion, site changes and charge state transitions
Hydrogen in Semiconductors II, Ed N Nickel (Academic Press) 61 Semiconductors and Semimetals **Ch8** p311 (1999)

R L Lichti, S F J Cox, M R Dawdy, T L Head, B Hitti, R J Molnar, C Schwab, R P Vaudo
Sites and motion of m-defect centres in n-type gallium nitride
Physica B **289-290** 542 (2000)

R L Lichti, M R Dawdy, T L Head, S F J Cox, B Hitti, C Schwab
Negatively charged muonium states in gallium nitride
Physica B **273-274** 116 (1999)

A Llobet, J L Garcia-Munoz, C Frontera, M Respaud, L Pinsard, A Revcolevschi, C A Scott
Magnetism and orbital-ordering in $La_{7/8}Sr_{1/8}MnO_3$
Physica B (in press 2000)

A Llobet, J L Garcia-Munoz, C Frontera, M Respaud, H Rakoto, J S Lord
Magnetic dynamics and discommensuration in charge-ordered $Pr_{1-x}Ca_xMnO_3$ (x=1/3 and 1/2)
Physica B **289-290** 73 (2000)

J S Lord, S P Cottrell, W G Williams
Muon spin relaxation in strongly coupled systems
Physica B **289-290** 495 (2000)

J S Lord, S P Cottrell, W G Williams
Muon sites and diffusion in doped lithium oxide
Physica B **289-290** 491 (2000)

J S Loveday, R J Nelmes, S Klotz, J M Besson, G Hamel
Pressure-induced hydrogen bonding: Structure of D_2S phase I'
Phys Rev Lett **85** 1024 (2000)

R Lovell, R M Richardson
Analysis methods in neutron and X-ray reflectometry
Current Opinion in Colloid and Interface Science **4** 197 (1999)

M R Lovell, R M Dalgliesh, R M Richardson, A C Barnes, J E Enderby, B Evans, J R P Webster
Depth of water incorporation into float glass surfaces studied by neutron reflection
Phys Chem Chem Phys **1** 2379 (1999)

S W Lovesey, S P Collins
Birefringence and dichroism in X-rays passing through magnetic material
RAL-TR-1999-078 (1999) and Rev Mod Phys (in press 2000)

S W Lovesey, K S Knight
Resonant X-ray Bragg diffraction from orbital moments in vanadium sesquioxide (V_2O_3) and hematite (a-Fe_2O_3)
J Phys:Condens Matter **12** L367 (2000)

B W Lovett, S J Blundell, F L Pratt, T Jestadt, W Hayes, S Tagaki, M Kurmoo
Spin fluctuations in the spin-Peierls compound $MEM(TCNQ)_2$ studied using μSR
Phys Rev B (in press 2000)

B W Lovett, S J Blundell, T Jestadt, F L Pratt, M Kurmoo, S Tagaki, W Hayes
Muon study of the spin dynamics in the organic spin-Peierls compound $MEM(TCNQ)_2$
Synthetic Metals **103** 2034 (1999)

B W Lovett, S J Blundell, F L Pratt, T Jestadt, W Hayes, S Tagaki, M Kurmoo
Very low temperature muon relaxation in an organic spin-Peierls compound
Physica B (in press 2000)

J R Lu, T J Su, R K Thomas, G Lawrie, G T Barnes, J Penfold
Neutron reflection study of the penetration of a spread octodecanol monolayer by the soluble surfactant $C_{16}TAB$
J Phys Chem B (in press 2000)

J R Lu, T J Su, M J Lawrence, D J Barlow, W Warisnoicharoen, T Zuberi
The structure and composition of ethyl hexadecanoate layers spread on aqueous solution of hexaethylene glycol monodecyl ether

G D Ma, D J Barlow, M J Lawrence, R K Heenan, P A Timmins
Small angle neutron scattering studies of non-ionic surfactant vesicles
J Phys Chem (in press 2000)

W A MacFarlane, P Mendels, J Bobroff, H Alloul, N Blanchard, A V Dooglav, G Collin, P G Picard, P J C King, J S Lord
Antiferromagnetism in water doped $YBa_2Cu_3O_{6+x}$ for x~0.5
Physica B **289-290** 291 (2000)

G MacGlashan, Y G Andreev, P G Bruce
The structure of $poly(ethylene\ oxide)_6$:$LiAsF_6$
Nature **398** 792 (1999)

I Z Machi, S H Connell, M Baker, J P F Sellschop, K Bharuth-Ram, S F J Cox
A new hydrogen trap in nitrogen-rich diamond discovered by μSR
Physica B **289-290** 507 (2000)

S Magazu
NMR, static and dynamic light and neutron scattering investigations on polymeric aqueous solutions
J Mol Structure (in press 2000)

E T Maguire, A M Coats, J M S Skakle, A R West
Stoichiometry and defect structure of $NdMnO_3$
J Mater Chem **9** 1337 (1999)

P R Mallinson, K Wozniak, C C Wilson, K L McCormack, D S Yufit
Charge density distribution in the 'proton sponge' compound 1,8-bis(dimethylamino)naphthalene
J Amer Chem Soc **121** 4640 (1999)

G Mao, M-L Saboungi, D L Price, M B Armand, W S Howells
Structure of liquid PEO-LiTFSI electrolyte
Phys Rev Lett **84** 5536 (2000)

G Mao, A G Baboul, L A Curtiss, D L Price, M-L Saboungi, M Armand, W S Howells, H E Fischer
Structure and dynamics of lithium polymer electrolytes
Proc 12th Symp on Molten Salts (Electrochemical Society, Pennington, NJ) (in press 2000)

G Mao, R Fernandez Perea, W S Howells, D L Price, M-L Saboungi
Relaxation in polymer electrolytes on the nanosecond time scale
Nature **405** 163 (2000)

S Margadonna, C M Brown, A Lappas, K Prassides, K Tanigaki, K D Knudsen, T L Bihan, M Mezouar
Pressure and temperature evolution of the structure of the superconducting Na_2CsC_{60} fulleride
J Solid State Chem **145** 471 (1999)

R J Marsh, R A L Jones, M Sferrazza, J Penfold
Neutron reflectivity study of the adsorption of β-lactoglobulin at a hydrophilic solid/liquid interface
J Coll Int Sci **218** 347 (1999)

P J M Marshall, D S Sivia, M A Adams, M T F Telling
Selection, rejection and optimisation of analyser crystals for the new IRIS pyrolytic graphite analyser
RAL-TR-2000-03 (2000)

D Martin, D Engberg, K H Andersen
The Polarisation Analysis Spectrometer and Diffractometer at ISIS
Physica B **276-278** 150 (2000)

D Martin
Polarisation analysis diffraction on a pulsed source
Mat Sci Forum **321-324** 290 (2000)

D Martin, D Engberg
OSIRIS: The Polarisation Analysis Spectrometer and Diffractometer at ISIS
Physica B **268** 134 (1999)

A Martucci, A Alberti, G Cruciani, P G Radaelli, P Ciambelli, M Rapacciulo
Location of Bronsted sites in D-ferrierite by neutron powder diffraction
Microporous and Mesoporous Materials **30** 95 (1999)

R Maschow
Neutrino oscillations: Accelerator experiments
Proc 17th Int Workshop on Weak Interactions and Neutrinos WIN'99, Eds C A Dominguez, R D Viollier (World Scientific) p426

M Matsuda, K Katsumata, R S Eccleston, S Brehmer, H J Mikeska
Magnetic excitations from the S=1/2 two-leg ladders in $La_6Ca_8Cu_{24}O_{41}$
J Appl Phys **87** 6271 (2000)

Y Matsushita
Studies on equilibrium structures of complex polymers in condensed systems
J Polym Sci **B** (in press 2000)

T Matsuzaki, K Nagamine, K Ishida, S N Nakamura, N Kawamura, M Tanase, M Kato, K Kurosawa, G H Eaton
m catalyzed fusion and m to ^{3}He transfer in solid T_2 studied by X-ray and neutron detection
Hyp Inter **118** 229 (1999)

J Mayers
Bose-Einstein condensation and spatial correlations in ^{4}He
Phys Rev Lett **84** 314 (2000)

J Mayers, F Albergamo, D N Timms
Measurements of the atomic kinetic energy of ^{4}He close to the superfluid transition
Physica B **276-278** 811 (2000)

L McBride, K Shankland, W I F David, G Steele
Crystal structures of remacemide base, nitrate and acetate from X-ray powder diffraction data
Acta Cryst **A55** Supplement (1999)

D F McCormack, W B Rowe, X Chen, A Bouzina, M E Fitzpatrick, L Edwards
Characterizating the onset of tensile residual stresses in ground components
Proc 6th Int Conf on Residual Stresses (in press 2000)

G S McGrady, J F C Turner, R M Ibberson, M Prager
Structure of the trimethylaluminium dimer as determined by powder neutron diffraction at low temperature
Organometallics (in press 2000)

G Meier, U Pawelzik, W Schweika, W Kockelmann
The static structure factor S(Q) of partially deuterated ethyl- and hexylmethacrylate polymers
Physica B **276-278** 369 (2000)

G I Meijer, R S Eccleston, H Mutka, C Rossel, J Karpinski, S Kazakov, P Wachter
Magnetic excitations in the quasi-one-dimensional magnet $Sr_{0.73}CuO_2$: Coexistence of the spin gap and long-range magnetic order
Phys Rev **B60** 9260 (1999)

A Mellergard, D A Keen, M Harris, R L McGreevy
Aspects of the structure and dynamics of the CMR material $Nd_{0.5}Pd_{0.5}MnO_3$
Physica B **276-278** 774 (2000)

L Menon, D T Adroja, B D Rainford, S K Malik, W B Yelon
Neutron scattering studies on CeRhSb
Solid State Comm **112** 85 (1999)

V Meyer, G H Eaton, K Jungmann, P G H Sandars, C A Scott et al
Measurement of the 1S-2S energy interval in muonium
Phys Rev Lett **84** 1136 (2000)

P C H Mitchell, D A Green, E Payen, J Tomkinson, S F Parker
Interaction of thiophene with a molybdenum disulfide catalyst: an inelastic neutron scattering study
Phys Chem Chem Phys **1** 3357 (1999)

P C H Mitchell, D A Green, E Payen, J Tomkinson, S F Parker
An inelastic neutron scattering study of the interaction of thiophene with a hydrodesulfurisation catalyst
Studies in Surface Science and Catalysis, Eds A Corma, F V Melo, S Mendioroz, J J G Fierro (Elsevier, Amsterdam) **130** 2789 (2000)

P C H Mitchell, D A Green, E Payen, S F J Cox, C A Scott
Modelling hydrogen transport in molybdenum disulfide catalysts with muon spin relaxation spectroscopy
Magnetic Resonance in Chemistry (in press 2000)

P C H Mitchell, M Bowker, N Price, S Poulston, D James, S F Parker
Iron antimony oxide selective oxidation catalysts - an inelastic neutron scattering study
Topics in Catalysis **11** 223 (2000)

A W Mombru, K Prassides, C Christides, R Erwin, M Pissas, C Mitros, D Niarchos
Neutron powder diffraction study (T=4.2 - 300K) and polarization analysis of $YBaCuFeO_{5+\delta}$
J Phys:Condens Matter **10** 1247 (1998)

F J Mompean, A Chahid, D Martin, B Ouladdiaf
Neutron-diffraction study of two organic liquids conducting under a low electric field
Phys Rev **E57** 4206 (1998)

K A Mort, K A Johnson, A N Burgess
The liquid-state structure of difluoromethane
Mol Phys **98** 999 (2000)

G Mountjoy, R Anderson, R J Newport, M E Smith
The effect of zirconia content on the structure of zirconia-silica xerogels as determined by X-ray and neutron diffraction and Zr K-edge EXAFS and XANES
J Phys:Condens Matter **12** 3505 (2000)

O Moze, W Kockelmann, J P Liu, F R de Boer, K H J Buschow
Magnetic structure $LaFe_{10.8}Al_{2.2}$ and $LaFe_{10.8}Al_{2.2}N_3$ cluster compounds
J Appl Phys **87** 5284 (2000)

M K Mukhopadhyary, M K Sanyal, A Datta, J K Basu, J Penfold
Interplay of hydrophilic-hydrophobic interactions and molecular orentation in Langmuir monolayers
Europhys Lett (in press 2000)

E Mytilineou
Muon studies of amorphous semiconductors
Proc 10th Int School on Condensed Matter Physics, Thin film materials and devices - Developments in Science and Technology, Eds J M Marshall, N Kirov, A Vavrek, J M Maud (World Scientific) (1999)

K Nagamine, T Matsuzaki, K Ishida, S N Nakamura, N Kawamura
Implications of the recent D-T muCF experiments at RIKEN-RAL and near-future directions
Hyp Inter **119** 273 (1999)

R Nagarajan, E Alleno, S J Blundell, C Mazumdar, D W Cooke, S P Cottrell, S F J Cox, C Godart, L C Gupta et al
Nature of the spin state in $TmNi_2B_2C$
Physica **B 261** 588 (1999)

A Navarro, M Fernandez Gomez, J J Lopez Gonzalez, F Partal, J Tomkinson, G J Kearley
Density functional theory and ab initio methods applied to the analysis of inelastic neutron scattering spectra
Neutrons and Numerical Methods - N2M, Eds M R Johnson, G J Kearley, H G Buttner (AIP, New York) p172 (1999)

A Navarro, M Fernandez Gomez, J J Lopez Gonzalez, M P Fernandez Liencres, E Martinez Torres, J Tomkinson, G J Kearley
Inelastic neutron scattering spectrum and quantum mechanical calculation of the internal vibrations of pyrimidine
J Phys Chem **103** 5833 (1999)

S Nave, J Eastoe, J Penfold
What is so good about Aerosol-OT? Part 1: aqueous systems
Langmuir (in press 2000)

E V Nefeodova, P A Alekseev, J M Mignot, V N Lazukov, I P Sadikov, Y B Paderno, N Y Shitsevalova, R S Eccleston
Inelastic neutron scattering study of the Kondo semiconductor YbB_{12}
Phys Rev **B60** 13507 (1999)

E V Nefeodova, P A Alekseev, J M Mignot, V N Lazukov, I P Sadikov, Y B Paderno, N Y Shitcevalova, R S Eccleston
Magnetic excitation spectrum of Kondo-insulator YbB_{12}
Physica **B 276** 770 (2000)

D Nemirovsky, R Moreh, K H Andersen, J Mayers
Anomalous kinetic energies of adsorbed ^4He on active carbon fibre (ACF)
J Phys:Condens Matter **11** 6653 (1999)

D Nemirovsky, R Moreh, K H Andersen, J Mayers
Study of the momentum distribution of a Zn single crystal using neutron Compton scattering
J Phys:Condens Matter **12** 4293 (2000)

J Neuefeind, H E Fischer, W Schroer
EPMC versus RMC modelling: the structure of supercritical HCF_3
Physica B **276-278** 482 (2000)

G B Nikiforov, A M Kusainova, P S Berdonosov, V A Dolgikh, P Lightfoot
The crystal structure of the new REE-Te oxychlorides: $NdTe_2O_5Cl$ and $GdTe_2O_5Cl$
J Solid State Chem **146** 473 (1999)

T Nishijima, M Arai, Y Endoh, S M Bennington, C D Frost, R S Eccleston, K Tomimoto, S Tajima, Y Shiohara
Incommensurate spin dynamics of high-Tc superconductor $YBa_2Cu_3O_{7-\delta}$
J Phys Chem Solids **60** 1091 (1999)

C J Nuttall, S G Carling, P Day
Muon spin rotation in the molecular-based layer ferrimagnets $AFe(II)Fe(III)(C_2O_4)_{(3)}$ ($A = N(n\text{-}C_4H_9)_{(4)}$, $P(C_6H_5)_{(4)}$)
Solid State Comm **110** 39 (1999)

C Oehler (KARMEN collaboration)
Analysis of the KARMEN time anomaly
Proc 6th Topical Seminar on Neutrino and Astroparticle Physics 1999 (in press 2000)

B Paci, M S Deleuze, R Caciuffo, A Arduini, F Zerbetto
Molecular motion in C_{60}@Calix(8)arene
Mol Phys (in press 2000)

J A Paixao, M R Silva, S A Sorensen, B Lebech, G H Lander, P J Brown, S Langridge, E Talik, A P Goncalves
Neutron-scattering study of the magnetic structure of $DyFe_4Al_8$
Phys Rev **B61** 6176 (2000)

H M Palmer, C Greaves
Structural, magnetic and electronic properties of $Fe_{0.5}Cu_{0.5}Cr_2S_4$
J Mater Chem **9** 637 (1999)

J W L Pang, T M Holden, T E Mason
The development of intergranular strains in a high strength steel
J Strain Analysis **33** 373 (1999)

S F Parker
High energy spectroscopy: Inelastic neutron scattering applications
Encylopedia of Spectroscopy and Spectrometry (Academic Press) **2** 894 (2000)

S F Parker
High energy spectroscopy: Inelastic neutron scattering instrumentation
Encylopedia of Spectroscopy and Spectrometry (Academic Press) **2** 905 (2000)

S F Parker, H Herman
The vibrational spectra of methyltrioxorhenium(VII)
Spec Acta **56A** 1123 (2000)

S F Parker, D J Champion, D Colognesi, J Tomkinson
The TOSCA I user-guide
RAL-TR-1999-060 (1999)

S F Parker, J Tomkinson, D A Braden, B S Hudson
Experimental test of the validity of the use of the n-alkanes as model compounds for polyethylene
J Chem Soc, Chem Comm **165** (2000)

J V Pearce, R T Azuah, W G Stirling, R M Dimeo, P E Sokol, M A Adams
High-resolution measurements of the temperature dependence of the roton energy of superfluid ^4He
Physica **B 276-278** 822 (2000)

J Penfold, E Staples, I Tucker, R K Thomas
The structure of mixed surfactants at the air-water interface
Coll and Surf **A 155** 11 (1999)

J Penfold, E Staples, I Tucker, L Soubiran, A Creeth, J Hubbard
The adsorption of di-chain cationic and non-ionic surfactants at the air-water interface
Phys Chem Chem Phys (in press 2000)

J Penfold, E Staples, I Tucker, R K Thomas
The adsorption of mixed cationic and non-ionic surfactants at the hydrophilic silicon surface from aqueous solution: the effect of solution composition and concentrations
Langmuir (in press 2000)

J Penfold
Neutron scattering for surface characterisation
Current Science **78** 1458 (2000)

N Peng, J T S Irvine, A G Fitzgerald
Synthesis and crystal structure of the distorted perovskite $Sr_{0.97}NbO_3$ determined by high resolution powder neutron diffraction
J Mater Chem **8** 1033 (1998)

S J Perkins
High-flux X-ray and neutron scattering studies
Protein-Ligand Interactions: a Practical Approach, Eds B Chowdhry, S E Harding (OUP) (2000)

T G Perring
Neutron scattering (mostly) from low dimensional magnetic systems
Frontiers of Neutron Scattering, Ed A Furrer (World Scientific) (2000)

P A Perry, A M Donald
SANS study of the granular composition of A type starches
Poly Preprint **39** 699 (1998)

Publications

S Peter, J Parise, H D Lutz, R I Smith
High-pressure neutron diffraction studies on laurionite-type Pb(OD)Br
J Phys Chem Solids **60** 1859 (1999)

I Petri, P S Salmon, H E Fischer
Structure of the liquid semiconductor GeSe
J Phys:Condens Matter **11** 7052 (1999)

I Petri, P S Salmon, W S Howells
Change in topology of the glass forming liquid $GeSe_2$ with increasing temperature
J Phys:Condens Matter **11** 10219 (1999)

C Petrillo, F Sacchetti, M Celli, M Zoppi, C A Checchi
An inverse geometry neutron scattering spectrometer with graphite venetian blind crystal analyser and a para-hydrogen filter
Nucl Instr Methods (in press 2000)

C Petrillo
The silicon/gadolinium detector for thermal neutrons: current status and future perspectives
Notiziario Neutroni e Luce di Sincrotrone **4** 14 (1999)

C Pitteloud, D H Powell, A K Soper, C J Benmore
The structure of interlayer water in Wyoming montmorillonite studied by neutron diffraction with isotope substitution
Physica **B 276-278** 236 (2000)

M Prager, H Grimm, S F Parker, S McGrady
Rotational potentials of bridging and terminal methyl groups in trimethylaluminium-dimers
Physica B **276-278** 250 (2000)

K Prassides, C M Brown, S Margadonna, K Kordatos, K Tanigaki, E Suard, A J Dianoux, K D Knudsen
Powder diffraction and neutron inelastic scattering studies of polymeric Na_2RbC_{60}
J Mater Chem (in press 2000)

F L Pratt, S J Blundell, T Jestadt, B W Lovett, A Husmann, I M Marshall, W Hayes, A Monkman et al
mSR of conducting and non-conducting polymers
Physica B (in press 2000)

F L Pratt, S J Blundell, B W Lovett, K Nagamine, K Ishida, W Hayes, T Jestadt, A P Monkman
Anisotropic polaron motion in conducting polymers studied by muon spin relaxation
Synthetic Metals **101** 323 (1999)

F L Pratt, S J Blundell, A Husmann, I M Marshall, B W Lovett, W Hayes, S L Lee, et al
BEDT-TTF superconductors studied by μSR
Physica B (in press 2000)

P G Radaelli, R M Ibberson, S-W Cheong, J F Mitchell
Neutron scattering studies of phase segregation in $Pr_{0.7}Ca_{0.3}MnO_3$
Physica B **276-278** 551 (2000)

P G Radaelli, D E Cox, L Capogna, S W Cheong, M Marezio
Wigner-crystal and bi-stripe models for the magnetic and crystallographic superstructures of $La_{0.333}Ca_{0.667}MnO_3$
Phys Rev **B59** 14440 (1999)

P G Radaelli, J D Jorgensen
Neutron diffraction from novel materials
MRS Bulletin **24** 24 (1999)

B D Rainford, D T Adroja, G J Bowden, I M Benson
Quadrupolar Kondo effect in $U_3Ni_3Sb_{4-x}Sn_x$ alloys
Physica B **261** 417 (1999)

A J Ramirez-Cuesta, P C H Mitchell, S F Parker, A P Wilkinson, P M Rodger
Molecular dynamics simulation of inelastic neutron scattering spectra of librational modes of water molecules in a layered aluminophosphate
Neutrons and Numerical Methods - N2M, (Eds M R Johnson, G J Kearley, H G Büttner) AIP Conf Proc **479** 195 (1999)

A J Ramirez-Cuesta, P C H Mitchell, S F Parker, P M Rodger
Dynamics of water and template molecules in the interlayer space of a layered aluminophosphate. Experimental inelastic neutron scattering spectra and molecular dynamics simulated spectra
Phys Chem Chem Phys **1** 5711 (1999)

P Rangaswamy, M B Prime, M R Daymon, M A M Bourke, B Clausen, H Choo, N Jayaraman
Texture and residual strain in two SiC/Ti-6-2-4-2 titanium composites
Metallurgical and Materials Transactions A **31** 889 (2000)

P Rangaswamy, M B Prime, M R Daymond, M A M Bourke, B Clausen, H Choo, N Jayaraman
Comparison of residual strains measured by X-ray and neutron diffraction in a titanium matrix composite
Materials Science & Engineering **A** (in press 1999)

M N Rao, S L Chaplot, N Choudhury, K R Rao, R T Azuah, W T Montfrooij, S M Bennington
Lattice dynamics and inelastic neutron scattering from sillimanite and kyanite Al_2SiO_5
Phys Rev **B60** 12061 (1999)

J Reading, M T Weller
Powder neutron diffraction analysis of the lanthanide barium copper oxyborates
Physica C **328** 31 (1999)

S A T Redfern, R J Harrison
Order-disorder phase transitions in silicates and oxides: recent observations of strain coupling
Ferroelectrics (in press 2000)

S A T Redfern, M D Welch, C M B Henderson, K S Knight
In situ high-T neutron diffraction studies of non-convergent order in minerals: from simple oxides to complex silicates
Phase Transitions **69** 17 (1999)

J J Reece, S A T Redfern, M D Welch, C M B Henderson
Mn-Mg disordering in cummingtonite: a high-temperature neutron powder diffraction study
Mineral Mag (in press 2000)

I D Reid, S F J Cox, U A Jayasooriya, G A Hopkins
Muon spin spectroscopy in selenium
Mag Res in Chemistry **38** S3 (2000)

I D Reid, S F J Cox
Muons in sulphur
Physica B **289-290** 620 (2000)

U Reusch, E Schweda
The transformation of $Sn(ND_3)_2F_4$ into $Sn(ND_2)_2F_2$. Synthesis and neutron crystal structure determination of $Sn(ND_2)_2F_2$
Solid State Sciences **1** 233 (1999)

P A Reynolds, B N Figgis, D Martin
Magnetic structure and covalence in tetrachlorobis(N-phenylacetamidinato)rhenium(IV) by neutron diffraction
J Chem Soc, Dalton Trans **945** (1999)

C J Rhodes, T C Dintinger, C A Scott
Rates of motion for free radicals in zeolites as directly measured by longitudinal field muon spin relaxation
Magnetic Resonance in Chemistry **38** 62 (2000)

C J Rhodes, T C Dintinger, I D Reid, C A Scott
Spin-labelling studies of benzene sorbed in carbon particles using muonium: a molecular view of sorption by environmental carbon
Magnetic Resonance in Chemistry (in press 2000)

C J Rhodes, T C Dintinger, C A Scott
Sorption of benzene in cation-exchanged zeolite X, as measured by muon spin relaxation
Magnetic Resonance in Chemistry (in press 2000)

C J Rhodes, T C Dintinger, I D Reid, C A Scott
Mobility of dichloroethyl radicals sorbed in kaolin and in silica: a potential model of heterogeneous atmospheric processes
Magnetic Resonance in Chemistry (in press 2000)

M A Ricci, F Bruni, P Gallo, M Rovere, A K Soper
Water in confined geometries: experiments and simulations
J Phys:Condens Matter **12** 345 (2000)

R Rinaldi, G Artioli, C C Wilson, G McIntyre
Octahedral cation ordering in olivine at high temperature. I: *in situ* neutron single crystal diffraction studies on natural mantle olivines (Fa_{12} and Fa_{10})
Phys Chem Minerals (in press 2000)

G A D Ritchie, D S Sivia
Foundations of Physics for Chemists (Book)
Oxford Chemistry Primers Series, OUP (2000) ISBN 0-19-850360-1

S Rosenkranz, M Medarde, F Fauth, J Mesot, M Zolliker, A Furrer, U Staub, R S Eccleston et al
Crystalline electric field of the rare-earth nickelates $RNiO_3$ (R = Pr, Nd, Sm, Eu, and $Pr_{1-x}Lax$, 0<=x<=0.7) determined by inelastic neutron scattering
Phys Rev **B60** 14857 (1999)

J L Ruggles, S A Holt, P A Reynolds, A S Brown, D C Creagh, J W White
Observation of a cubic phase in mesoporous silicate films grown at the air/water interface
Phys Chem Chem Phys **1** 323 (1999)

S Sakamoto, K Ishida, K Nagamine
X-ray studies on muon transfer reaction from excited states of muonic hydrogen atoms to deuterium atoms
Phys Lett **A 260** 253 (1999)

B R Saunders, H M Crowther, G E Morris, S J Mears, T Cosgrove, B Vincent
Factors affecting the swelling of poly(N-isopropylacrylamide) microgel particles: fundamental and commercial implications
Coll Surf **A 149** 57 (1999)

W Schafer, E Jansen, W Kockelmann, A Alker, A Kirfel, D Seitz, M Gronefeld
Variations of microstructure and texture of permanent magnetic Alnico alloys
Physica B **276-278** 866 (22000)

P F Schofield, K S Knight
Neutron powder diffraction studies of the thermal behaviour of deuterated chalcanthite
Physica B **276-278** 897 (2000)

R Senesi, C Andreani, Z A Bowden, D Colognesi, E Degiorgi, A L Fielding, J Mayers et al
VESUVIO: a novel instrument for performing spectroscopic studies in condensed matter with eV neutrons at the ISIS facility
Physica B **276-278** 200 (2000)

J Senker, H Jacobs, M Muller, W Press, H M Mayer, R M Ibberson
Structure determination of a low temperature phase of calcium and strontium amide by means of neutron powder diffrcation on $Ca(ND_2)_2$ and $Sr(ND_2)_2$
Z Anorg Allg Chem **625** 2025 (1999)

M Sferrazza, R A L Jones, J Penfold, D Bucknall, J R P Webster
Neutron reflectivity studies of the structure of polymer/polymer and polymer/substrate interfaces at the nanometer level
J Mat Chem **10** 127 (2000)

K Shankland, W I F David
Crystal structures of pharmaceuticals solved from powder data by global optimisation methods
Acta Cryst **A55** Supplement (1999)

K Shankland, W I F David
Method and apparatus for determining molecular crystal structures
International Patent Application PCT/GB98/02316 (1999)

K Shankland, T Csoka
A parallel computer for a genetic algorithm based crystal structure solution program
Acta Cryst **A55** Supplement (1999)

K Shankland, W I F David, L McBride, N Shankland
High throughput crystal structure solution from powder diffraction data
ESRF Highlights 1998/1999

T Shiroka, C Bucci, R De Renzi, F Galli, G Guidi, G H Eaton, P J C King, C A Scott
Polarized muon spins in pulsed magnetic fields: A new method to study delayed muonium formation
Phys Rev Lett **83** 4405 (1999)

L D A Siebbeles, S M Pimblott, S F J Cox
Muonium formation dynamics in radiolytic tracks
Physica B **289-290** 404 (2000)

L D A Siebbeles, S M Pimblott, S F J Cox
Simulation of muonium formation in hydrocarbons
J Chem Phys **111** 7493 (1999)

D C Sinclair, E Marinou, J M S Skakle
The crystal structure of a new oxide ion conductor $NaBi_3V_2O_{10}$ and oxide ion conductivity in $Pb_2Bi_2V_2O_{10}$
J Mater Chem **9** 2617 (1999)

P Sittner, P Lukas, M R Daymond, V Novak, G M Swallowe
Stress induced martensitic transformation in CuAlZnMn polycrystals investigated by *in situ* neutron diffraction
Proc Esomat 20 Conference on Shape Memory Alloys (in press 2000)

D S Sivia
The number of good reflections in a powder pattern
J Appl Cryst (in press 2000)

J M S Skakle, A R West
Crystal structure-Tc correlations in $LaBa_{1.5}Ca_{0.5}Cu_3O_\delta$
Physica C **321** 12 (1999)

P R Slater, J TS Irvine, T Ishihara, Y Takita
The structure of the oxide ion conductor $La_{0.9}Sr_{0.1}Ga_{0.8}Mg_{0.2}O_{2.85}$ by powder neutron diffraction
Solid State Ionics **107** 319 (1998)

P R Slater, J T S Irvine, T Ishihara, Y Takita
High-temperature powder neutron diffraction study of the oxide ion conductor $La_{0.9}Sr_{0.1}Ga_{0.8}Mg_{0.2}O_{2.85}$
J Solid State Chem **139** 135 (1998)

A K Soper
Probing the structure of water around biological molecules: concepts, constructs and consequences
Physica B **276-278** 12 (2000)

A K Soper, M A Ricci
Structures of high-density and low-density water
Phys Rev Lett **84** 2881 (2000)

J M Sorenson, G Hura, A K Soper, A Pertsemlidis, T Head-Gordon
Determining the role of hydration forces in protein folding
J Phys Chem B **103** 5413 (1999)

F E Stanley, M Perez, C H Marrows, B J Hickey, S Langridge
Inverse giant magnetoresistance in hybrid rare earth/transition metal multilayers
Europhys Lett **49** 528 (2000)

E Staples, I Tucker, J Penfold, N Warren, R K Thomas
The structure and composition of polymer-surfactant mixtures of SDS/$C_{12}E6$ and poly-dmdaac at the air-water interface
J Phys:Condens Matter (in press 2000)

E Staples, J Penfold, I Tucker
The adsorption of mixed surfactants at the oil-water interface
J Phys Chem **B 104** 606 (2000)

U Staub, M Gutmann, F Fauth, W Kagunya
Difficulty of probing the superconducting gap with relaxation measurements on 4f crystal-field transitions with neutron scattering
J Phys:Condens Matter **11** L59 (1999)

D Stefanescu, M E Fitzpatrick, L Edwards
On the stress analysis of cold expanded fastener holes
Buletinul Universitatii 'Petrol-Gaze' Ploiesti **LI-1999** 167 (1999)

M Steidl (KARMEN collaboration)
The search for neutrino oscillations anti-$\nu_\mu \rightarrow$ anti-ν_e with KARMEN
Proc Les Rencontres de Physique del la Vallee Aoste 1999 (in press 2000)

Publications

T Steiner, S A Mason, C C Wilson, I Majerz
Neutronendiffractionsstudie von sehr kurzen O-H··N and N-H··O Brucken
Z Kristallogr Suppl **17** 68 (2000)

T Steiner, C C Wilson, I Majerz
Neutron diffraction study of a very short O-H··N hydrogen bond: co-crystal of 2-methylpyridine and pentachlorophenol
Chem Comm (in press 2000)

A Steuwer, P J Withers, J R Santisteban, L Edwards, M E Fitzpatrick, M R Daymond, M W Johnson, G Bruno
Neutron transmission spectroscopy: a solution to the d0 problem?
Proc 6th Int Conf on Residual Stresses (in press 2000)

J R Stewart, R Cywinski
μSR evidence for the spin-liquid-to-spin-glass transition in β-$Mn_{1-x}Al_x$
Phys Rev **B59** 4305 (1999)

V G Storchak, D G Eshchenko, J H Brewer, G D Morris, S P Cottrell, S F J Cox
Electron localization in a disordered insulating host
Phys Rev Lett **85** 166 (2000)

V G Storchak, J H Brewer, D G Eshchenko, S P Cottrell, S F J Cox
Quantum diffusion and localization in molecular crystals
Physica **B 289-290** 473 (2000)

J Strutwolf, A L Barker, M Gonsalves, D J Caruana, P R Unwin, D E Williams, J R P Webster
Probing liquid/liquid interfaces using neutron reflection measurements and scanning electrochemical microscopy
J Electroanalytical Chem (in press 2000)

T Sugano, S J Blundell, F L Pratt, T Jestadt, B W Lovett, W Hayes, P Day
Several kinds of aminoxyl radicals and their metal ion complexes
Mol Cryst Liq Cryst **A 334** 477 (1999)

N M Suleimanov, S A Moiseev, M A Clark-Gayther, S P Cottrell, S F J Cox
Zero-field muon spin echo
Physica B **289-290** 676 (2000)

J Swenson, A Matic, L Borjesson, W S Howells
Experimental insight into the mixed mobile ion effect in glasses
Solid State Ionics (in press 2000)

J Swenson, A Matic, C Karlsson, L Borjesson, W S Howells
Free volume and dissociation effects in fast ion conducting glasses
J Non-Cryst Soldis **263-264** 73 (2000)

J Swenson, L Borjesson, W S Howells
Structure of $(AgI)_x.(Ag_2O_{.n}B_2O_3)_{1-x}$ glasses by neutron diffraction and reverse Monte Carlo simulations
J Phys:Condens Matter **11** 9275 (1999)

J Swenson, L Borjesson, R L McGreevy
Structure of multicomponent glasses using diffraction techniques and reverse Monte Carlo modelling
AIP Conference Proc **479** 57 (1999)

J Swenson, R Bergman, L Borjesson, W S Howells
Dielectric and quasi-elastic neutron scattering of monolayer water in a vermiculite clay
J Physique **IV** Pr7 195 (2000)

J Swenson, P Carlsson, L Borjesson, L M Torell, R L McGreevy, W S Howells
The application of reverse Monte Carlo modelling to a polymeric melt
Computational and Theoretical Polymer Science (in press 2000)

J Swenson, L Borjesson, R L McGreevy
Structure of multi-component glasses using diffraction techniques and reverse Monte Carlo modelling
Neutrons and Numerical Methods - N2M, Eds M R Johnson, G J Kearley, H G Buttner (AIP, New York) (1999)

J Swenson, R Bergman, W S Howells
Quasi-elastic neutron scattering of 2D-water in a vermiculite clay
J Chem Phys (in press 2000)

Yu V Taran, J Schreiber, J S Wright
The time-of-flight neutron diffraction measurements of residual stress in a shape welded steel tube
Mat Sci Forum (5th Eur Conf on Residual Stresses) (in press 2000)

A D Taylor
A second target station for ISIS
Physica B **276-278** 36 (2000)

F Tedoldi, A Campana, P Carretta
μSR evidence of low frequency spin fluctuations in the AF phase of hole-doped NiO
Eur Phys J B **7** 219 (1999)

M T F Telling, W S Howells
GUIDE - IRIS Data Analysis
RAL-TR-2000-004 (2000)

M T F Telling, S I Campbell
The optimisation of analyser geometry for a near back-scattering spectrometer - IRIS on the ISIS Pulsed Source
RAL-TR-1999-044 (1999)

M T F Telling, J A Dann, R Cywinski, J Bogner, W Steiner
Spin dynamics in the concentrated spin glass system $Y(Al_{1-x}\ Fe_x)_2$
Physica **B** (in press 2000)

M T F Telling, C Ritter, R Cywinski
Evolution of magnetic order in $(Tb_{1-x}Ho_x)Mn_2$ and $(Tb_{1-x}Dy_x)Mn_2$
Physica B **276-278** 740 (2000)

J B Thomson, A R Armstrong, P G Bruce
An oxygen rich pyrochlore with the fluorite composition
J Solid State Chem **148** 56 (1999)

P Tils, M Loewenhaupt, K H J Buschow, R S Eccleston
Exchange fields in Gd-Fe intermetallics studied by inelastic neutron scattering
J Magn Magn Mater **210** 196 (2000)

P Tils, M Loewenhaupt, K H J Buschow, R S Eccleston
Crystal and exchange fields in $SmCo_5$ studied by inelastic neutron scattering
J Alloys Comp **289** 28 (1999)

B L Tomberli, C J Benmore, P A Egelstaff, J Neuefeind, V Honkimaki
Isotopic quantum effects in water structure measured with high energy photon diffraction
J Phys:Condens Matter **12** 2597 (2000)

G J Tomka, C Ritter, P C Riedi, D T Adroja, J S Lord, C Kapusta, J Zukrowski
Magnetic structure of $^{154}SmMn_2(Ge_{0.9}Si_{0.1})_2$ as a function of temperature and pressure
Physica B **291** 317 (2000)

N Torikai, Y Matsushita, S Langridge, D G Bucknall, J Penfold, M Takeda
Interfacial structures of block and graft copolymers with lamellar microphase-separated structures
Physica **B** (in press 2000)

K Traeger et al
Production of pulsed ultraslow muons and first μSR experiments on thin metallic and magnetic films
Physica **B 289-290** 662 (2000)

K Traeger, G Allodi, W G Williams
A new pulsed slow muon source at RAL
Proc Workshop on Applications of Low Energy Muons in Solid State Phenomena, PSI Villigen (1999)

F Triolo, A Triolo, R Triolo, D E Betts, J B McClain, J M De Simone, D C Steytler, G D Wignall, B Deme, R K Heenan
Critical micellisation density: a SAS structural study of the unimer-aggregate transition of diblock copolymers in supercritical CO_2
J Appl Phys **33** 641 (2000)

F Triolo, A Triolo, M M Agamalian, J S Lin, R K Heenan, G Lucido, R Triolo
Fractal approach in petrology: combining USANS, SANS and IANS
J Appl Cryst **33** 863 (2000)

R Triolo, V Arrighi, A Triolo, P Migliardo, S Magazu, J B McClain, D Betts, J M DeSimone, H D Middendorf
QENS from polymer aggregates in supercritical CO_2
Physica B **276-278** 386 (2000)

F R Trouw, D L Price
Chemical applications of neutron scattering
Ann Rev Phys Chem **50** 571 (1999)

M G Tucker, M T Dove, D A Keen
Direct measurement of the thermal expansion of the Si-O bond by neutron scattering
J Phys:Condens Matter **12** L425 (2000)

S F Turner, S M Clarke, A R Rennie, P N Thirtle, Z X Li, R K Thomas, S Langridge, J Penfold
Adsorption of gelatin in combination with sodium dodecyl sulphate or hexadecyl trimethyl ammonium bromide to a polystyrene/water interface
ECIS proceedings (in press 2000)

C H Uffindell, A I Kolesnikov, J-C Li, J Mayers
Inelastic neutron scattering study of water in the sub- and super-critical region
Phys Rev **B** (in press 2000)

C H Uffindell, A I Kolesnikov, J-C Li, J Mayers
Inelastic neutron scattering study of water in the sub- and supercritical region
Physica B **276-278** 444 (2000)

H Uhlig, S M Bennington, J-B Suck
Dynamics of modified glass networks
J Phys:Condens Matter **12** 6979 (2000)

J Ulicny, N Leulliot, L Grajcar, M H Baron, H Jobic, M Ghomi
NIS, IR and Raman spectra with quantum mechanical calculations for analysing the force field of hypericin model compounds
Neutrons and Numerical Methods - N2M, Eds M R Johnson, G J Kearley, H G Buttner (AIP, New York) p183 (1999)

R R Urbano, A Garcia, E Granado, R Caciuffo, R M Ibberson
EPR of Ni^{3+} and structural changes in the $La_2Ni_{0.5}Li_{0.5}O_4$ compound
Phys Rev B (in press 2000)

P Vaqueiro, S Hull, B Lebech, A V Powell
High temperature neutron diffraction studies of phase transformations in $NiCr_2S_4$
J Mater Chem **9** 2859 (1999)

E G Vrieling, T P M Beelen, R A van Santen, W W C Gieskes
Diatom silicon biomineralization as an inspirational source of new approaches to silica production
J Biotechn **70** 39 (1999)

J K Walters, K W R Gilkes, J D Wicks, R J Newport
Progress in modeling the chemical bonding in tetrahedral amorphous carbon
Phys Rev **B58** 8267 (1998)

J K Walters, K W R Gilkes, J D Wicks, R J Newport
A new model for tetrahedral amorphous carbon (ta-C)
J Non-Cryst Solids **232-234** 694 (1998)

R I Walton, R I Smith, F Millange, I J Clarke, D C Sinclair, D O'Hare
An *in-situ* time-resolved neutron diffraction study of the hydrothermal crystallisation of barium titanate
Chem Commun 2000 1267 (2000)

Y Wang, J-C Li, A I Kolesnikov, S F Parker, S J Johnsen
Inelastic neutron scattering investigation of Greenland ices
Physica B **276-278** 282 (2000)

J C Wasse, P S Salmon
Structure of molten trivalent metal chlorides studied by using neutron diffraction: the systems $TbCl_3$, YCl_3 $HoCl_3$ and $ErCl_3$
J Phys:Condens Matter **11** 9293 (1999)

J C Wasse, P S Salmon, R G Delaplane
Structure of molten holmium and erbium trichlorides and tribromides
Physica B **276-278** 433 (2000)

J C Wasse, S Hayama, N T Skipper, C J Benmore, A K Soper
The structure of saturated lithium- and potassium-ammonia solutions as studied by neutron diffraction
J Chem Phys **112** 7147 (2000)

J C Wasse, S Hayama, N T Skipper, H E Fischer
Structure of a metallic solution of lithium in ammonia
Phys Rev (in press 2000)

I Watanabe, M Akoshima, Y Kolke, K Nagamine
Anomalous slowing down of Cu-spin fluctuations observed by muon spin relaxation in the Zn-substituted $Bi_2Sr_2Ca_{1-x}Y_x(Cu_{1-y}Zn_y)_2O_{8+d}$ system around the hole concentration of 1/8 per Cu
Phys Rev **B60** R9955 (1999)

I Watanabe, M Akoshima, Y Koike, K Nagamine
mSR study on the magnetic state of the Zn-substituted Bi-2212 system
Physica B **259-261** 557 (1999)

J H P Watson, B A Cressey, A P Roberts, D C Ellwood, J M Charnock, A K Soper
Structural and magnetic studies on heavy-metal-adsorbing iron sulfide nanoparticles
J Magn Magn Mater (in press 2000)

G A Webster
Role of residual stress in engineering applications
Proc ECRS-5 (in press 2000)

J R P Webster, S Langridge
Application of index matching in reflectometry, SANS and Brewster angle microscopy
Current Opinion in Colloid & Interface Science **4** 186 (2000)

B Webster, S H Kilcoyne
Muonium radical formation in apoferritin and ferritin
Phys Chem Chem Phys **1** 4805 (1999)

M T Weller, A M Healey, G M Johnson
The synthesis and structure by powder neutron diffraction of zeolite JBW
Microporous and Mesoporous Materials (in press 2000)

M T Weller, C S Knee
The structure of $TlSr_2NiO_{4+d}$ by high resolution powder neutron diffraction
J Solid State Chem **144** 62 (1999)

M T Weller, S J Skinner
Neutron and X-ray powder diffraction studies of the oxynitrides, $SrW(O,N)_3$, $Ba_3W_2(O,N)_8$ and $Ba_3Mo_2(O,N)_8$
Int J Inorg Materials (in press 2000)

M T Weller, S E Dann, G M Johnson, P J Mead
MASNMR-structure correlations
J Phys Chem (in press 2000)

R D Wesley, T Cosgrove, L Thompson
Interactions of star polymers with surfactants
Langmuir **15** 8376 (1999)

A G Whittaker, A Harrison, G S Oakley, I D Youngson, R K Heenan, S M King
Apparatus for the in situ study of a microwave-driven reaction by small angle neutron scattering
Rev Sci Inst (in press 2000)

R W Whitworth
Ferroelectricity in water ice
J Phys Chem **B 103** 8192 (1999)

A S Wills, A Harrison, C Ritter, R I Smith
Magnetic properties of pure and diamagnetically doped Jarosites: model Kagome antiferromagnetets with variable coverage of the magnetic lattice
Phys Rev **B61** 6156 (2000)

C C Wilson
Refinement of two different crystal structures simultaneously from a multiple-crystal sample: neutron study of 3-deazauracil and lead hydrogen arsenate at 100K
J Mol Struct (in press, 2000)

C C Wilson, K Shankland, T Csoka
XVIII IUCr Congress and General Asembly, Collected Abstracts (Eds)
Acta Cryst **A55** Supplement S1-S178 (1999)

C C Wilson, H Nowell
Methyl group librations in sterically hindered dimethylnaphthalene molecules: neutron diffraction studies of 1,8-dimethylnaphthalene between 50 and 200K
New J Chem (in press 2000)

R Winter, K Hochgesand
Neutron diffraction studies of liquid alloys up to high temperatures and pressures
High Pressure Molecular Science, Eds R Winter, J Jonas, NATO ASI E **358** (Kluwer Academic) p151 (1999)

D A Woodcock, P Lightfoot, R I Smith
Powder neutron diffraction studies of three low thermal expansion phases in the NZP family: $K_{0.5}Nb_{0.5}Ti_{0.5}(PO_4)_3$, $Ba_{0.5}Ti_2(PO_4)_3$ and $Ca_{0.25}Sr_{0.25}Zr_2(PO_4)_3$
J Mater Chem **9** 2631 (1999)

D A Woodcock, P Lightfoot, L A Villaescusa, M J Diaz-Cabanas, M A Camblor, D Engberg
Negative thermal expansion in the siliceous zeolites chabazite and ITQ-4: a powder neutron diffraction study
Chem Mater **11** 2508 (1999)

D A Woodcock, P Lightfoot
Comparison of the structureal behaviour of the low thermal expansion NZP phases $MTi_2(PO_4)_3$ (M=Li, Na, K)
J Mater Chem **9** 2907 (1999)

D A Woodcock, P Lightfoot, R I Smith
Negative thermal expansion behaviour in the NZP phase $NbTi(PO_4)_3$
Mater Res Soc Symp Proc **547** 191 (1999)

A C Wright, J Cho, S A Feller, A C Hannon, R N Sinclair et al
Neutron scattering studies of network glasses
Proc 13th Conf on Glas and Ceramics, Varna 1999 (in press 2000)

A C Wright, B A Shakhmatkin, N M Vedishcheva
The chemical structure of oxide glasses: a concept consistent with neutron scattering studies?
Glass Phys Chem (in press 2000)

J P Wright, D Martin, J P Attfield
TOF neutron powder diffraction study of the helimagnetic structures in the $Cr_xFe_{1-x}VO_4$-I system
Physica B **276-278** 682 (2000)

E Wu, S J Campbell, W A Kaczmarek, M Hofmann
Mechanochemical treatment of $BaFe_{12}O_{19}$ - Mossbauer investigation
J of Metastable and Nanocrystalline Materials **2-6** 127 (1999)

E Wu, S J Campbell, W A Kaczmarek, M Hofmann, S J Kennedy
Mechanochemical treatment of haematite - neutron diffraction investigation
J of Metastable and Nanocrystalline Materials **2-6** 121 (1999)

P Xiao, B Derby, J R P Webster, J Penfold
Microanalysis of buried metal/ceramic interfaces using neutron reflection
Ceramic Microstructures: Control at the Atomic Level, Eds A P Tomsia, A Glaeser (Plenum, New York) p377 (1998)

T Yamaguchi
New horizons in hydrogen bonded clusters in solution
Pure Appl Chem **71** (in press 1999)

A Yaouanc, P Dalmas de Reotier, P C M Gubbins, A M Mulders, Y Isikawa
Zero and longitudinal field muon spin depolarization measurements of CeNiSn
Physica B (in press 2000)

A Yaouanc, P Dalmas de Reotier, P Bonville, G Lebras, P C M Gubbins, A M Mulders, S Kunii
Dynamical magnetic correlations in the Kondo insulator YbB_{12}
Europhys Lett **47** 247 (1999)

T Yosihama, T Nishi, K Nakajima, N Aso, K Kakurai, Y Fujii, S Itoh, C D Frost, S M Bennington et al
Magnetic neutron scattering in the quarter-filled spin-ladder system NaV_2O_5
Physica B **281** 654 (2000)

A Zarbakhsh, J Bowers, J R P Webster
A new approach for measuring neutron reflection from a liquid/liquid interface
Meas Sci Technol **10** 783 (1999)

B Zeitnitz (KARMEN collaboration)
The KARMEN Time-Anomaly: Indications for a massive weakly interacting particle?
Proc 17th Int Workshop on Weak Interactions and Neutrinos WIN'99, Eds C A Dominguez, R D Viollier, (World Scientific) p150 (2000)

M Zoppi
TOSCA: A Thermal Original Spectrometer with Cylindrical Analyzers
Neutron News **11** 31 (2000)

N Zotov, F Bellido, M Dominguez, A C Hannon, R Sonntag
Continuous random network models of Cu-As-Te glasses
Physica B **276-278** 463 (2000)

G Zsigmond, F Mezei
Simulation of the time-of-flight backscattering neutron spectrometer IRIS: The Monte Carlo data reduction technique
Physica B **276-278** 106 (2000)

ISIS 99 Update

The following publications were listed as 'in press' in ISIS 99 and have since been published

A Aamouche, G Berthier, B Cadioli, E Gallinella, M Ghomi
Hydrogen bonding effects on quantum mechanical force fields of pyrimidine bases: uracil
J Mol Structure **426** 307 (1998)

R Akagi, K Handa, N Ohtori, A C Hannon, M Tatsumisago, N Umesaki
High temperature structure of K_2O-TeO_2 glasses
J Non-Cryst Solids **256-257** 111 (1999)

P W Albers, S Bosing, G Prescher, K Seibold, D K Ross, S F Parker
INS investigations of the products of thermally and catalytically driven catalyst coking
Appl Catal A **187** 233 (1999)

B Armbruster et al (KARMEN collaboration)
Measurement of the Energy Spectrum of n_e from Muon Decay and Implications for the Lorentz Structure of the Weak Interaction
Phys Rev Lett **81** 520 (1998)

B Armbruster, et al, (KARMEN collaboration)
The Search for Neutrino Oscillations anti-$\nu_\mu \rightarrow$ anti-ν_e with KARMEN
Proc XXXIII Rencontres de Moriond: '98 Electroweak Interactions and Unified Theories, Ed J Tran Thanh Van (Editions Frontiere) p327 (1998)

C J Benmore, S Sweeney, R A Robinson, P A Egelstaff, J-B Suck
Longitudinal excitations in Mg_20Zn_30 glass
J Phys:Condens Matter **11** 7079 (1999)

C Bilton, J A K Howard, N N L Madhavi, A Nangia, G R Desiraju, F H Allen, C C Wilson
When is a polymorph not a polymorph? Helical trimeris O-H··O synthons in trans-1,4,-diethynyl-1,4-cyclohexanediol
Chem Comm **1675** (1999)

S J Blundell, S L Lee, F L Pratt, C M Aegerter, Th Jestadt, B W Lovett, C Ager, E M Forgan, W Hayes
Stability of the vortex lattice in ET superconductors studied by μSR
Synthetic Metals **103** 1925 (1999)

M Braden, B Buchner, S Klotz, W G Marshall
Pressure dependence of the crystal structure of $CuGeO_3$ to 7 GPa by neutron diffraction
Phys Rev **B60** 9616 (1999)

D J Bull, D K Ross, M Kemali
Monte Carlo simulations of hydrogen diffusion in C_{15} Laves phase intermetallic compounds
J Alloys & Comp **293-295** 296 (1999)

A Bumajdad, J Eastoe, P Griffiths, D C Steytler, R K Heenan, P Timmins
Interfacial compositions and phase structures in mixed surfactant microemulsions
Langmuir **15** 5271 (1999)

S I Campbell, M Kemali, D K Ross, D J Bull, J F Fernandez, M R Johnson
Quasielastic neutron scattering study of the hydrogen diffusion diffusion in the C15 Laves phase structure, $TiCr_{1.85}$
J Alloys & Comp **293-295** 351 (1999)

J Crawshaw, M E Vickers, N P Briggs, R K Heenan, R E Cameron
The hydration of tencel cellulose fibres studied using contrast variation in small angle neutron scattering
Polymer **41** 1873 (2000)

P Dalmas de Reotier, A Yaouanc, P C M Gubbens
Spin dynamics in magnetic materials investigated by muon Spin Relaxation
Hyp Int **120-121** 31 (1999)

M R Daymond, C Lund, M A M Bourke, D C Dunand
Elastic strain distribution in copper reinforced with molybdenum particulates during deformation at low and high temperature
Met & Mat Trans **30A** 2989 (1999)

R De Renzi
μSR and NMR : fundamental concepts and selected examples
Muon Science: Muons in Physics, Chemistry and Materials, Eds S L Lee, S H Kilcoyne, R Cywinski (I O P Publishing, Bristol)

S L Dong, A I Kolesnikov, J-C Li
Neutron scattering study and lattice dynamical simulation of clathrate H_2O+He
Physica B **263-264** 429 (1999)

J Eastoe, A Downer, A R Pitt, J Penfold, R K Heenan
Adsorption and micellisation of partially and fully fluorinated surfactants
Coll and Surf A **156** 33 (1999)

H Ehrenberg, J McAllister, W G Marshall, J P Attfield
Compressibility of copper-oxygen bonds: High-pressure neutron diffraction on CuO
J Phys: Condens Matter **11** 6501 (1999)

K Eitel et al (KARMEN collaboration),
KARMEN: Neutrino Oscillation Limits and New Results with the upgrade
Nuclear Physics B (Proc Suppl) **70** 210 (1999)

D Engberg, L Borjesson, J Swenson, L M Torell, W S Howells, A Wannberg
The liquid-glass transition in a strong network glass former investigated by neutron scattering
Europhys Lett **47** 213 (1999)

L Fabrega, J Fontcuberta, A Calleja, A Sin, S Pinol, X Obradors, P J C King
Muon spin relaxation in Re-substituted $HgA_2Ca_{n-1}Cu_nO_{2n+2+x}$ (A=Sr, Ga; n=2,3) superconductors
Phys Rev **B60** 7579 (1999)
F Fillaux, N Leygue, J Tomkinson, A Cousson, W Paulus
Structure and dynamics of the hydrogen bond in potassium hydrogen maleate: a neutron scattering study
Chem Phys **244** 387 (1999)

M Geoghegan, C J Clarke, F Boue, A Menelle, T Russ, D G Bucknall
The kinetics of penetration of grafted polymers into a network
Macromolecules **32** 5106 (1999)

R J C Gilbert, R K Heenan, P A Timmins, J Rossjohn, M W Parker, R K Tweten, P W Andrew, O Byron
Studies on the structure and mechanism of a bacterial protein toxin by analytical ultracentrifugation and small-angle neutron scattering
J Mol Biol **293** 1145 (1999)

E M Gray, E H Kisi, R I Smith
Observation of a continuous phase transformation in $LaNi_5D_3$
J Alloys Comp **293-295** 135 (1999)

R Hagenmeyer, M Jansen, C J Benmore, J Neuefeind,
Structural studies of the amorphous silicon boron nitride $Si_3B_3N_7$
J Mat Chem **9** 2865 (1999)

J Haines, C Chateau, J M Leger, A Le Sauze, N Diot, R Marchand, S Hull
Crystal structure of moganite-type phosphorous oxynitride: relationship to other twinned-quartz based structures
Acta Cryst **B 55** 677 (1999)

B X Han, G Y Yang, H K Yan, Z X Li, R K Thomas, J Penfold, R K Heenan
The structure and thermodynamical properties of solutions of butane in aqueous SDS: a study using neutron scattering and solubility measurements
J Coll Interf Sci **218** 145 (1999)

A C Hannon, B G Aitken
Pulsed neutron diffraction from GeS_2-based sulphide glasses
J Phys Chem Solids **60** 1473 (1999)

A C Hannon
Neutron Diffraction, Theory
Encyclopedia of Spectroscopy and Spectrometry, Eds J Lindon, G Tranter, J Holmes (Academic Press, London) p1493 (2000)

R J Harrison, S A T Redfern, R I Smith
In-situ study of the R3(bar) to R3(bar)c phase transition in the ilmenite-hematite solid solution using time-of-flight neutron powder diffraction
Amer Min **85** 194 (2000)

A M Healey, M T Weller
The synthesis and structure of $NaZnSiO_3OH$: a new chiral zincosilicate framework material
Inorg Chem **38** 455 (1999)

S J Hibble, S P Cooper, S Patat, A C Hannon,
Total neutron diffraction: A route to the correct local structure of disordered $LaMo_2O_5$, and its application to the model compound $Zn_2Mo_3O_8$
Acta Cryst **B 55** 683 (1999)

S J Hibble, R I Walton, A C Hannon, G Bushnell-Wye
The structure of amorphous CrS_3 containing $[Cr^{III}_2((S\text{-}I)_2)_3]_x$ chains: an X-ray diffraction modelling study
J Solid State Chemistry 145 573 (1999)

N Hirose, J M S Skakle, A R West
Doping mechanism and permittivity correlations in Nd-doped $BaTiO_3$
J Electroceramics **3** 233 (1999)

F Hutchinson, A J Rowley, M K Walters, M Wilson, P A Madden, J C Wasse, P S Salmon
Structure of molten MCl_3 systems from a polarizable ion simulation model
J Chem Phys **111** 2028 (1999)

S Itoh, K Kakurai, Y Endoh, H Tanaka, M J Harris, K Nakajima
Magnetic correlations in $CsVCl_3$
J Phys Chem Solids **60** 1144 (1999)

H Jacobs, A Leineweber, W Kockelmann
Order-disorder phenomena in the e-phase of the system Fe/N
Mat Sci Forum **325** 117 (2000)

E Jericha, D-E Schwab, C J Carlile, M R Jakel, R Loidl, H Rauch
Storage of multiple cold neutron pulses with perfect crystals
Nucl Inst & Methods **A 440** 597 (2000)
G M Johnson, M T Weller
A powder neutron diffraction study of lithium substituted gallosilicate and aluminogermanate halide sodalites
Inorg Chem **38** 2442 (1999)

Publications

E B Karlsson, C A C Dreismann, T Abdul-Redah, R M F Streffer, B Hjorvarsson, O Ohrmalm, J Mayers
Anomalous neutron Compton scattering in Nb-hydride: indications of proton correlations
Europhys Lett **46** 617 (1999)

M Kemali, D K Ross, S I Campbell
Muon diffusion in metallic hydride systems
J Alloys & Comp **293-295** 292 (1999)

S M King, C Washington, D Attwood, C Booth, S-M Mai, Y-W Yang, T Cosgrove
Polymer bristles: a SANS study
J Appl Cryst **33** 664 (2000)

W Kockelmann, M Weisser, H Heinen, A Kirfel, W Schafer
Application spectrum and data quality of the time-of-flight neutron diffractometer ROTAX at ISIS
Mat Sci Forum **321-324** 332 (2000)

A I Kolesnikov, U Dahlborg, M Calvo-Dahlborg, O I Barkalov, E G Ponyatovsky, W S Howells, A I Harkunov
Neutron diffraction study of bulk amorphous $Al_{32}Ge_{68}$ alloy
Phys Rev **B60** 12681 (1999)

J Kraus, P Muller-Buschbaum, D G Bucknall, M Stamm
Roughness correlation and interdiffusion in thin films of polymer chains
J Pol Sci B:Pol Phys **37** 2862 (1999)

J Lam, J M Titman
Muon-proton correlated diffusion in TiHx
J Alloys & Compounds **293-295** 266 (1999)

G Lauhoff, J Lee, A Hirohita, J A C Bland, S Langridge, J Penfold
Magnetic anisotropy, magnetic moments and coupling for Co/Cu/Ni/Cu(001) structures
J Phys:Condens Matter **11** 6707 (1999)

G Lauhoff, J Lee, J A C Bland, S Langridge, J Penfold
Origin of the Co uniaxial volume anisotropy of the fcc Co/Ni/Cu(001) system
Phys Rev **B60** 4087 (1999)

G Lauhoff, J Lee, W Y Lee, A Hirohata, A Samad, J A C Bland, S Langridge, J Penfold
Perpendicular magnetic anisotropy of exchange coupled Co/Cu/Ni/Cu/Si(001) structures
J Magn Soc Japan **23** 872 (1999)

Z X Li, A Weller, R K Thomas, A R Rennie, J R P Webster, J Penfold, R K Heenan, R Cubitt
Preferential adsorption of the lamellar phase of AOT at the solid-liquid and air-liquid interfaces
J Phys Chem **B 103** 10800 (1999)

R L Lichti, S F J Cox, K H Chow, E A Davis, T L Estle, B Hitti, C Schwab
Charge-state transitions of muonium in germanium
Phys Rev **B60** 1734 (1999)

C D Ling, J G Thompson, R L Withers, S Schmid
Modelling and refinement of the crystal structure of $Bi_4Ta_2O_{11}$ based on that of $Bi_7Ta_3O_{18}$
J Solid State Chem **142** 33 (1999)

C D Ling, R L Withers, J G Thompson, S Schmid
Structures of $Bi_{14}WO_{24}$ and $Bi_{14}MoO_{24}$ from neutron powder diffraction data
Acta Cryst B **55** 306 (1999)

C D Ling, S Schmid, R L Withers, J G Thompson, N Ishizawa, S Kishimoto
Solution and refinement of the crystal structure of $Bi_7Ta_3O_{18}$ using single crystal X-ray and neutron powder diffraction data
Acta Cryst B **55** 157 (1999)

S W Lovesey, U Staub
A magnetic-elastic model for the relaxation of lanthanide ions in $YBa_2Cu_3O_{7-d}$ observed by neutron scattering
Phys Rev **B61** 9130 (2000)

J R Lu, J Penfold, R K Thomas
Surfactant mixtures (review article)
Adv in Coll and Int Sci **84** 143 (2000)

J R Lu, T J Su, J Penfold
Adsorption of serum albumins at the air/water interface studied by neutron reflection
Langmuir **15** 6975 (1999)

W G Marshall, R J Nelmes, J S Loveday, S Klotz, G Hamel, J M Besson, J B Parise
A high-pressure neutron diffraction study of FeS
Phys Rev **B61** 11201 (2000)

K A McEwen, M J Bull, R S Eccleston
Magnetic excitations and quadrupolar ordering in UNiSn
Physica B **281-282** 600 (2000)

T C B McLeish, J Allgaier, D K Bick, G Bishko, P Biswas, R Blackwell, N Clarke, R K Heenan, et al
Dynamics of entangled H-polymers: Theory, rheology and neutron scattering
Macromolecules **32** 6734 (1999)

F M Mulder, H Noijons, G J Nieuwenhuys, K S Knight
High-resolution neutron diffraction evidence for the strain-induced microdomains during the phase transition in UNi_2Sn
Physica B **262** 312 (1999)

A M Muslim, J R P Webster, J Penfold, M J Lawrence, D J Barlow
SURFISS: a program for modelling the 3-dimensional structures of interfacial surfactant layers
Langmuir **16** 1189 (2000)

B Noheda, J A Gonzalo, M Hagen
Pulsed neutron diffraction study of Zr-rich PZT
J Phys:Condens Matter **11** 3959 (1999)

C Panagopoulos, B D Rainford, J R Cooper, W Lo, J L Tallon, J W Loram, J Betouras, Y S Wang, C W Chu
Effects of carrier concentration on the superfluid density of high-T_c cuprates
Phys Rev **B60** 14617 (1999)

J B Parise, W G Marshall, R I Smith, H D Lutz, H Moller
The nuclear and magnetic structure of 'White Rust' - $Fe(OH_{0.86}D_{0.14})_2$
Amer Min **85** 189 (2000)

J-G Park, Y S Kwon, W Kockelmann, M J Bull, I P Swainson, K A McEwen, W J L Buyers
Neutron scattering study of $CeTe_2$
Physica **B 281&282** 451 (2000)

A Pavese, F Ferraris, V Pischedda, R M Ibberson
Tetrahedral order in phengite 2M1 upon heating, from powder neutron diffraction and thermodynamic consequences
European J Mineralogy **11** 309 (1999)

S K Peace, R W Richards, F T Kiff, J R P Webster, N Williams
Spread films of polymethyl methacrylate on aqueous solutions of polyethylene oxide
Polymer **40** 207 (1999)

J Penfold, E Staples, I Tucker, R K Thomas
The structure of mixed non-ionic monolayers at the air-water interface
J Coll Int Sci **201** 223 (1998)

I Petri, P S Salmon, H E Fischer
Structure of molten GeSe by neutron diffraction: the Ge coordination environment
J Non-Cryst Solids **250-252** 405 (1999)

A Pfitzner, S Reiser, T Nilges, W Kockelmann
Composite copper chalcogenide halides: Neutron powder diffraction of $CuClCu_2TeS_3$ and electrical properties of $CuClCu_2TeS_3$, $(CuI)_2Cu_3SbS_3$ and $(CuI)_3Cu_2TeS_3$
J Solid State Chemistry **147** 170 (1999)

D A Porter, A Harrison, D Visser, R C B Copley, A E Goeta, J A K Howard, K S Knight
Nuclear and magnetic structures of the distorted hexagonal perovskites ND_4FeCl_3 and NH_4FeCl_3
Physica B **241-243** 385 (1998)

R M Richardson, E B Barmatov, I J Whitehouse, V P Shibaev, T Yongjie, M H F Godinho
A small angle neutron scattering study of the effect of molecular weight on the conformation of side chain liquid crystal polymers in a smectic phase
Mol Cryst Liq Cryst **330** 167 (1999)

D K Ross, K Stefanopoulos, M Kemali
The use of small angle neutron scattering in the study of hydrogen trapping at defects in metals
J Alloys & Comp **293-295** 346 (1999)

A Samad, B-C Choi, J A C Bland, S Langridge, J Penfold
Layer dependent magnetic moment distribution in an epitaxial double spin valve structure: Si(001)/Cu/FeNi/Cu/Co/Cu/FeNi/Cu
Phys Rev **B60** 7304 (1999)

G Santoli, F Bruni, F P Ricci, M A Ricci, A K Soper
Orientational correlations in liquid hydrogen sulphide
Mol Phys **97** 777 (1999)

W Schafer, W Kockelmann, A Kirfel, W Potzel, F J Burghart, G M Kalvius, A Martin, W A Kaczmarek, S J Campbell
Structural and magnetic variations of $ZnFe_2O_4$ spinels - neutron powder diffraction studies
Mat Sci Forum **321-324** 802 (2000)

W Schafer, W Kockelmann, I Halevy, J Gal
Magnetic ordering in rare earth-iron-aluminium intermetallics studied by neutron diffraction
Mat Sci Forum **321-324** 670 (2000)

R N Sinclair, A C Wright, B Bachra, Y B Dimitriev, V V Dimitrov, M G Arnaudov
The structure of vitreous V_2O_5-TeO_2
J Non-Cryst Solids **232-234** 38 (1998)

D S Sivia, S G Rawlings
Foundations of Science Mathematics : Worked problems (Book)
Oxford Chemistry Primers Series, OUP (1999) ISBN 0-19-850429-2

J M S Skakle, R Herd,
Crystal chemistry of $(RE,A)_2M_3O_7$ compounds (RE=Y, lanthanide; A=Ba, Sr, Ca; M=Al, Ga)
Powder Diffraction **14** 195 (1999)

N T Skipper, G D Williams, A V C de Siqueira, C Lobban, A K Soper
Time-of-flight neutron diffraction studies of clay-fluid interaction under basin conditions
Clay Minerals **35** 287 (2000)

T J Su, J R Lu, Z F Cui, R K Thomas, R K Heenan
Identification of the location of protein fouling on ceramic membranes under dynamic filtration conditions
J Membrane Sci **163** 265 (1999)

J Swenson, A Matic, C Gejke, L Borjesson, W S Howells, M J Capitan
Conductivity enhancement in PbI_2-AgI-$AgPO_3$ glasses by diffraction experiments and reverse Monte Carlo modeling
Phys Rev **B60** 12023 (1999)

J Swenson, M V Smalley, H L M Hatharasinghe
Structure of bridging polymers
J Chem Phys **110** 9750 (1999)

C N Tome, M R Daymond, M A M M Bourke
Interpetation of experiments and modeling of internal strains using a polycrystal model: application to beryllium
Proc Int Conf on Nuclear Engineering **VI** (ASME) p658 (1998)

P L W Tregenna-Piggott, S P Best, H U Gudel, H Weihe, C C Wilson
Influence of the mode of water coordination on the electronic structure of the $[V(OH_2)_6]_3^+$ cation
J Solid State Chem **145** 460 (1999)

R Triolo, A Triolo, F Triolo, D C Steytler, C A Lewis, R K Heenan, G D Wignall, J M DeSimone
Structure of diblock copolymers in supercritical carbon dioxide and critical micellisation pressure
Phys Rev **E61** 4640 (2000)

R I Walton, R J Francis, P S Halasyamani, D O'Hare, R I Smith, R Done, R J Humphreys
A novel apparatus for the in situ study of hydrothermal crystallisation using time-resolved neutron diffraction
Rev Sci Instrum **70** 3391 (1999)

C Washington, S M King, D Attwood, C Booth, S-M Mai, Y-W Yang, T Cosgrove
Polymer bristles: adsorption of low molecular weight poly(oxyethylene)-poly(oxybutylene) diblock copolymers on a perfluorocarbon emulsion
Macromolecules **33** 1289 (2000)

J H P Watson, D C Ellwood, A K Soper, J Charnock
Nanosized strongly-magnetic bacterially-produced iron sulfide materials
J Magn Magn Mater **203** 69 (1999)

M T Weller, S J Skinner
The structure of $Ba_3Mo_2O_8$ by powder neutron diffraction
Acta Cryst **C 55** 154 (1999)

M T Weller, P F Henry, D B Currie, S E Dann
Synthesis of novel inorganic structures under unusual high pressure gas and hydrothermal conditions
J Materials Chemistry **9** 283 (1999)

G D Williams, A K Soper, N T Skipper, M V Smalley
High-resolution structural study of interfacial fluids in vermiculite clays
J Phys Chem **B 102** 10899 (1998)

C C Wilson
Modern Neutron Diffraction Methods
Implications of Molecular and Materials Structure for New Technologies, Eds F H Allen, J A K Howard, G P Shields, NATO Science Series E: Applied Sciences (Kluwer) **360** 11 (1999)

R L Withers, C D Ling, S Schmid
Atomic modulation functions, periodic nodal surfaces and the three-dimensionally incommensurate modulated
$(1-x)Bi_2O_3.xNb_2O_5$, $0.06 < x < 0.23$, solid solution
Z fur Kristallographie **214** 296 (1999)

A C Wright
Diffraction studies of glass structure: the first 70 years
Glass Phys Chem **24** 148 (1998)

E Wu, S J Campbell, W A Kaczmarek, M Hofmann
Mechanochemical treatment of $BaFe_{12}O_{19}$ - Mossbauer investigation
Materials Science Forum **312-314** 127 (1999)

E Wu, S J Campbell, W A Kaczmarek, M Hofmann, S J Kennedy, A J Studer
Mechanochemical treatment of haematite - neutron diffraction investigation
Materials Science Forum **312-314** 121 (1999)

T Yamaguchi, K Hidaka, A K Soper
Erratum: The structure of liquid methanol revisited: a neutron diffraction experiment at -80C and +25C
Mol Phys **97** 603 (1999)

T Yamaguchi, C J Benmore, A K Soper
The structure of subcritical and supercritical methanol by neutron diffraction, empirical potential structure refinement, and spherical harmonic analysis
J Chem Phys **112** 8976 (2000)

A Yaouanc, P Dalmas de Reotier, P C M Gubbens, C T Kaiser, P Bonville, J A Hodges, A Amato, A Schenck, P Lejay et al
μSR investigation of the quasielastic magnetic excitations in strongly correlated compounds
Physica **B 259-261** 126 (1999)

N Zotov, R Miletich, H Boysen, H Tietze-Jaensch, W Kockelmann
Copper substitution in $(Cu,Mn)_7O_{12}$ braunite: a combined neutron and x-ray powder diffraction study
Mat Sci Forum **321-324** 791 (2000)

ISIS Seminars 1999 - 2000

April 13 1999 **PCW Holdsworth** (UCL & Ecole Normale Superieure)
Huge universal ctatistics in curbulence and critical phenomena

April 19 1999 **I Anderson** (ILL, Grenoble, France)
Recent developments in neutron optics

April 27 1999 **D K Morr** (University of Illinois)
Inelastic neutron scattering in the superconducting state of high-T_c cuprates

May 25 1999 **W Montfrooij** (Oak Ridge National Laboratory, USA)
The superfluid phase of ^4He

June 25 1999 **I Goncharenko** (LLB, Saclay & Kurchatov Institute, Moscow)
Magnetic neutron diffraction under very high pressure: recent progress at LLB

June 29 1999 **GJ Baxter, P Wilson, K Bass** (Rolls-Royce PLC)
Intertia welding aerogengine components

August 6 1999 **J Carpenter** (Argonne National Laboratory, USA)
The rationale and concept development for a long-wavelength target station for the SNS

September 28 1999 **J E Lorenzo** (CNRS, Grenoble, France)
Neutron scattering studies on some antiferromagnetic S=1/2 chains and ladders

October 12 1999 **A Wildes** (ILL, Grenoble, France)
Recent developments in three-axis spectrometers at the ILL, or teaching an old dog new tricks

October 26 1999 **SJ Hibble** (University of Reading)
Total neutron diffraction studies of disordered crystalline materials including the CMR manganates

November 23 1999 **D Nees** (RAL)
Optical tweezers in colloid science - using the momentum of light for the measurement of particle pair interactions

December 3 1999 **JS Gardner** (Chalk River Laboratories, Canada)
$Y_2Mo_2O_7$: is it a spin glass?

December 7 1999 **S Lee** (University of St. Andrew's)
Using the complementarity of muon spin rotation and neutron scattering to probe the vortex lattice in exotic superconductors

December 20 1999 **Prof Kiyanagi** (Hokkaido University)
The development of neutron beam control devices

January 13 2000 **AS Rinat** (Wiezmann Inst. of Science, Israel)
Some theoretical developments on deep inelastic neutron scattering from fluid ^4He

February 29 2000 **P Böni** (PSI, Switzerland)
Neutron beam optics

March 28 2000 ***DN Argyriou*** *(Argonne National Laboratory, USA)*
Charge, orbital and magnetic ordering in the layered manganites

SDG Meetings

Informal meetings for the presentation and discussion of new ideas, latest results and recent developments

27th May, 1999	**Stephen Lovesey**	*YBCO, R and US*
11th June, 1999	**Ken Andersen**	*Polarisation analysis…*
24th June, 1999	**Mike Johnson**	*New lenses for neutrons?*
8th July, 1999	**Steve King**	*How not to drown a rat*
22nd July, 1999	**Steve Cottrell**	*Pulsed radio frequency μSR measurements*
5th August, 1999	**Ray Osborn**	*Why you should be using NeXus - the neutron and X-ray data format!*
12th August, 1999	**Chris Frost**	*Putting pressure on heavy fermions*
14th October, 1999	**Roger Eccleston**	*Hole migration in the superconducting spin ladder* $Ca_{11.5}Sr_{2.5}Cu_{24}O_{41}$
25th November, 1999	**Kevin Knight**	*Thermal expansion in gibbsite - a moral story*
9th December, 1999	**Alan Soper**	*The art of levitation on sandals*
20th January, 2000	**Jerry Mayers**	*Bose-Einstein condensation and pair correlations in superfluid helium*
10th February, 2000	**Oleg Petrenko**	*Frustrated anti-ferromagnets in a magnetic field*
17th February, 2000	**Clemens Glaubitz**	*Solid state NMR of membrane proteins*
9th March, 2000	**Mark Daymond**	*Strain anisotropy - a fingerprint of deformation?*
6th April, 2000	**John Webster**	*The liquid-liquid interface*